INVESTIGATING THE ROLE OF DTX3L IN THE REPLICATION STRESS RESPONSE

LUCINDA ANN CURNOW

THE INSTITUTE OF CANCER RESEARCH, UNIVERSITY OF LONDON

SUPERVISOR: PROF. WOJCIECH NIEDZWIEDZ

Thesis submitted for the degree of

Doctor of Philosophy,

University of London

January 2022

Declaration

I hereby declare all the work presented in this thesis is my own unless where otherwise stated.

I hereby declare that this thesis has not been and will not be submitted in whole or in part to another University for the award of any other degree.

Signed: *Lucinda Ann Curnow*

Date: 25/01/2022

Acknowledgements

Joining the Niedzwiedz lab in late 2017, the lab itself having recently re-established after moving from the University of Oxford, I couldn't envision the lab growing into the community that it has become now. Starting off as a lab of just four, we've now bloomed into a lab of ten- we've been to Greece together, we've navigated a pandemic together; it's certainly been an experience! I would like to thank Wojciech especially for his guidance and giving me this valuable opportunity, as well as the Niedzwiedz lab for their company and remedying trips to the pub.

I would also like to express my gratitude for the support, guidance, and good company of Lu Yu, who made one of the more challenging parts of this project not only possible, but enjoyable. I want to extend thanks to Theo Roumeliotis for his contributions and for making the time to answer my numerous questions.

On a personal level, I want to express gratitude for the support and shoulders of my friends who have been on this journey with me. You've made the effort to feign interest about cells and proteins, tried to use your GCSEs in biology to help me solve my experimental problems and used your hearts to solve the rest. The last four years have been transformative, and I wouldn't have done it without the healing escapism you give. I'd also like to express thanks to Anna, who I had met after the first year of my PhD studies; it's fair to say you found me at a low point but through your immeasurable understanding, kindness, and encouragement, you've helped me immensely to believe and have confidence in what I can achieve. I absolutely would not have done this without you.

Finally, I'd like to thank my family for their support. Especially, I want to hold my mum, Julie, up in particular as a beacon of values and intellect in my life. You have endured and achieved so much; you are my daily inspiration of strength. Your encouragement and support (and whacky humour) throughout the years have been crucial. I hope you enjoy your new doorstop!

Abstract

DNA replication must be carried out with high fidelity to ensure accurate transfer of genetic information upon cell division. The mechanisms by which damage upon DNA is repaired are extensive and are increasingly well characterised; in contrast, the mechanisms that maintain DNA replication the face of these challenges, known as the replication stress response (RSR), are less well understood. Cancer cells often harbour mutations in these pathways to enable carcinogenesis; conversely, a reliance on remaining pathways provides opportunity for their selective targeting to elicit genomic instability and cancer cell death. Therefore, the identification of novel factors of the RSR will provide new opportunities for drug development. Through the use of isolation of proteins on nascent DNA (iPOND), E3 ubiquitin ligase DTX3L has been identified as a novel factor present at the progressing replisome. DNA fibre analysis has suggested DTX3L to be an important factor in maintaining replication fork dynamics to both endogenous and amplified replication stress, with evidence of defective replication fork regression and resection. Quantification of DNA damage response (DDR) markers suggests that altered replication dynamics as a result of DTX3L depletion are consequential, resulting in increased genomic instability. Furthermore, an enhanced sensitivity to clastogen treatment in DTX3L deficient cells is observed, demonstrating clinical relevance. Mechanistically, through abrogation of ubiquitin ligase domain functionality, DTX3L ubiquitination is essential for its replication stress associated role. Evidence presented here suggests DTX3L depletion may result in defective ATR activation and this may be mediated through DTX3L association with TOPBP1. Furthermore, ubiquitome enrichment analysis reveals other potential targets of DTX3L ubiquitination that may contribute to its role in maintenance of DNA replication. Ultimately, the work here evidences DTX3L as a newly identified factor of the RSR.

Table Of Contents

DECLARATION **2**

ACKNOWLEDGEMENTS **3**

ABSTRACT **4**

TABLE OF CONTENTS **5**

LIST OF FIGURES **9**

LIST OF TABLES **11**

LIST OF ABBREVIATIONS **12**

CHAPTER 1: INTRODUCTION **16**

1.1. Outline **18**

1.2. Cancer **20**

1.3. DNA Replication & the S-phase Checkpoint **22**

1.4. Replication Stress & Cancer **26**

1.5. DNA Damage and Repair **30**

1.5.1. DNA Damage Signalling 30

1.5.2. MMR, BER & NER 31

1.5.3. Double Strand Break Repair 32

1.5.3.1. Non-Homologous End Joining (NHEJ) 32

1.5.3.2. Homologous Recombination (HR) 34

1.6. The Replication Stress Response **39**

1.6.1. Replication Fork Reversal 42

1.6.2. Replication Fork Restart 44

1.6.3. Fork Reversal is a Double-edged Sword 45

1.6.4. Post Replication Repair 46

1.6.5. Exploiting Cancer's Replication Stress Burden 47

1.7. Ubiquitin Signalling in the DDR & RSR **50**

1.7.1. The DTX3L E3 Ubiquitin Ligase 53

1.7.1.1. DTX3L & Cancer 56

1.7.1.2. DTX3L & the DNA Damage Response 57

CHAPTER 2: MATERIALS & METHODS **60**

2.1. Materials **61**

2.1.1. siRNA 61

2.1.2. Antibodies 61

2.2. Methods 63
2.2.1. Cell Culture 63
2.2.2. siRNA Gene Silencing 63
2.2.3. Plasmid Cloning & Transfection 64
2.2.3.1. Site Directed Mutagenesis of FLAG-DTX3L 65
2.2.4. CRISPR *DTX3L*$^{-/-}$ Cell Line Generation 66
2.2.5. Single Molecule DNA Fibre Immunofluorescence 67
2.2.6. Cell Proliferation Assays 69
2.2.7. Drug Sensitivity Assays 69
2.2.8. Western Blotting 70
2.2.9. qPCR 71
2.2.10. Flow Cytometry and Cell Sorting 71
2.2.11. DDR Immunofluorescent Staining 72
2.2.11.1. 53BP1/OPT/Micronuclei, RAD51 and γH2AX IF Staining 72
2.2.11.2. RPA IF Staining 72
2.2.12. EdU Labelling and Proximity Ligation Assays (PLAs) 73
2.2.12.1. EdU Labelling for PLA 73
2.2.12.2. PLA Assay 74
2.2.13. GFP Co-Immunoprecipitation (Co-IP) and Mass Spectrometry (MS) 75
2.2.13.1. GFP-DTX3L Co-IP 75
2.2.13.2. FLAG-DTX3L Co-IP 76
2.2.13.3. MS Sample Preparation 77
2.2.13.4. Desalting & Fractionation 78
2.2.13.5. LC-MS/MS Analysis 79
2.2.14. Ubiquitome Enrichment Profiling 80
2.2.14.1. Sample Preparation 80
2.2.14.2. Ubiquitin Remnant Peptide Immunoprecipitation 81
2.2.14.3. Ubiquitome Enrichment MS Acquisition 84
2.2.14.4. Ubiquitome Enrichment MS Result Analysis 85

CHAPTER 3: DEPLETION OF DTX3L AFFECTS DNA REPLICATION DYNAMICS 86

3.1. Identification of E3 Ubiquitin Ligases Present at the DNA Replication Fork by iPOND 87
3.1.1. Isolation of Proteins On Nascent DNA 87
3.1.2. E3 ubiquitin ligases identified by iPOND-MS 88

3.2. DNA Fibre Analysis Upon Depletion of Fork-Associated E3 Ubiquitin Ligases 91
3.2.1. Depletion of select E3 ubiquitin ligases leads to altered replication dynamics 91

3.3. HeLa Cells Depleted for DTX3L Have Reduced Proliferation 99

3.4. Depletion of DTX3L in HeLa Cells Leads to Clastogen Sensitivity.....100

3.5. Conclusion 104

CHAPTER 4: DTX3L PREVENTS REPLICATION STRESS-ASSOCIATED DNA DAMAGE 106

4.1. Exogenous Replication Stress Leads to Increased DNA Damage in DTX3L Depleted Cells 107

4.1.1. 53BP1 Foci, OPT Domains and Micronuclei Formation in DTX3L Depleted HeLa Cells.....107

4.1.2. RPA Foci Formation is Increased in HeLa and U2OS Cells Deficient for DTX3L 112

4.1.3. CHK1 Phosphorylation is Reduced in HeLa Cells Upon DTX3L Silencing 114

4.1.4. DTX3L Depletion Leads to Increased DNA Damage Foci Formation Upon Ionising Radiation 116

4.2. Conclusion 120

CHAPTER 5: PHENOTYPIC VALIDATION IN *DTX3L*$^{-/-}$ CELLS.....122

5.1. Generation of DTX3L Deficient Cell Models by CRISPR.....123

5.1.1. Characterisation of *DTX3L*$^{-/-}$ HeLa & RPE-1 Cells by DNA Fibre Analysis 125

5.1.2. HeLa *DTX3L*$^{-/-}$ cells exhibit enhanced clastogen sensitivity.....130

5.1.3. HeLa *DTX3L*$^{-/-}$ cells exhibit reduced proliferation but unimpeded cell cycle progression.....134

5.1.4. HeLa and RPE-1 *DTX3L*$^{-/-}$ cells have increased RPA foci formation ...136

5.2. Conclusion 138

CHAPTER 6: ELUCIDATING THE MECHANISTIC ROLE OF DTX3L AT THE STALLED REPLICATION FORK 139

6.1. Complementation of HeLa *DTX3L*$^{-/-}$ Cells 140

6.1.1. Suppression of Regressed Replication Fork Degradation Requires the E3 ubiquitin ligase activity of DTX3L 140

6.1.2. Clinically Relevant Y403X DTX3L Mutation Demonstrates Fork Resection Defect Seen in *DTX3L*$^{-/-}$ cells.....144

6.1.3. Abolishment of PARP9 Does Not Account For Fork Resection Defect 148

6.2. Fork Degradation in *DTX3L*$^{-/-}$ Cells is Rescued Through Modulation of Fork Repair Factors 150

6.2.1. Silencing of SMARCAL1 Rescues Fork Resection in HeLa *DTX3L*$^{-/-}$ Cells 150

6.2.2. MRE11 Inhibition Rescues Fork Resection in HeLa *DTX3L*$^{-/-}$ Cells 152

6.2.3. Recruitment of RAD51, BRCA1 and MRE11 to the Replication Fork Are Unaffected by DTX3L Deficiency.....154

6.3. Complementation of HeLa *DTX3L*$^{-/-}$ Cells by Ectopic Expression of GFP-DTX3L 158

6.3.1. Generation and Characterisation of HeLa *DTX3L*$^{-/-}$ Cells Recomplemented With GFP-DTX3L 158

6.3.2. Exploring the DTX3L Interactome Through GFP-Nanotrap Co-Immunoprecipitation Coupled to LC-MS/MS 160

6.4. TOPBP1 Associates With DTX3L 162

6.4.1. FLAG-DTX3L-WT Co-IP Corroborates DTX3L and TOPBP1 Interact *In Vivo* 162

6.4.2. DTX3L and TOPBP1 Associate More Frequently Under Conditions of Replication Stress 163

6.5. Ubiquitome Enrichment Profiling of *DTX3L*$^{-/-}$ Cells 165

6.5.1. Pathway Enrichment Analysis of Ubiquitinated Peptides 167

6.5.2. Ubiquitin Peptide Enrichment between HeLa WT and *DTX3L*$^{-/-}$ cells 169

6.6. Conclusion 172

CHAPTER 7: DISCUSSION 174

7.1. Summary 176

7.2. DTX3L Acts at the Stalled Replication Fork to Overcome Challenges to Replication 178

7.3. DTX3L and the Maintenance of Genome Stability 180

7.4. Mechanistic Action of DTX3L in the RSR 182

7.4.1. DTX3L Requires Ubiquitination Function to Mediate Replication Stress Tolerance 182

7.4.2. Contribution of PARP9 to Observed Fork Defects 184

7.4.3. Fork Resection Arising Through DTX3L Deficiency is Mediated by SMARCAL1 and MRE11 185

7.4.4. Recruitment of Fork Repair Factors is Not Significantly Affected by DTX3L Depletion 186

7.4.5. DTX3L Associates With TOPBP1 Under Conditions of Enhanced Replication Stress 188

7.4.6. *DTX3L*$^{-/-}$ Ubiquitome Enrichment Analysis 191

REFERENCES 197

List of Figures

Figure 1. Mechanism and proteins involved in replication origin firing. ... 24
Figure 2. Structures and lesions that hinder DNA replication and cellular outcomes. ... 28
Figure 3. Mechanisms of HR, NHEJ and Alt-EJ in DSBR. ... 36
Figure 4. RSR factor recruitment at the stalled replication fork promotes fork reversal. ... 40
Figure 5. Schematic depicting the process of replication fork reversal. ... 43
Figure 6. Enhancement of replication stress can lead to specific targeting of cancer cells. ... 48
Figure 7. The ubiquitin-dependent DNA damage response. ... 52
Figure 8. DTX3L domain structure. ... 55
Figure 9. Illustration depicting DNA fibre labelling protocol. ... 68
Figure 10. Schematic of iPOND labelling protocol. ... 88
Figure 11. DNA fibre analysis of unchallenged replication fork dynamics arising from siRNA-mediated depletion of candidate E3 ubiquitin ligases. ... 94
Figure 12. DNA fibre analysis of replication fork stalling dynamics arising from siRNA-mediated depletion of candidate E3 ubiquitin ligases in HU challenged cells. ... 95
Figure 13. DNA fibre analysis of replication fork recovery arising from siRNA-mediated depletion of candidate E3 ubiquitin ligases in HU challenged cells. ... 96
Figure 14. Silencing of DTX3L in HeLa cells by siRNA treatment. ... 97
Figure 15. Fork dynamics are impeded upon DTX3L silencing. ... 98
Figure 16. Cell proliferation is reduced in cells silenced for DTX3L. ... 99
Figure 17. DTX3L depletion enhances cell sensitivity to replication stress inducing drug treatments. ... 102
Figure 18. DTX3L depleted cells have increased 53BP1 focus formation. ... 108
Figure 19. DTX3L deficient cells have increased micronuclei formation. 110
Figure 20. DTX3L depletion results in increased frequency of OPT domains. ... 111
Figure 21. HeLa cells depleted for DTX3L have increased RPA foci intensity. ... 113
Figure 22. CHK1 phosphorylation is reduced in DTX3L depleted cells compared to controls. ... 115
Figure 23. Quantification of cells positive for RAD51 foci following 10Gy IR. ... 117
Figure 24. DTX3L depleted cells display increased γH2AX DNA damage foci upon IR treatment. ... 119
Figure 25. DTX3L knockout by CRISPR-Cas9 transfection is successful in HeLa and RPE-1 cells. ... 124
Figure 26. Preliminary DNA fibre analysis of DTX3L$^{-/-}$ clones shows replication stress phenotypes. ... 126
Figure 27. DNA fibre analysis of specific HeLa DTX3L$^{-/-}$ clones validates replication stress phenotypes. ... 128
Figure 28. RPE-1 DTX3L$^{-/-}$ cells exhibit increased fork stalling. ... 129
Figure 29. HeLa DTX3L$^{-/-}$ cells are more sensitive than wild-type to replication stress inducing drug treatments. ... 132

Figure 30. Cell proliferation is reduced in DTX3L$^{-/-}$ cells. 134
Figure 31. Loss of DTX3L does not cause changes in cell cycle profile. 135
Figure 32. HeLa and RPE-1 DTX3L$^{-/-}$ clones exhibit an increase in RPA foci compared to WT under conditions of enhanced replication stress. 137
Figure 33. FLAG-DTX3L-M2 Sequencing trace. 142
Figure 34. Western blot depicting ectopic expression of WT DTX3L and M2 DTX3L. 142
Figure 35. DNA fibre analysis of HDKO cells re-complemented with FLAG-DTX3L-WT or FLAG-DTX3L-M2 expressing constructs. 143
Figure 36. Multi sequence alignment of the DTX3L gene in different species of vertebrate demonstrating conservation of the 502A residue. 146
Figure 37. FLAG-DTX3L-Y403X does not rescue DTX3L$^{-/-}$ fork resection defect, compared to FLAG-DTX3L-A502V expressing constructs. 147
Figure 38. Silencing of PARP9 induces a mild fork degradation defect compared to DTX3L depletion. 149
Figure 39. Silencing of SMARCAL1 rescues the fork resection defect seen in HeLa DTX3L$^{-/-}$ cells. 151
Figure 40. Inhibition of MRE11 by mirin rescues the fork resection defect seen in HeLa DTX3L$^{-/-}$ cells. 153
Figure 41. Schematic of the proximity ligation assay. 154
Figure 42. Recruitment of RAD51 to the replication fork is not affected by DTX3L deficiency. 156
Figure 43. Recruitment of BRCA1 to the replication fork is not affected by DTX3L deficiency. 157
Figure 44. Recruitment of MRE11 to the replication fork is not affected by DTX3L deficiency. 157
Figure 45. DTX3L is transgenically expressed in HeLa DTX3L$^{-/-}$ cells via the pDEST-GFP-DTX3L construct and localises to the nucleus. 159
Figure 46. TOPBP1 interaction in vivo with DTX3L is suggested by GFP co-IP-MS. 161
Figure 47. TOPBP1 in vivo interaction with DTX3L is validated by FLAG co-IP. 162
Figure 48. Frequency of TOPBP1 and DTX3L association in vivo is greater in conditions of enhanced replication stress. 164
Figure 49. Pearson sample correlation analysed using scaled abundances. 166
Figure 50. Differentially ubiquitinated peptides. 171

List of Tables

Table 1. Human syndromes associated with DDR and RSR genetic mutations. 38
Table 2. siRNAs used in the present study. 61
Table 3. Primary antibodies used in the present study. 62
Table 4. Site Directed Mutagenesis primers used for generation of FLAG-DTX3L-M2/Y403X/A502V plasmid constructs. 66
Table 5. gRNA oligos cloned into the CRISPR pAIO-NK vector. 66
Table 6. Samples included in ubiquitin remnant peptide IP. 81
Table 7. E3 ubiquitin ligase iPOND hits. 90
Table 8. DNA damage repair and immune system related pathways are significantly represented in ubiquitome enrichment analysis comparing DTX3L$^{-/-}$ against WT cells. 168

List of Abbreviations

pAIO	All In One plasmid
Alt-EJ	Alternative end joining
AT	Ataxia Telangiectasia
ATM	Ataxia-telangiectasia mutated
ATR	ATM and Rad-3 related
ATRi	ATR inhibitor
BAL	B aggressive lymphoma protein
BCL2	B-cell lymphoma 2
BBAP	B-lymphoma- and BAL-associated protein
BER	Base excision repair
BLM	BLM RecQ like helicase
BSA	Bovine serum albumin
BRCA1	BRCA1, DNA repair associated
BRCA2	BRCA2, DNA repair associated
BIR	Break induced replication
BrdU	Bromodeoxyuridine
Cas9	Cas9 nickase
NK	Cas9-D10A-nickase
CMG	Cdc45, MCM2-7, GINS complex
CDC25A	Cell division cycle 25 homologue A
CDC45	Cell division cycle 45
CDC6	Cell division cycle 6
CHK1	Checkpoint kinase 1
CHK2	Checkpoint kinase 2
CldU	Chlorodeoxyuridine
CDT1	Chromatin licensing and DNA replication factor 1
CRISPR	Clustered regularly interspaced short palindromic repeats
Co-IP	Co-immunoprecipitation
CtIP	CTBP-interacting protein
cGAS	Cyclic GMP-AMP synthase
CCND1	Cyclin D1
CDK2	Cyclin-dependent kinase 2
DDK	Dbf4-dependent kinase
DUB	De-ubiquitinating enzyme
DTX1	Deltex E3 ubiquitin ligase 1
DTX3	Deltex E3 ubiquitin ligase 3
DTX3L	Deltex E3 ubiquitin ligase 3-like
dNTP	Deoxynucleoside triphosphate
DNA	Deoxyribonucleic acid
DLBCL	Diffuse large B cell lymphoma
DDR	DNA damage response

DF	DNA fibre
MutH	DNA mismatch repair protein H
MutL	DNA mismatch repair protein L
MutS	DNA mismatch repair protein S
DNA2	DNA replication helicase/nuclease 2
TOPBP1	DNA topoisomerase II binding protein 1
DNA-PKcs	DNA-dependent protein kinase catalytic subunit
DSB	Double strand break
DSBR	Double strand break repair
EtOH	Ethanol
EdU	Ethynyldeoxyuridine
ETAA1	Ewing tumour-associated antigen 1
EXO1	Exonuclease 1
EXD2	Exonuclease 3'-5' domain containing 2
FBH1	F-box DNA helicase 1
FANCD2	FA complementation group D2
FANCI	FA complementation group I
FA	Fanconi Anaemia
FBS	Fetal bovine serum
FACS	Fluorescence activated cell sorting
γH2AX	Gamma H2AX
GINS	Go-ichi-ni-san complex
Gy	Gray
GFP	Green fluorescent protein
gRNA	Guide RNA
HDKO	HeLa DTX3L Knockout
HLTF	Helicase like transcription factor
HPLC	High performance liquid chromatography
H2AX	Histone 2AX
H4	Histone 4
H4K20	Histone 4 lysine 20
H4K91	Histone 4 lysine 91
HAT4	Histone acetyltransferase 4
HJ	Holliday junction
HR	Homologous recombination
HECT	Homologous to the E6-AP carboxyl terminus
HDR	Homology directed repair
HU	Hydroxyurea
IF	Immunofluorescent
IP	Immunoprecipitation
ICR	Institute of Cancer Research
IFN-γ	Interferon gamma
ISG	Interferon stimulated gene
ICL	Interstrand crosslink

IdU	Iododeoxyuridine
IR	Ionising radiation
iPOND	Isolation of proteins on nascent DNA
KO	Knockout
Ku	Ku70-Ku80 heterodimer
LC	Liquid chromatography
SET8	Lysine methyltransferase 5A
MS	Mass spectrometry
MDC1	Mediator of damage checkpoint 1
MetOH	Methanol
MUS81	Methyl methanesulphonate ultraviolet sensitive gene clone 81
MMEJ	Microhomology mediated end joining
MCM	Minichromosome maintenance
MMR	Mismatch repair
mtDNA	Mitochrondrial DNA
MRE11	MRE11 homologue, double strand break repair nuclease
MRN	MRE11/RAD50/NBS1
NHEJ	Non-homologous end joining
XLF	Non-homologous end joining factor 1
NLS	Nuclear localisation sequence
NER	Nucleotide excision repair
ORC	Origin recognition complex
53BP1	P53 binding protein 1
PFA	Paraformaldehyde
PARPi	PARP inhibitor
PALB2	Partner and localiser of BRCA2
PTIP	Pax transactivation domain-interacting protein
PBS	Phosphate buffered saline
pDNA	Plasmid DNA
PARP1	Poly (ADP-ribose) polymerase-1
PARP9	Poly (ADP-ribose) polymerase-9
PAR	Poly(ADP-ribose)
PAH	Polycyclic aromatic hydrocarbon
PRR	Post replicative repair
PTM	Post translational modification
pre-RC	Pre-replisome complex
PCNA	Proliferating cell nuclear antigen
PPase	Protease and Phosphatase
PPI	Protein-protein interaction
PLA	Proximity ligation assay
qPCR	Quantitative real-time polymerase chain reaction
RAD51	RAD51 recombinase
RING	Really interesting new gene
RECQ1	RecQ like helicase

RPA	Replication protein A
RSR	Replication stress response
RIF1	Replication timing regulatory factor 1
pRb	Retinoblastoma protein
RNA	Ribonucleic acid
RFWD3	Ring finger and WD repeat domain 3
RNF168	Ring finger protein 168
RNF8	Ring finger protein 8
SIOD	Schimke Immuno-osseous Dysplasia
SS	Seckel Syndrome
STAT1	Signal transducer and activator of transcription 1
siLuc	siLuciferase
SSB	Single stranded break
ssDNA	Single stranded DNA
SFR	Sister fork ratio
SDM	Site directed mutagenesis
SMX	SLX1-SLX4-MUS81-EME1-XPF-ERCC1 complex
SLX4	SLX4 structure-specific endonuclease subunit
siRNA	Small interfering RNA
SDS-PAGE	Sodium dodecyl sulphate-polyacrylamide gel electrophoresis
SEM	Standard error of the mean
STING	Stimulator of interferon genes
SMARCAL1	SWI/SNF-related matrix-associated actin-dependent regulator of chromatin subfamily A-like protein 1
SDSA	Synthesis-dependent strand annealing
TBK1	Tank binding kinase 1
TS	Template switching
TMEJ	Theta mediated end joining
TLS	Translesion synthesis
TBST	Tris-buffered saline with Tween
p53	Tumour protein p53
UBD	Ubiquitin binding domain
UPS	Ubiquitin proteosome system
UV	Ultraviolet
WRN	Werner syndrome RecQ like helicase
WB	Western blot
WT	Wild-type
XRCC4	X-ray repair cross-complementing protein 4
ZRANB3	Zinc finger RANBP2-type containing 3

Chapter 1: Introduction

Cellular propagation and the maintenance all life depends on the timely and accurate replication of the complete genetic material contained within the nucleus, so that it may be divided among two daughter cells and growth of the organism can continue. Deoxyribose nucleic acid (DNA) synthesis, in concert with DNA damage repair processes, are responsible for ensuring high fidelity of this genomic transmission. Failures in these processes result in consequences of varying severity based on the offending lesion produced, the spatiotemporal context and the magnitude of resultant mutations. The field of DNA damage and repair aims to identify both the source and remedy of these lesions, so that advances may be made in the treatment of disease and aging that arise as a result. It was over 60 years ago at the Institute of Cancer Research (ICR) that the first conclusive evidence emerged that the fundamental cause of cancer is DNA damage; today research is ongoing to expand our depth of knowledge ever deeper, with the hope of identifying better treatments for cancer.

1.1. Outline

Human cells, despite harbouring around three billion bases of genomic material that must be replicated each cell division, reproduce with an estimated mutation rate of less than 2 mutations per mitosis (Werner et al., 2020). To maintain such high fidelity, cells have evolved numerous DNA damage response pathways, of which defects can lead to deleterious DNA alterations and genomic instability (Ciccia & Elledge, 2010). Replication of DNA is one of the most vulnerable cell processes. At its initiation, replication machinery is assembled at discrete replication origins to ensure duplication of the genome once per cell division. The replication machinery permits unwinding of the DNA duplex and semi-conservative synthesis by establishing a replication fork, elongating as the DNA is traversed (Gaillard et al., 2015).

DNA replication must be carefully orchestrated to overcome replication challenges that arise, a phenomenon termed 'replication stress'. These challenges manifest as DNA damage lesions, which in turn propagate further replication stress and genomic instability, and ultimately, carcinogenesis (Gaillard et al., 2015). Many of the components of the DNA damage response (DDR) are also recruited by the DNA replication stress response (RSR) to facilitate strategic DNA restructuring at the fork or for removal of the offending lesion. While the DNA damage response has been extensively characterised in terms of the various lesions recognised and their repair sub-pathways, the RSR remains relatively uncharacterised.

This study aims to provide evidence that the deltex E3 ubiquitin ligase (3-like) 3L, DTX3L (synonym: BBAP) is a novel factor involved in the RSR. Through the use of isolation of proteins on nascent DNA (iPOND) coupled to mass spectrometry (MS), DTX3L has been identified by this lab (unpublished data) to be recruited to

the active replication fork in conditions of endogenous and induced replication stress, suggesting that DTX3L plays a functional role in the maintenance of replication. Additionally, DTX3L has previously been identified to play a role in the DNA damage response (Wu et al., 2019; Yan et al., 2009). Furthermore, DTX3L has been found to be overexpressed in cancers of the breast and prostate, as well as chemotherapy-resistant lymphoma suggesting a role in cancer biology. Elucidating the role of DTX3L in preventing replication stress may explain its implication in cancer and will be the focus of this study. Ultimately, DTX3L may provide a novel therapeutic targeting strategy.

1.2. Cancer

The collection of diseases that is encapsulated by the term ‘cancer’ were considered to share six hallmarks that influence tumour growth and metastasis, as outlined in the eminent review by Hanahan and Weinburg in 2000 (Hanahan & Weinberg, 2000). The most fundamental trait of cancer is the ability to maintain constant proliferation, where non-cancer cells carefully regulate proliferative homeostasis for sustaining organismal viability. Conversely, cancer cells must evade the action of growth suppressors; prototypical examples being the retinoblastoma (pRb) and p53 proteins. Additional hallmarks include the resistance of apoptosis, induction of new blood vessel formation for sustained energy supply, achieving replicative immortality and the acquisition of the ability to metastasize (Hanahan & Weinberg, 2000). These hallmarks have since been revisited and now include the ability for cancer cells to rewire their cellular metabolism and avoid immune surveillance, as well as cancer-enabling characteristics such as its emergence through inflammation and more pertinently, genomic instability (Hanahan & Weinberg, 2011).

Cancer is the leading cause of death worldwide, resulting in almost ten million deaths in 2020 (Sung et al., 2021). In 2020, the most common forms of cancer diagnosed were those of the breast, lung, colon & rectum, prostate, skin (non-melanoma) and stomach, ranging from 2.26 million cases to 1.09 million cases respectively. Cancers that resulted in the highest mortality were those of the lung, colon & rectum, liver, stomach and breast, with mortality ranging between 1.8 million deaths and 0.7 million deaths (Ferlay et al., 2020).

Cancer incidence is dependent on an individual’s genotype and its interplay with environmental carcinogens, which can be physical, chemical or biological in

nature. Examples of exogenous causes of cancer that directly lead to DNA damage include tobacco smoke, ultraviolet (UV) and ionizing radiation (IR), as well as pollutants such as asbestos and polycyclic aromatic hydrocarbons (PAHs) (Pfeifer et al., 2002; Rose Li et al., 2020; Soehnge et al., 1997; Stec et al., 2018).

As discovered by Philip Lawley and Peter Brookes at the ICR during the later 20th century, carcinogens produce mutations to DNA and these mutations often hinder DNA replication and cell division (Venitt & Phillips, 2012). It has since been revealed that many genes mutated in cancer are involved in DNA repair. Non-cancer cells will respond to DNA lesions through the activation of the DNA damage checkpoint and DNA damage repair pathways. Unresolved DNA damage will result in apoptosis or senescence of the non-cancer cell, however mutations in the cancer cell permit cell survival and DNA damage tolerance. A state of chronic genomic instability in cancer cells leads to a dependency on remaining DNA damage repair pathways to permit sustained DNA replication and cancer cell division; consequentially, cancer cells are inherently subject to a higher degree of replication stress relative to the non-cancer cell (Gaillard et al., 2015).

1.3. DNA Replication & the S-phase Checkpoint

DNA replication is a process in cells that must be carried out with high fidelity in order to maintain genomic stability. It is a process that is carefully orchestrated and initiates once per cell cycle through the licensing and activation of replication origins located throughout the DNA (Leonard & Grimwade, 2017; Masai et al., 2010; Sclafani & Holzen, 2007).

Eukaryotic DNA synthesis begins with the formation of pre-replisome complexes (pre-RC) at multiple replication origins during the G1 phase of the cell cycle. This initiation stage of replication ensures that the genome duplicates only once per cell division, as origins licensed in G1 can then initiate replication in the following S-phase (Masai et al., 2010; Sclafani & Holzen, 2007). Initiation of pre-RC formation begins with origin-association of the origin recognition complex (ORC), facilitating the recruitment of cell division cycle 6 (Cdc6) protein. Cdc6, along with chromatin licensing and DNA replication factor 1 (Cdt1), provide a recruitment scaffold at these origins for loading of the minichromosome maintenance complexes (MCM2-7), which will produce bidirectional replication forks (Gambus et al., 2011). Once the pre-RC has permitted loading of MCM2-7 complexes onto the origin, they are then able to act as platforms for replisome assembly. Upon G1 to S-phase transition, pre-RCs form functional initiation complexes through the action of cyclin-dependent kinase 2 (CDK2) and Dbf4-dependent kinase (DDK), which permit further recruitment of replication factors that make up the replisome and dissociation of Cdc6 (Petersen et al., 1999).

The main component of the replisome consists of Cdc45 and GINS which bind to MCM2-7 to form the CMG helicase (Ilves et al., 2010). Origin firing during early S-phase initiates the replication process, whereby the parental DNA duplex is unwound by the CMG complex. At these origins, DNA polymerase α synthesises

RNA primers upon the leading strand, and primers are formed on the lagging strand for Okazaki fragment initiation (Foiani et al., 1997). Altogether, this results in a Y-shaped structure known as the DNA replication fork (**Figure *1***). In phase with this continuous helix unwinding, associated leading and lagging DNA polymerases (ε and δ, respectively), clamped to chromatin by proliferating cell nuclear antigen (PCNA), extend the nascent DNA strand producing the new DNA duplexes in a semi-conservative fashion (Georgescu et al., 2017; Miyabe et al., 2011). Importantly, coupling of the DNA helicase and DNA polymerases ensures minimal exposure of single-stranded DNA (ssDNA).

Many of the replication origins that were licensed do not proceed with replication but instead remain dormant, primed for replication later on upon replication fork stalling or collapse (Blow, Jackson 2011).

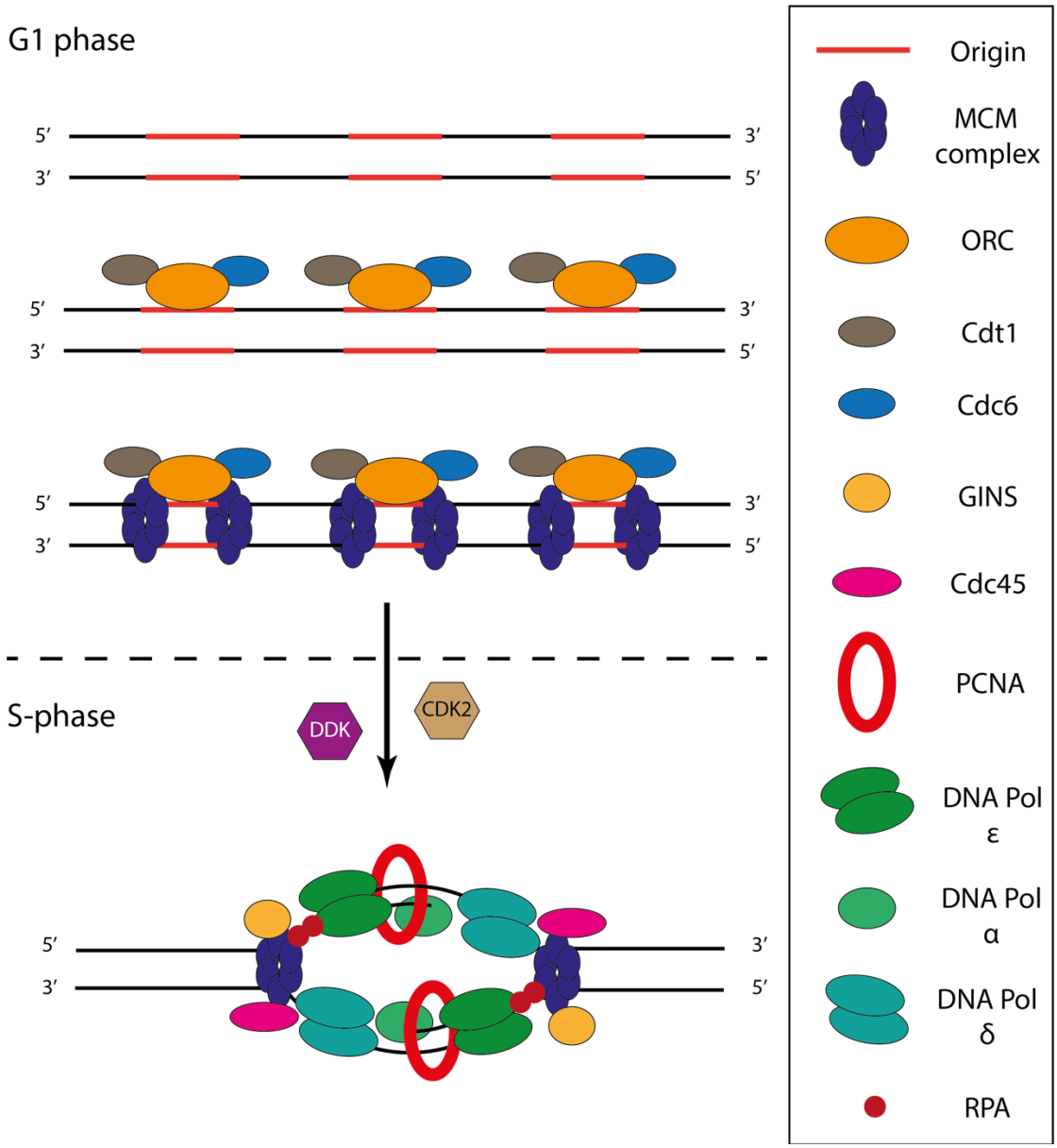

Figure 1. Mechanism and proteins involved in replication origin firing.

Replication origins are licensed in G1 phase through sequential loading of the ORC and MCM complexes, forming a pre-replication complex. In S-phase, functional initiation complexes are formed through recruitment of factors that form the CMG helicase for DNA unwinding and subsequent synthesis by DNA polymerases.

To ensure fork integrity during the DNA replication process, cells possess an S-phase checkpoint that encapsulates the cellular responses of the regulatory ataxia telangiectasia Rad3-related (ATR) and ataxia telangiectasia-mutated (ATM) protein kinases (Cimprich & Cortez, 2008; Lopes et al., 2001; Masai et al., 2010). These kinases act in response to replication fork stalling (through the presence of ssDNA) and DNA damage (such as double strand breaks (DSBs)) through the phosphorylation of checkpoint kinase 1 (CHK1) and checkpoint kinase 2 (CHK2) respectively, and those elicited by ATR are referred to as the DNA replication stress response (RSR). The S-phase checkpoint pathways ensure complete and accurate DNA replication through fork maintenance and coordination of the DNA damage response, ultimately to prevent genomic instability.

1.4. Replication Stress & Cancer

The faithful duplication of genetic material is challenged every time a cell, cancerous or not, divides. A condition which hampers the progression of DNA replication is commonly referred to as replication stress (Gaillard et al., 2015). Common challenges to DNA replication include local limited substrate availability for DNA synthesis, such as histone shortages and depletion of the deoxyribonucleotide triphosphate (dNTP) pool (Groth et al., 2007; Técher et al., 2017). Other sources of endogenous replication stress include heterochromatinised regions of repetitive DNA sequences, secondary DNA structures such as DNA hairpins, G4 quadruplexes and telomeric loops (Hickson & Bhowmick, 2017; Vannier et al., 2012). Topological stress that arises infront of and behind the replication fork through the process of DNA unwinding can also produce fork stalling, when not resolved by DNA topoisomerases (Nedelcheva-Veleva et al., 2006). Furthermore, replication stress is also a consequence of replication-transcription machinery conflicts where replication forks will stall, and even undergo fork reversal, upon approaching a region of active transcription (Bermejo et al., 2012; Neelsen & Lopes, 2015). Accumulation of transcription-associated R-loops (DNA:RNA hybrids) can also result in replication fork arrest (Schwab et al., 2015). Endogenous aldehydes have also been identified as a source of fork stalling DNA lesions, although the specific DNA lesion formed is still disputed (Garaycoechea et al., 2018). Finally, replisome conflicts may also arise when encountering DNA-protein crosslinks, an outcome of endogenous reactive chemical species inducing the formation of covalent bonds between DNA and proximal protein factors, or exogenously through the action of topoisomerase poisons such as camptothecin and doxorubicin (**Figure *2***) (Berti & Vindigni, 2016; Riccio et al., 2020; Stingele et al., 2017).

Replication stress, through its propensity to generate genome instability, has mutagenic potential if left unchecked by the ATR-activated S-phase checkpoint. This is supported by the observation that in pre-cancerous lesions in patients, DNA damage signalling is constitutively activated to induce apoptosis or senescence and prevent malignant transformation (Bartkova et al., 2005; Gorgoulis et al., 2005). ATR activation (as well as ATM) mediates this through phosphorylation of downstream targets such as p53. However, DNA damage checkpoint and repair pathway proteins are often mutated in cancer (Halazonetis et al., 2008; Kandoth et al., 2013). Indeed, ATR haploinsufficiency leads to carcinogenesis in mouse models, particularly when in combination with oncogene expression or other DNA damage repair pathway mutations (Brown & Baltimore, 2000). The link between replication stress and cancer development is further exemplified by observation of ATR somatic mutations in humans, found in tumours with microsatellite instability caused by the loss of mismatch repair (MMR) activity (Menoyo et al., 2001; Vassileva et al., 2002).

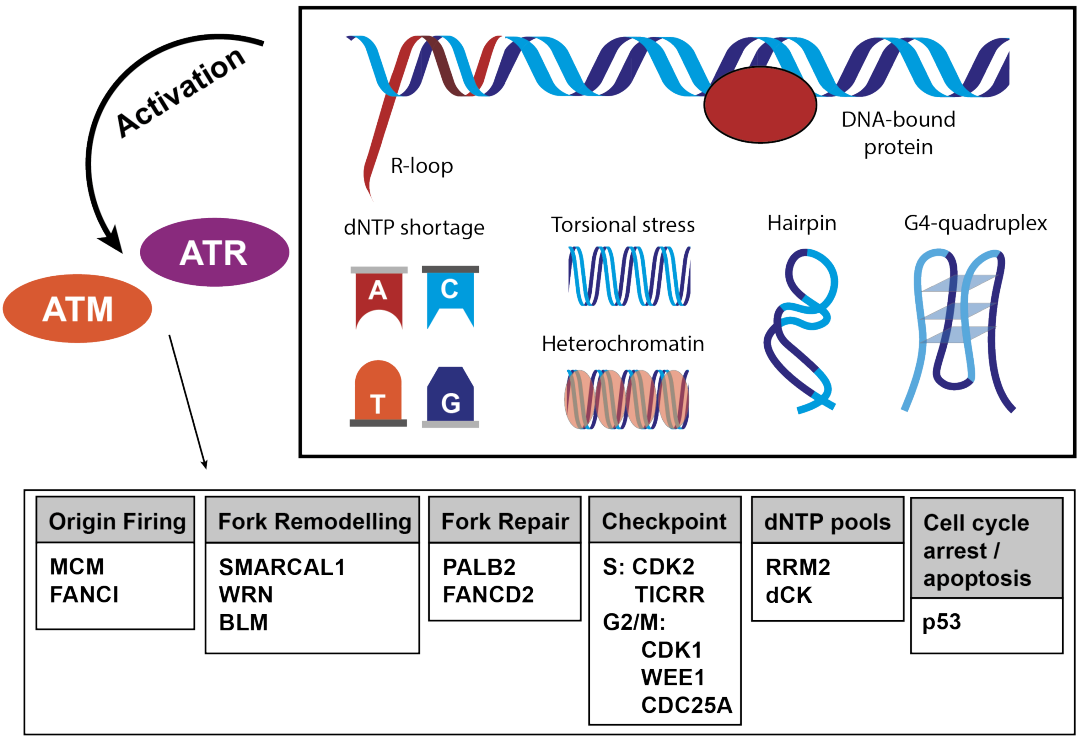

Figure 2. Structures and lesions that hinder DNA replication and cellular outcomes.

Replication stress may be induced by a variety of lesions that occur upon DNA to impede replication fork progression, or through local substrate shortages. Numerous cellular pathways may be promoted through the RSR and DDR to respond to these challenges.

Replication stress is a double-edged sword for the cancer cell. While a defective S-phase checkpoint is advantageous for cancer development, persistent replication stress can lead to a level of genomic instability that is incompatible for cancer cell survival. Compared to non-cancerous dividing cells, cancer cells have a higher burden of replication stress due to oncogene activation that drives cell proliferation through deregulation of pathways that control cell cycle progression (Macheret & Halazonetis, 2015). Deregulation of such pathways includes inefficient origin licensing, through overexpression of cyclin-E for example, that leads to under-replicated DNA (Jones et al., 2012). Unscheduled origin licensing can also result in re-replication, such as through the oncogenic expression of MYC (Curti & Campaner, 2021). Oncogenes can also directly impede fork

progression, such as BCL2 overexpression that reduces dNTP availability through ribonucleotide reductase inhibition (Xie et al., 2014).

Consequential alterations in replication timing and progression lead to an increased incidence of replication fork stalling (Gaillard et al., 2015). A higher burden of replication stress in cancer cells produces greater dependence on the RSR to maintain a level of genome stability and cell viability. Indeed, upregulation of the main replication stress response ATR-CHK1 pathway is found in several cancers, and the complete loss of ATR or CHK1 compromises cancer cell survival (Abdel-Fatah et al., 2015; López-Contreras et al., 2012).

1.5. DNA Damage and Repair

The cell has evolved numerous mechanisms to rectify the array of insults faced by the genome and these have been described collectively as the DNA damage response (DDR). A complex array of signalling networks exist to detect, signal and mediate the repair of DNA lesions to maintain cellular physiology.

Recruitment of DDR factors is a coordinated and spatiotemporally regulated process (Ciccia & Elledge, 2010). Pertinently, various elements of DNA damage response mechanisms are employed by the cell to specifically handle lesions faced by the replisome on actively replicating DNA, and this encapsulates the replication stress response. The RSR engages upon replication fork stalling in attempt to stabilise the fork, and to excise the offending lesion for maintenance of replication.

1.5.1. DNA Damage Signalling

Apical kinases ATR and ATM respond to DNA damage lesions at the replication fork to initiate the most appropriate DNA damage response based on the type of damage, cellular context, cell cycle stage and genetic background (Liang et al., 2008; O'Connor, 2015). In S-phase, ATR initiates the replication stress response for fork stabilisation and to respond to minor lesions such as SSBs and replication errors through processes such as base excision repair (BER), nucleotide excision repair (NER) and mismatch repair (MMR) (Cimprich & Cortez, 2008; Saldivar et al., 2017). Additionally, ATR can respond to other fork stalling lesions such as interstrand crosslinks (ICLs) through the promotion of repair pathways such as the Fanconi Anaemia (FA) pathway (Andreassen et al., 2004; Jing Huang et al., 2019; Schwab et al., 2010). Furthermore, ATR has also been found to play a role

in mitosis, ensuring chromosome alignment and segregation, as well as regulating the spindle assembly checkpoint (Kabeche et al., 2018).

Failure to repair these lesions or stabilise forks can result in persistent replication fork stalling, leading to fork collapse and the generation of DSBs. These DSBs then require the action of ATM to initiate HR and NHEJ pathways for double strand break repair (DSBR). ATM phosphorylation of histone variant 2AX (γH2AX) permits further DDR factor recruitment (Goodarzi & Jeggo, 2013). Recruitment of mediator of DNA damage checkpoint 1 protein (MDC1) leads to ring finger protein 8 (RNF8) and 168 (RNF168) recruitment for H2A ubiquitination, leading to downstream DDR factor recruitment including p53 binding protein 1 (53BP1) and BRCA1 (Doil et al., 2009; Stewart et al., 2003, 2009).

1.5.2. MMR, BER & NER

The replication stress response can respond to small lesions that do not significantly distort the DNA helix through MMR & BER processes (Jiricny, 2006; Krokan & Bjørås, 2013). Incision/excision, end processing, repair synthesis and ligation are common steps in these pathways however the factors involved vary depending on the lesion involved. MMR recognises and resolves misincorporated nucleotides through action of mismatch repair proteins MutS, MutH and MutL (Jiricny, 2006). BER utilises DNA glycosylases to recognise and remove damaged or inappropriate bases (Krokan & Bjørås, 2013). A third excision pathway, the NER pathway responds to UV-induced lesions and other bulky adducts (Marteijn et al., 2014). The FA pathway handles ICLs and contributes to HR, and also has a role in preventing R-loop accumulation (Schwab et al., 2015).

ATR acts to promote FANCD2 mono-ubiquitination, where it is then localised to DNA damage foci (Andreassen et al., 2004). Subsequent orchestration of DNA incision, lesion unhooking, translesion synthesis and break repair is coordinated (L. C. Wang & Gautier, 2010).

1.5.3. Double Strand Break Repair

The most deleterious lesions formed upon DNA are double-strand breaks (DSBs) which are repaired by two distinct pathways in mammalian cells: non-homologous end joining (NHEJ), active during all stages of the cell cycle, and S/G2-phase specific homologous recombination (HR) (**Figure *3***). Pathway choice between NHEJ and HR is influenced by cell cycle stage, availability of a homologous repair template and the regulation of DSB resection through recruitment of DDR factors such as 53BP1 and BRCA1 (Symington & Gautier, 2011). These pathways can be further sub-divided into non-canonical 'alternative' (alt-) pathways, characterised by the key effector proteins involved. In eukaryotes, HR is usually relied upon for the repair of replication-associated damage, however it has been reported that NHEJ is also active during DNA replication in prokaryotes and metazoans (Audoynaud et al., 2021).

1.5.3.1. Non-Homologous End Joining (NHEJ)

NHEJ is initiated through DSB recognition by the Ku70-80 (Ku) heterodimer, permitting the recruitment and retention of other repair proteins that can facilitate joining of the separated DNA ends (Weterings & Chen, 2008). Ku heterodimers, being highly abundant and having high affinity for broken DNA ends, often bind to DSBs making NHEJ the predominant repair pathway in cells throughout the cell cycle (Chang et al., 2017). In the context of the replication stress response

during mid-to-late S-phase and G2 phase, where a sister chromatid template is available, HR is preferentially engaged for error-free repair. However, when an intact repair template is unavailable, NHEJ may be relied upon to sustain cell proliferation through non-canonical engagement (Langerak & Russell, 2011).

DNA-dependent protein kinase catalytic subunit (DNA-PKcs), with its high affinity for Ku-bound DNA ends forms the DNA-PK complex (Chang et al., 2017).
X-ray repair cross-complementing protein 4 (XRCC4) and DNA ligase IV are the most central eukaryotic components of NHEJ, recruited by Ku and capable of facilitating direct ligation of DSB ends (Chang et al., 2017). DNA Polymerase (Pol) μ, DNA Pol λ, Artemis and non-homologous end joining factor 1 (XLF) may also be recruited by the NHEJ pathway to facilitate end-processing, removing overhangs and creating regions of non-templated microhomology for ligating DNA ends (Davis & Chen, 2013; Weterings & van Gent, 2004).
Other NHEJ components such as 53BP1, RIF1 and the shieldin complex are recruited to DSBs to inhibit end resection of the break and promote NHEJ in G1 (Chapman et al., 2013; Setiaputra & Durocher, 2019). These factors also serve to protect and repair DSBs at the stalled fork and can work in concert with HR to repair damage (Garzón et al., 2019; W. Liu et al., 2020; Mukherjee et al., 2019). 53BP1 in particular plays a crucial role in promoting NHEJ pathway choice at DSBs; indeed loss of 53BP1 in BRCA1 deficient backgrounds has been found to restore homologous recombination repair (HRR) (Bouwman et al., 2010; Bunting et al., 2010).
Interestingly, it has recently been observed that RNAs, acting as DDR factor scaffolds, may contribute to NHEJ activity at the replication fork to assist in avoidance of mutagenic repair (Audoynaud et al., 2021).

1.5.3.2. Homologous Recombination (HR)

HR repair requires the presence of a homologous sequence, usually in the form of a sister chromatid, to serve as a template for DNA synthesis. This requirement restricts the action of HR repair to cells in the mid S-phase to G2 phases of the cell cycle (Heyer et al., 2010).

Stalled and collapsed forks depend on homologous recombination for their error-free repair and sometimes, in conditions of heightened replication stress, eukaryotic cells will engage fork restart through a HR-mediated process known as break induced replication (BIR) (Kramara et al., 2018).

HR will respond to one-ended DSB like structures formed through reannealing of nascent DNA during fork reversal, or through DSBs formed through fork collapse. DSBs are recognised by the MRE11/RAD50/NBS1 (MRN) complex, leading to recruitment of CTBP-interacting protein (CtIP) and initiation of 5' strand endonucleolytic resection. Short range 3'-5' resection is performed by MRE11 exonuclease activity in combination with EXD2 exonuclease activity (Broderick et al., 2016). Extensive 5'-3' exonucleolytic resection is then performed by exonuclease 1 (EXO1) and the BLM-DNA2 helicase-endonuclease complex (Symington, 2014).

BRCA proteins, while also being vital for fork protection upon fork stalling and reversal, are also key factors in mediating HR over error-prone NHEJ repair. BRCA1 functions to remove 53BP1 from DSBs and promotes DNA resection (Bouwman et al., 2010; Bunting et al., 2010). 5'-3' resection of the DSB allows for the generation of RPA coated 3'-ssDNA. BRCA2 acts to replace this RPA with RAD51 to form stable nucleofilaments that are required for homology search with the repair template (Ait Saada et al., 2018; Ochs et al., 2016). PALB2 binding

with BRCA1 assists with BRCA2 recruitment to sites of DNA damage. Indeed, the importance of these proteins in promoting error-free repair to maintain genomic stability is exemplified by their frequent defective status producing breast and ovarian cancer predisposition (Ait Saada et al., 2018; Connor et al., 1997; Ludwig et al., 2001). RAD51 nucleofilaments carry out homology search for a sister chromatid to invade, displace and anneal to, forming a D-loop structure with the displaced, RPA coated non-complimentary strand. The D-loop permits the invading strand to provide the stalled fork with an undamaged template for repriming DNA synthesis and continuing DNA replication by DNA polymerase δ (Petermann et al., 2010; Wright et al., 2018). The D-loop is often resolved by synthesis-dependent strand annealing (SDSA), resulting in non-crossover and maintenance of heterozygosity (Wright et al., 2018).

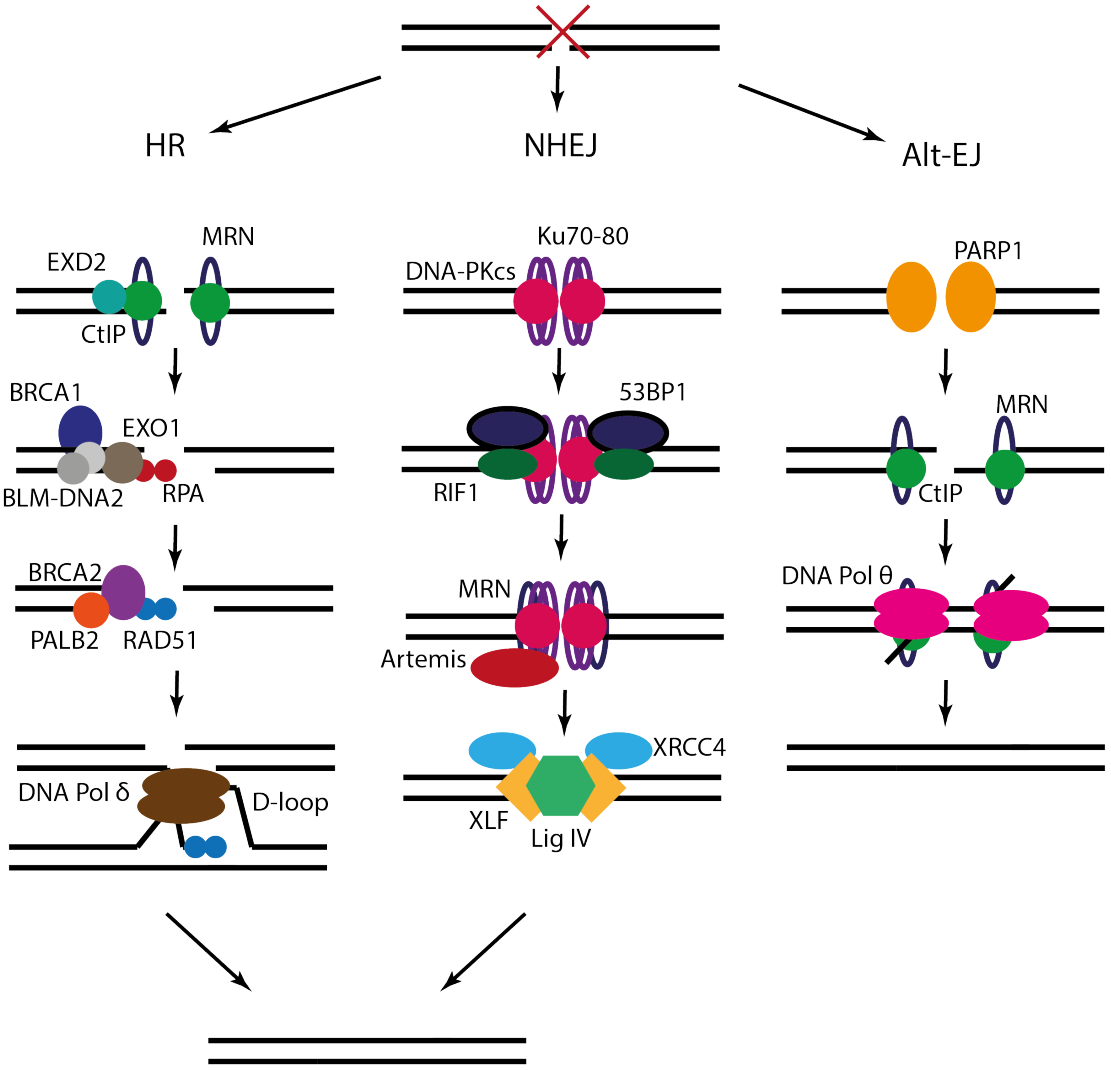

Figure 3. Mechanisms of HR, NHEJ and Alt-EJ in DSBR.

Upon formation of a double strand break, repair pathway choice is influenced by cell cycle stage, availability of a repair template substrate and repair factor recruitment regulation.

Alternative end joining (Alt-EJ) components are relied upon in the absence of a functional HR pathway; alt-EJ, also referred to as microhomology (MMEJ) or Pol θ-mediated end joining (TMEJ), requires minimal homology (<25bp) for repair of DNA ends (Ceccaldi et al., 2015; Chang et al., 2017). Alt-EJ requires Pol θ, PARP1, CtIP and MRN components. It is an error-prone pathway that can result in chromosomal end-to-end fusions, but in the context of BRCA deficiency can promote cell survival (Mateos-Gomez et al., 2015).

Recently, functional analyses have provided evidence to suggest that alt-EJ protects cells in a variety of background deficiencies not limited to BRCA1/BRCA2 deficiency, but the DDR more widely (such as BER, NER, TLS, MMR, DNA metabolism and the FA pathway) (W. Feng et al., 2019). A common feature of these gene mutations was postulated to be an increase in endogenous replication associated DSBs. Indeed, cells defective for alt-EJ were associated with increased fork instability (W. Feng et al., 2019). This work indicates the contribution of the alt-EJ to maintenance of genome stability derived from replication stress when preferential repair pathways may be unavailable.

The crucial role of these collective DNA damage repair pathways for cell viability is most evident in the context of their deficiency (**Table *1***). Many cancers, immune defects and neurodegenerative diseases originate from inherited DDR pathway defects. In cancer, these defects may promote tumour cell survival and proliferation, despite an increased mutational burden and genome instability. Where ongoing formation of DNA damage leads to activation of DDR signallers ATR/ATM, inactivation of such components permits avoidance of senescence & apoptosis and malignant progression. Severe developmental conditions such as Seckel Syndrome (SS) and Ataxia Telangiectasia (AT) arise without the functional contributions of ATR and ATM, respectively (Alderton et al., 2004; X. L. Liu et al., 2016; McKinnon, 2012; O'Driscoll & Jeggo, 2003). SS results in intellectual disability, microcephaly and dwarfism whereas AT symptoms exhibit neurodegeneration, immune dysfunction and cancer predisposition (McKinnon, 2012; O'Driscoll & Jeggo, 2003). These clinical phenotypes are often common to many DNA repair deficiency syndromes (Knijnenburg et al., 2018; McKinnon, 2009; O'Driscoll & Jeggo, 2002). Mutations in many of the identified FA proteins

result in bone marrow failure, genomic instability and cancer pre-disposition phenotypes in those with the condition (Duxin & Walter, 2015). Mutations in key promoters of the HR pathway such as BRCA1 and BRCA2 are now widely known to contribute to the elevated risk of breast and ovarian cancer development and are established targets for selective therapy (C.-C. Chen et al., 2018).

Syndrome	Clinical Phenotypes	Mutated Gene(s)
Lig4 / Human Immunodeficiency with microcephaly	Microcephaly, developmental defects, immunodeficiency, leukemia	DNA Ligase IV, XLF
Radio-sensitive Severe Combined Immunodeficiency	IR hypersensitivity, immunodeficiency, lymphomas	Artemis
Breast cancer 1, early onset	Breast and ovarian cancer	BRCA1
Breast cancer 2, early onset	Breast and ovarian cancer, pancreatic, prostate, gastric and melanoma predisposition	BRCA2
Fanconi Anaemia	Bone marrow failure, congenital abnormalities, cancer predisposition	FANCA-FANCL, BRCA2
Ataxia telangiectasia	Cerebellar ataxia, telangiectases, immune defects, cancer predisposition	ATM
Ataxia telangiectasia-like disorder	Similar yet mild to A-T, potential cancer predisposition	MRE11
Nijmegen breakage syndrome	Immunodeficiency, cancer predisposition, growth & mental retardation, microcephaly	NBS1
RIDDLE syndrome	Immunodeficiency, radiosensitivity, dysmorphic features, learning difficulties	RNF168
Seckel syndrome	Primordial dwarfism, dysmorphic features, mental retardation, microcephaly, possible leukemia risk	ATR, SCKL2, SCKL3
Li-Fraumeni syndrome	Breast cancer, brain tumours, soft tissue sarcomas	p53
Bloom syndrome	Dysmorphic features, mental retardation, cancer predisposition, microcephaly	BLM
Werner's syndrome	Cancer predisposition, premature aging	WRN
Meier-Gorlin syndrome	Primordial dwarfism, growth retardation, microcephaly	ORC1, ORC4, ORC6, CDT1, CDC6

Table 1. Human syndromes associated with DDR and RSR genetic mutations.

1.6. The Replication Stress Response

Stalling of the DNA replication fork produces an uncoupling of the DNA helicase and DNA polymerase components of the replisome (Byun et al., 2005). This phenomenon is a precise molecular definition for the term 'replication stress' and is characterised by the accumulation of replication protein A (RPA) coated-single stranded DNA (ssDNA) that forms at the fork after helicase unwinding, but before complimentary strand synthesis by the polymerase (Lecona & Fernández-Capetillo, 2014). Formation of this ssDNA is suppressed by several factors including the claspin-timeless-tipin axis, which act to restrain helicase movement (Forment & O'Connor, 2018).

ATR is essential in proliferating cells and is activated every S-phase for the regulation of origin firing & fork stabilisation, and for the repair and restart of forks after DNA damage (Cimprich & Cortez, 2008; de Klein et al., 2000). However, the replication stress response arises through the accumulation of ssDNA-RPA at the stalled fork (**Figure *4***). The ssDNA-RPA signal leads to recruitment of the apical replication checkpoint kinase ATR and its constitutive binding partner ATRIP (López-Contreras & Fernandez-Capetillo, 2010), as well as recruitment of fork remodeller SWI/SNF-related matrix-associated actin-dependent regulator of chromatin subfamily A-like protein 1 (SMARCAL1) (Bansbach et al., 2009; Ciccia et al., 2009). ATRIP mediates association of DNA topoisomerase II binding protein 1 (TOPBP1), recruited by the Rad9-Hus1-Rad1 (9-1-1) clamp, with ATR for its activation (Kumagai et al., 2006; Mordes & Cortez, 2008). ATR is also activated by Ewing tumour-associated antigen 1 (ETAA1) and it has recently been suggested that TOPBP1 and ETAA1 dimerization is important for optimal ATR signalling (Thada & Cortez, 2021).

Persistent ssDNA-RPA leads to subsequent phosphorylation of downstream kinase CHK1 by ATR, and this leads to cell cycle checkpoint activation and growth arrest (by phosphorylation of WEE1 and CDC25A) (Furnari et al., 1997; O'Connell et al., 1997). The S-phase checkpoint activation results in recruitment of replication stress response proteins that can elicit stabilisation of the stalled fork and facilitate DNA damage repair or tolerance (Osborn et al., 2002).

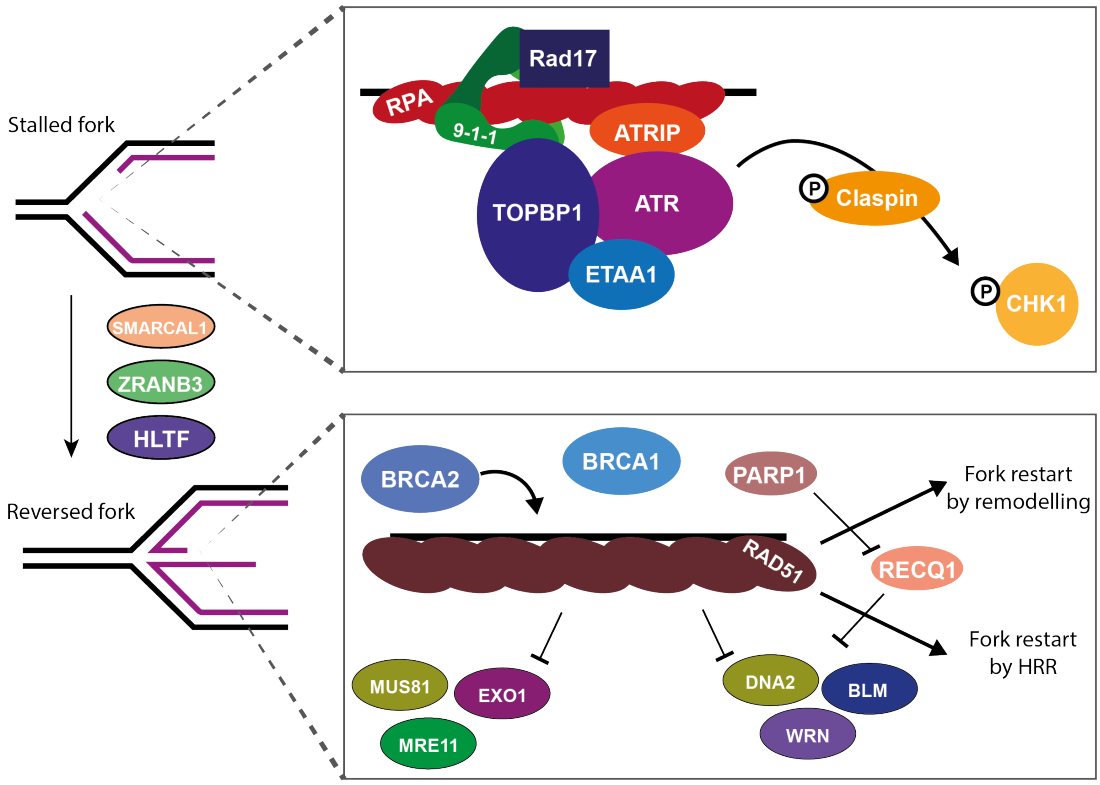

Figure 4. RSR factor recruitment at the stalled replication fork promotes fork reversal.

During fork stalling, RPA bound ssDNA leads to ATR-ATRIP recruitment. TOPBP1, recruited by the 9-1-1 complex, and ETAA1 activate ATR for activation of the replication stress response. ATR will phosphorylate CHK1 and additional factors for regulation of origin firing, cell cycle progression and apoptosis. Fork reversal is mediated by translocases SMARCAL1, ZRANB3 and HLTF. RAD51, loaded by the actions of BRCA1/2 protects the reversed fork from nuclease-mediated degradation. PARP1 counteracts RECQ1 to maintain fork regression. Once the replication challenge has been overcome, forks may undergo restart through various pathways.

ATR stabilises the stalled replication fork through multiple approaches. Firstly, new origin firing is prevented (via CHK1) to limit RPA pool depletion (Ge & Blow, 2010). RPA is required to protect single stranded DNA at stalled forks, thereby preventing ssDNA cleavage, consequential DSB formation and replication catastrophe (Fanning et al., 2006; Toledo et al., 2013). Secondly, ATR regulates fork repair protein activity to prevent collapse of existing forks, such as that mediated by fork remodeller SMARCAL1. Without ATR regulation of SMARCAL1 during replication, inappropriate formation of DNA structures through excessive fork reversal can lead to DSB formation and nascent DNA degradation (Bétous et al., 2013; Couch et al., 2013; Ragland et al., 2013). Interestingly, it has recently been revealed that replisome stabilisation itself is not a major function of the ATR replication checkpoint (Dungrawala et al., 2015).

In cases where replication stress cannot be overcome to restore replication, ATR phosphorylation of CHK1 may induce downstream phosphorylation of p53, inducing cell cycle arrest or apoptosis (López-Contreras & Fernandez-Capetillo, 2010). This is a key step to be overcome in many cases of tumorigenesis and for survival of the genomically-unstable cancer cell. Indeed, p53 mutations have been reported to occur in almost every type of cancer, at rates varying between 10% (i.e. for haematopoietic cancers) to almost 100% (high-grade serous ovarian carcinoma) (Peller & Rotter, 2003; Petitjean, Achatz, et al., 2007; Petitjean, Mathe, et al., 2007).

To overcome replication fork stalling in the face of DNA lesions and resume DNA synthesis, the S-phase checkpoint can stimulate various responses. Eukaryotic cells can stimulate dormant origins to re-initiate replication and complete DNA

synthesis, stimulated by factors such as Fanconi Anaemia complementation group I protein (FANCI) during mild replication stress (Y. H. Chen et al., 2015). As well as this, a two-step fork reversal and fork restart programme may also be instigated. Failure to initiate this response results in fork collapse, potential formation of DSBs and genomic instability.

1.6.1. Replication Fork Reversal

Replication fork reversal (also termed fork regression) is a process whereby stalling of the replisome leads to backtracking of the DNA through the formation of a four-stranded 'chicken-foot' structure, through the action of translocases such as SMARCAL1, zinc finger RANBP2-type containing 3 (ZRANB3) and helicase like transcription factor (HLTF) (Berti & Vindigni, 2016; Mouli Kolinjivadi et al., 2017; Taglialatela et al., 2017a; Vujanovic et al., 2017). The two nascent DNA strands are released from template DNA at the fork, and subsequently the parental strands and nascent strands re-ligate forming a Holliday junction (HJ)-like structure (**Figure *5***). This structure provides stability to the fork by permitting repair processes to remedy the lesion on the parental template or, in the case of continued lagging strand synthesis, by providing a substrate for template switching for lesion bypass (Osborn et al., 2002). These translocases have been proposed to respond to stalled forks formed from specific contexts, such as blockage of the leading strand polymerase and presence of persistent RPA-ssDNA gaps in the case of SMARCAL1 (Bétous et al., 2013). ZRANB3 requires polyubiquitinated PCNA, which is also dependent on RPA-ssDNA at the stalled fork for PCNA ubiquitination (Vujanovic et al., 2017). HLTF reverses forks either lacking ssDNA, or those with a leading strand gap, however studies with other substrates have not been reported (Poole & Cortez, 2017).

RAD51 is a crucial factor in promoting fork reversal, as well as in homologous recombination repair. The absence of RAD51 leads to extensive fork degradation by MRE11, and this is seen in BRCA1/BRCA2 deficient backgrounds due to their function stabilising RAD51 filaments of regressed arms on reversed forks (Schlacher et al., 2011). RAD51 also interacts with DNA polymerase α to facilitate DNA synthesis and prevent single stranded gap formation. These ssDNA gaps are remodelled by SMARCAL1 to reverse the fork (Mouli Kolinjivadi et al., 2017).

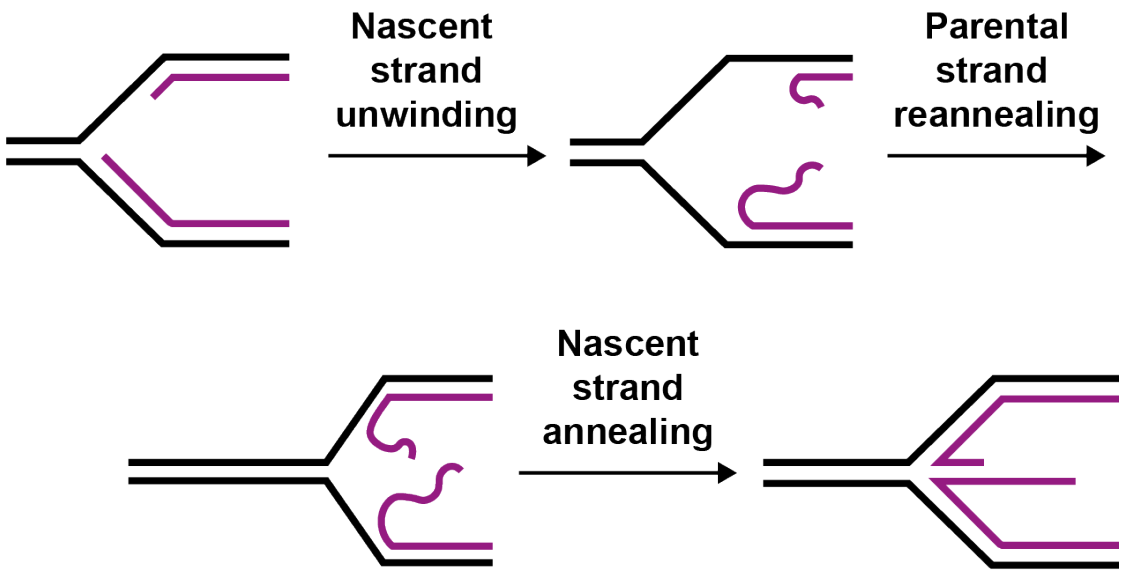

Figure 5. Schematic depicting the process of replication fork reversal.

Newly synthesized DNA strands (purple) unwind to permit backtracking of the fork through reannealing of the parental DNA strands (black). Nascent strands anneal to form a four way 'chicken-foot', structurally resembling a Holliday junction.

Specific fork reversal and repair processes may be elicited in response to lesions such as ICLs, which act as a physical impediment to the progression of the replisome and extensive DNA unwinding. Fork reversal can provide opportunity for a second converging replication fork to encounter the offending lesion (J.

Zhang et al., 2015). This second fork may then permit replication-coupled ICL repair by the FA pathway (Knipscheer et al., 2009; L. C. Wang & Gautier, 2010). The importance of fork reversal in maintaining complete and accurate DNA replication is evidenced by the existence of severe conditions where these translocases are mutated. Inherited mutations leading to defective SMARCAL1 activity result in the developmental disorder Schimke Immuno-osseous Dysplasia (SIOD), characterised by immune deficiencies, microcephaly and growth defects (Boerkoel et al., 2002). Mutations in ZRANB3 and HLTF have also been linked to cancer (Poole & Cortez, 2017).

1.6.2. Replication Fork Restart

Replication fork regression must be resolved through replication restart or through fork rescue by a converging fork from a nearby origin. Stabilisation and restart of the regressed fork is mediated through the action of RecQ like helicase (RECQ1) and poly(ADP-ribose) polymerase-1 (PARP1) and can also be restored by SMARCAL1 and ZRANB3 remodellers (Poole & Cortez, 2017).

RECQ1 is a specialised ATP-dependent helicase that primes reversed forks for their restart through branch migration. RECQ1 is inhibited by PARP1, but becomes activated through replication stress mediated inhibition of PARP1 (Berti et al., 2013). RECQ1 also acts to inhibit an alternative fork restart pathway mediated by DNA unwinding and nucleolytic degradation, through the action of DNA replication helicase/nuclease 2 (DNA2) assisted by Werner syndrome RecQ like helicase (WRN) (Berti 2013, Thangavel 2015). Here, controlled resection of the regressed fork may permit the recruitment of alternative branch migration factors or promote HRR and restart of the reversed fork. RAD51 filament formation at the resected nascent ssDNA promotes strand invasion of the

upstream parental dsDNA duplex, forming a D-loop intermediate for repriming of DNA synthesis. The lagging strand may also be resected and fork backtracking produces an extruded leading strand for RAD51 loading and invasion (Ait Saada et al., 2018).

1.6.3. Fork Reversal is a Double-edged Sword

Fork reversal provides opportunity for the proliferating cell to repair DNA lesions and restart replication. However, excessive fork reversal can be pathophysiological and become a source of genomic instability. One way this instability can occur physiologically is when frequent fork reversal occurs upon repetitive sequences, potentially leading to repeat expansion through misalignment of DNA strands (Fouché et al., 2006). Indeed, excessive fork reversal through overexpression of SMARCAL1 has also been shown to interfere with DNA replication, leading to fork breakage (Bansbach et al., 2009).

More generally, reannealed nascent arms of the reversed replication fork resemble a one-ended DSB, which if unprotected, can be targeted by nucleases. To mitigate this, fork protection factors such as BRCA1 and BRCA2, in concert with RAD51 prevent extensive fork degradation, such as that induced upon hydroxyurea (HU) treatment by MRE11, CtIP and EXO1 dependent resection, a process also requiring pax transactivation domain-interacting protein (PTIP) and PARP1 (Schlacher et al., 2011; Ying et al., 2012). Protection of the fork also prevents its degradation by MUS81, a nuclease that targets Holliday junctions formed during HR and HJ-like structures, and SLX4, a scaffold for assembly of the SLX1-SLX4-MUS81-EME1-XPF-ERCC1 (SMX) complex that aids HJ resolution (Couch et al., 2013; Dehé & Gaillard, 2017; Malacaria et al., 2017;

Wyatt et al., 2013). Holliday junctions are four-stranded DNA structures of which the regressed replication fork is structurally similar.

In BRCA-deficient tumours, extensive fork degradation is responsible for sensitivity to DNA damaging chemotherapies, highlighting the consequential magnitude of this phenomenon to the cell (Chaudhuri et al., 2016).

Conversely, MUS81 can also elicit fork rescue through cleavage of ssDNA regressed fork tails and promotion of POLD3-dependent DNA synthesis (required for BIR, a specialised HR pathway for DSBR at stalled forks and fork restart) demonstrating the careful orchestration of nuclease activity within the stalled fork context (Lemaçon et al., 2017).

1.6.4. Post Replication Repair

In some cases, repair of a fork-stalling lesion is not always possible and replication through bulky lesions would result in a high frequency of fork stalling and fork collapse. To avoid this, the cell can instead tolerate these lesions by engaging post replicative repair (PRR) pathways (Petermann et al., 2010). PRR can reconfigure the replisome to perform translesion synthesis (TLS) and strand invasion (Neelsen & Lopes, 2015; Vaisman & Woodgate, 2017). Low fidelity 'Y-family' DNA polymerases (such as DNA polymerases η, ζ, I and κ) utilise damaged DNA templates to maintain replication of the genome. These polymerases are downregulated in some types of cancer, suggesting a tumour suppressive role despite their low fidelity (Lange et al., 2011; Pan et al., 2005). Alternatively, PRR can induce a more error-free, HR-mediated template switching (TS) pathway where the nascent DNA strand of the sister DNA duplex may be used as a primer to continue DNA synthesis, if available (Gao et al., 2017).

Failure in these pathways can lead to chromosomal rearrangements through faulty repair by the non-homologous end joining (NHEJ) pathway (Audoynaud et al., 2021). While these processes reduce the possibility of more deleterious outcomes of perturbed replication such as the formation of DSBs, excessive accumulation of ssDNA or incomplete replication of DNA, they have recombinogenic potential.

1.6.5. Exploiting Cancer's Replication Stress Burden

The persistence of replication stress and a reliance on the RSR in cancer cells provides opportunity for targeted therapy. While non-cancerous cells possess alternative DNA damage response and repair pathways to overcome exogenous insults, the reliance of cancer cells on remaining functional pathways, such as the ATR-CHK1 axis, may be exploited. This is a concept referred to as synthetic lethality and has the potential to spare non-cancerous cells while inducing cancer cell death (O'Neil et al., 2017) (**Figure *6***). UCN-01 is a well-known inhibitor of CHK1 that has been observed to enhance the sensitivity of p53-deficient cancer cells to genotoxic treatment (Ma et al., 2013). ATR inhibitors (ATRi) such as AZD6738 and VX-970 are currently in clinical trials (Lee et al., 2020; Shapiro et al., 2021).

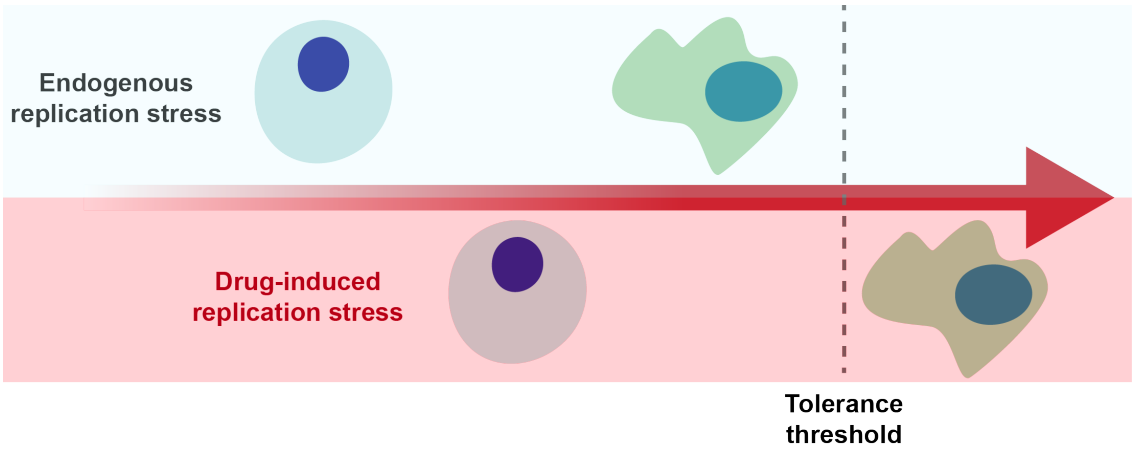

Figure 6. Enhancement of replication stress can lead to specific targeting of cancer cells.

Non-cancerous cells (round, blue) and cancer cells (irregular, green) are subject to different levels of endogenous replication stress. Cancer cells have higher levels of replication stress due to oncogenic signalling and defective DNA repair pathways and checkpoints, which will typically induce apoptosis or senescence in non-cancer cells. Enhancing replication stress through replication-perturbing and DNA-damaging drug treatments, and abolishing remaining RSR pathways through drug targeting can promote genomic instability and selective death of the cancer cell.

Targeted inhibition of other tumour-reliant DNA damage repair pathways has also shown promise. PARP inhibitors (PARPi) are a class of drug that have shown particular efficacy and tumour selectivity for tumours with defects in homologous recombination repair, BRCA-deficient tumours being a common example (Audeh et al., 2010; Fong et al., 2009; Tutt et al., 2010). PARP is required for the repair of single stranded breaks (SSBs), however through its inhibition, PARP-DNA complexes unable to dissociate lead to the formation of double strand breaks (DSBs) through DNA replication fork stalling at these lesions (Helleday, 2011). HRR is required for the repair of these replication stress associated DSBs, therefore cancers with HR deficiency are subject to greater genomic instability and eventual cell death (Mccabe et al., 2006). Combining targeting approaches of cancer dependencies also provides an opportunity to overcome drug resistance, such as through ATRi treatment of PARPi resistant BRCA-deficient tumours (Yazinski et al., 2017). Expanding our knowledge of cancer reliant

pathways and their molecular characterisation will provide greater opportunities to overcome chemotherapy resistance.

1.7. Ubiquitin Signalling in the DDR & RSR

The protein kinase network is one of the most studied and significant post-translational modification signalling systems in the cell and is encoded by over 500 genes (Madhani, 2006). In relation to this, the significance of the ubiquitin signalling system can be emphasised by the fact there are >600 genes coding E3 ubiquitin ligases alone (George et al., 2018). In addition, E1 ubiquitin activating enzymes and E2 ubiquitin conjugating enzymes are also required of which they are encoded by 2 and >35 genes, respectively (George et al., 2018). Ubiquitination is the process of conjugating a 76aa moiety known as ubiquitin to specific protein substrates, via the C-terminal glycine residue of ubiquitin. E3 ubiquitin ligases dictate target specificity for ligation of the ubiquitin moiety (Hershko & Ciechanover, 1998). Targets for ubiquitination can be subject to mono-ubiquitination on a substrate lysine or poly-ubiquitination on lysine residues of a sequence of ubiquitin entities (Komander & Rape, 2012). This can produce varied outcomes for the target protein, from proteasome mediated degradation, to modulation of protein-protein interactions (PPIs), protein localisation and modulation of function (Z. J. Chen & Sun, 2009). Chains formed via Lys48, Lys29 and Lys11 generally target proteins for proteasomal degradation whereas Lys63 chains regulate PPIs. Ubiquitination of proteins is a reversible process with more than 100 de-ubiquitinating enzymes (DUBs) that catalyse the removal of the ubiquitin peptide (Wilkinson, 2000).

Although the canonical role for ubiquitin modification is targeted protein degradation through the 26S proteosome (ubiquitin proteosome system, UPS), the importance of the ubiquitin pathway in modulation of protein activity, localisation and interaction is gaining further traction (Z. J. Chen & Sun, 2009;

Wilkinson, 2000). Ubiquitination has been found to have a crucial role in the DNA damage response, first identified in yeast through PCNA-K164 ubiquitination to facilitate post-replicative repair and has since been observed in other DNA repair pathways such as NER and DSBR (Al-Hakim et al., 2010; Bekker-Jensen & Mailand, 2011; S. P. Jackson & Durocher, 2013; Schmid et al., 2018). Ubiquitination of various components can exert control over DNA damage pathway choices, as well as DNA damage signalling. A paradigmatic example of ubiquitination involvement in the DNA damage response was discovered through E3 RING-type ligases ring finger proteins RNF8 and RNF168 and their involvement in the recruitment of 53BP1 and BRCA1 to modified chromatin at DSB sites (**Figure 7**) (Kolas et al., 2007; Mailand et al., 2007; Mattiroli et al., 2012). After the initial phosphorylation of H2AX and MDC1 by ATM at DSB sites, subsequent phospho-site occupation by RNF8 results in RNF8-mediated ubiquitination of multiple targets including H2A histones, resulting in RNF168 ubiquitin binding domain (UBD) recognition (Stewart, 2009). Ubiquitination by RNF168 ultimately results in the amplified ubiquitination of H2A histones and the recruitment and retention of DSB response factors at the site such as 53BP1 and BRCA1 (Messick & Greenberg, 2009).

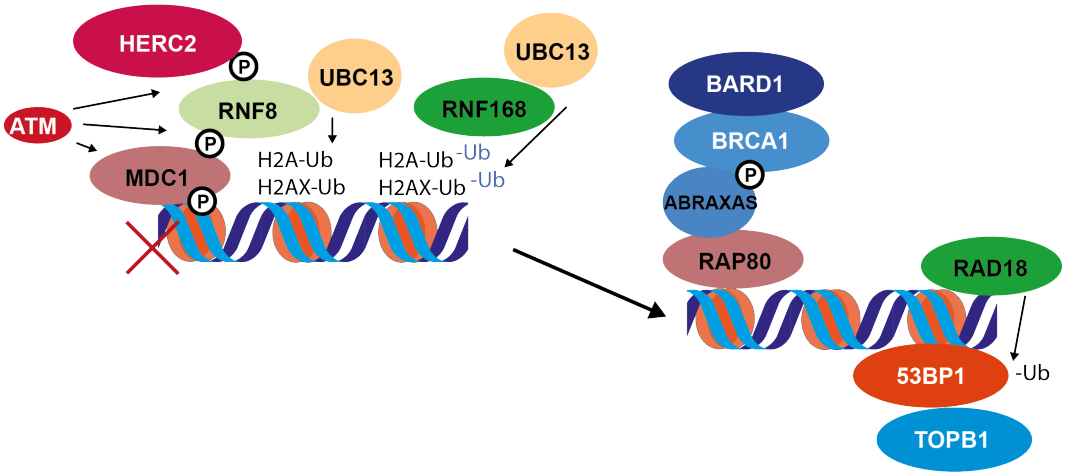

Figure 7. The ubiquitin-dependent DNA damage response.

Chromatin proximal to DNA damage is enriched with K63 polyubiquitin chains, produced through the action of phosphorylated RNF8, coordinated by phosphorylated MDC1. A ubiquitylation cascade is induced through RNF168 recruitment. Ultimately, through ubiquitin signalling at these sites, BRCA1 and 53BP1 are recruited to mediate the DDR.

Specific examples of the role of ubiquitination in regulation of the RSR include the mono-ubiquitination of PCNA at K164 for recruitment of TLS polymerases during PRR (Kannouche et al., 2004; Watanabe et al., 2004). Polyubiquitin chains linked by K63 may also form, instead shifting lesion tolerance to the template switching (TS) pathway- demonstrating signal modulation for diverse responses (Takahashi et al., 2020). Recently, it has been identified that PCNA requires ubiquitination during unchallenged S-phase progression to promote cellular proliferation and prevent genome instability. Loss of PCNA ubiquitination resulted in DNA2-dependent degradation at stalled forks in response to endogenous replication stress, as well as nucleosome deposition interference (Thakar et al., 2020).

PCNA also has a role in stabilising the E3 RING type ubiquitin ligase RFWD3 at the active replication fork, however this E3 ligase instead ubiquitinates RPA and RAD51 for their timely removal to ensure replication and facilitation of HR (Inano et al., 2017; Lin et al., 2018). RFWD3 is also recruited by RPA during fork stalling

to induce RPA and RAD51 removal, promoting HR and ICL repair (Elia, Wang, et al., 2015; Feeney et al., 2017).

From these examples, it is clear that ubiquitination is an important PTM for dynamic regulation of both active and stalled replication fork functionality and composition, however ubiquitin regulation and the factors involved are still not well defined. Further elucidation of the numerous E3 ubiquitin ligases and their roles in the regulation of DNA replication and the RSR will provide greater depth on the mechanistic details of these responses, that may then be engineered for a wider variety of targeted cancer treatments.

1.7.1. The DTX3L E3 Ubiquitin Ligase

Many factors of the ubiquitination system are identified in a substrate-first manner. In some cases, involved E3 ubiquitin ligases may be identified from exploratory (non-hypothesis driven) approaches such as large-scale screens to identify a dataset of candidates whose involvement may then be validated in follow-up studies (Bakos et al., 2018; Elia, Boardman, et al., 2015; Peng et al., 2003; G. Xu & Jaffrey, 2013; P. Xu & Peng, 2006). In this study, iPOND (isolation of nascent proteins on DNA) was previously utilised to identify E3 ubiquitin ligases present at the actively replicating and challenged replication fork (Higgs et al., 2015). Here, E3 ubiquitin ligase DTX3L has been identified and investigated as a factor involved in the RSR.

The B-lymphoma and BAL-asssociated protein (BBAP, synonymous with DTX3L) was discovered in yeast as a B-aggressive lymphoma 1 (BAL1) protein

/ARTD9/PARP9) interactor and novel member of the deltex (DTX) family of proteins (Takeyama et al., 2003). These proteins have been discovered to be modifiers of notch signalling, a highly conserved signalling pathway crucial for development and implicated in malignant transformation, and they may also have roles in regulation of transcription (Artavanis-Tsakonas et al., 1999). Additionally, they have all been identified to be functional E3 ubiquitin ligases (Takeyama et al., 2003) and evidence suggests that DTX3L in particular may have a role in the DNA damage response (Yan et al., 2009).

Human DTX3L is an 84kDa protein consisting of 740 amino acids and possesses a unique 560aa N-terminus (containing two potential nuclear localisation signals and a nuclear export signal), differing it from other members of the deltex family (Juszczynski et al., 2006; Takeyama et al., 2003). Indeed, DTX3L has been evidenced to shuttle between the nucleus and cytoplasm, along with binding partner PARP9 (Aguiar et al., 2005; Juszczynski et al., 2006).

Conversely, the C-terminus is common to all family members, and in DTX3L contains specifically a RING-HC type domain (shared only by the DTX3 protein) (Takeyama et al., 2003). The RING domain encompasses specific cysteine and histidine topology for zinc ion coordination in a ‘cross-braced’ fashion (Saurin et al., 1996). The RING-HC domain is distinguished from other configurations due to histidine at the fourth position, compared to RING-H2 with an additional histidine at the fifth position (Saurin et al., 1996).

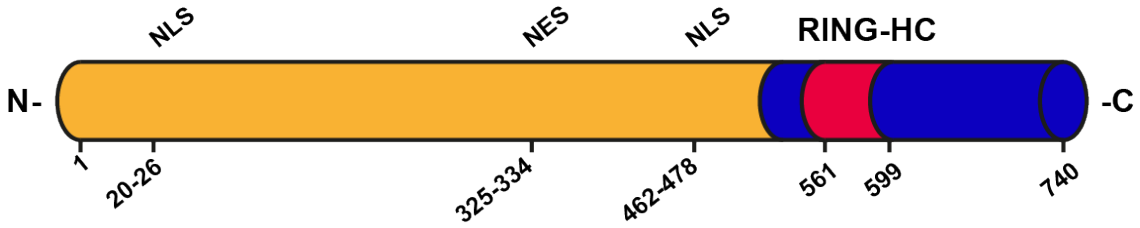

Figure 8. DTX3L domain structure.

DTX3L consists of a unique N-terminus (yellow) compared to other members of the deltex family. This region is predicted to contain two nuclear localisation signals (NLS) and a nuclear export signal (NES). DTX3L also has a functional E3 ubiquitin ligase RING-HC domain (pink) in the C-terminus (blue).

E3 ligase enzymes classically possess either a RING domain or HECT domain, essential for ubiquitin ligase activity (Uchida & Kitagawa, 2016). While HECT domains transiently bind ubiquitin from the E2 conjugating enzyme, RING domains bind to the E2-ubiquitin thioester for direct transfer of the ubiquitin moiety by the E3 ligase (Metzger et al., 2012). Indeed, the importance of the DTX3L RING domain for its ubiquitination activity (and self-ubiquitination) has been demonstrated in *in vitro* ubiquitination assays, where a RING finger deletion mutant was found to be inactive (Takeyama et al., 2003).

DTX3L has been reported to interact with a number of binding partners via its N-terminus, such as PARP9. Interestingly, PARP9 is found to be more highly expressed in aggressive tumours (Takeyama et al., 2003). Heterodimerization of DTX3L with PARP9 has been shown to restrain E3 ubiquitin ligase activity through PARP9-mediated PARylation of ubiquitin (Yang et al., 2017).

PARP9 is also important for localisation of the heterodimer to sites of DNA damage, of which the PARP9 macrodomains recognise ADPr and PAR formed upon histones by PARP1 (Yan et al., 2013). Nevertheless, the role of the DTX3L-PARP9 heterodimer in the DDR is unknown.

DTX3L, through its N-terminal domain has also been found to interact with other members of the deltex family such as DTX1, modulating DTX3L ligase activity (Takeyama et al., 2003). While this was found to enhance DTX3L self-ubiquitination relative to the homodimer, it is not known whether ubiquitination is enhanced on other substrates of DTX3L.

1.7.1.1. DTX3L & Cancer

As previously mentioned, DTX3L was originally identified as a binding partner of PARP9, in turn identified as a risk-related gene in diffuse large B cell lymphoma (DLBCL) (Yan et al., 2009, 2013). These two proteins are orientated head-to-head and are regulated by the same interferon-γ (IFN-γ) responsive bidirectional promoter.

Initial interest in these proteins was generated due to the observation that both DTX3L and PARP9 are most abundant in an aggressive 'host-response' subtype of chemotherapy-resistant DLBCLs, characterised by prominent inflammatory infiltrate and increased IFN-γ production, suggestive of a role for DTX3L/PARP9 in immune response modulation (Juszczynski et al., 2006; Monti et al., 2005).

DTX3L (and PARP9) has also been found to be overexpressed in a variety of solid cancers such as Ewing tumour malignancy, cervical carcinomas and metastatic prostate cancer (Grunewald et al., 2012; Qin et al., 2019; Wilting et al., 2008). DTX3L has also been identified to be overexpressed in melanoma, and glioma, where the level of expression was correlated with the grade of malignancy (Thang et al., 2015; P. Xu et al., 2017).

Overexpression of DTX3L in multiple cancers suggests that DTX3L expression is oncogenic, and that the function of DTX3L is advantageous for cancer cell

growth, viability and/or metastasis. How the potential role of DTX3L at the nascent replication fork, especially under conditions of enhanced replication stress, facilitates this is yet to be identified. Recently, evidence has implicated DTX3L in the DNA damage response, of which the RSR may share aspects (Yan et al., 2009, 2013).

1.7.1.2. DTX3L & the DNA Damage Response

Histone 4 lysine 91 (H4K91) is a ubiquitination target of DTX3L, of which mutations in H4K91 had originally been identified to lead to chemosensitivity in yeast (Hyland et al., 2005). Later work demonstrated that DTX3L catalyzes H4K91 mono-ubiquitination *in vitro* and *in vivo*, limiting the cell sensitivity to DNA damaging agents (Yan et al., 2009). Of note, while depletion of DTX3L was found to reduce proliferation in drug treated cells, it was also found to reduce cell proliferation even in untreated cells, suggesting a growth advantage role of DTX3L overexpression in cancer, possibly mediated by H4K91 mono-ubiquitination.

Furthermore, following DNA damage, DTX3L depletion was found to alter the DDR response concerning 53BP1 accumulation kinetics, where up to 4 hours after doxorubicin treatment, significantly fewer 53BP1 foci positive cells were identified compared to controls. A similar finding was also seen in response to low dose (100cGy) ionising radiation (Yan et al., 2009). 53BP1 recruitment is dependent on H4K20 mono and dimethylation (Hsiao & Mizzen, 2013). It was also found that DTX3L depletion prior to doxorubicin treatment led to a significant decrease in H4K20 methylation and a slight increase in H4K91 acetylation. Chromatin-associated PR-SET7/SET8 (required for H4K20 monomethylation) was also significantly decreased in DTX3L depleted cells (Yan et al., 2009).

The above study was one of the first to associate DTX3L with the DDR. In support of this, another study also demonstrated the role of DTX3L in the DNA damage response in relation to H4K91 modification (Tessadori et al., 2017). Originally identified in three patients, mono-allelic missense mutations in H4K91 produced clinical phenotypes of intellectual disability, microcephaly and growth delay. Recapitulating these mutations in zebrafish reproduced similar phenotypes. Additionally, an increase in DNA damage through γH2AX foci accumulation was observed which importantly was rescued by co-expression of DTX3L. Co-expression of H4K91 acetyl transferase HAT4 did not rescue the damage phenotype, suggesting that H4K91 mono-ubiquitination is important for DNA damage repair and prevention of these clinical phenotypes. H4K91 mutations also resulted in increased apoptosis and cell cycle defects (Tessadori et al., 2017).

Furthermore, it has also been observed that ubiquitination of DTX3L is decreased in response to UV treatment; given the canonical role of ubiquitination in the UPS, this may suggest increased stability of DTX3L in response to DNA damage and may further support a requirement of DTX3L in the DDR and RSR (Elia, Boardman, et al., 2015).

Interestingly, DTX3L heterodimerisation partner PARP9 has also been shown to play a role in enhancing the nuclear DNA damage response upon induced mitochondrial DNA (mtDNA) damage and mtDNA release by genotoxic agents such as doxorubicin. mtDNA stimulates an antiviral response through activation of the cyclin GMP-AMP synthase (cGAS)- stimulator of interferon genes (STING)-tank binding kinase 1 (TBK1) pathway, leading to signal transducer and activator

of transcription 1 (STAT1)-dependent expression of interferon stimulated genes (ISGs) which include PARP9. 53BP1 and γH2AX kinetics were blunted in PARP9 depleted cells, of which this was attributed to the previously described role of DTX3L recruitment to histones at DNA damage sites by PARP9 (Wu et al., 2019; Yan et al., 2009).

While the above work demonstrates a role of DTX3L in the DDR, it is yet to be established whether DTX3L, identified as being present at the nascent replication fork by iPOND, is specifically involved in the RSR. Additionally, given the promiscuous nature of E3 ubiquitin ligases for target substrates, it is important to identify potential novel targets of DTX3L as these may also contribute to the DNA damage phenotypes described above.

Establishing a role for DTX3L in the RSR may provide future therapeutic opportunities. Targeted inhibition of DTX3L, or DTX3L ubiquitinated targets, may increase efficacy of DNA damaging chemotherapeutics or enhance sensitivity of cancer cells further to replication stress. Additionally, understanding how DTX3L elicits protection in the face of DNA damage and replication stress may contribute to our understanding of, and strategies to overcome, chemotherapy resistance.

Ultimately, the following study sets out to characterise the role of DTX3L during replication and establish the protein as a *bona fide* factor contributing to the RSR. Additionally, this study attempts to mechanistically unpin DTX3L function in context of the RSR.

Chapter 2: Materials & Methods

2.1. Materials

2.1.1. siRNA

Custom siRNA oligonucleotides and ON-TARGETplus SMARTpool siRNAs (Dharmacon), combining four gene-specific siRNAs into a single reagent pool to ensure knockdown, were utilised.

siRNA	Catalogue Number/Sequence (Manufacturer)
siDTX3L (SMARTpool)	L-007143-00-0005 (Dharmacon)
siLuciferase (Custom)	5'- CGTACGCGGAATACTTCGA -3' (Dharmacon)
siPARP9 (SMARTpool)	L-014734-00-0005 (Dharmacon)
siRFWD3 (SMARTpool)	L-017095-00-0005 (Dharmacon)
siRNF169 (SMARTpool)	L-032290-00-0005 (Dharmacon)
siSMARCAL1 (SMARTpool)	L-013058-00-0005 (Dharmacon)
siTRIM25 (SMARTpool)	L-006585-00-0005 (Dharmacon)

Table 2. siRNAs used in the present study.

2.1.2. Antibodies

Applications include Western Blotting (WB), Immunofluorescent Staining (IF), Proximity Ligation Assay (PLA) and DNA Fibre (DF), with indicated application-dependent dilutions.

Primary Antibody Target	Dilution (Application)	Catalogue Number (Manufacturer)
α-tubulin (Mouse)	1:10000 (WB)	66031-10IG (ThermoFisher)
γH2AX (Mouse)	1:500 (IF)	JBW301 (Merck)
53BP1 (Mouse)	1:1000 (IF)	MAB3802 (Sigma)

Biotin (Mouse)	1:1000 (PLA)	200-002-211 (Jackson ImmunoResearch)
Biotin (Rabbit)	1:3000 (PLA)	A150-109A (Bethyl)
BRCA1 (Mouse)	1:500 (PLA)	sc6954 (Santa Cruz)
BrdU (Mouse)	1:20 (DF)	347580 (BD Biosciences)
BrdU (Rat)	1:400 (DF)	ab6326 (Abcam)
CHK1 (Mouse)	1:1000 (WB)	sc-8408 (Santa Cruz)
CHK1-pS345 (Rabbit)	1:1000 (WB)	133D3 (Cell Signaling)
Cyclin-A (Rabbit)	1:500 (IF)	ab181591 (Abcam)
DTX3L (Rabbit)	1:500 (PLA) 1:1000 (WB)	D5F2J (Cell Signaling)
GFP (Mouse)	1:500 (PLA)	11814460001 (Roche)
MRE11 (Mouse)	1:200 (PLA)	ab214 (Abcam)
RAD51 (Rabbit)	1:1000 (PLA)	133534 (Abcam)
RAD51 (Rabbit)	1:100 (IF)	63801 (Abcam)
RPA (Mouse)	1:200 (IF)	NA18 (Sigma)
SMARCAL1 (Mouse)	1:500 (WB)	sc-376377 (Santa Cruz)
TOPBP1 (Mouse)	1:500 (PLA) (WB)	sc-271043 (Santa Cruz)

Table 3. Primary antibodies used in the present study.

2.2. Methods

2.2.1. Cell Culture

HeLa and U2OS, RPE-1 and HEK293FT cells were a generous gift from Dr. Fumiko Esashi, Dr. Andrew Blackford and Dr. Roger Grand, respectively. All cells were maintained in Dulbecco's Modified Eagle's Medium supplemented with streptomycin sulphate and benzylpenicillin antibiotics (DMEM w/ antibiotics, ICR stores) and 10% fetal bovine serum (FBS). Cells were maintained at 37°C, 5% CO_2 in a humidified atmosphere in vented T75 flasks with 10ml medium. Cells were passaged upon 70-90% confluency. To passage cells, media was aspirated and cells were washed in 5ml PBS, before the addition of 1ml 1X trypsin. Cells were incubated for 3-5 mins to permit cell detachment. Media was replaced at a volume appropriate for splitting to achieve 20% confluency for continued growth. Cells would be passaged for a maximum of 4 weeks before disposal. Frozen cell stocks were made, with cells stored at 30-40% confluency in 10% DMSO + FBS. Cell vials were then frozen in an isopropanol box and stored at -80°C. Additional vials were stored in liquid nitrogen.

For experiments, cells were trypsinised and media was added to neutralise the trypsin. Cells were centrifuged at 300 x g for 3 mins, media was aspirated and cells resuspended in the appropriate volume to acquire the required seeding density. For harvesting of cells, cells were similarly collected, washed twice in PBS and pellets were frozen on dry ice.

2.2.2. siRNA Gene Silencing

For the targeted knockdown of genes, small interfering ribonucleic acids (siRNA) were chemically transfected into cells. Cells were seeded at a density of 0.5 x 10^6

in 6cm dishes, with 2.5ml media. Liposome-siRNA complexes were formed by combining 90μL Opti-MEM (11058021, ThermoFisher), 3μL siRNA (at 20μM stock) and 12μL HiPerfect (301704, Qiagen) per transfection reaction. After seeding, cells were transfected in suspension. After 24h, media was refreshed and adherent cells were transfected again. At 48h, cells were split for experimental seeding. After 72h, cells were used in experiments. siRNA targeting luciferase (siLuc) was used as a transfection control.

2.2.3. Plasmid Cloning & Transfection

Plasmid constructs for GFP-DTX3L and FLAG-DTX3L expression were generated using Gateway LR clonase II technology, as described in the manufacturer's protocol (11791043, ThermoFisher). pENTR223-DTX3L (DNASU plasmid repository) was used as the gateway donor vector for recombination of the DTX3L CDS into the pDEST-EGFP-C1 (for N-terminal GFP tag; a kind gift from Prof. C. Green) and pHAGE-N-FLAG-HA (for N-terminal FLAG tag; a kind gift from Dr. R. Chapman) gateway destination vectors. Successful cloning was verified by Sanger sequencing. All plasmids were transfected, purified and concentrated using standard molecular biology techniques.

For the GFP-DTX3L construct, plasmid DNA (pDNA) was chemically transfected into HeLa *DTX3L*$^{-/-}$ clones using Lipofectamine 2000 (11668019, ThermoFisher). Cells were left to recover for 48h before media was refreshed with media supplemented with 1000μg ml^{-1} G418 (11811031, ThermoFisher). Cell lines were grown until parental cell death was observed, upon which transfected cell lines were sorted for GFP-positive (GFP background determined using non-transfected parental cells) cell pools and for single cell clones, using the BD

FACSAria III cell sorter. Cell lines were then maintained in 500μg ml^{-1} G418-containing media.

For the FLAG-DTX3L construct, two eppendorfs containing 1.1μg pDNA incubated with OptiMEM, and 10μL Lipofectamine 2000 incubated with OptiMEM were mixed and incubated at RT for 10 mins. The transfection mix was added to cells seeded 24h previously, at a density of 0.4 x 10^6 per well in 6-well plates. Cells were then used for experiments 48h post-transfection.

2.2.3.1. Site Directed Mutagenesis of FLAG-DTX3L

For generation of FLAG-DTX3L-M2, FLAG-DTX3L-Y403X and FLAG-DTX3L-A502V plasmid constructs, the FLAG-DTX3L plasmid was used as a template for site directed mutagenesis (SDM). Primers were designed using the Agilent QuikChange Primer Design tool (https://www.agilent.com/store/primerDesignProgram.jsp).

Marathon Polymerase was used for SDM PCR and template plasmid was digested by Dpn-I (R0176S, NEB) digestion for 1 hour at 37°C. SDM was verified by Sanger Sequencing.

Construct	SDM primers	Tm (°C)
FLAG-DTX3L-M2 (T1729A, C1735A, A1736G, T1744A, T1753A)	Forward: 5'- ACATGGCTTTGTTGATACTAGGGGCGCTGA ATTCACTCTTGCTCTTTGGTAGCACTTTTTT -3' Reverse: 5'- AAAAAAGTGCTACCAAAGAGCAAGAGTGAAT TCAGCGCCCCTAGTATCAACAAA GCCATGT-3'	59
FLAG-DTX3L-Y403X (T1209G)	Forward: 5'- GAAACCTTGCTGCAAATGTCCTACCTTTTT TCGATCTCTGATATC -3' Reverse: 5'- GATATCAGAGATCGAAAAAAGGTAGGACAT TTGCAGCAAGGTTTC -3'	54
FLAG-DTX3L-A502V (C1505T)	Forward: 5'- CTTTTAGAACATACTGCTTCACCTTTGCAA GGTGATTTGGC -3'	54

Reverse:
5'- GCCAAATCACCTTGCAAAGGTGAAGCAGTA
TGTTCTAAAAG -3'

Table 4. Site Directed Mutagenesis primers used for generation of FLAG-DTX3L-M2/Y403X/A502V plasmid constructs.

2.2.4. CRISPR *DTX3L*$^{-/-}$ Cell Line Generation

HeLa and RPE-1 *DTX3L*$^{-/-}$ cell lines were generated by CRISPR-SpCas9D10A (Cas9 double nickase) mediated deletion using paired guide RNAs (gRNAs) targeting exon 1 of DTX3L. gRNAs were designed using the Deskgen online CRISPR gRNA design tool (www.deskgen.com). gRNA oligos were custom ordered from IDT (adapter sequences underlined in red), annealed and cloned into the pAIO-NK vector (a kind gift from Dr. A. Blackford):

gRNA Primer	Sequence
gRNA DTX3L KO F Primer 'A'	5'- ACCGCAGAGCTCTAAGTCCTCGGG -3'
gRNA DTX3L KO F Primer 'B'	5'- AAACCCCGAGGACTTAGAGCTCTG -3'
gRNA DTX3L KO R Primer 'A'	5'- ACCGCCAGCTTCCTTCGTACTCGG -3'
gRNA DTX3L KO R Primer 'B'	5'- AAACCCGAGTACGAAGGAAGCTGG -3'

Table 5. gRNA oligos cloned into the CRISPR pAIO-NK vector.

Successful generation of the pAIO-NK-DTX3L CRISPR plasmid was confirmed by Sanger sequencing. The DTX3L knockout (KO) construct was transfected into cells using Lipofectamine 3000 Transfection Reagent (L3000001, ThermoFisher) and after 24 hours, cells were sorted (BD FACSAria III cell sorter) for cells expressing GFP-Cas9D10A-nickase from the pAIO-NK construct. Cells were

sorted into GFP positive pools. After 7 days, non-GFP expressing single cells were then sorted for into round bottom 96-well plates and colonies were allowed to develop. Upon confluency, clonal pellets were harvested. Clones were validated for absence of DTX3L expression by western blot and positive clones were taken forward for downstream analysis.

2.2.5. Single Molecule DNA Fibre Immunofluorescence

Specific DNA fibre labelling was performed as indicated. Generally, cells were seeded at 0.2 x 10^6 in 6cm dishes and allowed to adhere. After 24h, cells media was refreshed with 3ml media containing 25μM iododeoxyuridine (IdU) and incubated for the indicated period. For chlorodeoxyuridine (CldU) incubation, media was refreshed with media containing 125μM CldU and incubated as indicated. After labelling, cells were washed in PBS, resuspended to 0.5 x 10^6 cells/ml in PBS and kept on ice.

Glass slides were spotted with 2μL of the cell suspension and allowed to dry for 1 minute. Cells were lysed through the addition of 7μL of DNA fibre lysis solution (50mM EDTA and 0.5% SDS in 200mM Tris-HCl, pH 7.5), gently stirred by the pipette tip.

Slides were tilted to approximately 15°, allowing spreading of DNA fibres along the length of the glass slide. Slides were air-dried overnight. Slides were then immersed in methanol/acetic acid (3:1) in a slide staining jar and incubated for 10 mins.

Slides were then washed in distilled H_2O and immersed in 2.5M HCl for 80 minutes, followed by three PBS washes. Slides were then placed into a humidity chamber and blocked for 30 mins with the addition of 150μL of 5% BSA-PBS per

slide, covering each slide with a glass coverslip to ensure homogenous distribution. Coverslips were then removed and excess blocking solution removed from each slide by tissue dabbing. Slides were then replaced in the humidity chamber and primary antibodies were added 60μL/slide: 1:20 anti-bromodeoxyuridine (BrdU) (mouse) and 1:400 anti-BrdU (rat) in 5% BSA-PBS, incubating at RT (room temperature) for 2 hours. Slides were washed three times in PBS before the addition of 60μL/slide secondary antibodies: 1:500 anti-mouse Cy3 (sheep) and 1:400 anti-rat Alexa Fluor 488 (goat), incubated for 1 hour. Slides were washed for a minimum of three times in PBS, immersed in 70% ethanol (EtOH) and subsequently immersed in 100% EtOH. Slides were air dried and mounted with Vectashield mounting medium (H-1000, Vectorlabs). Images were acquired using a 60x oil-immersion lens on Zeiss 710 and Leica SP8 laser confocal microscopes.

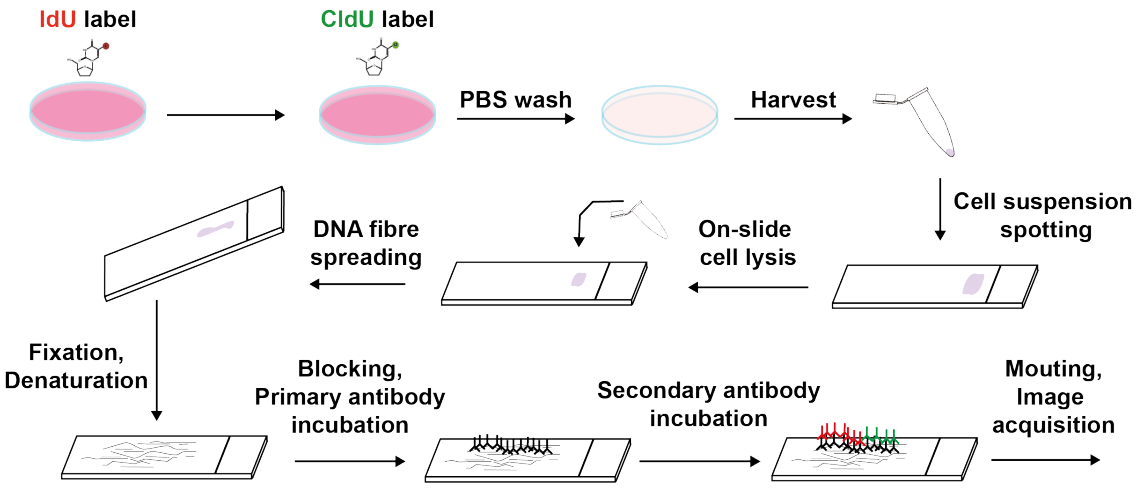

Figure 9. Illustration depicting DNA fibre labelling protocol.

Cells are labelled with IdU and CldU, in which drug treatments may be included. Various incubations may be performed to interrogate different replication scenarios. Cells are then harvested and lysed on-slide. DNA fibres are spread, fixed and denatured before blocking, primary and secondary antibody incubation. Images are then acquired by confocal microscopy.

2.2.6. Cell Proliferation Assays

Cells were seeded at 500 cells per well (in 100μL), 6 technical replicates per cell type, into duplicate flat bottomed 96 well plates, one plate per each day of the assay. Starting with Day 0, 10μL of alamarBlue (BUF012A, BioRad), a non-toxic cell viability assay reagent containing resazurin, was added to each well and incubated at 37°C for 6 hours. Quantification of cell proliferation through alamarBlue redox reaction was measured by fluorescence (excitation 550nm / emission 590nm). Background fluorescence was subtracted from each reading. Cell proliferation derived from fluorescence (measured in arbitrary units (a.u.) was normalised to a cell line's respective day 0 within individual experiments, and then normalised subsequently across three biological repeats for plotting.

2.2.7. Drug Sensitivity Assays

To all wells of a flat-bottomed 96 well plate (100μL in media only control column), 50μL of media was added. Drug concentrations were made to 4X the desired top dose in media. Using a multichannel pipette, the drug-media solution was serially diluted from right to left across the 96 well plate, diluting 50μL the drug 1:1 in 50μL media (1/2) subsequently across each column. Cells were seeded at 500 cells per well (in 50μL, for a final volume of 100μL per well), from left to right, with 6 technical repeats per drug dilution. Cells were incubated for 7 days, upon which 10μL AlamarBlue was added per well and incubated for 2 hours. Fluorescence was measured as described for cell proliferation. Percentage survival was calculated relative to untreated controls for each cell line.

2.2.8. Western Blotting

Cell pellets collected for western blotting were harvested as previously described and snap-frozen on dry ice before being stored at -80°C. Pellets were then resuspended in urea lysis buffer (9M urea, 50mM Tris HCl, pH 7.3, with 150 mM β-mercaptoethanol added before use) followed by sonication at 10mA for 10s. Lysate protein concentration was determined by spectrophotometry using either the NanoDrop 2000 (ThermoFisher) or DeNovix DS-11 (DeNovix). Western blot samples were made to an equal protein concentration and SDS loading buffer was added to 1X (2% SDS, 10% glycerol, 2% 2-Mercaptoethanol, 62.5 mM Tris-HCl, pH 6.8, 0.01% bromophenol blue) followed by boiling at 95°C for 10 min. Samples were resolved by SDS-PAGE on in-house prepared 10% Tris-Glycine gels or commercially available 3-8% Tris-Acetate (EA0375BOX, Invitrogen) and 4-12% Bis-Tris (NP0321BOX, Invitrogen) gels, using the corresponding running buffers; 1X Tris-glycine running buffer (prepared in-house), 1X MES Running Buffer (prepared in-house), 1X NuPAGE Tris Acetate SDS Running Buffer (LA0041, ThermoFisher). Gels were transferred to 0.45μm nitrocellulose (GE10600016, Merck) or PVDF (GE10600023, Merck), at 90V for 90 mins on ice, in Tris-glycine transfer buffer (prepared in-house) containing 20% methanol. Membranes were blocked in 5% milk- Tris Buffered Saline and 0.01% Tween 20 (TBST). Immunoblotting was carried out using the indicated primary antibodies, in 5% milk-TBST (5% BSA-TBST was used for CHK1-pS345) at 4°C overnight on a rocking platform. Membranes were washed five times with 1X TBST. Antigens were visualised using HRP-conjugated secondary antibodies (Dako) in 5% milk-TBST, for 1 hour at RT, and Immobilon Western chemiluminescent HRP substrate (WBKLS0500, Merck). Chemiluminescence was detected using X-ray film or digitally using the Azure C300 (Azure Biosystems).

2.2.9. qPCR

Analysis of PARP9 silencing by qPCR was performed by Dr. Charlotte Smith (ICR). In brief, RNA from cells was harvested using the RNeasy Mini Kit (74004, QIAGEN) according to manufacturer protocol. cDNA was synthesized using the Applied Biosystems High-Capacity cDNA Reverse Transcription Kit (4368814, Applied Biosystems). qPCR using SYBR Green PCR Master Mix (4309155, Applied Biosystems) was performed using the following primers for PARP9:

PARP9 qPCR Forward primer: 5'- GGCAAAGAGGTCCAAGATGCTG -3'

PARP9 qPCR Reverse primer: 5'- GCCTCACACATCTCTTCCACGT -3'

2.2.10. Flow Cytometry and Cell Sorting

For cell cycle analysis, cells were seeded in 10cm dishes for 70% confluency upon treatment and harvesting. Cells were harvested, washed twice in PBS and spun at 1000 x g for 3 mins. Pellets were then resuspended in 200μL PBS, on ice. To fix the cells, 5mL of cold 70% EtOH was added drop-wise to resuspended cells on vortex and incubated on ice for 30 mins. Cells were centrifuged at 1000 x g for 3 mins and the supernatant was aspirated. Pellets were loosened by vortexing and 1mL 2M HCl/ 0.5% Triton-X100 was added to cells in a drop-wise manner, on vortex. Cells were incubated at RT for 30 mins and centrifuged at 1000 x g for 3 mins. Supernatant was aspirated and 1mL PBS was added to resuspend cells. Samples were centrifuged again, supernatant aspirated and 1mL 0.5% Tween/ 1% BSA-PBS used to resuspend pellets.

Cells were centrifuged and resuspended in 1mL PBS containing 250μg RNase A (10109142001, Merck) and 20μg propidium iodide (P4170-10MG, Merck).

Samples were then analysed on the BD LSR II flow cytometer, where a minimum of 10,000 events were recorded per sample.

2.2.11. DDR Immunofluorescent Staining

Cells were seeded onto round glass coverslips (631-0150, VWR) in 6-well plates, at a seeding density of 1.5 x 10^6 cells per well. After 24h, cells were treated as indicated. Coverslips were washed twice in PBS before subsequent treatment. Steps were carried out at RT unless stated otherwise. Microscopy was performed as described previously:

2.2.11.1. 53BP1/OPT/Micronuclei, RAD51 and γH2AX IF Staining

Coverslips were fixed in 4% paraformaldehyde (PFA) in PBS for 10 mins, washed twice in PBS and permeabilised with 0.1% Triton-X100 in PBS for 10 mins. Coverslips were washed three times in PBS, transferred to a humidified chamber covered in parafilm and blocked by the addition of 200μL of 10% fetal bovine serum (FBS) in PBS to each coverslip for 30 mins. Blocking buffer was aspirated and 40μL primary antibodies, diluted in 0.1% FBS-PBS, was immediately added to each coverslip and incubated for 1 hour. Coverslips were washed three times in PBS for 5 mins before the addition of 40μL secondary antibodies, diluted in 0.1% FBS-PBS, for 1 hour. Coverslips were washed four times in PBS before mounting onto glass slides with Vectashield mounting medium containing DAPI (H1200, Vectorlabs).

2.2.11.2. RPA IF Staining

Coverslips were pre-extracted on ice using freshly prepared CSK extraction buffer (produced in-house; 10mM PIPES, pH 6.8, 300mM sucrose, 100mM NaCl, 1.5mM $MgCl_2$ and 0.5% Triton-X100) for 2 mins. Coverslips were then fixed with

4% PFA-PBS for 10 mins and washed three times in PBS for 5 mins each. Blocking, primary and secondary antibody addition and coverslip mounting were performed as described in the previous section.

2.2.12. EdU Labelling and Proximity Ligation Assays (PLAs)

2.2.12.1. EdU Labelling for PLA

Analysis of the association of proteins to nascent DNA through EdU labelling and the PLA assay was performed as previously described (Nieminuszczy et al., 2019; Taglialatela et al., 2017). Cells were seeded on coverslips as described in the previous section. For cells requiring ethynyldeoxyuridine (EdU) labelling, cells were pulse-labelled with 10μM EdU in 2ml media for 10 mins. Media was then refreshed and for HU treated cells, 2ml media containing either 1mM HU or 4mM HU, still with EdU, was added to wells, for 1 hour or 3 hours respectively. Treatment was staggered to enable simultaneous collection of coverslips. After treatment, coverslips (in 6-well plates) were placed on ice, washed and then permeabilised at 4°C with 0.5% Triton-X100 for 10 mins. Coverslips were washed with PBS and fixed with 3%PFA/2% sucrose in PBS at RT for 10 mins. For GFP-TOPBP1:DTX3L PLAs, cells were fixed in cold MetOH for 10 mins and washed three times in PBS. Coverslips were washed three times in PBS and blocked in 200μL 3% bovine serum albumin (BSA) in PBS for 30 mins. Coverslips were washed twice in PBS and transferred to a humidified chamber covered in parafilm, with the immediate addition of PBS upon each coverslip to maintain hydration.

For EdU labelling, components of the Click-iT EdU kit (C10337, ThermoFisher) were combined (80% 5mM Copper Sulphate Solution, 10% Reaction Buffer, 10% Buffer Additive) with the addition of 2% 1mM Biotin Azide in DMSO. To each

coverslip, 40μL of the reaction mix was added. The humidified chamber was incubated at RT for 30 mins. After labelling, coverslips were washed twice with PBS for 5 mins.

2.2.12.2. PLA Assay

Primary antibodies were diluted in 0.1% saponin/ 1% BSA-PBS and 40μL was added to each coverslip. The humidified chamber was sealed using parafilm and incubated overnight at 4°C. Coverslips were washed twice in PBS for 5 mins before the addition of PLA probes (Duolink In Situ PLA Probe; anti-mouse PLUS (DUO92001-100RXN) and anti-rabbit MINUS (DUO92005-100RXN), Merck). Mouse and rabbit PLA probes were diluted together 1 in 5 in provided antibody diluent solution and 40μL was added per coverslip. Coverslips were incubated in the sealed humidity chamber for 1 hour at 37°C. Coverslips were washed twice with PLA Buffer A solution (DUO82049-4L, Merck), stored at 4°C but warmed to RT prior to use.

For the PLA ligation and amplification reactions, the Duolink In Situ Detection Reagents (Red) were used (DUO92008-100RXN, Merck). Ligation buffer was diluted 1 in 5 in dH_2O, upon which ligase was diluted 1 in 40 in the ligation buffer. To each coverslip, 40μL of reaction mix was added and coverslips were incubated in the humidified chamber at 37°C for 30 mins. Coverslips were washed twice in Buffer A for 2 mins. Similarly, amplification buffer was diluted 1 in 5 in dH_2O and polymerase was diluted 1 in 80 in amplification buffer. To each coverslip, 40μL of reaction mix was added and coverslips were incubated in the humidified chamber at 37°C for 100 mins.

Coverslips were washed twice in PLA Buffer B (DUO82049-4L, Merck) for 10 mins, stored at 4°C but warmed to RT prior to use. 0.01X PLA Buffer B was added

to coverslips for 1 min prior to immediate mounting using Vectashield mounting medium containing DAPI (Vectorlabs).

2.2.13. GFP Co-Immunoprecipitation (Co-IP) and Mass Spectrometry (MS)

2.2.13.1. GFP-DTX3L Co-IP

HEK293FT cells were seeded into 15cm dishes and grown to 25% confluency for transfection. The pDEST-GFP-DTX3L was chemically transfected; two eppendorfs containing 5μg pDNA and 1.8ml OptiMEM and 45μL Lipofectamine 2000 with 1.8ml OptiMEM were combined and incubated for 10 mins. Cell media was refreshed with OptiMEM for transfection, and regular media was replaced after 6 hours. Cells were treated with drug as indicated 48 hours post transfection and pellets were harvested at 1500rpm for 5 mins at 4°C. Pellets were washed twice in PBS. For cell pellets of >80μL packed cell volume, pellets were divided into multiple eppendorfs to avoid protein precipitation. Pellets were stored at -80°C.

For immunoprecipitation, cell pellets were resuspended on ice in 1.2ml IP Buffer I (in-house preparation; 100mM NaCl, 0.2% NP40, 1mM $MgCl_2$, 10% glycerol, 5mM NaF, 50mM Tris-HCl, pH 7.5) supplemented with Halt Protease and Phosphatase (PPase) Inhibitor Cocktail, EDTA-free (78443, ThermoFisher) and 25U/mL benzonase nuclease (E1014, Merck). Cell suspensions were incubated for 90 mins at 4°C with rotation. Cell suspensions were adjusted to 200mM NaCl with 2mM EDTA and incubated for 30 mins at 4°C with rotation. Cell suspensions were then centrifuged at 16,000 x g for 25 mins at 4°C. Binding control agarose beads (bab-20, ChromoTek), used for sample lysate preclearance, were

prepared by washing three times in IP Buffer II (in-house preparation; 200mM NaCl, 0.1% NP40, 10% glycerol, 5mM NaF, 50mM Tris-HCl, pH 7.5, 2mM EDTA), supplemented with PPase Inhibitor. Remaining buffer was removed from beads and lysate supernatant was added, incubate the lysate-bead mixture for 1 hour at 4°C with rotation. Protein concentration of lysates were quantified by DeNovix Spectrophotometry. 5mg of lysate protein at 1mg/ml was taken forward for IP; remaining lysate was stored at -20°C for the 'Input' samples. GFP Nano-Trap Agarose beads (gta20, ChromoTek) were equilibrated by washing 25μL of packed bead volume three times in 500μL IP Buffer II. Beads were then added to 5mL of lysate protein and incubated for 2 hours at 4°C with rotation. The bead-lysate mix was pelleted at 2500 x g for 2 min at 4°C. Supernatant was stored as 'Flowthrough' at -20°C. Beads were washed three times with 500μL IP Buffer II supplemented with PPase Inhibitor and centrifuged again.

For analysis by western blot, proteins were eluted by resuspending beads in 50μL of 2X SDS IP Buffer (in-house preparation; 120mM Tris-HCl, pH 6.8, 20% glycerol, 4% SDS, 0.04% bromophenol blue, 10% β-mercaptoethanol). Input samples were thawed and protein samples were made for western blotting, adding SDS IP buffer to a final volume of 50μL. Input and lysate-bead mixtures were boiled at 95°C for 10 mins. IP samples were centrifuged at 2500 x g for 2 mins to pellet beads and supernatant was collected. Samples were analysed by western blotting as previously described, on 1.5mm gels.

2.2.13.2. FLAG-DTX3L Co-IP

The FLAG-DTX3L co-IP was performed similarly to that previously described but with some differences. HEK293FT cells were seeded in 10cm dishes. The

transfection mix consisted of two eppendorfs containing 2.2μg pDNA and 750μL OptiMEM and 20μL Lipofectamine 2000 with 750μL OptiMEM, mixed and incubated. For co-IP, lysis was performed as described above, but using Anti-FLAG M2 Affinity Gel beads (A2220-1ML, Merck). To elute peptides, 40μL 3X FLAG peptide was used (in-house preparation), diluted in IP buffer II to 100μg/mL. Samples were incubated at 4°C for 30mins with gentle agitation. Eluates were centrifuged as before, transferred to fresh tubes, 5X SDS IP buffer added and boiled at 95°C for 10mins.

2.2.13.3. MS Sample Preparation

For analysis by mass spectrometry, on bead digestion was performed. Beads were washed with 10 volumes of cold IP Buffer II. Beads were then washed three times with 10 volumes of cold 50mM triethylammonium bicarbonate buffer, pH 8.5 (TEAB; T7408-100ML, Merck). With the last wash, beads were transferred to a new, cold, protein lo-bind tube (EP0030108116-100EA, Merck). Beads were microfuged and residual liquid removed. 100μL of 100mM TEAB was added to beads, ensuring bead coverage, and samples were placed into an ultrasonic bath for 5s to aid resuspension.

To the beads, 1μg Pierce MS grade trypsin (90057, ThermoFisher) in 0.5% formic acid (FA; 15667520, ThermoFisher) was added. Bead digests were incubated for 18 hours with Thermomixer shaking, at 1400rpm,at 37°C. Digest supernatant was collected and reserved. 50μL 100mM TEAB was added to the remaining beads, resuspended, supernatant removed and pooled with reserved. This step was repeated once, and supernatant was then dried by SpeedVac (to almost dry).

Sample filtering was then performed to remove residual beads in the samples, followed by desalting and hpH fractionation (these steps were performed by Lu

Yu, ICR). Briefly, to filter the samples, 65% acetonitrile (ACN; 10193051, ThermoFisher) / 0.5% FA was added to dried peptides and sonicated for resolubilisation. Resolubilised peptides were filtered using Pierce Spin Columns (69705, ThermoFisher) and redried by SpeedVac. Samples were then resuspended in 100mM tris(2-carboxyethyl)phosphine hydrochloride solution, pH 8.5 (TCEP; 646547, Merck) and 0.5% FA was added. Desalting, fractionation and LC-MS/MS analysis were then performed (Lu Yu, ICR).

2.2.13.4. Desalting & Fractionation

Eluates were desalted in home-made C18 tips (ReproSil-Pur 120 ODS-3, 50 µm, Dr. Maisch), and flow-through samples were further desalted by SDB-XC (Empore^{TM}, 3M) tips to ensure antibody removal. Samples were dried by SpeedVac. Peptides were resuspended in 20 µl H_2O and peptide concentration was measured by Nanodrop (DeNovix DS-11) at A280nm to estimate peptide amount. Samples were then TMT labelled according to manufacturer's instructions: 21 µl of 0.2 M TEAB was added to each sample for a final concentration at 0.1 M, and 0.5 mg TMT10plex reagents (ThermoFisher) in 20 µl extra dry CH_3CN (Fisher Scientific) was added and mixed immediately. The mixture was incubated for 1 hour at RT with shaking at 650 rpm in a Thermomixer. The reaction was quenched by adding 6 µl of 5% hydroxylamine and incubated for another 15 min at RT, with shaking. The 10 labelled samples were combined, then dried by SpeedVac.

The pooled sample was resuspended in 0.1% NH_4OH/100% H_2O, and fractionated on an XBridge BEH C18 column (2.1 mm i.d. x 150 mm, Waters) with an initial 5 min loading with 5% ACN/0.1% NH_4OH (pH 10), then linear gradient

to 35% CH_3CN /0.1% NH_4OH in 35 min, then to 80% CH_3CN /0.1% NH_4OH in 5 min, incubated for another 5 min, then back to 5% ACN/0.1% NH_4OH in 5 min and incubated for 5min, i.e. total 60 min. The flow rate was at 200 µl/min. Fractions were collected every 42 seconds from retention time 8.5 min to 50 min and then concatenated to 12 fractions at equal time intervals and dried by SpeedVac. Each fraction was resuspended in 40 µl of 0.1% FA/ H_2O before LC-MS/MS analysis.

2.2.13.5. LC-MS/MS Analysis

LC-MS/MS Analysis was performed on the Orbitrap Fusion Lumos Tribrid mass spectrometer coupled with U3000 RSLCnano UHPLC system. Both instrument and columns used below are from ThermoFisher. The peptides were first loaded to a PepMap C18 trap (100 µm i.d. x 20 mm, 100 Å, 5 µm) for 5 min at 10 µl/min with solvent A, then separated on a PepMap C18 column (75 µm i.d. x 500 mm, 2 µm) over a linear gradient of 5 - 38% B in 120 min / cycle time at 150 min at a flow rate at 300 nl/min, where A was 0.1% formic acid (FA)/ 100% H2O, and B was 80%CH3CN/0.1% FA. Gradient time was 90 min with total cycle time at 120 min, and 120 min gradient time /total cycle time 150min for ubiquitin fractions. The MS acquisition used standard Data-Dependent Acquisition (DDA) method with the Top Speed 3 sec cycle time. Briefly, the full MS survey scan in Orbitrap was m/z 375 – 1500 with AGC (Automatic Gain Control) set at 400,000 and maximum injection time at 50 msec. The resolution was set at 120,000 at m/z 200. For IP samples, multiply charged ions (2+ to 5+) with intensity threshold above 7,000 were fragmented in HCD (higher energy collision-activated dissociation) at 30% normalized collision energy (NCE) with isolation width at 1.6 Da in quadrupole, and detected in the ion trap with the AGC at 10,000 with

maximum injection time at 50 msec. The dynamic range was 40 sec at ±10 ppm mass tolerance.

All LC-MS/MS data were processed in Proteome Discoverer (PD) software v.2.4 (ThermoFisher Scientific). For GFP-DTX3L IP samples, both Mascot (Matrix Science) and Sequest HT search engines were used to search against the reviewed UniprotKB protein database of Homo sapiens (Version February 2020) plus the in-house contaminate database. The precursor mass tolerance was set at 20 ppm and the fragment ion mass tolerance was set at 0.5 Da. Spectra were searched for fully tryptic peptides with maximum 2 miss-cleavages with the dynamic modifications included N-acetylation (Protein N-terminus), Deamidation (N, Q), GlyGly (K), Oxidation (M), and Phosphorylation (S, T, Y). The search result was validated by Percolator with q value setting, where the protein FDR settings were 0.01 (strict) and 0.05 (relaxed). Only master proteins with at least 1 high confidence peptide were reported. The label-free protein quantification used Precursor ion intensities by feature mapping. Only unique peptides were considered for quantification.

2.2.14. Ubiquitome Enrichment Profiling

2.2.14.1. Sample Preparation

For cell sample preparation, a minimum of six 15cm dishes per sample were seeded at an appropriate density to account for proliferate rate differences and ensure homogenous confluency (estimated 80%) upon treatment and harvesting. Cell media was refreshed with media containing 5μM MG-132 (474787, Merck) proteosome inhibitor and incubated for 30 min prior to drug treatment. For HU

treated cells, 3mM HU was added to media and incubated for 4 hours. All samples were then harvested after 4h and 30 mins. Cells were scraped and collected into falcon tubes on ice, centrifuged at 2500 x g for 10 mins and pellets were washed three times in PBS, centrifuging between for 3 mins. Pellets were divided between two 2ml eppendorfs, then snap-frozen and stored at -80°C.

The following samples were collected; a ten sample maximum was necessitated by the PTMScan Ubiquitin Remnant Motif (K-ε-GG) IP kit (5562, Cell Signaling Technology):

Biological Repeat n1	**Biological Repeat n2**
UT (untreated) WT (HeLa Wild-type)	UT WT
UT DTX3L KO Clone 1 (HeLa *DTX3L*$^{-/-}$ clone. 20)	UT DTX3L KO Clone 2
UT DTX3L KO Clone 2 (HeLa *DTX3L*$^{-/-}$ clone. 24)	HU WT
HU (3mM HU, 4h) WT	HU DTX3L KO Clone 2
HU DTX3L KO Clone 1	
HU DTX3L KO Clone 2	

Table 6. Samples included in ubiquitin remnant peptide IP.

Ten samples were selected for immunoprecipitation using the PTMScan Ubiquitin Remnant Motif (K-ε-GG) Kit.

2.2.14.2. Ubiquitin Remnant Peptide Immunoprecipitation

Cell pellets were briefly thawed on ice and 200mM 2-chloroacetamide (CAA; C0267, Merck) was prepared in high-performance liquid chromatography (HPLC) H_2O just before use. CAA was added to lysis buffer (5% SDS/100mM TEAB) at a final concentration of 5mM. 500μL of lysis buffer was used to resuspend cell pellets before probe sonication at 40% power (1s On, 1s Off, fifteen repeats). Samples were heated to 90°C for 10 mins, allowed to cool and microfuged, before

being sonicated again. Lysate was cleared by centrifugation at 16000 x g for 15 mins and supernatant was moved to a new clean tube. Lysate protein concentration was then measured by Pierce 660nm Protein Assay (22660, ThermoFisher) using Ionic Detergent Compatible Reagent (IDCR; 22663, ThermoFisher).

To perform protein digest, 5mg protein was aliquoted to 15ml falcon tubes and made up to 500μL with lysis buffer (without CAA), with two aliquots per condition for a total protein amount of 10mg per IP. To each tube, 20μL of 500mM TCEP, pH 7 was added, vortexed briefly and incubated at 56°C for 15 mins. Samples were cooled to RT before adding 25μL of freshly prepared 200mM CAA. Samples were protected from light, mixed and incubated at RT for 30 mins, with agitation. Chloroform (CH_3Cl)/methanol protein precipitation was performed to remove contaminates. To each sample, 2mL 100% HPLC MetOH, 0.5mL CH_3Cl and 1.5mL HPLC H_2O was added, vortexed vigorously for 10s and centrifuged at 9000 x g for 5 mins. The top layer of liquid was carefully removed, avoiding contact with the protein pellet. 4mL MetOH was added, samples were vortexed for 10s and left in an ultrasonic bath until complete pellet dispersion. Samples were centrifuged at 9000 x g for 5 mins and all liquid was removed. 1mL 100mM TEAB was added and samples were replaced in the ultrasonic bath. To the resuspended protein, 100μg Pierce Trypsin Protease MS grade (90059, ThermoFisher) in 0.5% FA was added per sample and incubated at 37°C for 4 hours with shaking at 600rpm. Another 100μg trypsin was added to each sample and incubated for a further 15 hours. Samples were then heated to 70°C for 10 mins and the two 5mg aliquots per condition were combined, then dried by SpeedVac for several hours.

For immunoprecipitation of ubiquitin remnant peptides, 1.5mL PTMScan IAP Buffer (1X) was added to each sample and placed in an ultrasonic bath for 1 min to dissolve peptides. Samples were centrifuged at 16,000 x g for 5 mins and supernatant was transferred to a new clean 2mL protein LoBind tube. Vials of PTMScan Ubiquitin Branch Motif (K-ε-GG) Immmunoaffinity Beads were centrifuged at 2000 x g for 30s and all buffer was removed. Beads were washed four times with 1mL PBS and resuspended in 40μL PBS in the provided vial. Peptide solution was incubated with the beads for 2 hours at RT with rotation. One spin column per sample was prepared by adding 500μL 0.15% trifluoroacetic acid (TFA; 302031-10X1ML, Merck), vortexing for 5s and microfuging briefly to remove all liquid, repeated a further two times. Spin columns were then washed three times with 500μLHPLC H_2O. Peptide-bead solution was centrifuged at 2000 x g for 30s, supernatant was removed and stored as 'Flowthrough'. Beads were washed twice with 1mL cold IAP Buffer, inverting the tube 5 times, centrifuging and removing the liquid. Similarly, beads were washed with 1mL cold PBS. 500μL cold PBS was added to the beads to transfer the bead slurry to the spin column. Spin columns were microfuged for 10s and liquid removed. 500μL was added to the original bead tube, and transferred again to ensure efficient bead transfer. 500μL cold HPLC H_2O was added to the column, inverted 5 times, microfuged and liquid removed. Similarly, 500μL H_2O was added but this time columns were centrifuged at 2000 x g for 30s. After removing liquid, spin columns were transferred to a clean tube for peptide elution.

To elute ubiquitin remnant peptides, 100μL of 0.15% TFA was added to the beads in the spin columns and incubated for 10 mins at RT with shaking at 650rpm. Columns were centrifuged as before and eluate reserved. Elution was repeated once again and eluates pooled. Samples were then frozen at -20°C for further

processing by the proteomics core before LC-MS/MS acquisition, including desalting, TMT labelling and hpH fractionation (performed by Lu Yu, ICR).

LC-MS/MS was performed as previously described, with adjustments:

Full MS survey scan range was at m/z 375 – 1800. The multiply charged ions (3+ to 6+) with intensity threshold above 10,000 were fragmented in HCD with NCE at 38% and isolation width at 0.7 Da in quadrupole, and detected in Orbitrap in the scan mode of defined first m/z at 100. The resolution was set at 50,000 at m/z 200, the AGC at 100,000 with maximum injection time at 100 msec. The dynamic range was 40 sec at ±7 ppm mass tolerance.

2.2.14.3. Ubiquitome Enrichment MS Acquisition

The Ubiquitome raw files were processed in Proteome Discoverer 2.4 (Thermo Fisher) using the Sequest HT search engine to search against reviewed UniprotKB database of Homo Sapiens (March 2021) and in-house contaminate database. Search parameters were: trypsin with 2 maximum miss-cleavage sites, mass tolerances at 20 ppm for the precursor, and 0.1 Da for the fragment ions. Spectra were searched for fully tryptic peptides with maximum 2 miss-cleavages. Carbamidomethyl (C) and TMT6plex (Peptide N-terminus) were set as static modify cations, and N-acetylation (Protein N-terminus), Deamidation (N, Q), Oxidation (M), TMT6plex (K) and GlyGlyTMT6plex (K) as dynamic modifications. For reporter ion intensity detection, the integration window tolerance was set 15 ppm. Only unique peptides were considered for quantification. TMT Quan value correction factor, provided by the manufacturer's certificate of analysis, was applied. Co-isolation threshold was set at 100, and reporter ions average S/N threshold at 3. Reporter ion intensities were normalized by total peptide amount,

and then scaled on all average to correct the variation by different sample loading in each channel.

2.2.14.4. Ubiquitome Enrichment MS Result Analysis

MS result acquisition, processing and normalisation was carried out by Lu Yu (ICR). Statistical analysis and pathway enrichment analysis was performed by Theo Roumeliotis (ICR), using Perseus software (v. 1.6.2.2.). Data was processed to include results with two maximum equal modification per peptides, and peptide abundance normalised by GG-peptides. Samples were then log_2 transformed. Pearson sample correlation analyses revealed a batch effect (greater variation between biological repeats) therefore samples were rescaled within each biological repeat to normalise for this, according to the respective controls (e.g. log_2(DTX3L KO clone 2 (n1) / WT (n1)) and log_2(DTX3L KO clone 2 (n2) / WT (n2)). For statistical analysis, clone 2 samples were averaged to enable two sample t-test and ANOVA comparisons between groups, i.e. WT vs KO or UT vs HU. Samples were then filtered for significance ($P < 0.05$) and a minimum of 30% fold change (>1.3 enrichment factor). Pathway enrichment was performed using the Gene Ontology Biological Processes (GOBP) database.

Chapter 3: Depletion of DTX3L Affects DNA Replication Dynamics

3.1. Identification of E3 Ubiquitin Ligases Present at the DNA Replication Fork by iPOND

In order to understand how cells reliably replicate their genomic material and tolerate challenges to replication, it is important to identify the factors that facilitate this process. Despite many of its components being shared with the DSBR, the replication stress response is relatively poorly characterised.

3.1.1. Isolation of Proteins On Nascent DNA

Within the last decade, technology that permits the detection of proteins at active, stalled and collapsed replication forks, as well as newly deposited chromatin, in mammalian cells was developed by Cortez and colleagues, known as the isolation of proteins on nascent DNA (iPOND) (Sirbu et al., 2011, 2012). The importance of this technique lies in the fact that previously, site-specific analysis of active and stalled mammalian replisomes had not been possible.

In short, the thymidine analogue 5-ethynyl-2'-deoxyuridine (EdU) is incorporated into actively replicating DNA within the cell, followed by subsequent formaldehyde treatment to cross-link proteins (**Figure *10***). The protein-DNA complexes are washed and cells are permeabilised before subsequent biotin conjugation. DNA-protein complexes are sheared and resulting fragments are isolated by streptavidin purification. Eluted proteins may then be identified by western blot or mass spectrometry (MS).

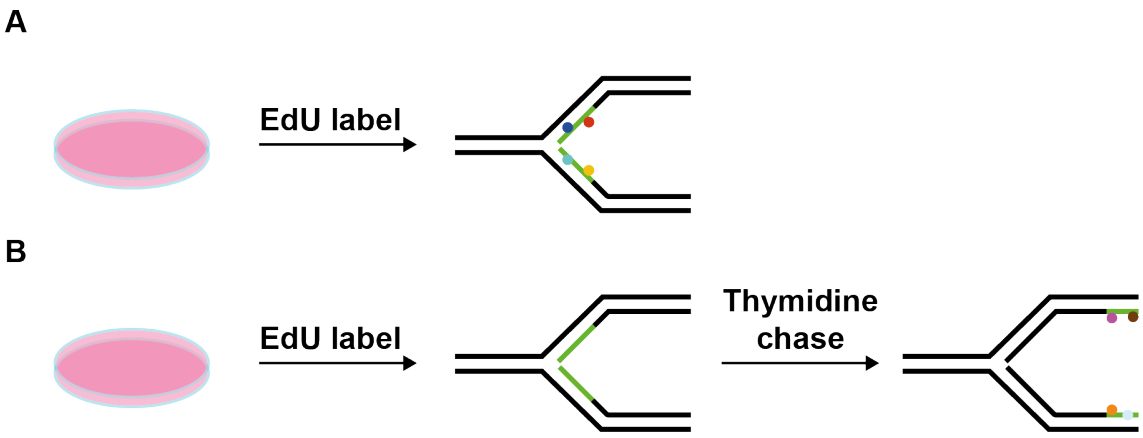

Figure 10. Schematic of iPOND labelling protocol.

A) *Short EdU labelling (in green) followed by immediate fixation for detection of proteins that localise to the nascent replication fork.* ***B)*** *EdU labelling followed by thymidine chase prior to fixation allows the detection of proteins deposited at mature chromatin.*

3.1.2. E3 ubiquitin ligases identified by iPOND-MS

An iPOND screen was previously undertaken to identify factors recruited to stalled replication forks, in which factors such as EXD2 and BOD1L were identified and established to be fork protection factors against uncontrolled fork degradation (iPOND performed by Alicja Winczura (Higgs et al., 2015; Nieminuszczy et al., 2019)). Other known fork associated factors were identified such as replication machinery components MCM subunits, RPA and DNA replication polymerases (Higgs et al., 2015). From this screen, a range of E3 ubiquitin ligases were also identified and found to be present at both unchallenged and hydroxyurea treated (3mM for 4h) stressed forks. The specificity of these factors to *nascent* DNA was established through confirming their absence after thymidine-chase, differentiating actively progressing replication forks from mature chromatin (**Figure *10***).

Secondary candidate stratification was carried out on a selection of the E3 ubiquitin ligases retrieved (see **Table *7***, highlighted in red); some of these proteins

were identified to be present at HU-treated replication forks as well as in untreated conditions. Other proteins were only identified from the iPOND-MS screen in untreated conditions but are known to have a role in the DDR- suggesting they may have a potential role in the RSR but their recruitment may be dependent on different types of lesion than that arising from 3mM HU treatment for 4 hours. These E3 ubiquitin ligases have been indicated to have a role in replication and/or DNA damage responses, providing precedent for their investigation (J. Chen et al., 2012; Elia, Wang, et al., 2015; Inano et al., 2017; Yan et al., 2009; P. Zhang et al., 2015). Candidates were considered in greater detail with regards to their cellular localisation, and potential for their involvement in DNA related processes through the presence of domains that allude to cellular function (such as nuclear localisation sequence (NLS) domains, predicted (ST)Q motifs, etc) to validate potentially relevant targets to take forward.

Here, initial phenotypic characterisation was carried out to establish a potential functional role for these factors at the replication fork, where selected E3 ligases were depleted and preliminary DNA fibre analysis was carried out.

A

EdU only:			
E3 Ubiquitin Ligase	**PROT SCORE**	**PROT MATCHES**	**PROT SEQUENCE**
UBR5	293	33	11
RING1	111	6	3
PIAS2	103	6	1
E3A	58	10	4
ARIH2	55	4	3
MMS21 (NSE2)	54	3	2
HERC2	47	34	4
RNF123	47	13	1
KCMF1	45	3	3
XIAP	45	1	1
RNF14	45	1	1
ARIH1	42	6	2
LRSAM1	42	15	1
RNF169	41	14	2
RING2	39	8	1
RNF170	39	2	1
RAD18	35	5	1
UHRF2	31	6	1
CNOT4	31	6	1
PRAJA2	30	6	1
HERC6	28	6	1
RFWD3	27	3	2
MYCBP2	24	23	1

B

EdU + 3mM HU (4h) chase:			
E3 Ubiquitin Ligase	**PROT SCORE**	**PROT MATCHES**	**PROT SEQUENCE**
HUWE1	1918	112	84
TRIM28	900	44	29
HECTD1	721	41	35
RANBP2	582	49	44
UBR4	575	72	59
RNF213	415	48	46
TRIM25	405	25	20
TRIP12	350	26	25
UHRF1	289	12	11
NEDD4	141	11	8
CHIP	134	9	9
TRIM33	132	14	11
UFM1	131	17	15
KCMF1	130	7	6
FIP-2	108	9	7
RNF160	106	17	17
UBR5	101	21	20
HERC4	97	10	8
BRE1A	96	15	15
TRIM56	90	8	7
DTX3L	87	11	10
TRIM24	79	5	5
RBBP6	75	13	11
LRSAM1	68	18	14
TRIM32	63	5	5
BRE1B	63	20	19

Table 7. E3 ubiquitin ligase iPOND hits.

A) *HeLa S3 cells were pulsed with 10μM EdU****,*** *and in* ***B)*** *followed with a 3mM hydroxyurea chase for 4h. E3 ligases shown in* ***B*** *were also identified in EdU only samples.* (Higgs et al., 2015) *E3 ligases in red were characterised by DNA fibre.*

3.2. DNA Fibre Analysis Upon Depletion of Fork-Associated E3 Ubiquitin Ligases

To investigate the putative role of these E3 ubiquitin ligases at the replication fork, DNA fibre analysis was utilised, a quantitative method for direct observation of replication fork dynamics on single DNA molecules. This *in vivo* fluorescence microscopy-based technique depends on the incorporation of two halogenated nucleoside analogues into actively replicating DNA. The protocol may be modified to investigate different replication contexts. In its simplest form, unchallenged replication dynamics may be observed through a double, sequential pulse of 5-iodo-2'-deoxyuridine (IdU) and 5-Chloro-2'-deoxyuridine (CldU). These two labels are incorporated into the nascent DNA and the progression of the replication fork can be monitored as a result. The labelling protocol can be modified to experimentally interrogate various scenarios at the replication fork; replication stress inducing agents such as HU can permit investigation of fork stalling and fork collapse, as well as fork resection upon persistent induction of replication stress (see **Chapter 2.2.5**, **Figure *9***).

3.2.1. Depletion of select E3 ubiquitin ligases leads to altered replication dynamics

As the selected E3 ubiquitin ligases (RFWD3, TRIM25, RNF169 and DTX3L) were identified in the iPOND screen to be present at unimpeded, nascent replisomes, I sought to investigate whether their absence would affect unchallenged fork progression. It should be noted that the following experiments in this sub-chapter are single and preliminary; therefore without statistical analysis, the results should be regarded with caution.

Given that two forks emanating from the same replication origin (sister replication forks) should theoretically progress at the same speed in unimpeded wild-type cells (producing an average sister fork ratio (SFR) of 1), it may be assumed that a difference in length of SFRs and resulting deviation from a ratio of 1 arises from slowed or stalled replication forks. The four selected candidates were depleted by siRNA in HeLa cells and for all four E3 ligases, the sister fork ratio (SFR) was found to increase above 1 compared to cells treated with control siRNA targeting Luciferase (siLuc), suggesting an increased frequency of fork stalling arising from endogenous sources of replication stress in their absence (***Figure 11***).

E3 ligases TRIM25 and DTX3L were also identified in the iPOND screen as being present at replication forks stalled through the addition of high-dose replication-stress inducing agent hydroxyurea, suggesting a role in tolerance of exogenous replication stress and fork stabilisation.

To validate this further, and investigate whether these candidate E3 ligases contribute to the tolerance of HU-induced stress to aid fork progression, the fibre protocol was modified to include a low dose of HU during incorporation of the second CldU analogue. Again, a decrease was observed in the ratio between CldU and IdU upon depletion of all four candidates compared to siLuc-treated control, suggesting an increase in fork slowing and stalling (**Figure *12***). To see whether this extended to a role in fork recovery, this time a low dose of HU was used in-between DNA labelling. A decrease in the CldU and IdU ratio compared to control treated cells suggests that in the absence of RFWD3 and DTX3L, replication forks had a reduced ability to restore replication upon removal of the replication inhibitor. This did not seem to be the case for TRIM25 or RNF169,

suggesting that fork stability in response to HU may not be dependent on the action of these E3 ligases (**Figure *13***).

From this DNA fibre analysis, RFWD3 and DTX3L depletion demonstrated the most severe phenotypes. Given that RFWD3 has a previously known role in ICL repair at stalled replication forks, DTX3L was taken forward as a high-confidence candidate, displaying similar DNA fibre replication phenotypes to RFWD3 (DNA fibre analysis in this study and (Lin et al., 2018) but with an undocumented role in the replication stress response. Although there has been some indication that DTX3L is involved in the DDR, a replication stress specific role is yet to be identified (Yan et al., 2009, 2013).

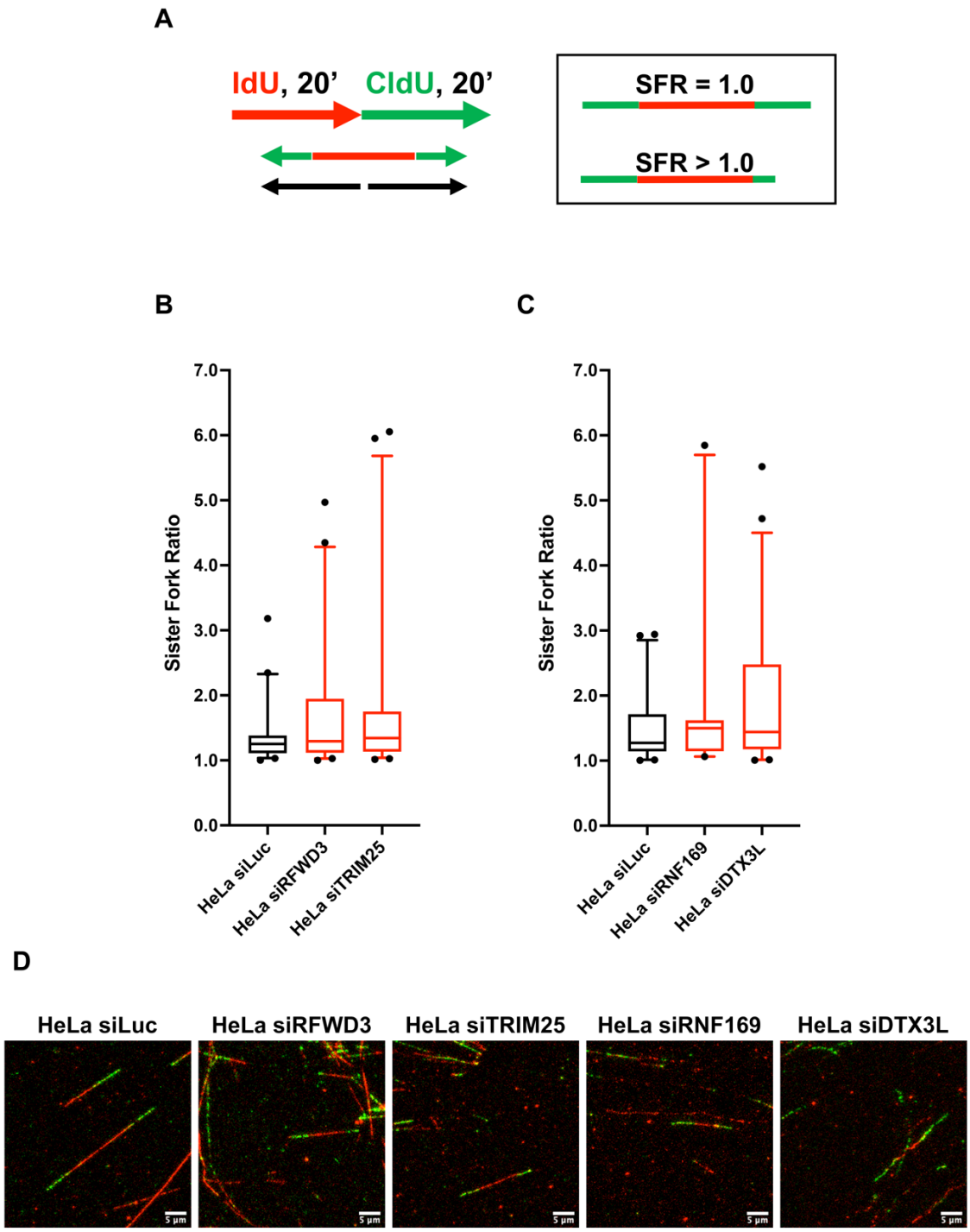

Figure 11. DNA fibre analysis of unchallenged replication fork dynamics arising from siRNA-mediated depletion of candidate E3 ubiquitin ligases.

A) *Schematic of nucleoside analogue incubation protocol for unchallenged fibres. Black arrows represent replication forks emanating from the same origin, termed 'sister forks'.* ***B)*** *&* ***C)*** *CldU ratios (long / short tract) of sister forks from HeLa cells, treated with control siRNA (siLuc) or siRNA targeting the indicated E3 ligase. (n ≥ 20 sister fork ratios from one experiment, 5-95th percentile boxplots).* ***D)*** *Representative images of sister fork fibres; white scale bars are 5µm in length.*

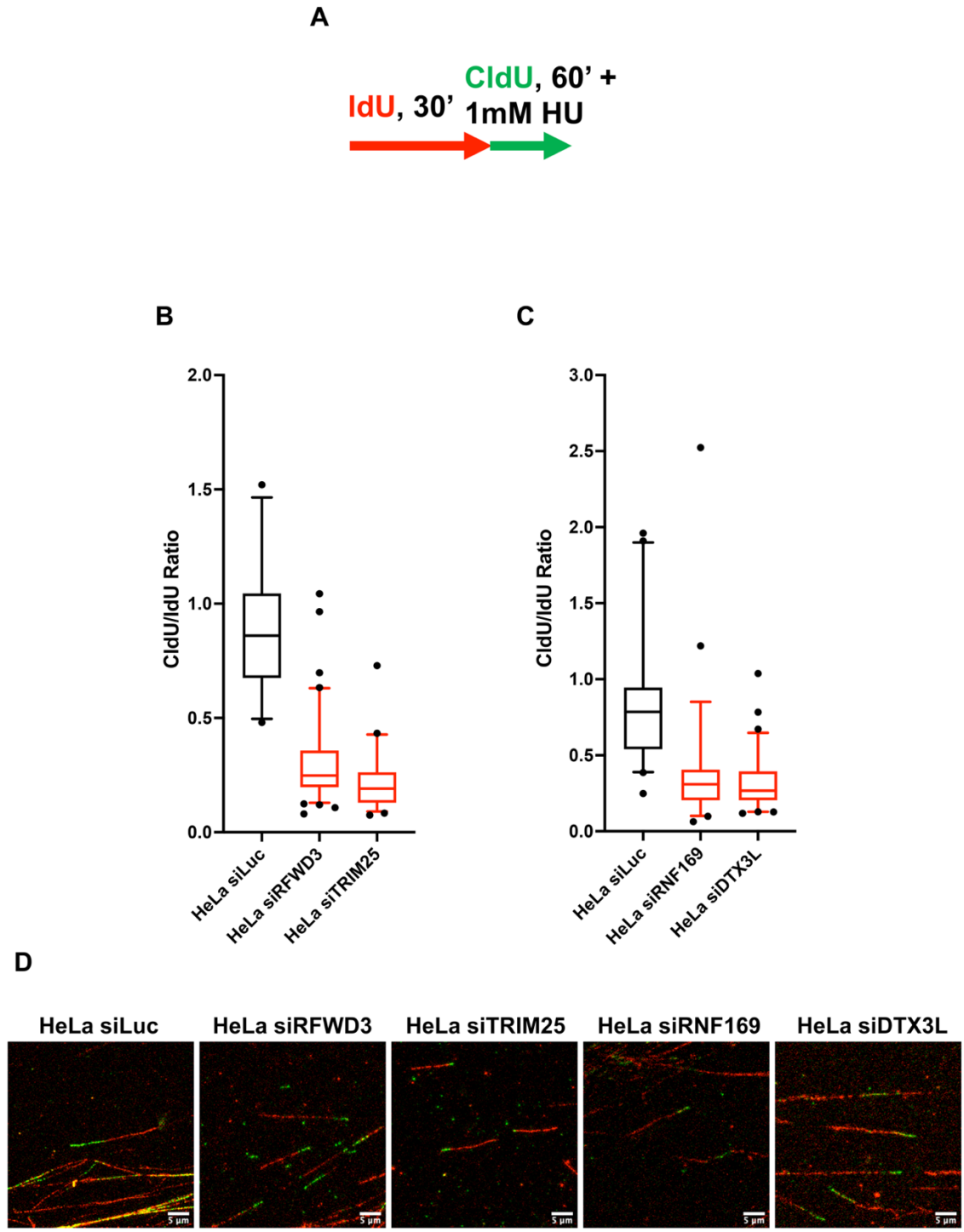

Figure 12. DNA fibre analysis of replication fork stalling dynamics arising from siRNA-mediated depletion of candidate E3 ubiquitin ligases in HU challenged cells.

A) *Schematic of nucleoside analogue incubation protocol for fibres challenged with 1mM HU to induce fork stalling during the CldU pulse.* ***B)*** *&* ***C)*** *CldU/IdU ratios of forks from HeLa cells, treated with control siRNA (siLuc) or siRNA targeting the indicated E3 ligase. (n ≥ 40 tracts from one independent experiment).* ***D)*** *Representative images of HU challenged fibres.*

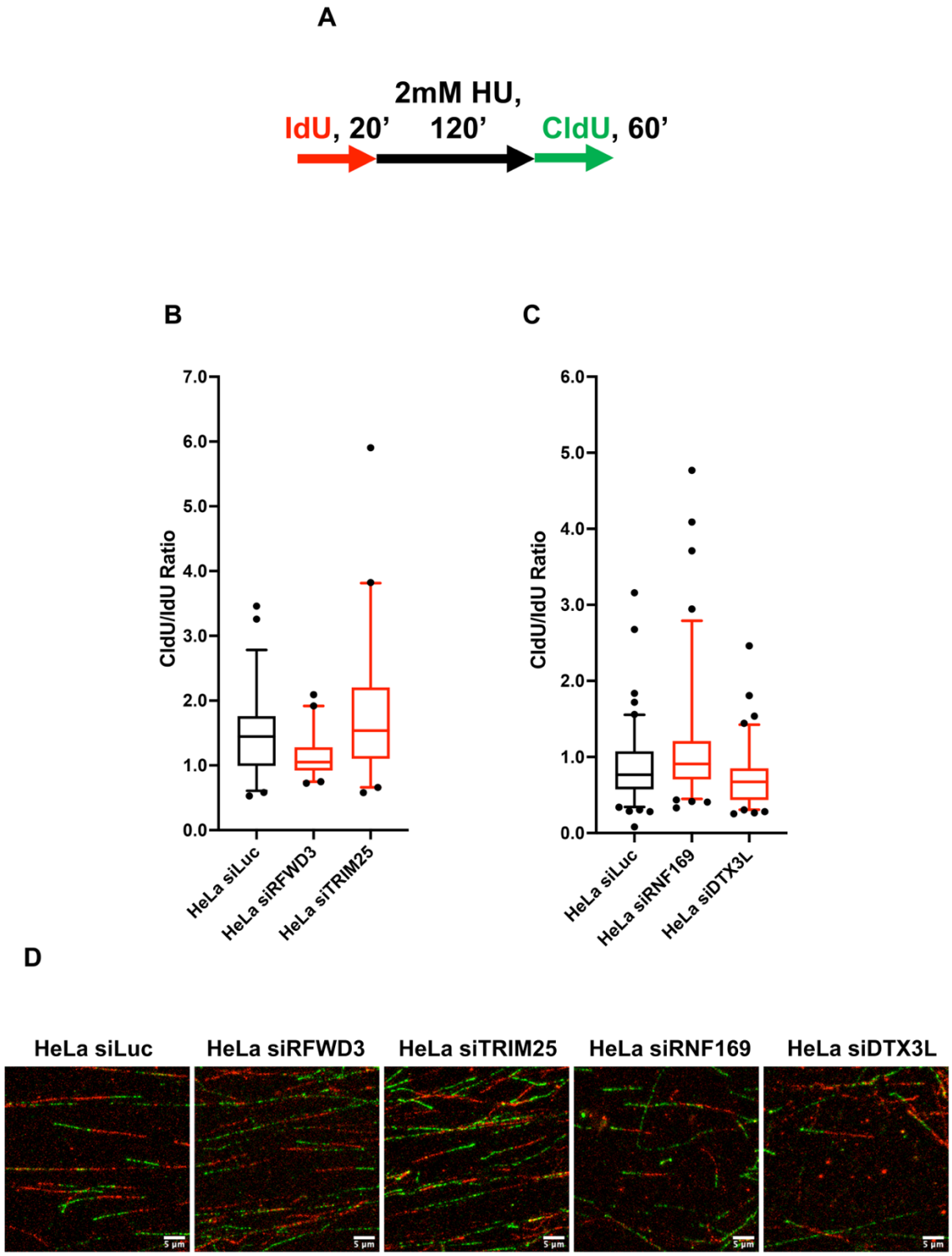

Figure 13. DNA fibre analysis of replication fork recovery arising from siRNA-mediated depletion of candidate E3 ubiquitin ligases in HU challenged cells.

A) *Schematic of nucleoside analogue incubation protocol for fibres challenged with 2mM HU to induce fork stalling, with replication recovery permitted during the CldU pulse.* ***B)*** *&* ***C)*** *CldU/IdU ratios of forks from HeLa cells, treated with control siRNA (siLuc) or siRNA targeting the indicated E3 ligase. (n ≥ 40 tracts from one independent experiment).* ***D)*** *Representative images of HU challenged fibres.*

The potential role for DTX3L was investigated more thoroughly through two additional repeats, establishing a *significant* replication stress defect in DTX3L depleted cells (**Figure *14***), as demonstrated initially (**Figure *15, A-C***).

Additionally, to investigate the role of DTX3L in protecting stalled forks from fork resection, a high dose HU was added for a prolonged period after the second CldU label. Fork resection is inferred upon a shortening of the second label in relation to the first. A significant reduction in CldU/IdU ratio was again observed upon DTX3L depletion, suggesting a role for this protein in fork protection against extensive fork degradation by nucleases (**Figure *15, D***).

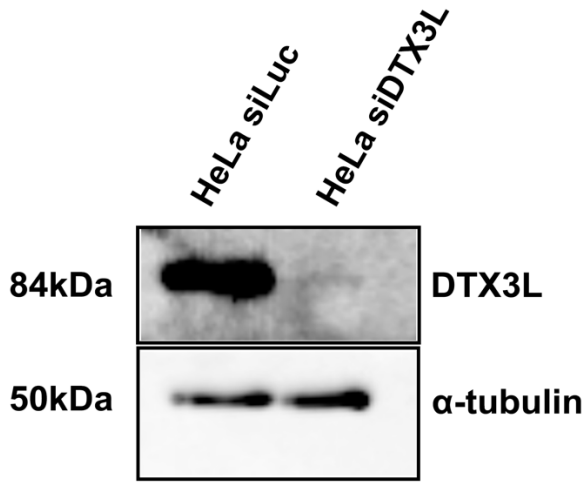

Figure 14. Silencing of DTX3L in HeLa cells by siRNA treatment.

40μg of whole cell lysate was analysed by western blot. HeLa WT cells treated with control siRNA (siLuc) was included as a negative control of endogenous DTX3L expression. α-tubulin serves as loading control.

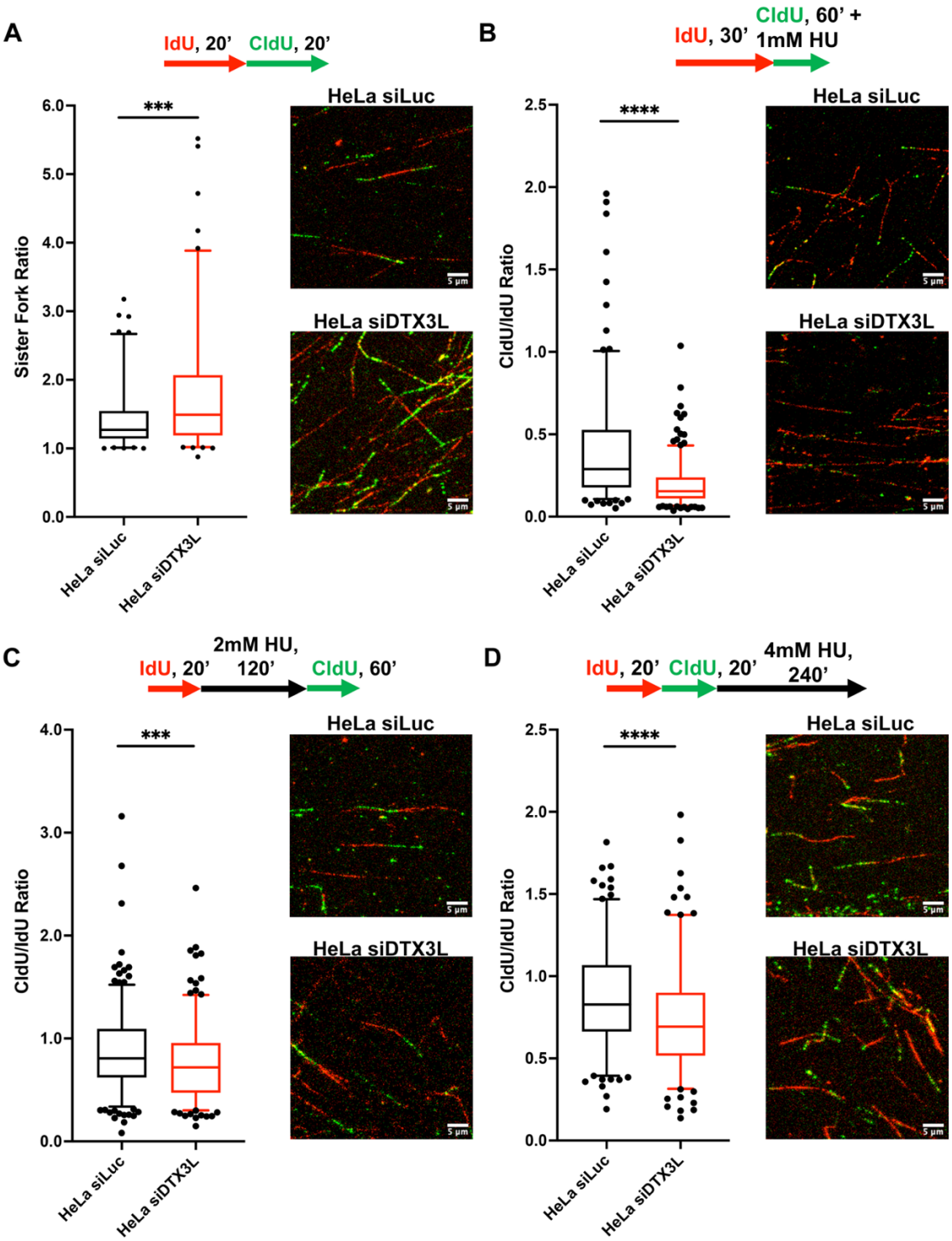

Figure 15. Fork dynamics are impeded upon DTX3L silencing.

*__A__) CldU ratios of sister forks from HeLa cells, treated with non-targeting luciferase siRNA or siRNA targeting DTX3L ($n \geq 100$ sister fork ratios, from three independent experiments, *** = $P = 0.0004$). __B)__ CldU/IdU ratios from HeLa cells treated with 1mM HU during 60min CldU pulse ($n \geq 189$ tracts from three independent experiments, **** = $P < 0.0001$). __C__) As before, but with 2mM HU for 120min followed by CldU 60min incubation ($n \geq 234$ tracts from three independent experiments, *** = $P = 0.0002$). __D__) As in __A__, followed by 4mM HU treatment for 240mins ($n \geq 185$ tracts from two independent experiments, **** = $P < 0.0001$). (5-95th percentile boxplots, Mann-Whitney). Representative images depict DNA fibre spreads. White scale bars are 5μm in length.*

3.3. HeLa Cells Depleted for DTX3L Have Reduced Proliferation

As DTX3L appears to have a role in the replication stress response, and may also play a more general role in replication, it was important to investigate the proliferative capacity and cell cycle profile of DTX3L depleted cells.

It may be expected that cells with a reduced ability to tolerate replication stress would have reduced rates of replication and hence reduced cellular proliferation. To see if this was the case in cells depleted for DTX3L, cell proliferation was investigated. Depletion of DTX3L was found to decrease cell proliferation by 10% at day 5 and 20% at day 7 in siDTX3L treated cells (**Figure *16***).

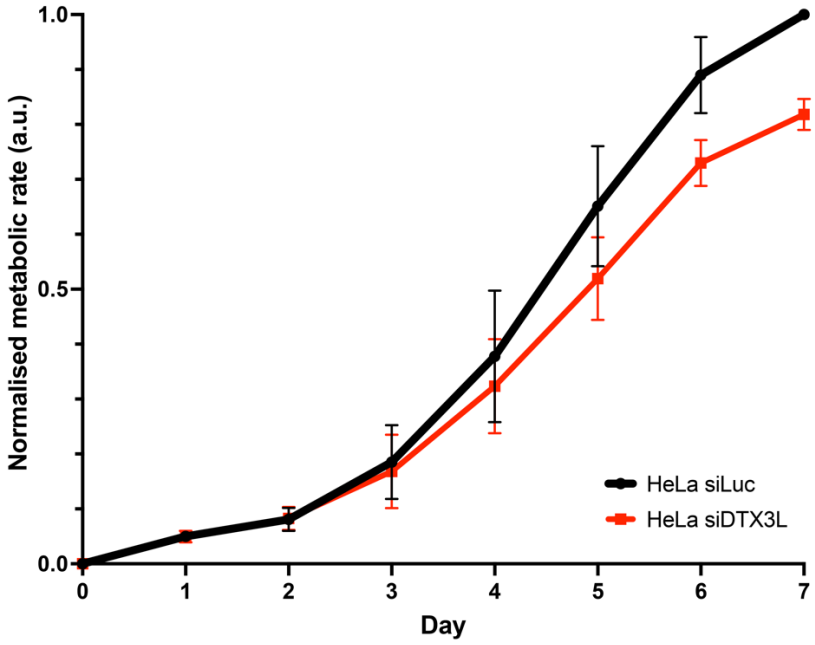

Figure 16. Cell proliferation is reduced in cells silenced for DTX3L.

Alamar blue assay measuring cell proliferation in HeLa cells treated with control siRNA (siLuc) or siRNA targeting DTX3L (Mean ± SEM from three independent experiments, normalised to maximal metabolic rate per experiment).

3.4. Depletion of DTX3L in HeLa Cells Leads to Clastogen Sensitivity

Based on the above results, it would be expected that cells with a reduced ability to tolerate replication stress would be more sensitive to agents that impede replication. Agents that produce physical obstacles to the DNA replication machinery such as ICLs, or dNTP synthesis inhibitors that deplete DNA replication substrates will induce a replication stress response in treated cells through impeded replisome progression. Cells with a reduced tolerance to this replication stress will become more sensitive to these treatments.

To put these replication stress response phenotypes into clinical context, the sensitivity of DTX3L-depleted cells to drugs that impede replication fork progression was investigated. Cisplatin is a chemotherapeutic agent used in a variety of cancers and induces DNA damage primarily through cross-linking of purine bases on DNA, ultimately resulting in apoptosis of the cell. Replication stress arises due to the inability of the replisome to proceed through the intra- and interstrand crosslinks. The ATR-CHK1 pathway is engaged to enable cells to survive cisplatin treatment (Wagner & Karnitz, 2009). Therefore, I wanted to see whether cells deficient for DTX3L, and hence a fully functioning replication stress response, would be sensitized to cisplatin.

Silencing of DTX3L in HeLa cells revealed an increased sensitivity to cisplatin (**Figure *17, A***), with an IC_{50} of 0.243μM compared to HeLa WT at 0.404μM. This suggests that cells deficient for DTX3L are less able to survive with damage induced by cisplatin treatment, and this may be due to a reduced ability to overcome challenges to DNA replication or through other pathways regulated by the replication stress response.

Next, I tested DTX3L deficient cell sensitivity to gemcitabine. Gemcitabine acts to inhibit DNA synthesis by being incorporated into newly synthesized strands, preventing ongoing replication and evading base excision repair. Resultant inhibition of DNA synthesis leads to apoptosis of the cell. In cells silenced for DTX3L, the IC_{50} response to gemcitabine was 5.755nM compared to WT at 8.93nM (**Figure *17, B***).

I then investigated the sensitivity of DTX3L silenced cells to hydroxyurea. Hydroxyurea is a potent inhibitor of ribonucleotide reductase and leads to the depletion of the dNTP pools required for DNA synthesis. HeLa cells treated with siDTX3L showed increased sensitivity to HU with an IC_{50} of 40.82mM compared to 57.31mM in HeLa siLuc cells (**Figure *17, C***).

Given the previously documented role of DTX3L in the wider DDR, to investigate if cells depleted for DTX3L were more sensitive to DSB-inducing drugs, zeocin sensitivity was also investigated. Zeocin is a radiomimetic that directly causes DNA damage through intercalation with DNA. Surprisingly, a similar degree of sensitivity was seen between cells treated with siDTX3L and siLuc (**Figure *17, D***).

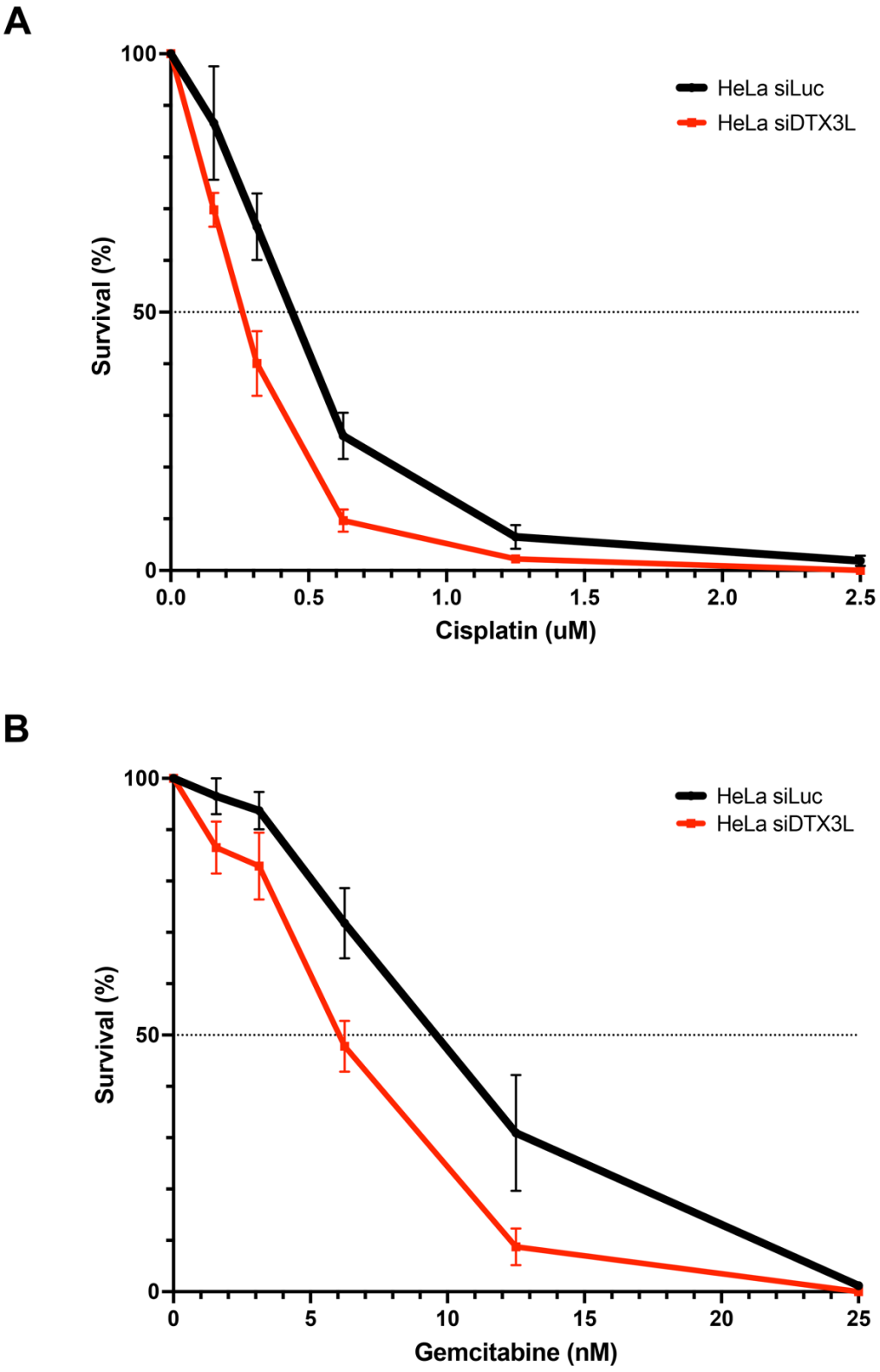

Figure 17. DTX3L depletion enhances cell sensitivity to replication stress inducing drug treatments.

*HeLa cells treated with non-targeting luciferase siRNA or siRNA targeting DTX3L were treated continuously with **A**) cisplatin **B**) gemcitabine **C**) hydroxyurea **D**) zeocin and left to grow for one week. Proportion of surviving cells compared to untreated cells was determined by Alamar blue cell proliferation assay (Mean ± SEM from three independent experiments).*

C

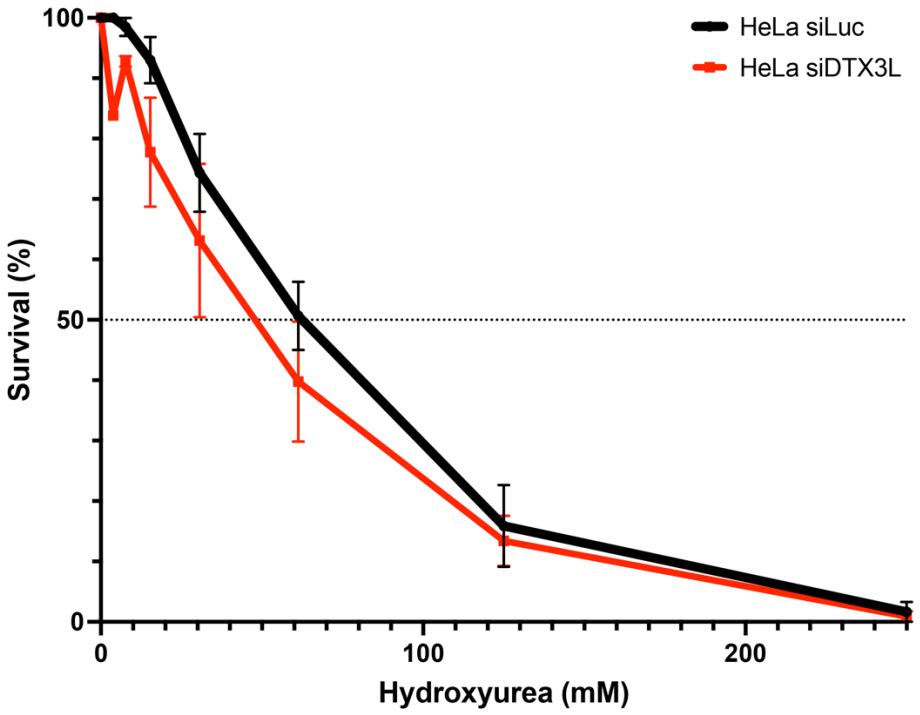
HeLa siLuc
HeLa siDTX3L
Survival (%)
100
50
0
0
100
200
Hydroxyurea (mM)

D

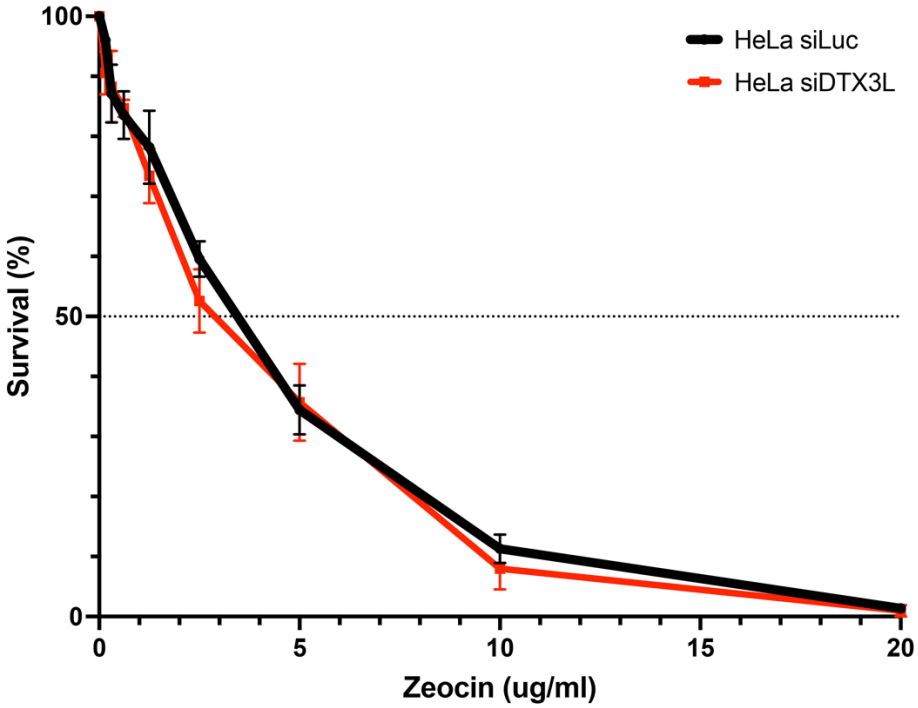
HeLa siLuc
HeLa siDTX3L
Survival (%)
100
50
0
0
5
10
15
20
Zeocin (ug/ml)

3.5. Conclusion

Overall, this data reveals a role for DTX3L in the replication of DNA and in the tolerance of challenges to replication. Through the use of iPOND-MS and DNA fibre techniques, DTX3L has been identified as an E3 ubiquitin ligase with a potential role directly at the DNA replication fork.

Interrogating different replication scenarios suggests that in cells deficient for DTX3L there is a decreased tolerance to endogenous replication challenges, as inferred through a reduced SFR. Additionally, a decreased tolerance to exogenous replication stress was observed, resulting in an increase in fork stalling in the presence of 1mM HU treatment. Although cells will generally possess mechanisms to overcome replication challenges, elicited through the replication stress response, in cells deficient of DTX3L it appears that the ability to overcome this challenge is decreased.

A decreased ability to restart replication forks after HU treatment was observed in cells where DTX3L was depleted. Likewise, in cells treated with 4mM HU for 240mins after CldU pulse, a decrease in CldU tract length arises through fork reversal and fork resection by endonucleases. While these responses are part of a regulated replication stress response, upon deregulation, this can lead to unscheduled fork reversal and resection, as seen here in the case of DTX3L deficiency with decreased CldU/IdU ratio.

Furthermore, this work demonstrates that DTX3L deficiency leads to decreased cell proliferation in untreated cells, in support of a previous study showing proliferation reduction (Figure 4B, Yan et al., 2009). The work here also demonstrates an increased sensitivity to clastogen treatment, similar to previous

work where enhanced sensitivity was observed to DNA damage-inducing drug doxorubicin (Figure 4B, Yan et al., 2009).

A variety of DNA damage inducing drugs were investigated and found to produce enhanced sensitivity in a DTX3L deficient background. Sensitivity to cisplatin could suggest a role for DTX3L in the ICL repair pathway, however it is also likely that due to the sensitivity observed with hydroxyurea and gemcitabine DTX3L may have a role in tolerance of replication stress more generally.

In summary, these data support a novel role for DTX3L in the maintenance of replication and as part of the replication stress response. Loss of DTX3L leads to decreased fork stability in the face of both endogenous and exogenous replication stress, resulting in decreased cell proliferation and enhanced sensitivity to drugs that impede replication.

Chapter 4: DTX3L Prevents Replication Stress-Associated DNA Damage

4.1. Exogenous Replication Stress Leads to Increased DNA Damage in DTX3L Depleted Cells

Given the putative role of DTX3L in the replication stress response, as evidenced in the previous chapter, it was then important to establish the consequence of DTX3L depletion and resultant alteration of DNA replication dynamics on DNA damage and genome instability.

4.1.1. 53BP1 Foci, OPT Domains and Micronuclei Formation in DTX3L Depleted HeLa Cells

53BP1 forms discrete foci as assayed by immunofluorescence staining and these foci represent sites of DNA damage and break processing. Through the induction of damage by agents that lead to increased fork stalling and DSBs, they may be interpreted as an indicator of damage arising from collapsed forks due to increased replication stress (Harrigan et al., 2011; Lukas et al., 2011).

Here, a significant increase in the incidence of 53BP1 foci was observed in untreated DTX3L depleted cells compared to HeLa WT cells, suggesting increased DSB arising from DTX3L depletion even in unchallenged conditions. This was further exacerbated with low dose (1mM HU for 1h) and high dose (4mM HU for 3h) HU treatment, of which high dose HU was found to induce the greatest increase in 53BP1 foci in DTX3L deficient cells. This suggests prolonged fork stalling leads to increased DNA damage and the capacity to overcome this enhanced replication stress is reduced in cells depleted of DTX3L, potentially resulting in greater fork collapse and break formation (**Figure *18***).

Micronuclei are also a key indicator of reduced replicative ability and resultant chromosomal instability due to under-replicated DNA. DTX3L depletion in HU-treated cells was found to significantly increase the frequency of micronuclei observed (**Figure *19***). Similarly, the number of G1 cells with OPT domains, foci representing DNA damage arising from impaired replication from the previous S phase, were found to significantly increase with treatment in DTX3L-depleted cells (***Figure 20***).

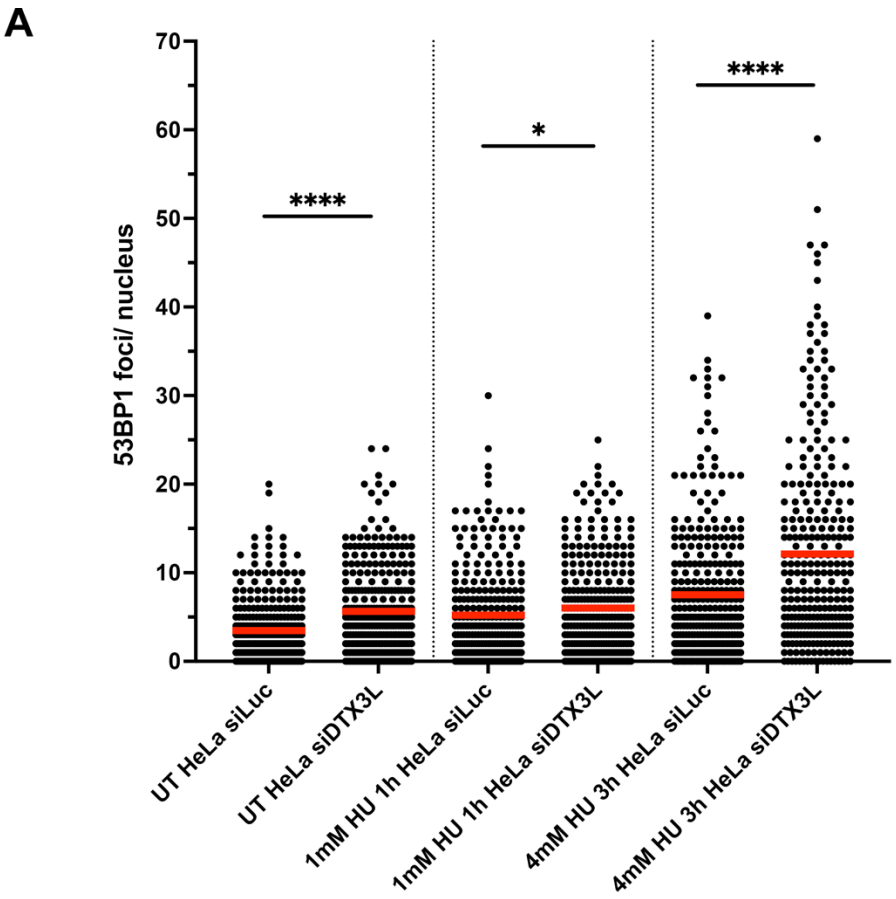

***Figure* 18. DTX3L depleted cells have increased 53BP1 focus formation.**

A) *HeLa cells were treated with siLuc or siDTX3L and treated as described. 53BP1 foci counts per cell (mean, n ≥ 270 nuclei, from three independent experiments. Analysed by Mann-Whitney, * = P = 0.0158, **** = P < 0.0001).* ***B)*** *(Next page) Representative images. White scale bar is 10μm in length.*

(Landscape)

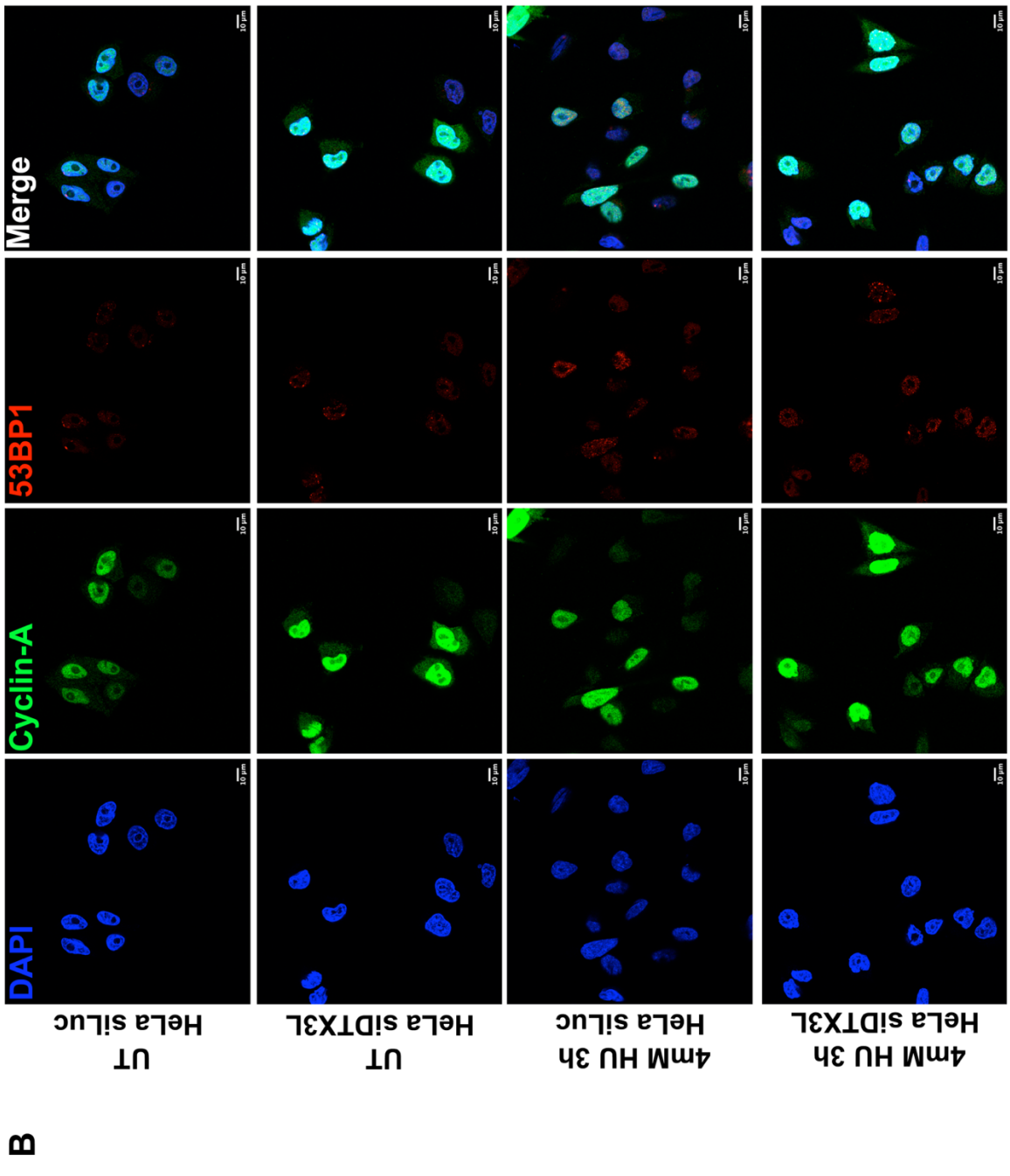
B
UT
HeLa siLuc
UT
HeLa siDTX3L
4mM HU 3h
HeLa siLuc
4mM HU 3h
HeLa siDTX3L
DAPI
Cyclin-A
53BP1
Merge

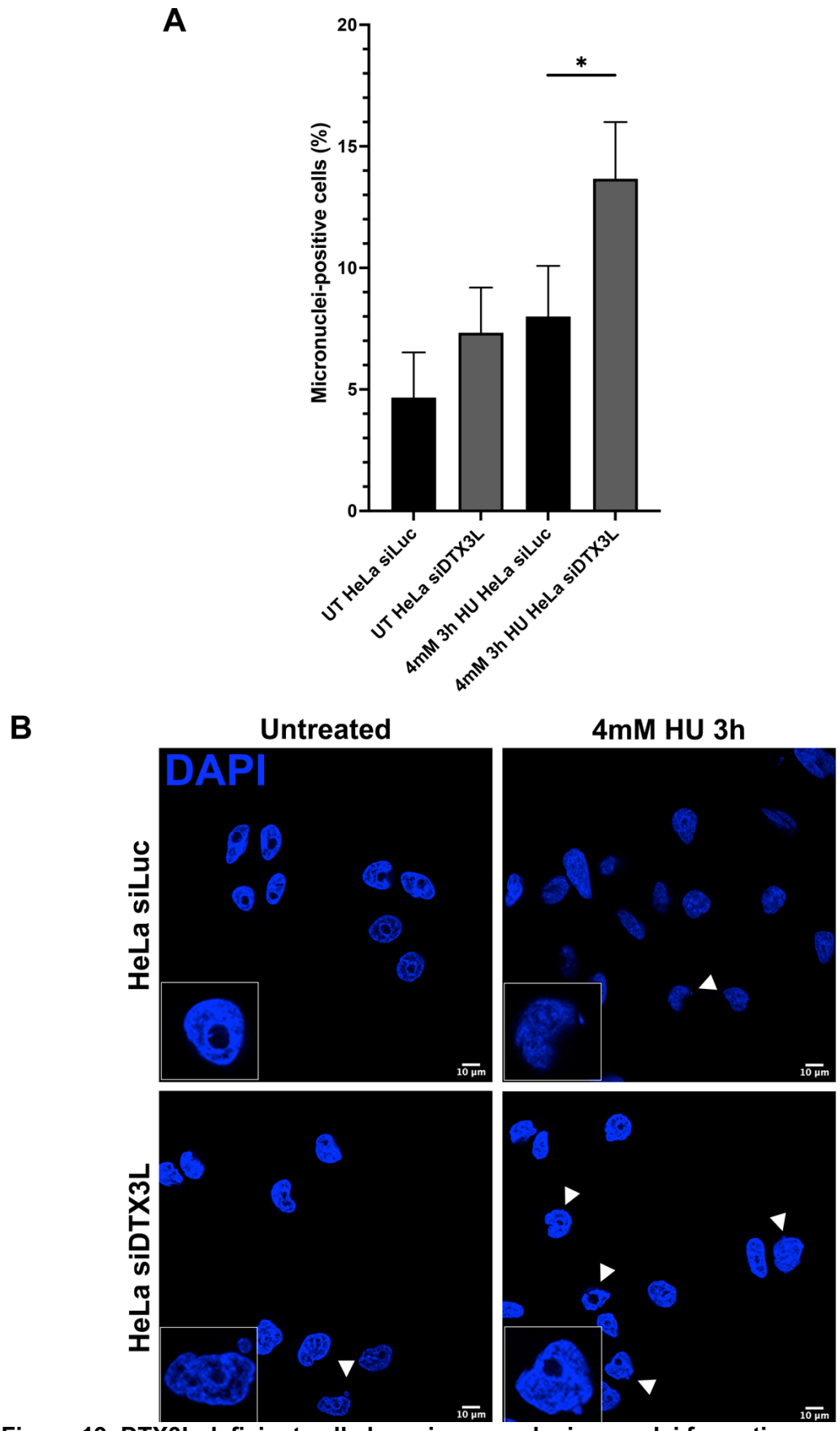

Figure 19. DTX3L deficient cells have increased micronuclei formation.

A) *Percentage of cells with associated micronuclei (mean ± SEM, from three independent experiments. Analysed by Chi-square, * = P = 0.0214).* ***B)*** *Representative images. White scale bar is 10μm in length. Micronuclei are indicated by white arrows, with representative nuclei enlarged in white boxes.*

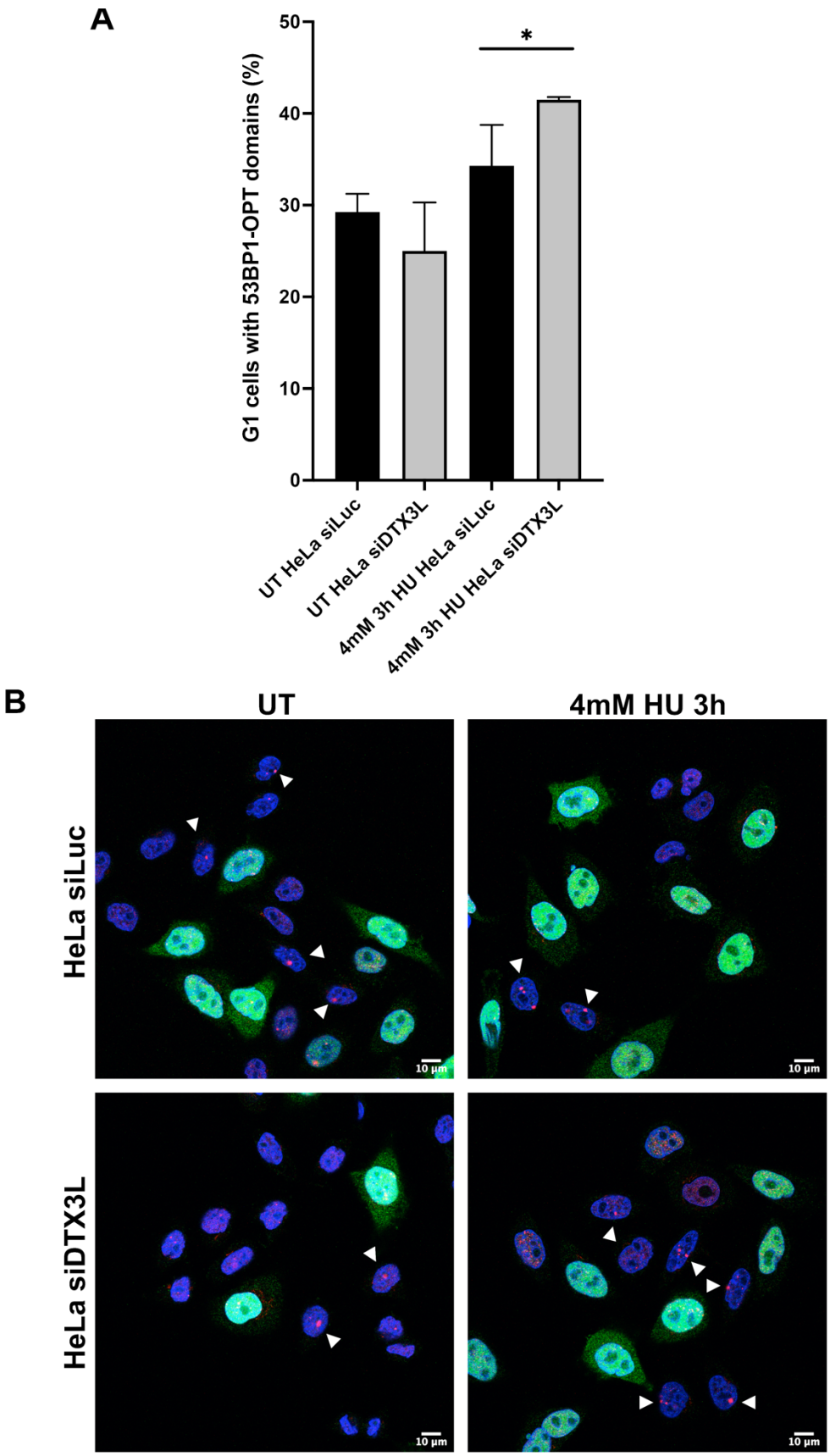

Figure 20. DTX3L depletion results in increased frequency of OPT domains.

A*) Quantification of HeLa cells in G1, as indicated by an absence of cyclin-A, with 53BP1-OPT domains (mean ± SEM, from three independent experiments. Analysed by Chi-square, * = P = 0.0164).* ***B)*** *Representative images, where OPT domain containing G1 cells are indicated by white arrows. White scale bars are 10µm.*

4.1.2. RPA Foci Formation is Increased in HeLa and U2OS Cells Deficient for DTX3L

Prolonged replication fork stalling can lead to replication fork collapse and the resultant formation of a one-ended DSB. Consequentially, forks that are not able to stabilise and resume replication are prone to degradation, leading to the formation of ssDNA that must then be protected through the binding of RPA. RPA coated ssDNA is also formed at stalled replication forks through the uncoupling of the DNA helicase and polymerase components (Nam & Cortez, 2011). To investigate the formation of ssDNA as a result of DTX3L depletion and to validate fork phenotypes further, quantification of nuclear RPA foci through immunofluorescent staining was performed.

In unchallenged cells, a significant increase in RPA intensity was observed in the U2OS cells, but not in HeLa cells (**Figure *21***). This could be attributed to cell-line difference in the ability to tolerate replication stress in the absence of DTX3L. Interestingly however, in both cell lines with mild HU treatment (1mM for 1h), a significant increase was observed in RPA intensity in those depleted for DTX3L, suggesting an increased deposition of RPA at DNA.

Low dose (1mM HU treatment for 1h) is likely to induce fork stalling, but should not predominantly induce collapse of stalled replication forks (Bétous et al., 2018). As a result, it is likely to be the case that the increase in RPA intensity observed arises due to ssDNA formation from fork stalling, as opposed to ssDNA formation from the DSB resection in this circumstance.

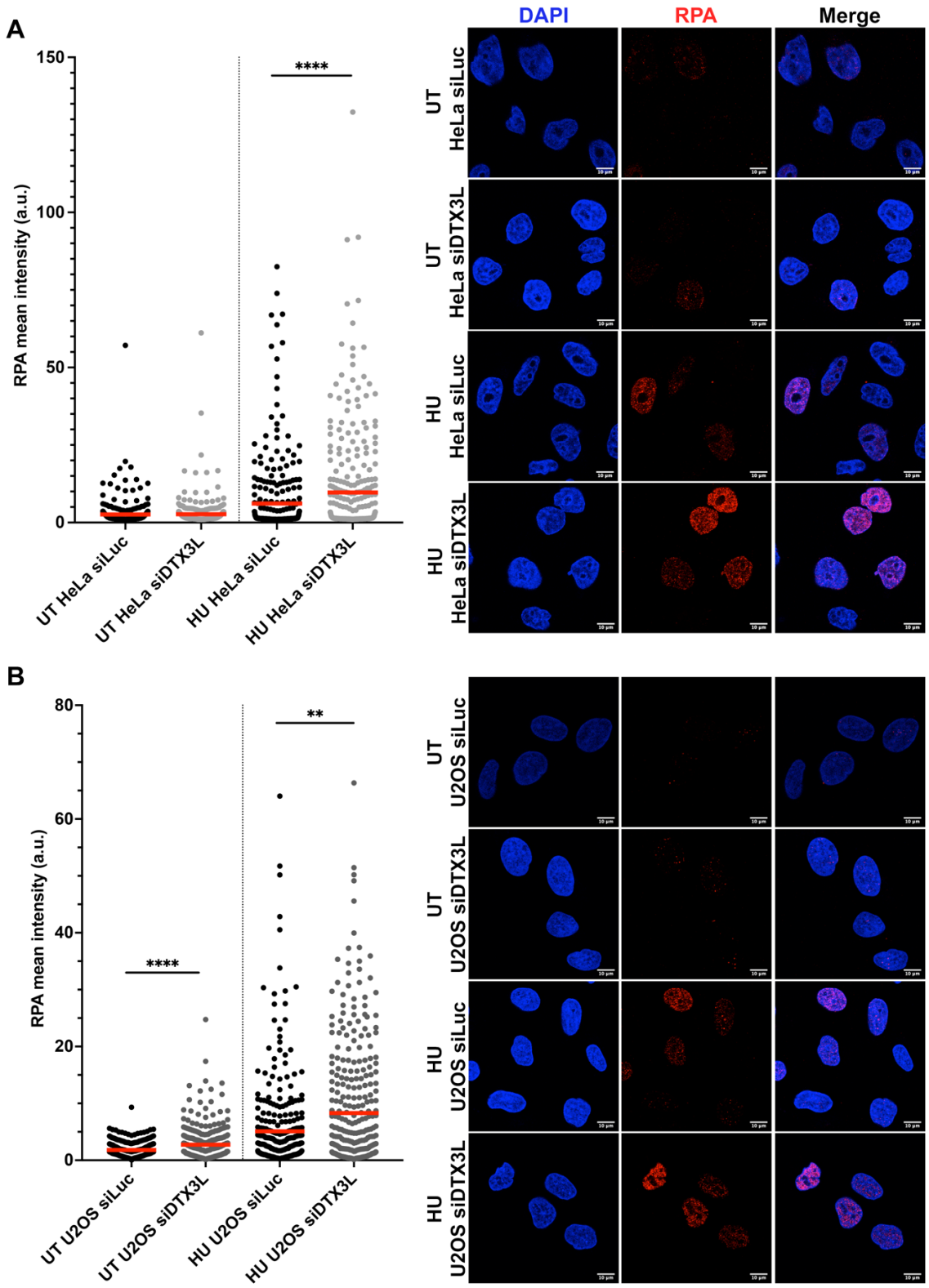

Figure 21. HeLa cells depleted for DTX3L have increased RPA foci intensity.

A) *Mean intensity of RPA in HeLa cells treated with siLuc or siDTX3L, with or without 1mM HU treatment for 1 hour (n ≥ 300 nuclei, from three independent experiments).* ***B)*** *As in* ***A****, but in U2OS cells. Mean intensity was measured by ImageJ macro. (n ≥ 300 nuclei, from three independent experiments). Red lines depict mean. Analysed by Mann-Whitney test. ** = P = 0.0021, **** = P < 0.0001. Representative images of nuclei shown; white scale bars are 10μm in length.*

4.1.3. CHK1 Phosphorylation is Reduced in HeLa Cells Upon DTX3L Silencing

In response to replication stress, the apical kinase ATR is recruited to RPA-coated ssDNA at the stalled replication fork. ATR induces a signalling cascade through phosphorylation of CHK1 on downstream substrates to regulate the replication stress response and checkpoint activation.

To investigate whether the phenotypes observed are a product of defective replication stress signalling, activation of CHK1 through phosphorylation at S345 was analysed. As expected, upon induction of replication stress by low dose (1mM) HU, CHK1 was phosphorylated at serine 345 in both siLuc and siDTX3L treated cells (**Figure *22***). Interestingly, there seemed to be a time-dependent induction of DTX3L in response to HU induced replication stress (HeLa siLuc 0min vs 60min), of which a such rapid change in protein levels suggests this is due to increased DTX3L protein stabilisation. Most notably, a significant defect in normalised CHK1-pS345 was observed, with phosphorylation in HeLa siDTX3L cells decreasing significantly to half that seen in HeLa siLuc treated cells. This could suggest defective ATR activation in response to HU induced replication stress.

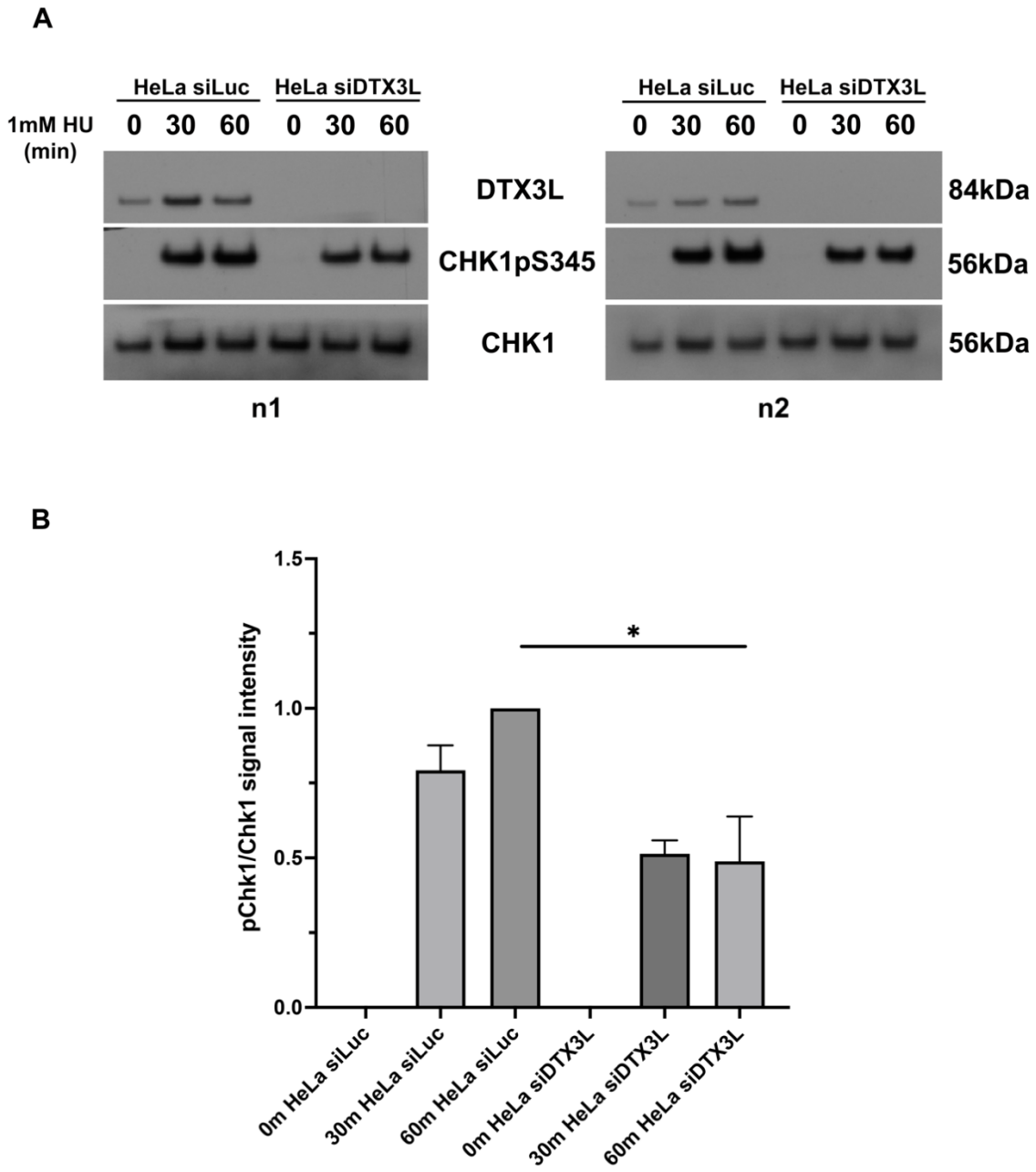

Figure 22. CHK1 phosphorylation is reduced in DTX3L depleted cells compared to controls.

A) *Two independent western blot repeats are shown. HeLa whole cell lysates (20μg) were treated with siLuc or siDTX3L and treated 1mM HU for the indicated durations before harvesting.* ***B)*** *Quantification of CHK1-pS345p, normalised to total CHK1 (Two independent repeats. Quantification analysed by two tailed, unpaired t-test. * = P < 0.05).*

4.1.4. DTX3L Depletion Leads to Increased DNA Damage Foci Formation Upon Ionising Radiation

Given the previously identified role of DTX3L in the DNA damage response, ionising radiation (IR) was used to investigate the effect of DTX3L depletion on the DSBR to see whether a similar increase in DNA damage burden was observed upon depletion of DTX3L (Yan et al., 2009, 2013). As previously described, RAD51 has a major role in HR repair of DSBR and phosphorylation of H2AX at serine 139 (γH2AX) is considered to be a surrogate marker of DNA damage induction and early repair response (Sharma et al., 2012).

Following siRNA treatment, HeLa cells were subsequently treated with 10Gy IR followed by a 6hr recovery period to permit foci formation. Cells depleted for DTX3L showed no significant difference in the incidence of RAD51 foci formation (**Figure *23***).

Interestingly, depletion of DTX3L was found to significantly increase the γH2AX signal observed compared to control siRNA treated cells, suggesting an increased incidence of DNA damage arising from DSB formation in its absence (**Figure *24***).

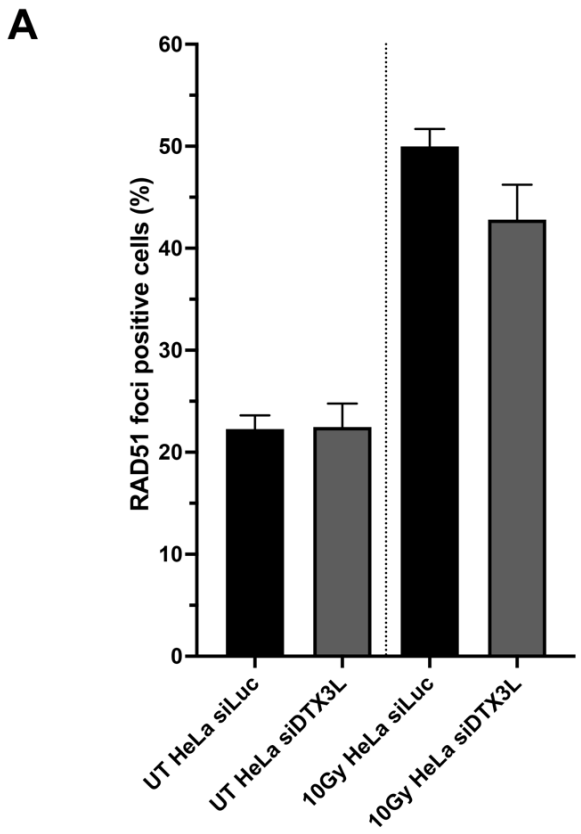

Figure 23. Quantification of cells positive for RAD51 foci following 10Gy IR.

A*) HeLa cells treated with siLuc or siDTX3L were then treated with 10Gy IR, followed by 6h recovery. Cells containing >6 distinct foci were deemed positive. (Mean ± SEM, from three independent experiments).* ***B)*** (Next page) *Representative images, RAD51-foci positive cells are circled in white. White scale bars are 10μm.*

(Landscape)

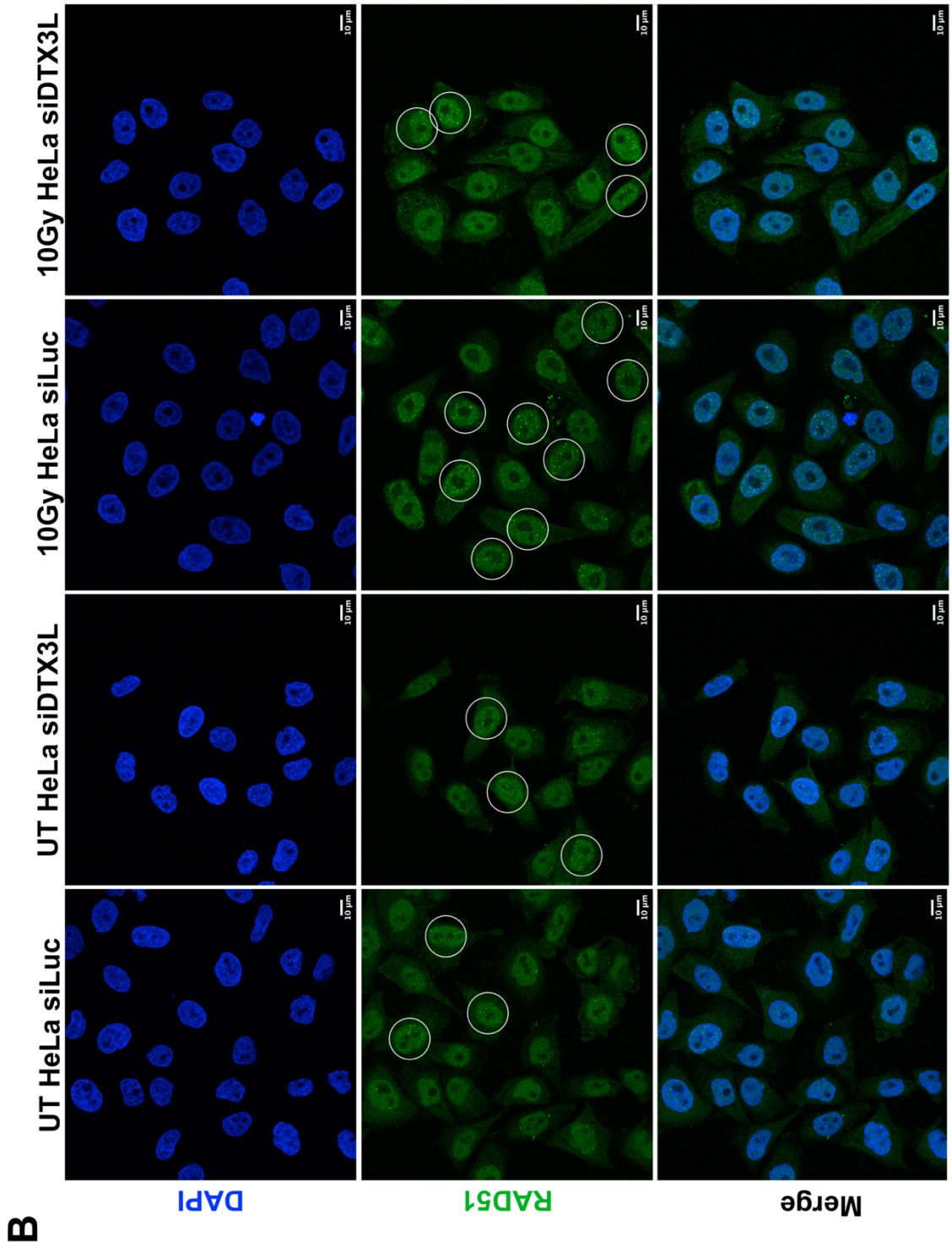
B
UT HeLa siLuc
UT HeLa siDTX3L
10Gy HeLa siLuc
10Gy HeLa siDTX3L
DAPI
RAD51
Merge

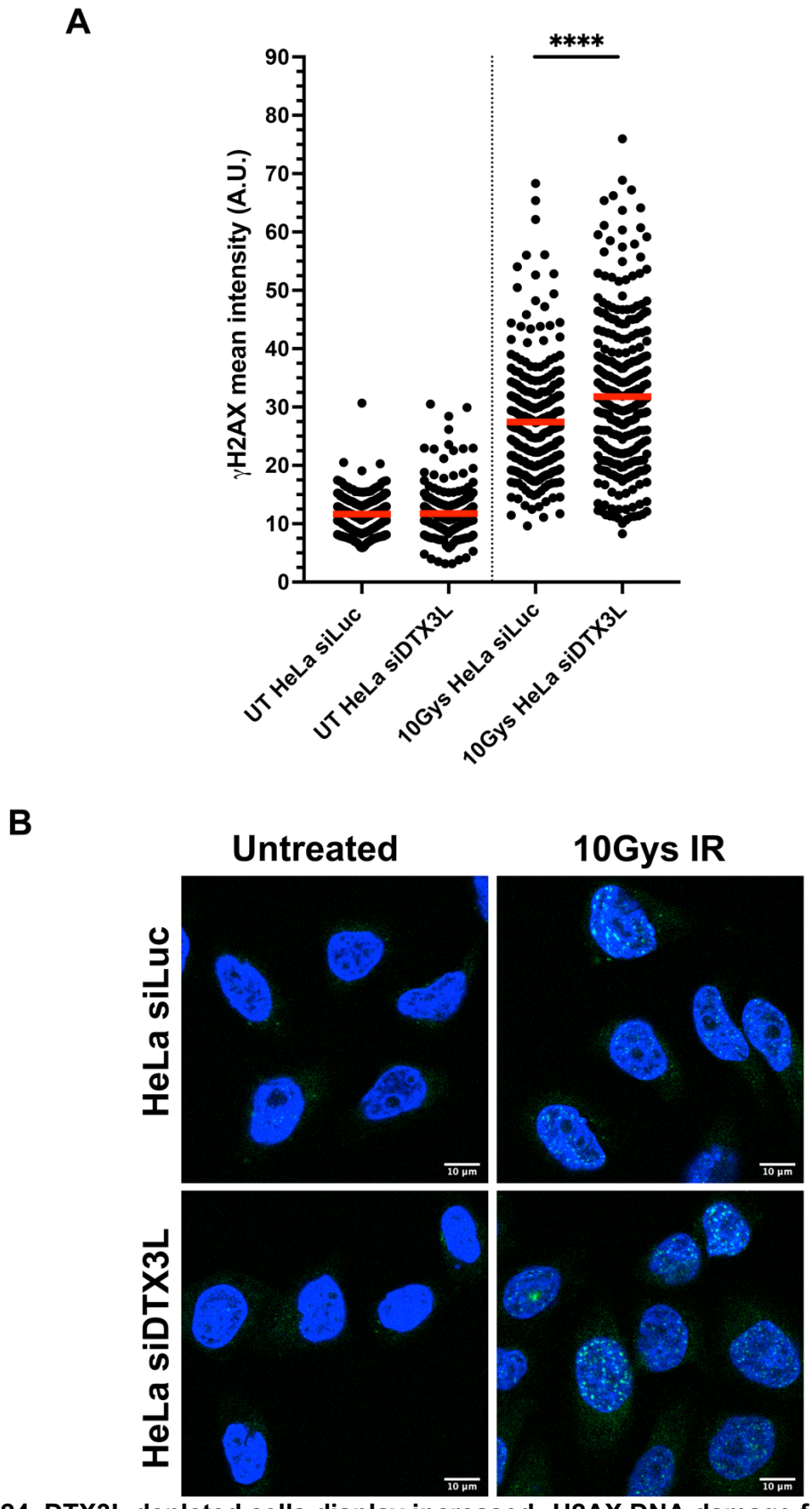

Figure 24. DTX3L depleted cells display increased γH2AX DNA damage foci upon IR treatment.

A) *Mean γH2AX intensity obtained from immunofluorescent staining. HeLa cells treated with siLuc or siDTX3L were then treated with 10Gy IR where indicated, followed by 6h recovery. Mean intensity was acquired by ImageJ macro ($n \geq 260$ nuclei from three independent experiments. Analysed by Mann-Whitney, **** = $P < 0.0001$.)*
B) *Representative images with γH2AX foci in green. White scale bars are 10μm.*

4.2. Conclusion

A reduced ability to tolerate challenges to replication results in greater genomic instability. In the previous chapter, DTX3L was identified as a novel factor contributing to the maintenance of replication and tolerance of replication stress. The data presented here suggests that, as a result of reduced stress tolerance from DTX3L deficiency, increased DNA damage arises likely through increased fork collapse and fork degradation. An increase in 53BP1 foci in untreated and HU treated conditions was observed. Correspondingly, an increase in 53BP1-OPT domains in G1 cells and an increase in micronuclei were observed suggesting incomplete DNA synthesis and genomic instability arising as a result of unrepaired DNA damage during S-phase (Harrigan et al., 2011; Luzhna et al., 2013) .

Increased RPA foci was observed in HeLa, U2OS and RPE-1 DTX3L deficient cells, likely as a result of increased ssDNA formation from DNA helicase-polymerase uncoupling and unscheduled DNA degradation arising from excessive fork regression. Furthermore, quantifying CHK1 phosphorylation in response to HU treatment revealed that DTX3L silencing results in decreased CHK1 phosphorylation, suggesting suboptimal ATR activation.

Interestingly, depletion of DTX3L was found to result in an increase in DSBs as inferred by γH2AX foci arising from IR treatment, however this may be rapidly repaired as no difference was observed in sensitivity of siDTX3L treated cells in response to zeocin treatment, observed in the previous chapter. This may suggest that the main function of DTX3L is in replication-dependent repair.

Taken together, these data indicate that the reduction in tolerance to replication stress arising as a result of DTX3L deficiency is consequential, resulting in greater DNA damage and genomic instability and supporting the enhanced sensitivity observed to clastogen treatment. The fate of the stalled replication fork is also implied, with greater DSBs and RPA coated ssDNA indicating fork collapse and degradation.

Chapter 5: Phenotypic Validation in *DTX3L*$^{-/-}$ Cells

5.1. Generation of DTX3L Deficient Cell Models by CRISPR

While siRNA technology is useful for rapid and efficient knockdown of a protein target, off-target consequences remain a concern. To validate the phenotypic consequences of DTX3L depletion observed through silencing of DTX3L, and to generate a cell model that could be taken forward for further interrogation, CRISPR-Cas9D10A nickase technology was utilised to generate DTX3L deficient cell lines.

The mutational variant D10A of Cas9 requires two guide RNAs (gRNA) to target a gene of interest; gRNA pairs introduce two single strand breaks (SSBs) in proximity on respective target strands, and the resultant double strand break (DSB) may then repaired by homology directed repair (HDR) should a repair template be present. As gene knockouts were required, no repair template was provided and the resultant break is repaired through non-homologous end joining (NHEJ). Insertions and deletions (indels) are likely to be introduced, resulting in a gene knock-out. The use of two gRNAs reduces the probability of off-target editing.

All-in-one (pAIO) plasmid constructs containing insertion sites for targeting gRNA pairs and an expression cassette for the Cas9-D10A-nickase (NK) enzyme were used. Guides targeting exon 1 of the DTX3L protein coding region were designed for abolition of all DTX3L isoforms (**Figure *25, A***). Through restriction cloning techniques, sequences encoding gRNAs were cloned into the pAIO-NK construct and incorporation verified by sequencing (see Chapter 2.2.4). Constructs were transfected into cancerous HeLa WT cells and non-cancerous RPE-1 WT cells. Multiple clones were obtained after single cell sorting and an expansion period.

Clones were screened by western blot analysis for complete abrogation of DTX3L expression (**Figure *25, B & C***).

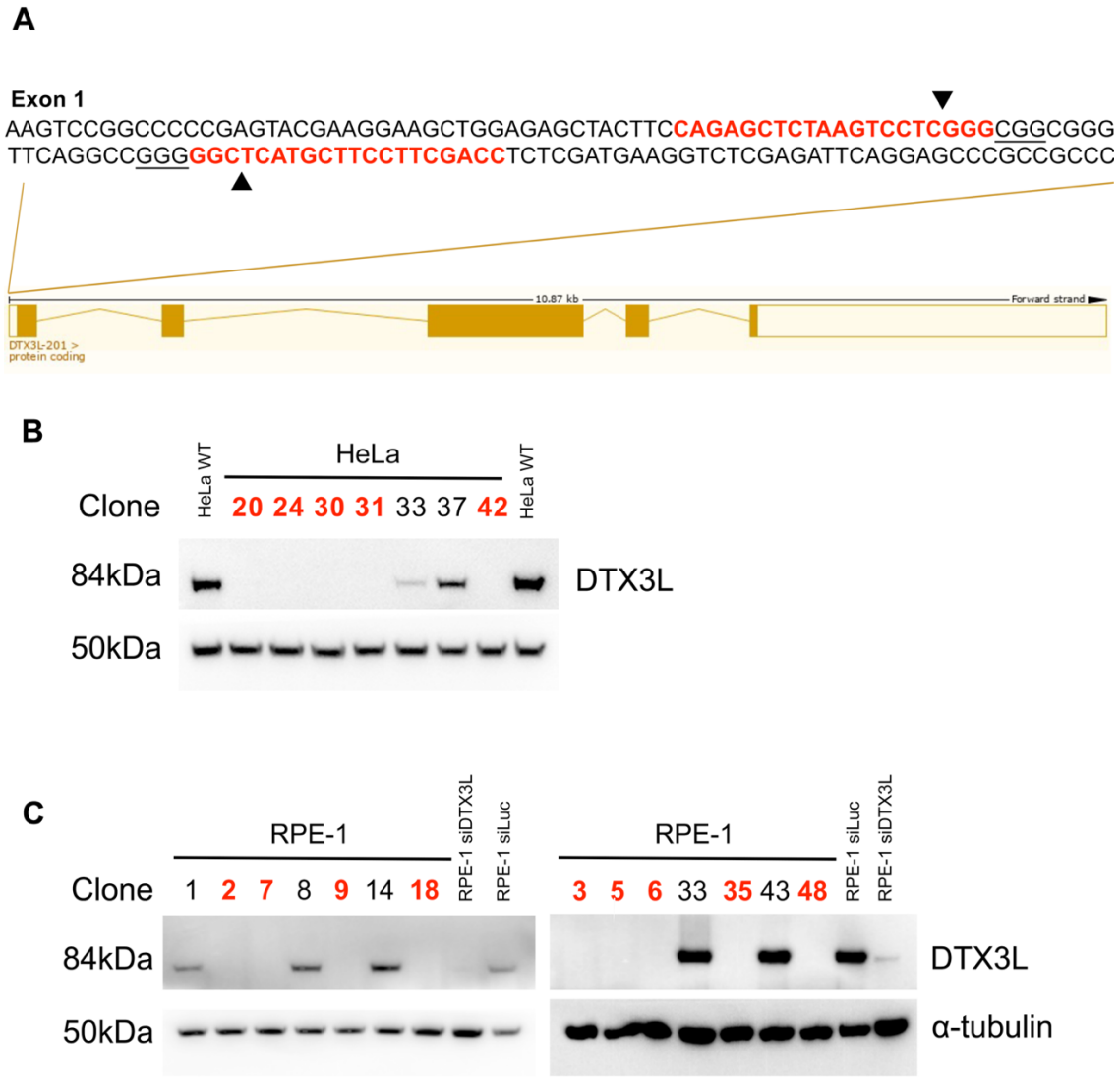

Figure 25. DTX3L knockout by CRISPR-Cas9 transfection is successful in HeLa and RPE-1 cells.

A) *Nucleotides highlighted in red indicate target sequences of the gRNA pair, located in exon 1 of the DTX3L protein coding region, with exon map below. Arrows indicate predicted cut sites. Whole cell lysate from* ***B)*** *HeLa clones, with HeLa WT as negative control and* ***C)*** *RPE-1 clones, with RPE-1 siLuc negative control and RPE-1 siDTX3L positive control for DTX3L depletion, were analysed by western blot for DTX3L expression. Putative positive clones in red. α-tubulin serves as loading control.*

5.1.1. Characterisation of *DTX3L*$^{-/-}$ HeLa & RPE-1 Cells by DNA Fibre Analysis

To validate the phenotypes observed in HeLa WT cells upon silencing of DTX3L, and to establish my CRISPR knock-out clones as *bona-fide* cell models for DTX3L deficiency through replication of these phenotypes, the DNA fibre assay was employed. As numerous knock-out clones were identified by western blot, a subselection of these were used for preliminary DNA fibre phenotypic analysis. Previously, it was shown that knockdown of DTX3L lead to a decreased tolerance to replication stress; increased fork asymmetry was observed for replicating sister fork pairs, an increase in fork stalling and fork resection was observed in conditions of exogenous replication stress, and the ability for forks to recover was impaired after replication challenge in comparison to wild-type cells. As DTX3L silencing produced the most severe defect in fork stalling and fork resection phenotypes, I focused on these two assays going forward.

Compared to HeLa WT cells, all positive HeLa *DTX3L*$^{-/-}$ clones displayed a reduced CldU/IdU ratio when HU was included in the second nucleoside analogue labelling pulse (**Figure *26***). Wild-type cells retain some capacity to overcome the challenge to replication introduced by HU, however replication is still impeded with a CldU/IdU ratio of around 0.45. In the absence of DTX3L, this falls to as low as 0.25 (clone 30), with a decrease observed in all tested clones, 0.35 ratio maximum (clone 24).

In a different replication scenario, following labelling pulses with treatment of high dose 4mM HU for 4h, HeLa WT cells are unaffected with CldU/IdU ratio of 1. DTX3L deficient clones produce a ratio of almost half that seen in WT, between 0.6 and 0.7. These decreases observed in respective CldU/IdU ratios is similar

to what was observed previously upon DTX3L silencing, indicating that these phenotypes are due to the loss of DTX3L.

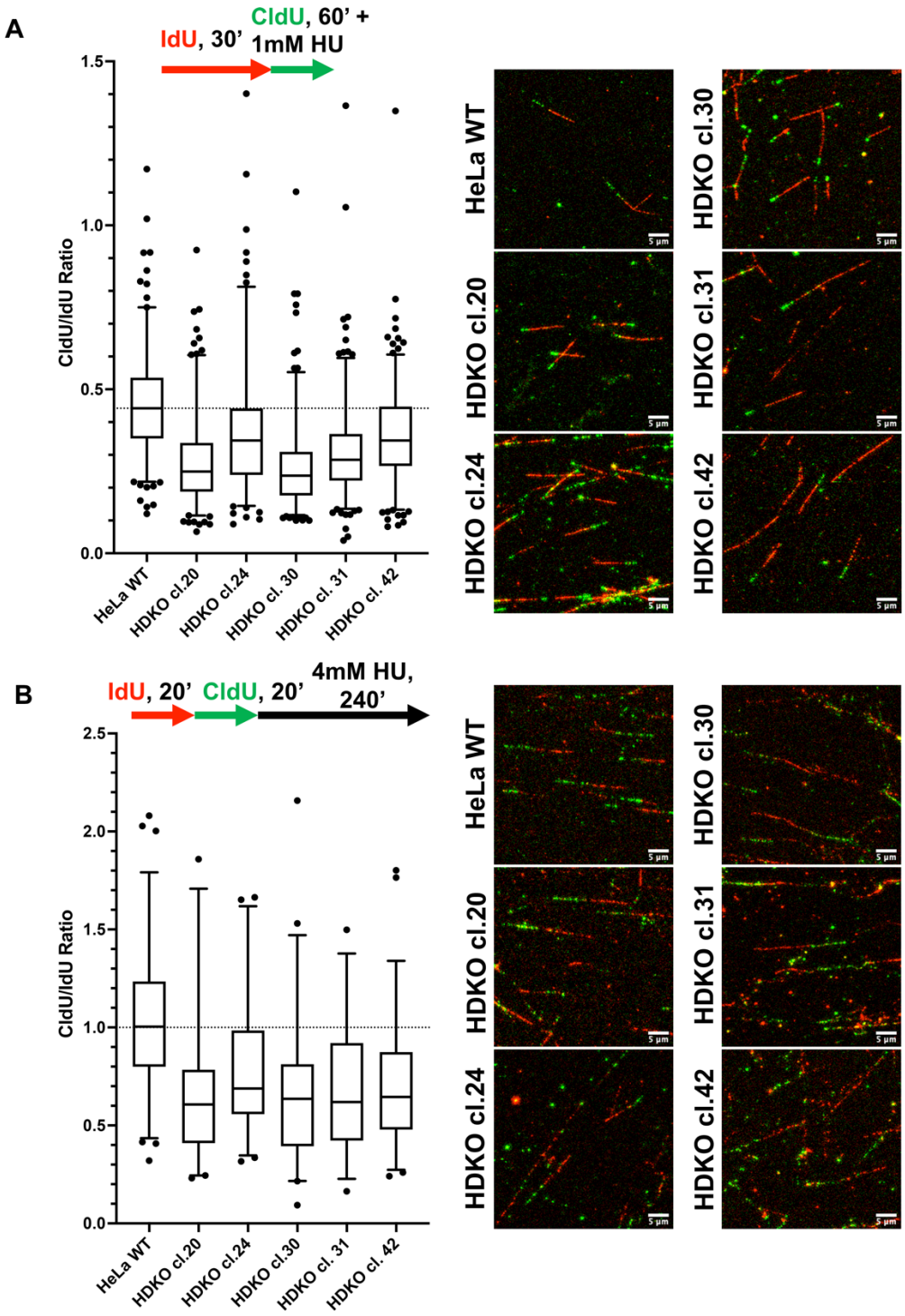

Figure 26. Preliminary DNA fibre analysis of *DTX3L*$^{-/-}$ clones shows replication stress phenotypes.

CldU/IdU tract ratios from HeLa cells selected as DTX3L$^{-/-}$ *clones by western blot analysis.* ***A)*** *Cells were pulsed with IdU for 30min, before treatment with 1mM HU during the second CldU pulse for 60 mins (5*th*-95*th *percentile, n ≥ 150 tracts from two independent experiments).* ***B)*** *Cells were pulsed with IdU for 20 mins, then CldU for 20 mins before treatment with 4mM HU for 240mins. (5*th*-95*th *percentile, n ≥ 30 tracts from one experiment). White scale bars are 5μm.*

Two clones (denoted HDKO clone 20 and HDKO clone 24) were taken forward for further repeats to establish significance of the differences observed in ratios between HeLa WT and *DTX3L*$^{-/-}$ cells.

The trend observed in the preliminary experiment was robust and observed in subsequent repeats. Upon addition of 1mM HU during the 60min CldU pulse, a ratio of 0.42 was observed for HeLa WT cells, compared to 0.24 for HDKO clone 20 and 0.32 for *DTX3L*$^{-/-}$ clone 24 (**Figure *27, A***).

In the second replication scenario where cells were treated with 4mM HU for 240mins, again a robust decrease in CldU/IdU ratio was observed. HeLa WT cells produced a ratio of 0.87 compared to 0.57 in *DTX3L*$^{-/-}$ clone 20 and 0.66 in *DTX3L*$^{-/-}$ clone 24 (**Figure *27, B***).

As HeLa cells are a cellular model for cancer, I wanted to see whether these phenotypes were also conserved in a non-cancer cell model, as well as in an alternative cell model. To this end, the CRISPR plasmid construct targeting DTX3L was utilised in RPE-1 WT cells, and once again clones were selected for interrogation with the DNA fibre technique. Similarly to HeLa *DTX3L*$^{-/-}$ clones, a decrease in CldU/IdU ratio was observed in RPE-1 *DTX3L*$^{-/-}$ cells suggesting a defective RSR (***Figure 28***).

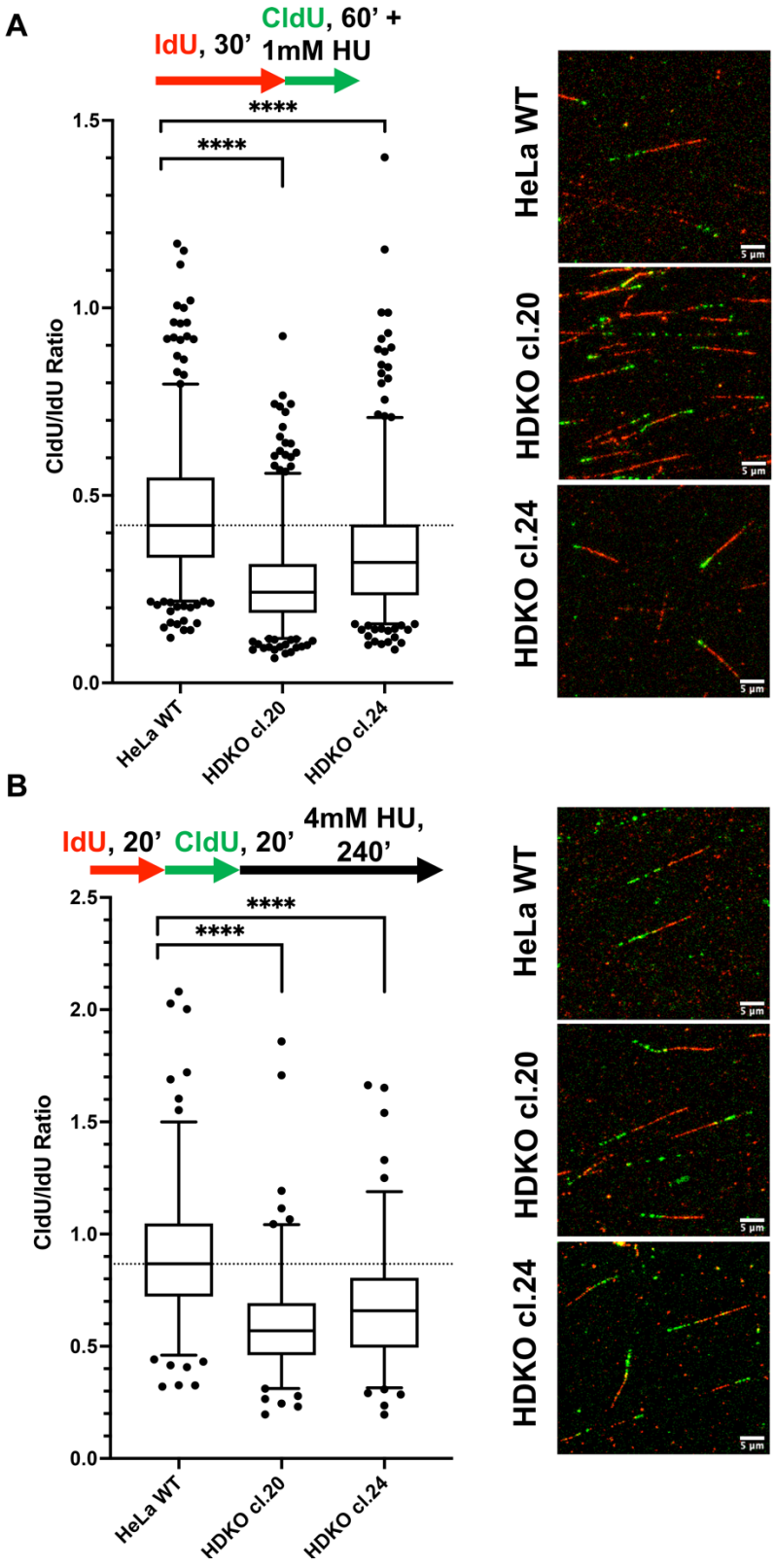

Figure 27. DNA fibre analysis of specific HeLa *DTX3L*$^{-/-}$ clones validates replication stress phenotypes.

CldU/IdU tract ratios from HeLa DTX3L$^{-/-}$ clones. ***A)*** *Cells were pulsed with IdU for 30min, before treatment with 1mM HU during the second CldU pulse for 60 mins (5th-95th percentile, n ≥ 360 tracts from four independent experiments. Analysed by Mann-Whitney, **** = P < 0.0001).* ***B)*** *Cells were pulsed with IdU for 20 mins, then CldU for 20 mins before treatment with 4mM HU for 240mins (5th-95th percentile, n ≥ 115 tracts from two independent experiments. Analysed by Mann-Whitney, **** = P < 0.0001).*

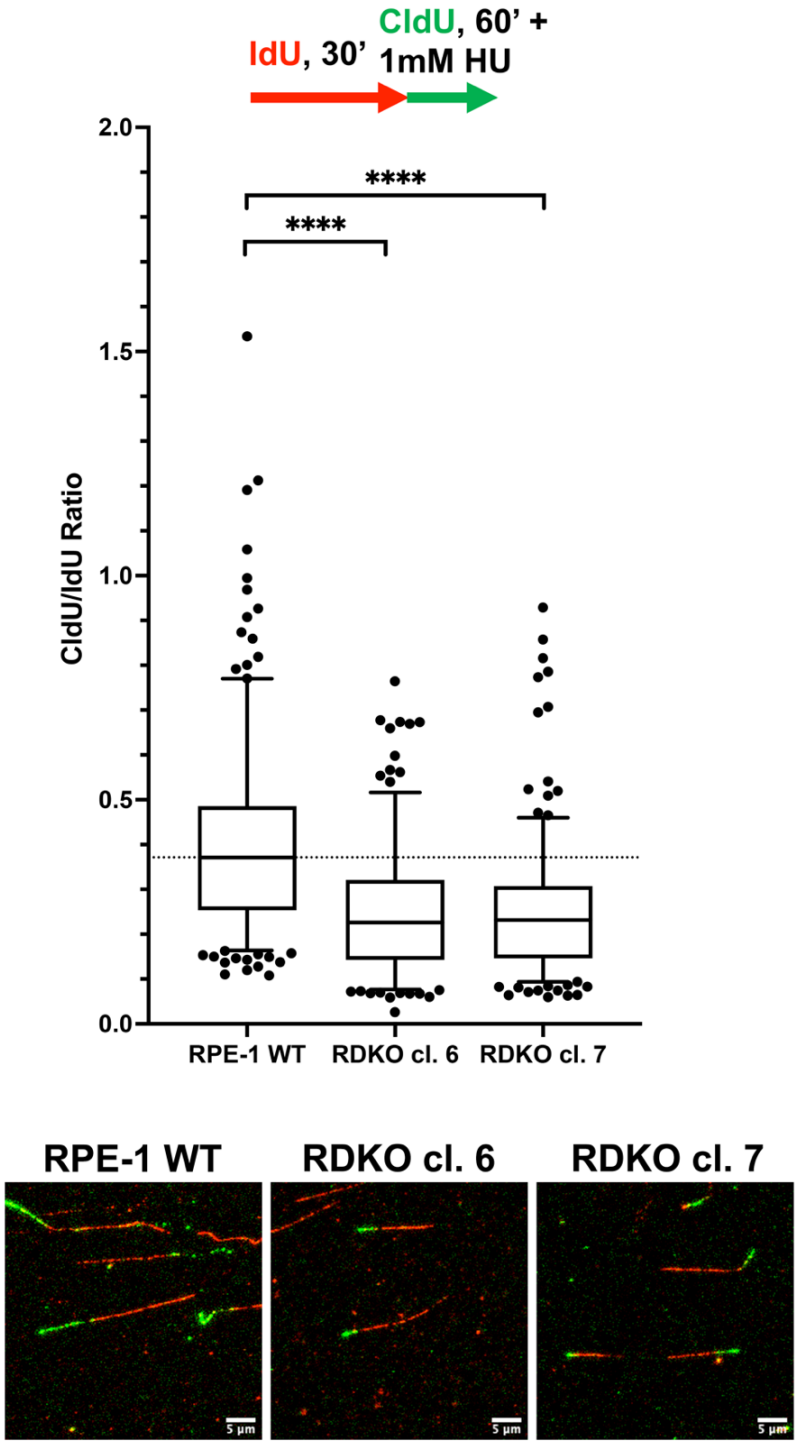

Figure 28. RPE-1 *DTX3L*$^{-/-}$ cells exhibit increased fork stalling.

*CldU/IdU tract ratios from RPE-1 cells, selected as DTX3L knockout clones by western blot analysis. Cells were pulsed with IdU for 30min, before treatment with 1mM HU during the second CldU pulse for 60 mins (5th-95th percentile, n ≥ 228 tracts from three independent experiments. Analysed by Mann-Whitney, **** = P < 0.0001). Representative images of DNA fibres; white scale bars are 5µm.*

5.1.2. HeLa *DTX3L*$^{-/-}$ cells exhibit enhanced clastogen sensitivity

The sensitivity of *DTX3L*$^{-/-}$ cells to clastogen treatment was analysed. To validate the enhanced sensitivity previously observed upon DTX3L silencing in HeLa cells, *DTX3L*$^{-/-}$ sensitivity to cisplatin and gemcitabine was investigated.

Similarly to siDTX3L treated cells, in *DTX3L*$^{-/-}$ cells there was a marked increase in sensitivity to cisplatin compared to WT cells (**Figure *29, A***). HeLa WT cells exhibited an IC_{50} of 0.193μM compared to HDKO clone 20 and clone 24 with IC_{50}s of 0.110μM and 0.055μM respectively.

In a similar fashion, testing gemcitabine sensitivity, HeLa WT cells demonstrated an IC_{50} of 7.29nM compared to 5.95nM and 4.65nM in HDKO clone 20 and clone 24 respectively, indicating an increased sensitivity to gemcitabine in *DTX3L*$^{-/-}$ cells (**Figure *29, B***).

To further characterise the sensitivity of HeLa *DTX3L*$^{-/-}$ cells to replication stress inducing drugs, I then tested an inhibitor of DNA replication aphidicolin. Aphidicolin is a specific inhibitor of DNA polymerase alpha and delta, polymerases crucial for DNA replication. HeLa WT cells demonstrated an IC_{50} of 0.163μM whereas the IC_{50} for DTX3L knockout cells fell by a third with IC_{50}s of 0.108μM and 0.096μM respectively (**Figure *29, C***). Again, this suggests that DTX3L is important for tolerance to challenges to replication.

Finally, I also investigated cell sensitivity to camptothecin. Camptothecin is a topoisomerase I (topo-I) inhibitor that leads to the formation of a covalently bound ternary protein-DNA complex that prevents the re-ligation step after topo-I

cleavage. This leads to collisions between elongating replication forks and the complex, resulting in S-phase specific DNA damage.

This time, only one *DTX3L*$^{-/-}$ clone exhibited a marked difference in sensitivity compared to WT cells (**Figure *29, D***). HeLa WT had an IC_{50} of 6.18nM compared to HDKO clone 20 with an IC_{50} of 5.91nM and clone 24 with an IC_{50} of 3.70nM. The difference observed here between clones could be due to clonal differences within the genetic background of the cells, may be due to a greater effect of experimental variation as these results are only from two experimental repeats, or could simply be a result of the fact that clone 20 is consistently less sensitive to drug treatment as seen from the graphs shown previously. Any increase in sensitivity to camptothecin may therefore be relatively subtle in this clone.

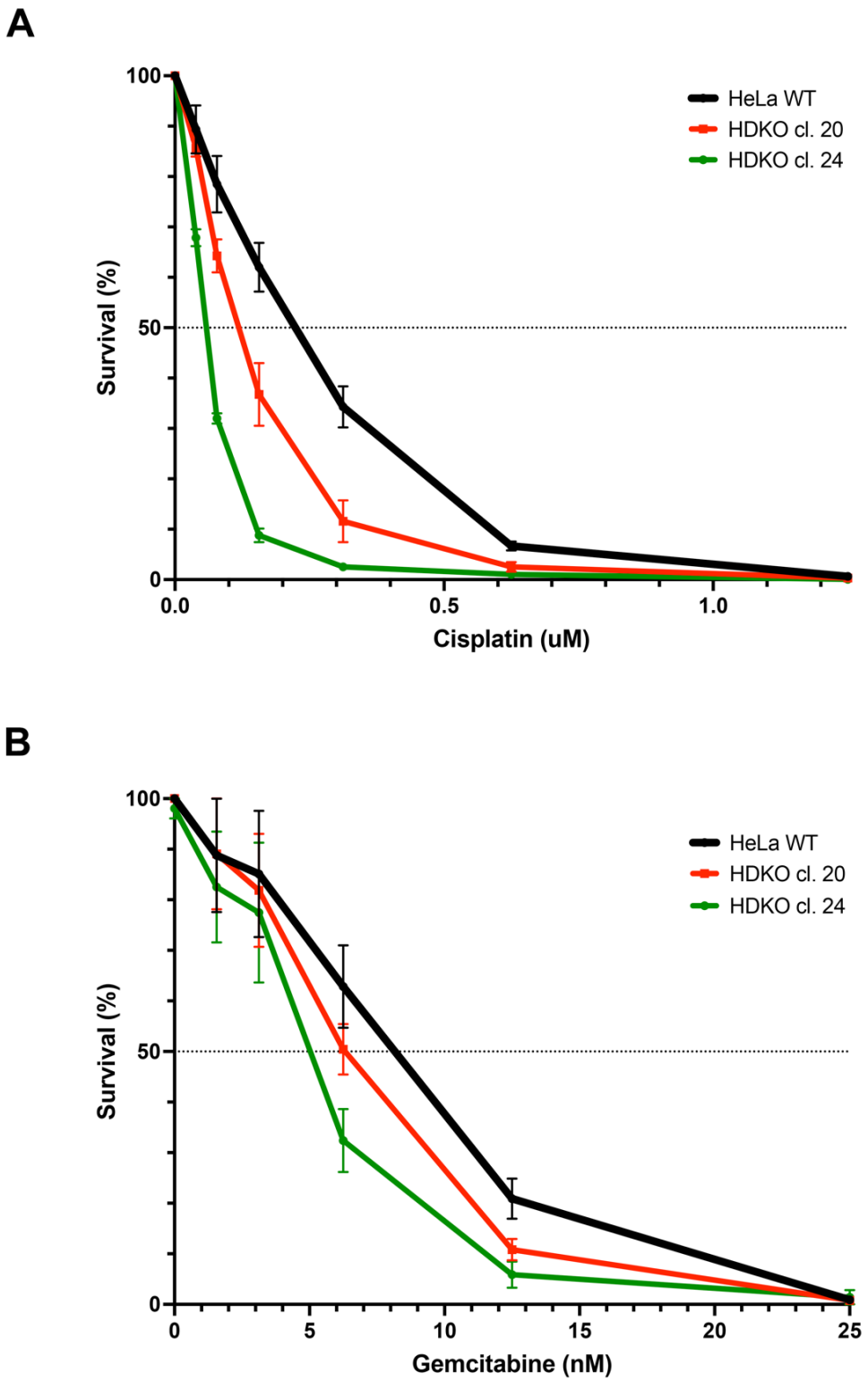

Figure 29. HeLa *DTX3L*$^{-/-}$ cells are more sensitive than wild-type to replication stress inducing drug treatments.

*Drug sensitivity to **A)** cisplatin **B)** gemcitabine **C)** aphidicolin **D)** camptothecin. HeLa WT or HeLa DTX3L$^{-/-}$ cells were treated continuously with a range of drug doses and left to grow for one week. Proportion of surviving cells compared to untreated cells was determined by alamar blue cell proliferation assay (Mean ± SEM from three independent experiments, except **D** from two independent experiments).*

C

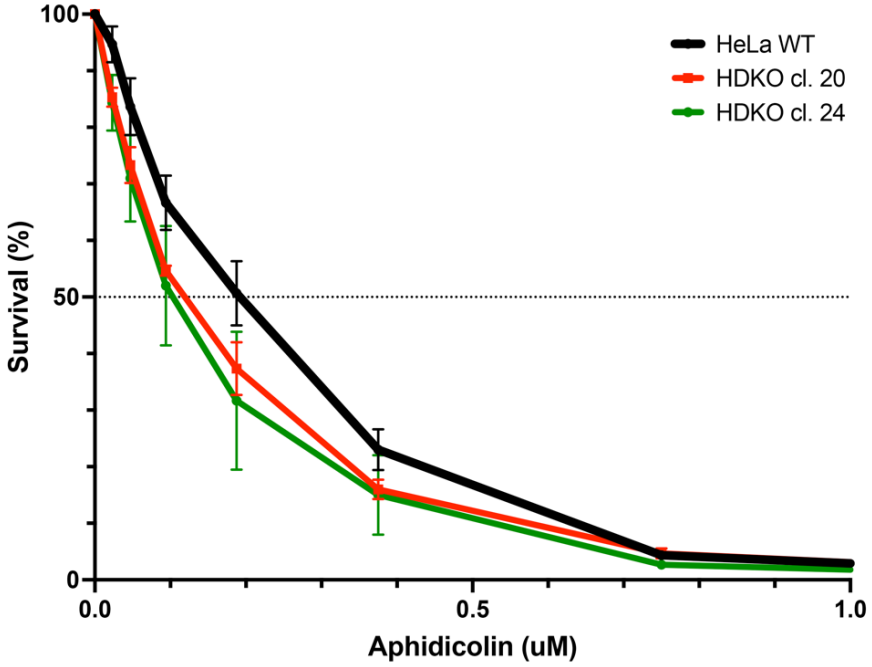
100
50
0
Survival (%)
0.0
0.5
1.0
Aphidicolin (uM)
HeLa WT
HDKO cl. 20
HDKO cl. 24

D

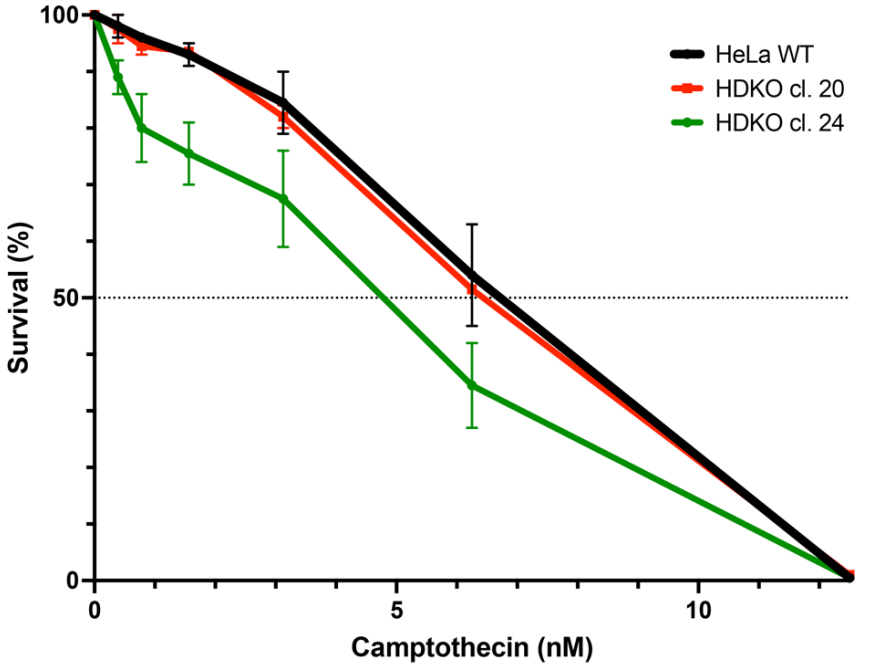
100
50
0
Survival (%)
0
5
10
Camptothecin (nM)
HeLa WT
HDKO cl. 20
HDKO cl. 24

5.1.3. HeLa *DTX3L*$^{-/-}$ cells exhibit reduced proliferation but unimpeded cell cycle progression

To validate the cell proliferation defect seen in HeLa cells silenced for DTX3L, *DTX3L*$^{-/-}$ cells were also analysed by cell proliferation assay. Similarly, a reduction of 10% was observed in the normalised metabolic rate between HeLa WT and *DTX3L*$^{-/-}$ clones by day 5, suggesting a reduced rate of proliferation in cells depleted for DTX3L (**Figure *30***).

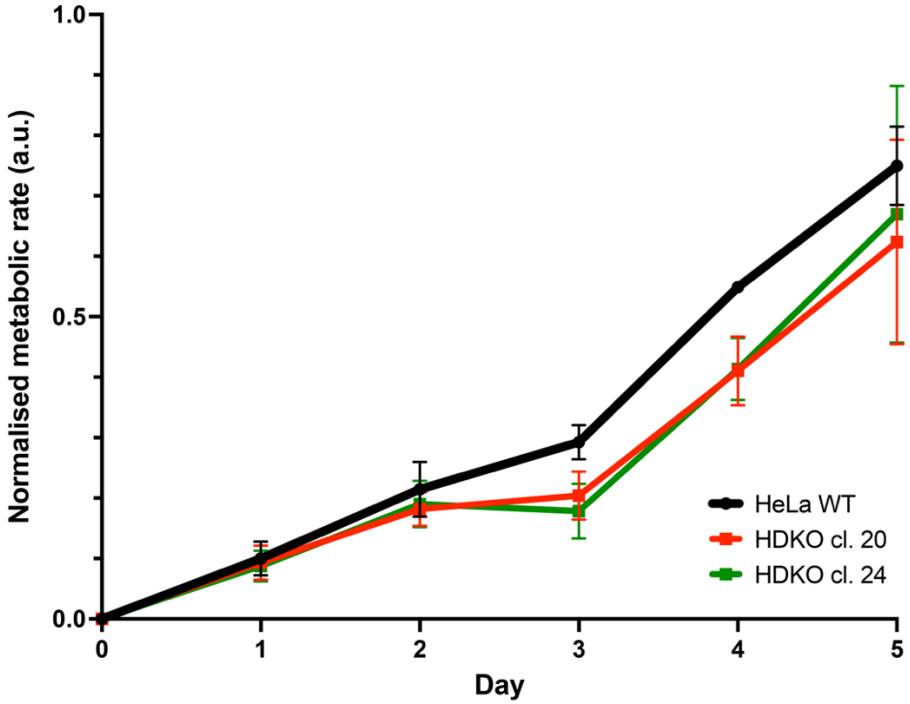

Figure 30. Cell proliferation is reduced in *DTX3L*$^{-/-}$ cells.

Alamar blue assay measuring cell proliferation in HeLa WT cells compared to HeLa DTX3L$^{-/-}$ *clones (Mean ± SEM from two independent experiments).*

Given the reduced rate of proliferation, it was important to investigate the cell cycle profile of these cells. Cell cycle analysis through the use of DNA staining with propidium iodide and fluorescence activated cell sorting (FACS) revealed little difference in the cell cycle profile of HeLa *DTX3L*$^{-/-}$ cells compared to WT (**Figure *31***).

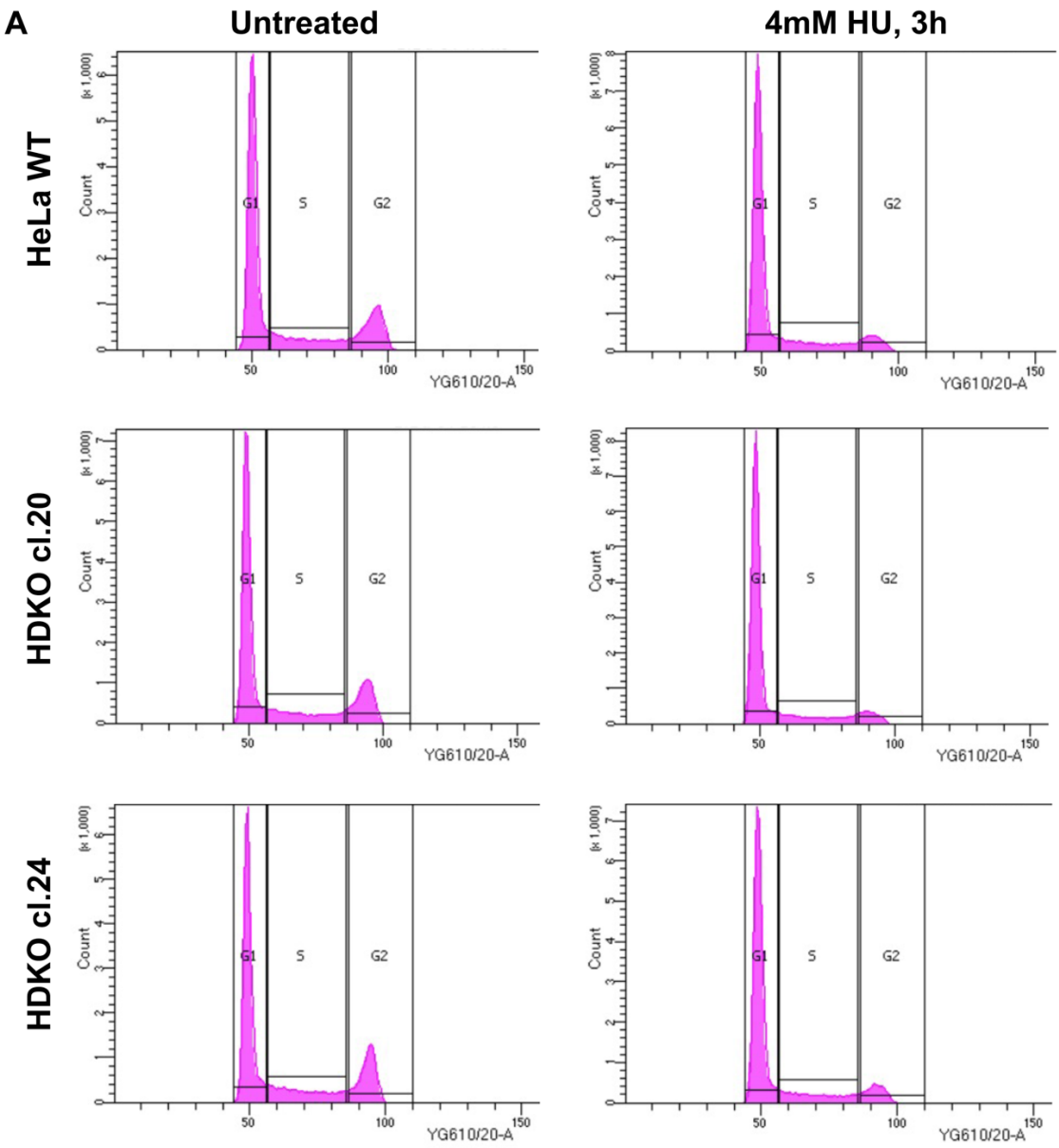

B

	G0/G1 (%)	S (%)	G2/M (%)
N1			
UT HeLa WT	59.0	18.9	18.8
UT HDKO20	60.2	17.1	19.8
UT HDKO24	55.4	19.6	21.7
4mM HU HeLa WT	71.8	16.4	9.1
4mM HU HDKO20	72.8	16.3	9.1
4mM HU HDKO24	68.7	17.6	11
N2			
UT HeLa WT	58.6	17.8	20.2
UT HDKO20	59.8	17.6	20
UT HDKO24	55.7	19.5	21.4
4mM HU HeLa WT	71.3	16.6	9.2
4mM HU HDKO20	73.2	16.1	8.1
4mM HU HDKO24	70.5	16	10.5

Figure 31. Loss of DTX3L does not cause changes in cell cycle profile.

A) *Cytometer plots showing propidium iodide fluorescence (x-axis) vs cell count (y-axis).* ***B)*** *Table showing proportion of cells in each cell cycle phase.*

5.1.4. HeLa and RPE-1 *DTX3L*$^{-/-}$ cells have increased RPA foci formation

To further validate the HeLa and RPE-1 *DTX3L*$^{-/-}$ clones and the replication stress phenotypes observed in DTX3L deficient cells, RPA foci quantification was analysed in clone 20 and clone 24. This time, a higher dose of HU was utilised to assess RPA foci formation under conditions likely to induce fork collapse.

HeLa WT cells were either left untreated or treated with 4mM HU for 3 hours prior to fixation. In WT cells, a robust induction of RPA foci was induced upon HU treatment, with the mean RPA intensity increasing four-fold from 5.77 to 19.41 (arbitrary units). In HeLa *DTX3L*$^{-/-}$ clones, this increase of RPA foci was even greater, with a five-fold induction from 6.10 to 31.83 and nine-fold of 5.27 to 44.92 in HDKO clone 20 and HDKO clone 24 respectively (**Figure *32, A***). A similar trend was seen in RPE-1 *DTX3L*$^{-/-}$ clones where RPA foci intensity was significantly greater compared to RPE-1 WT in HU treated conditions, from 0.05 to 0.08 (**Figure *32, B***).

Greater mean RPA intensity in cells deficient for DTX3L, as a result of 4mM HU treatment for 3 hours, in the context of reduced tolerance to replication challenges, suggests increased RPA recruitment to sites of single stranded DNA that arise through increased fork stalling and resection. In the absence of DTX3L, as replication forks are less able to tolerate these challenges, more single stranded DNA may form through fork degradation which requires stabilisation by RPA binding.

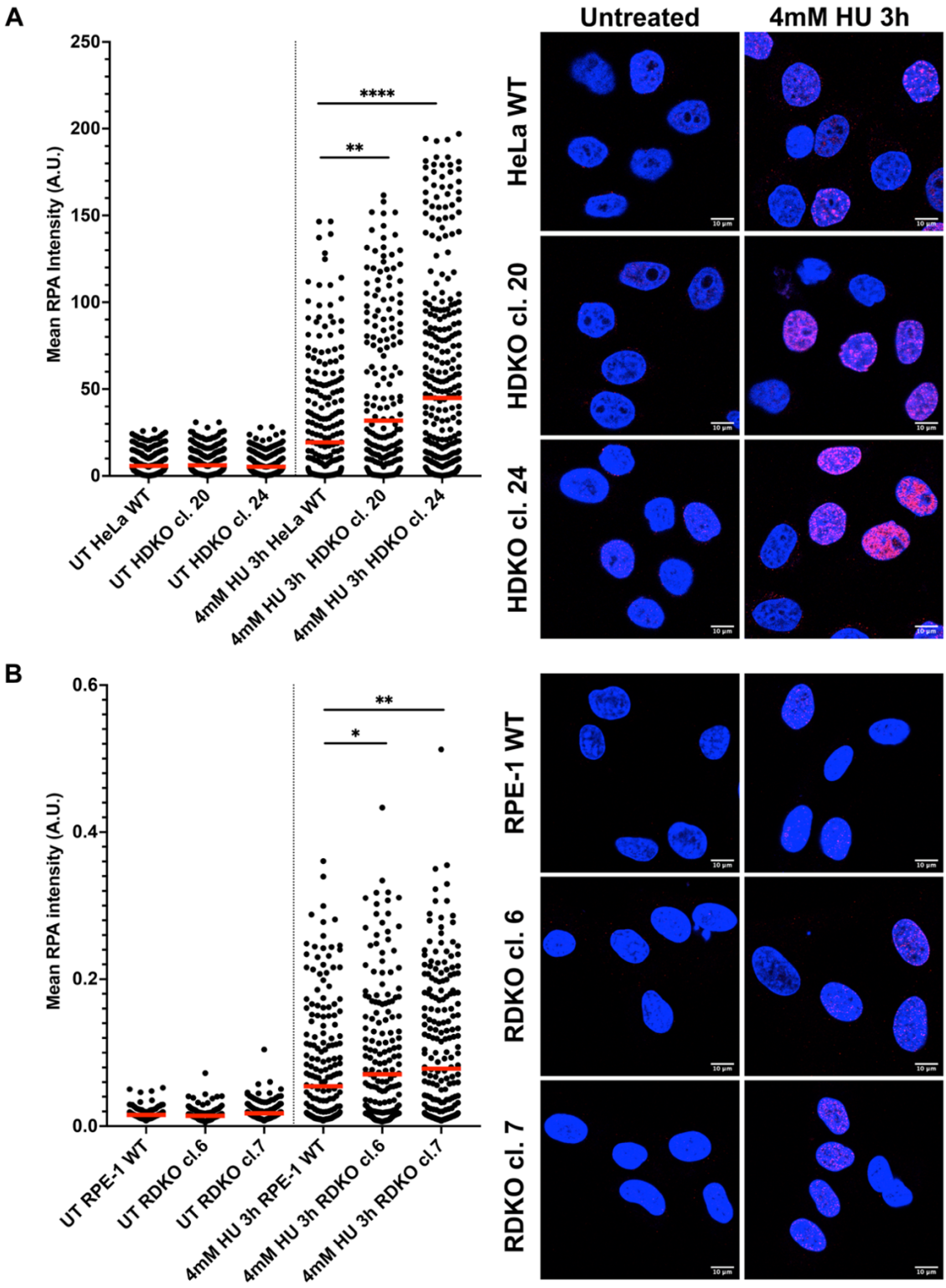

Figure 32. HeLa and RPE-1 *DTX3L*$^{-/-}$ clones exhibit an increase in RPA foci compared to WT under conditions of enhanced replication stress.

Mean RPA intensity acquired through immunofluorescent staining. WT cells or DTX3L$^{-/-}$ clones were either untreated or treated with 4mM HU for 3 hours prior to fixation. Each point represents the mean intensity per nucleus. ***A)*** *HeLa cells ($n \geq 270$ cells, from three independent experiments. Analysed by Mann-Whitney, ** = P= 0.0028, **** = P < 0.0001.).* ***B)*** *RPE-1 cells ($n \geq 252$ cells, from two independent experiments. Analysed by Mann-Whitney,* = P= 0.0497, ** = P < 0.0036). Red lines indicate mean. Representative images of nuclei shown; white scale bars are 10μm.*

5.2. Conclusion

Here, a cellular model to interrogate the role of DTX3L in the replication stress response was generated through the use of CRISPR technology. Validating the replication stress phenotypes observed in the previous chapters with siDTX3L treatment, increased replication fork stalling and defective fork regression were observed. Additionally, increased fork stalling as a result of DTX3L depletion was also observed in a non-cancer cell line, suggesting a general role of DTX3L in replication.

Clastogen sensitivity was investigated in *DTX3L*$^{-/-}$ cells, reproducing the enhanced sensitivity to cisplatin and gemcitabine seen in siDTX3L treated cells. Sensitivity to aphidicolin and camptothecin was also observed, further supporting a role for DTX3L in tolerance of challenges that lead to increased replication stress.

Furthermore, similarly to siDTX3L treated cells, reduced cellular proliferation was observed in *DTX3L*$^{-/-}$ cells compared to HeLa WT. Interestingly, no differences were observed in cell cycle distribution despite this.

Finally, RPA foci quantification in *DTX3L*$^{-/-}$ cells was investigated. In response to 4mM HU 3h treatment, *DTX3L*$^{-/-}$ cells had greater RPA foci intensity compared to WT, in both HeLa and RPE-1 cells suggesting increased formation of RPA bound ssDNA in both cancerous and non-cancerous cell lines.

Establishing consistent phenotypic behaviour of *DTX3L*$^{-/-}$, these cells are taken forward for mechanistic interrogation of the role of DTX3L at the replication fork.

Chapter 6: Elucidating the Mechanistic Role of DTX3L at the Stalled Replication Fork

6.1. Complementation of HeLa *DTX3L*$^{-/-}$ Cells

From the previous two chapters, there is evidence to implicate DTX3L in the replication stress response, a novel role for this DNA damage repair associated protein. To validate the defect observed in replication fork regression upon DTX3L deficiency, I wanted to see whether the defect could be rescued by ectopic expression of WT DTX3L. Additionally, given the primary function of DTX3L as an E3 ubiquitin ligase and utilising a previously described DTX3L RING domain mutation (M2), I wanted to investigate if the ubiquitination function was crucial for the role of DTX3L at the replication fork (Tessadori et al., 2017). Furthermore, complementation has been utilised to characterise the functional outcome of patient associated mutations within DTX3L, relating DTX3L function with clinical impact.

6.1.1. Suppression of Regressed Replication Fork Degradation Requires the E3 ubiquitin ligase activity of DTX3L

To expand the toolset available for the investigation of DTX3L in the replication stress response, plasmid constructs for the introduction of FLAG tagged DTX3L protein to cells were generated. The pDEST-FLAG-DTX3L-WT construct was produced via the gateway LR cloning system as described in **Chapter 2.2.3**, using the pHAGE-N-FLAG-HA destination vector (a kind gift from Dr. R. Chapman). Upon validation of the wild-type DTX3L FLAG-tagged construct by sequencing, the WT construct was used as a plasmid template for site-directed-mutagenesis (SDM), as described in **Chapter 2.2.3.1**. Through the design of primers incorporating four point mutations into the DTX3L WT sequence (see **Table *4***), the pDEST-FLAG-DTX3L-M2, a construct encoding for FLAG-DTX3L with a disrupted RING domain was amplified. RING domain amino acid mutations

consisted of: Cys576Ser, His578Ser, Cys581Ser, Cys584Ser. Purified plasmid was sequenced to confirm the M2 point mutations were introduced (**Figure *33***).

The pDEST-FLAG-DTX3L was transiently transfected into the HeLa *DTX3L*$^{-/-}$ clone 20 and clone 24 cell lines. In comparison to parental controls, both the FLAG-DTX3L-WT and FLAG-DTX3L-M2 transfected knockout cells were found to express DTX3L at a similar level to endogenous DTX3L in HeLa WT cells (**Figure *34***).

To establish that the degradation of regressed replication forks observed through silencing and knockout of DTX3L could be rescued through complementation with WT DTX3L, the FLAG-DTX3L-WT construct was transfected into HeLa *DTX3L*$^{-/-}$ cells and analysed by DNA fibre analysis. As DTX3L is an E3 ubiquitin ligase, I also wanted to investigate whether this emergent excessive fork resection defect was due to the specific loss of DTX3L ubiquitination activity or due to an alternative role of the DTX3L protein. To this end, I also included FLAG-DTX3L-M2 for analysis.

As expected, knockout of DTX3L induced a robust fork resection defect in both clones as observed previously, with CldU/IdU ratio decreasing from 0.927 in HeLa WT to 0.635 and 0.586 respectively. Reintroduction of functional DTX3L protein through transfection of FLAG-DTX3L-WT was found to rescue this defect in both clones, restoring the CldU/IdU ratio to 0.881 and 0.976 in HDKO clone 20 and HDKO clone 24 respectively. Transfection of FLAG-DTX3L-M2 was not able to rescue the defect in fork resection, producing CldU/IdU ratios of 0.686 for clone 20 and 0.696 in clone 24 (**Figure *35***).

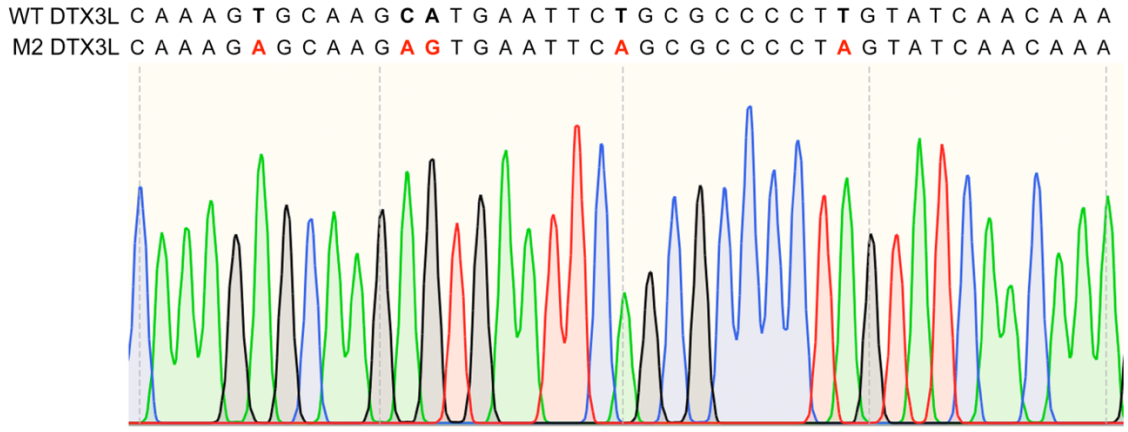

Figure 33. FLAG-DTX3L-M2 Sequencing trace.

Sequencing primer was designed to sequence the RING region of the FLAG-DTX3L-M2 construct. Top sequence depicts WT DTX3L sequence, with nucleotides to be mutated highlighted in bold. Below, FLAG-DTX3L-M2 is shown, with corresponding mutated bases in red.

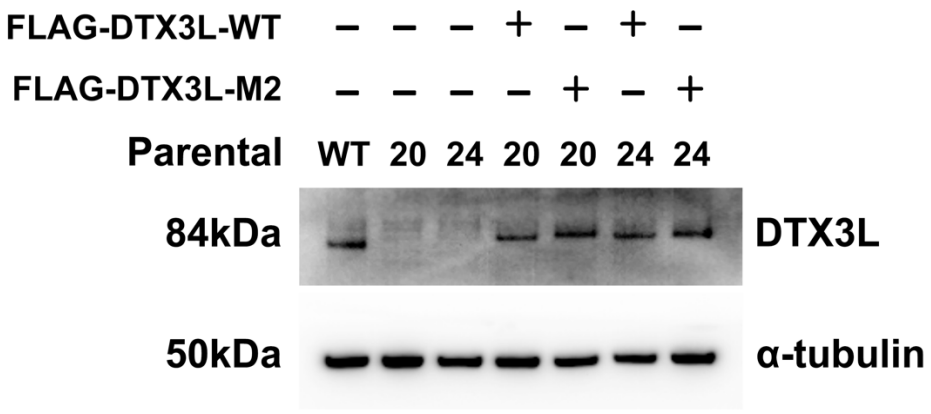

Figure 34. Western blot depicting ectopic expression of WT DTX3L and M2 DTX3L.

Parental HeLa DTX3L$^{-/-}$ cells were transiently transfected with 1.1μg pDEST-FLAG-DTX3L-WT or FLAG-DTX3L-M2 constructs to test for successful expression of the transgene product. Cell pellets were harvested 48h post-transfection. Transgene expression was detected by immunoblotting using DTX3L antibody.

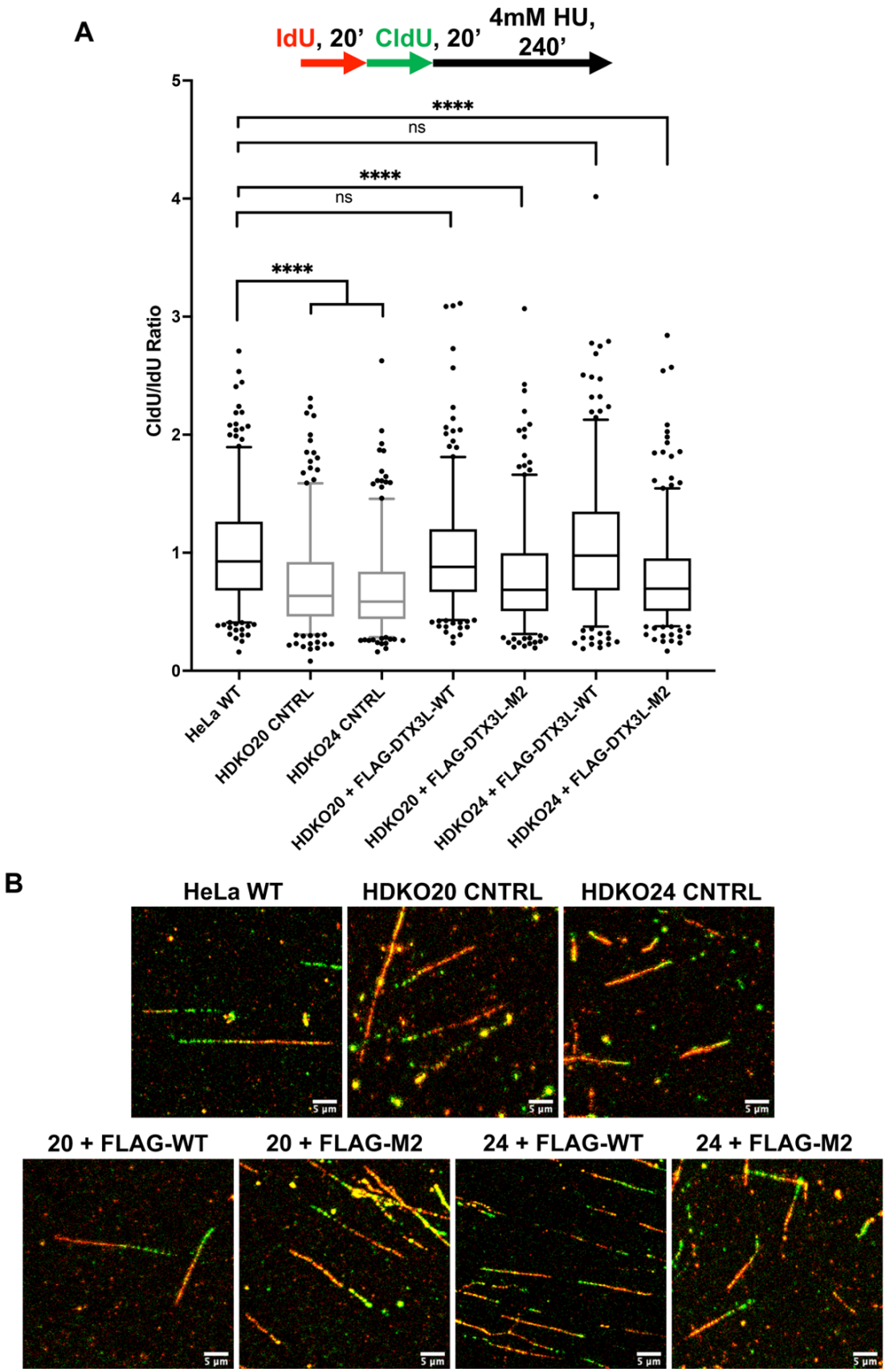

Figure 35. DNA fibre analysis of HDKO cells re-complemented with FLAG-DTX3L-WT or FLAG-DTX3L-M2 expressing constructs.

A) *Arrow schematic depicts nucleoside pulse labelling of DNA and HU treatment before cells were harvested. Boxplots represent 5th-95th percentile. (ns = Non-significant, **** = P < 0.0001, Mann-Whitney test, n ≥ 288, from three independent experiments).*
B) *Representative images of DNA fibres; white scale bars are 5µm.*

6.1.2. Clinically Relevant Y403X DTX3L Mutation Demonstrates Fork Resection Defect Seen in *DTX3L*$^{-/-}$ cells

DTX3L is overexpressed in numerous cancers, however this study has brought to light that the absence of DTX3L is also detrimental to the cell, resulting in defects in DNA replication and tolerance to replication stress.

To investigate the clinical relevance of DTX3L functional abrogation, clinical mutations in DTX3L were identified through the Genematcher database, where Daniel Wegner (Undiagnosed Diseases Network, Washington University School of Medicine in St. Louis) kindly shared information of their patient carrying heterozygous mutations. These mutations were identified in two independent sequencing assays (whole genome sequencing and whole exome sequencing), with inheritance of each DTX3L gene variant from respective parents clearly observed. One copy of the DTX3L gene possesses a T1209G point mutation, resulting in amino acid conversion of tyrosine at position 403 in the amino acid sequence to a stop codon (Y403X). This likely results in expression of a truncated protein of predicted size 46kDa. Expression of this truncated protein was in fact observed (**Figure *37, B***) as expected. As this truncated protein does not include the RING domain located downstream (positions 561 to 600), this truncated protein is predicted to be functionally inactive for E3 ubiquitin ligase activity.

The second inherited allele encodes a C1505T point mutation, converting alanine at position 502 to valine (A502V). The functional implications of this mutation are less obvious as this is a conservative substitution. A commonly used strategy to identify functional sequences within the genome and more specifically to assess conservation of amino acids within genes is to perform sequence alignment. It follows that if a residue is highly conserved, it is likely to be important for protein function. To shed light on the potential consequence of these point mutations,

multiple sequence alignment was carried out (**Figure *36***). From this analysis, the alanine at 502 in the human DTX3L gene appears to be highly conserved, with a score of '*', indicating absolute conservation across the five sequences. This suggests that this residue may be important for gene function in at least vertebrates.

To investigate if the clinical mutations described here have functional consequence and produce a fork regression defect as seen in the case of DTX3L deficiency, parental HeLa *DTX3L*$^{-/-}$ cells were re-complemented by transient transfection of plasmid constructs modified by site directed mutagenesis for these patient mutations. As seen in the previous chapters, a robust defect in fork resection was observed in HeLa *DTX3L*$^{-/-}$ cells (**Figure *37***). Interestingly, complementation of *DTX3L*$^{-/-}$ clones with the Y403X patient mutation construct demonstrated no rescue to the fork resection defect seen in the respective *DTX3L*$^{-/-}$ clones alone, in comparison to HeLa WT cells. Complementation with the A502V construct was found to fully rescue the fork resection phenotype to that seen in HeLa WT cells, with no significant difference in the CldU/IdU ratios observed. Attempting to replicate the genetic context observed in our patient and investigating the possibility of compounding heterozygous DTX3L mutations, the Y403X and A502V constructs were co-transfected in *DTX3L*$^{-/-}$ cells (0.55μg of each plasmid was used per transfection compared to 1.1μg of plasmid for single plasmid transfections). Interestingly, simultaneous ectopic expression of both mutated DTX3L proteins were not able to fully rescue the fork regression defect compared to HeLa WT cells (1.21 in WT, 1.08 in re-complemented clone 20 and 1.05 in clone 24), but did partially restore the CldU/IdU compared to *DTX3L*$^{-/-}$ cells (0.77 and 0.84 for clone 20 and clone 24 respectively).

Unfortunately, clinical phenotypes for the patient are not known due to limited correspondence with the clinician and therefore cannot be commented on further.

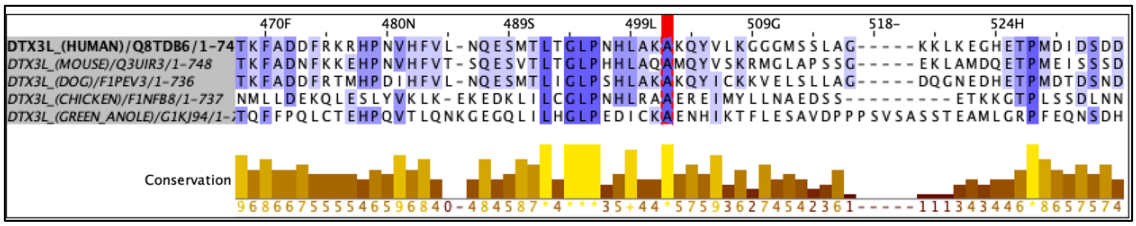

Figure 36. Multi sequence alignment of the DTX3L gene in different species of vertebrate demonstrating conservation of the 502A residue.

*Conservation histogram depicts conservation scores between 0-9, 0 being least conserved. – no conservation, + conservation of residue properties, * absolute conservation. Sequences obtained from UniProt, alignment performed with ClustalOWS on Jalview 2.11.1.4.*

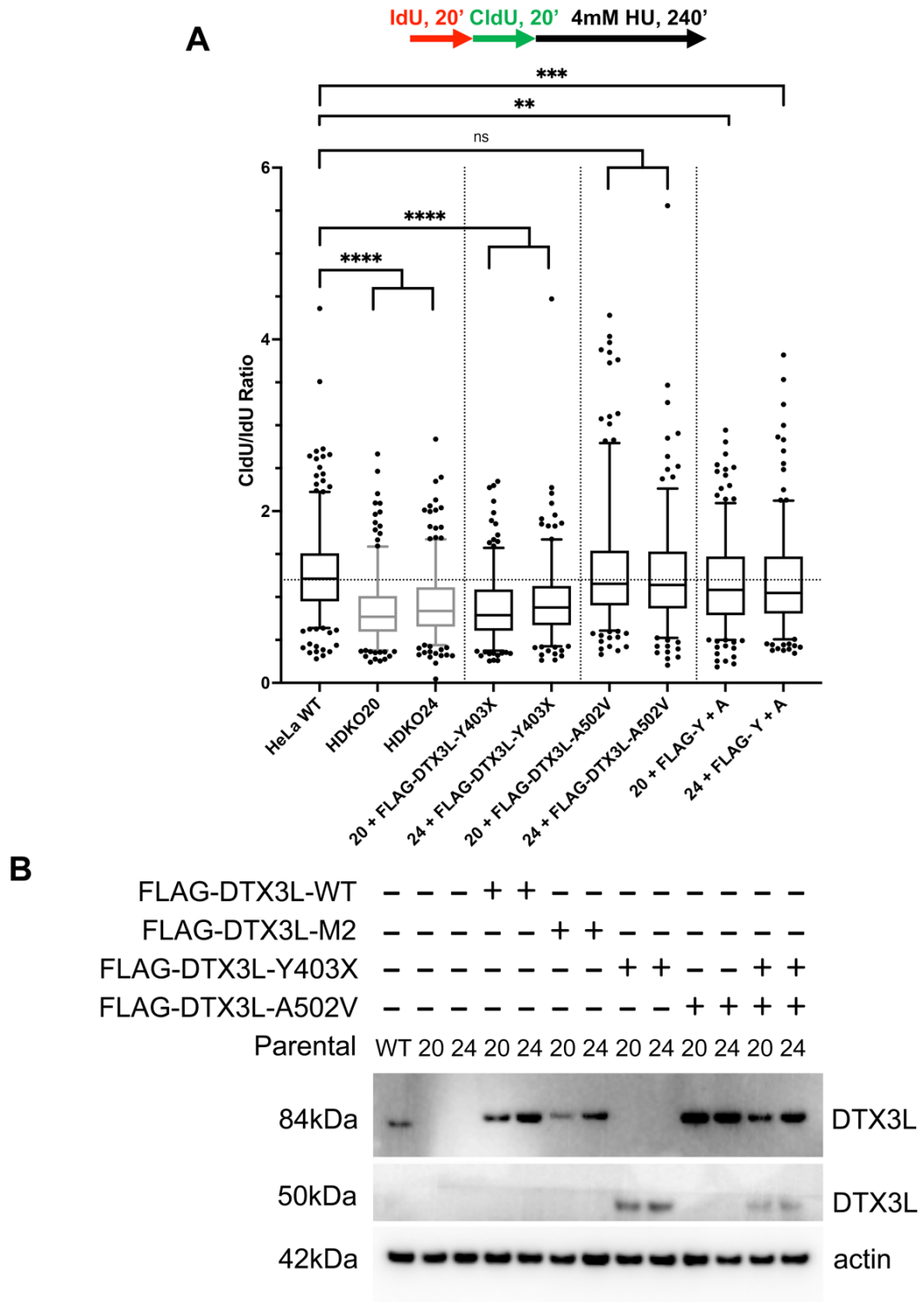

Figure 37. FLAG-DTX3L-Y403X does not rescue *DTX3L*$^{-/-}$ fork resection defect, compared to FLAG-DTX3L-A502V expressing constructs.

A) *Arrow schematic depicts nucleoside pulse labelling and treatment before cells were harvested (5th-95th percentile, n ≥ 219 tracts from three independent experiments. Analysed by Mann-Whitney, ** = P=0.0017, *** = P=0.0006, **** = P<0.0001).* ***B) Western blot comparing expression levels of FLAG-DTX3L from constructs transiently transfected into HDKO cell lines.*** *For single transfections, 1.1μg pDNA was used; for co-transfections, 0.55 μg was used per plasmid. Transgenic DTX3L was immunoblotted with DTX3L antibody. The FLAG-DTX3L-Y403X is predicted to express a truncation protein of estimated size 46kDa. Actin serves as a loading control.*

6.1.3. Abolishment of PARP9 Does Not Account For Fork Resection Defect

PARP9 is a binding partner of DTX3L and has been found to restrain DTX3L catalytic activity through its ADP-ribosylation activity on ubiquitin, as mentioned in **Chapter 1.7.1** (Yang et al., 2017). DTX3L in association with PARP9 plays a role in DNA damage repair, and therefore it was important to investigate if silencing of PARP9 contributes to the fork resection defect observed with DTX3L deficiency. Firstly, to establish if PARP9, in association with DTX3L, is responsible for the defect observed, I wanted to investigate if knockdown of PARP9 alone in HeLa WT cells resulted in a similar defect seen with DTX3L deficiency. PARP9 knockdown efficiency resulted in 25% of PARP9 expression in WT, and between 30% and 50% in respective HDKO clones, indicating a reduction in PARP9 expression (**Figure *38*B**). Interestingly, a mild reduction in the CldU/IdU ratio from 0.86 to 0.76 is observed compared to HeLa WT siLuc, suggesting knockdown of PARP9 leads to a mild fork regression defect (**Figure *38***). However, in comparison to CldU/IdU ratios in HDKO clone 20 and clone 24 treated with control siLuc, the fork regression defect is significantly less pronounced compared to ratios of 0.56 and 0.50 respectively.

Secondly, to investigate epistasis between PARP9 and DTX3L, silencing of PARP9 in *DTX3L*$^{-/-}$ cells was also investigated. Interestingly, siPARP9 treatment was found to slightly, yet significantly, reduce the CldU/IdU ratios observed in both HDKO clones even further compared to siLuc control, despite incomplete abrogation of PARP9 expression. Silencing of PARP9 in HDKO clone 20 and clone 24 produced ratios of 0.48 and 0.42 respectively, suggesting a multiplicative defect in fork regression upon deficiency of both DTX3L and PARP9.

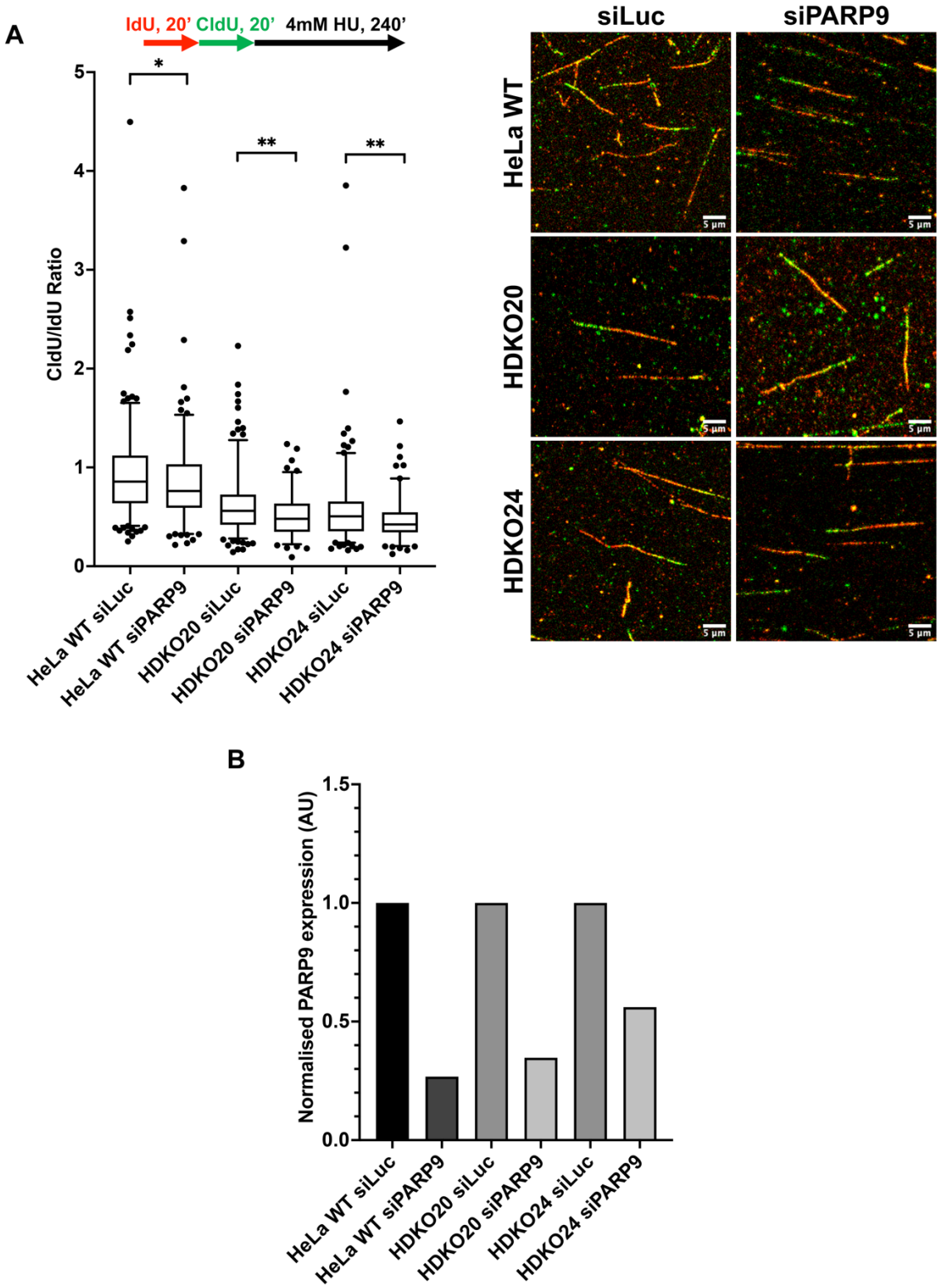

Figure 38. Silencing of PARP9 induces a mild fork degradation defect compared to DTX3L depletion.

A) *DNA fibre analysis of HDKO cells treated with siLuc or siPARP9. Arrow schematic depicts nucleoside pulse labelling and HU treatment. Boxplots represent 5th-95th percentile. (* = P = 0.0266, ** = P ≥ 0.0039. Analysed by Mann-Whitney test, n ≥ 106 fibres, from two independent experiments).* ***B)*** *qPCR demonstrating knockdown efficiency. siPARP9 was normalised to respective siLuc cell line (from one experiment, performed by Dr. Charlotte Smith, ICR).*

6.2. Fork Degradation in *DTX3L*$^{-/-}$ Cells is Rescued Through Modulation of Fork Repair Factors

6.2.1. Silencing of SMARCAL1 Rescues Fork Resection in HeLa *DTX3L*$^{-/-}$ Cells

Cells tolerate challenges to DNA replication through reversal of the ongoing replication fork. While controlled orchestration of this process can be advantageous to permit repair of the fork stalling lesion, providing opportunity for fork restart, excessive fork reversal can provide a substrate for unscheduled degradation of nascent DNA, resulting in genomic instability. To investigate whether the extensive fork degradation seen in *DTX3L*$^{-/-}$ cells could be rescued through prevention of inappropriate regression of stalled forks, knockdown of SMARCAL1, a key fork remodeller that promotes fork reversal, was performed for DNA fibre analysis.

As seen previously, a significant decrease in CldU/IdU ratio was observed for both siLuc treated DTX3L knockout clones compared to WT siLuc. Ratios decreased from 0.891 to 0.666 and 0.728 for clone 20 and clone 24 respectively (***A*Figure *39A***). SMARCAL1 knockdown using siRNA was effective (***A*Figure *39B***). Interestingly, knockdown of SMARCAL1 was found to increase CldU tract length in all 3 cell lines compared to their control counterpart, as shown by the increase in CldU/IdU ratio. HeLa WT cells treated with siSMARCAL1 produced a ratio of 1.046, and 1.069 and 1.065 in the case of *DTX3L*$^{-/-}$ cells. Most importantly, *DTX3L*$^{-/-}$ cells treated with siSMARCAL1 were rescued to WT levels, suggesting that extensive fork reversal, leading to fork degradation in the absence of DTX3L, is mediated by fork remodellers such as SMARCAL1.

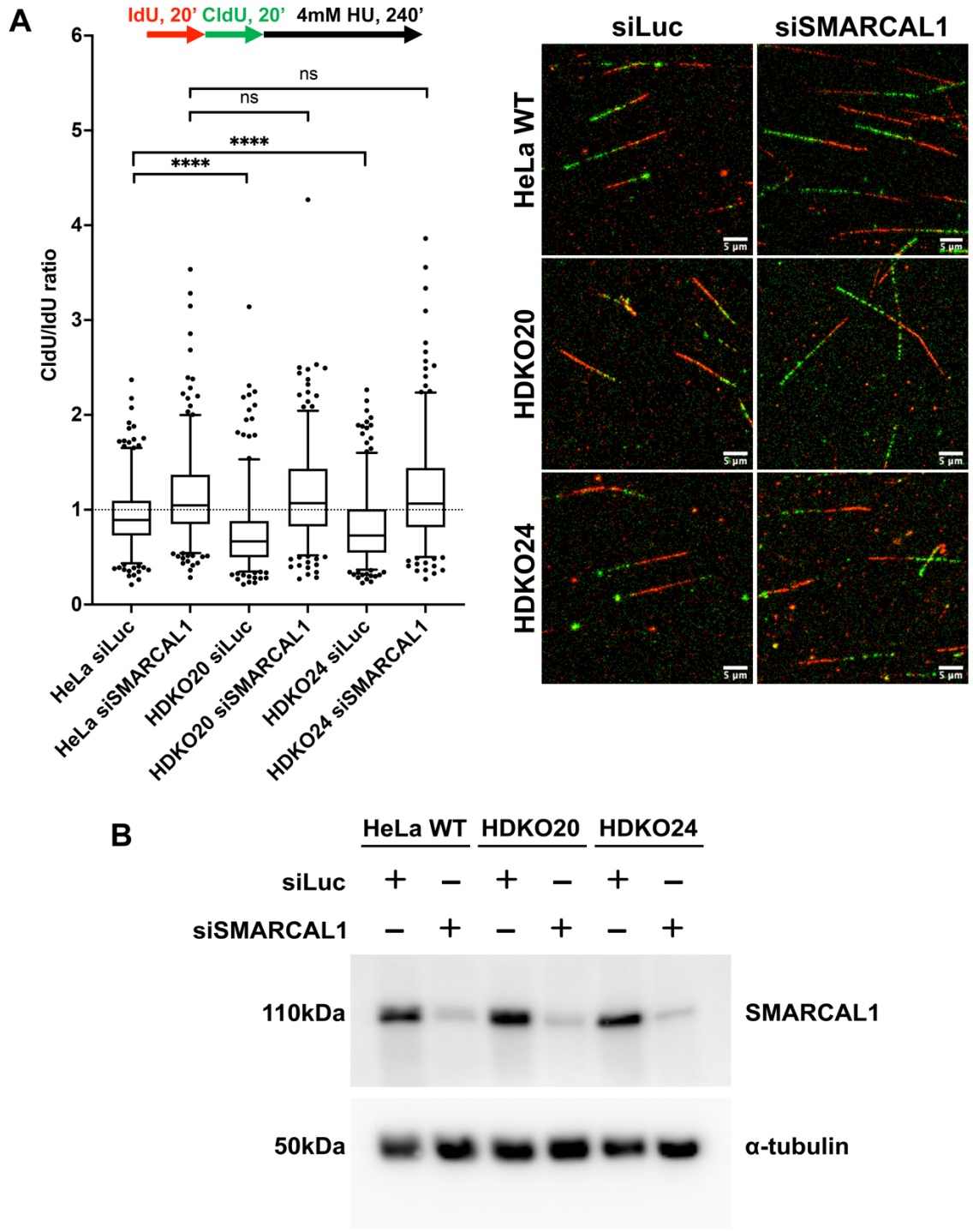

AFigure 39. Silencing of SMARCAL1 rescues the fork resection defect seen in HeLa *DTX3L*$^{-/-}$ cells.

A) *DNA fibre analysis of HDKO cells treated with siLuc or siSMARCAL1. Arrow schematic depicts nucleoside pulse labelling and treatment before cells were harvested. Boxplots represent 5th-95th percentile. (**** = P < 0.0001, Mann-Whitney test, n ≥ 269 fibres, from three independent experiments).* ***B)*** *Western blot showing knockdown of SMARCAL1 by siRNA, where α-tubulin serves as a loading control.*

6.2.2. MRE11 Inhibition Rescues Fork Resection in HeLa *DTX3L*$^{-/-}$ Cells

Following on from this, I then wanted to investigate whether SMARCAL1 reversed forks result in degradation by MRE11 in the absence of DTX3L. To this end, I employed the extensively characterised MRE11 inhibitor mirin in the DNA fibre assay (Dupré et al., 2008; Nieminuszczy et al., 2019).

Once again, the fork resection defect observed in *DTX3L*$^{-/-}$ cells was recapitulated, with a decrease in CldU/IdU ratio from 1.063 in HeLa WT cells to 0.753 in clone 20 and 0.869 in clone 24 (**Figure *40***).

As seen previously with siSMARCAL1 treatment, all three cell lines treated with mirin saw an increase in CldU tract length and a resultant increase in the CldU/IdU ratio. Strikingly, mirin treatment was found to rescue CldU/IdU to at least WT levels, with 1.107, 1.252 and 1.203 and in WT, clone 20 and clone 24 respectively.

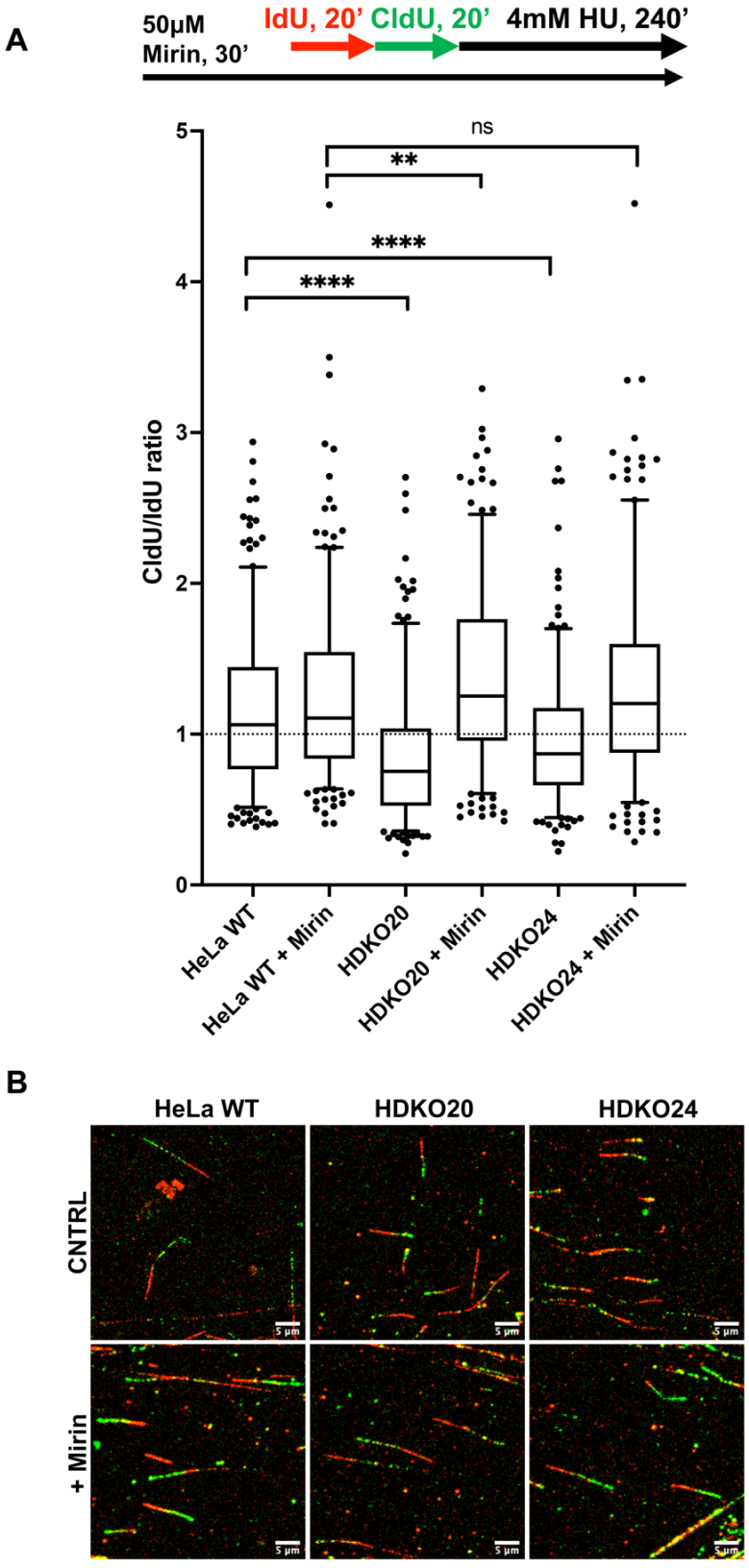

Figure 40. Inhibition of MRE11 by mirin rescues the fork resection defect seen in HeLa *DTX3L*$^{-/-}$ cells.

A) *DNA fibre analysis of cells treated with mirin as indicated. Arrow schematic depicts nucleoside pulse labelling and treatment before cells were harvested. Boxplots represent 5th-95th percentile. (** = 0.0024, **** = P < 0.0001, Mann-Whitney test, n ≥ 269 fibres, from three independent experiments).* ***B)*** *Representative images of DNA fibres; white scale bars are 5μm.*

6.2.3. Recruitment of RAD51, BRCA1 and MRE11 to the Replication Fork Are Unaffected by DTX3L Deficiency

To investigate if recruitment/retention of crucial fork repair components to the ongoing replication fork are defective as a result of DTX3L deficiency, resulting in defective fork resection, the proximity ligation (PLA) assay was utilised (Nieminuszczy et al., 2019; Taglialatela et al., 2017). Foci are formed as a result of fluorescent DNA probes binding to the product of rolling circle PCR amplification that can occur once two secondary probes are in proximity. These probes bind to primary antibodies of which here mouse and rabbit biotin antibodies were used as a positive control for the assay (**Figure *41***).

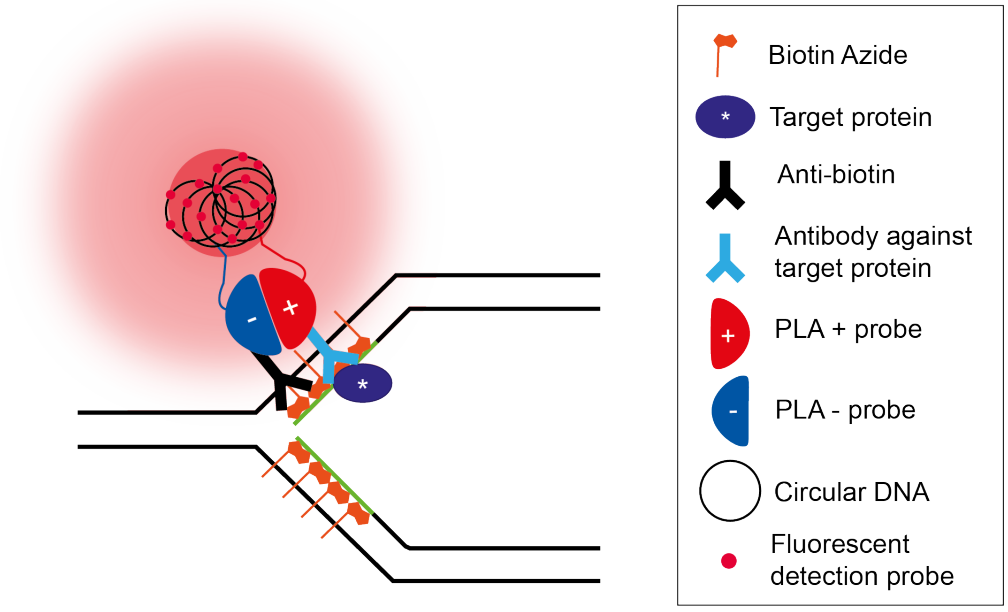

Figure 41. Schematic of the proximity ligation assay.

The EdU labelled replication fork (green) is biotin labelled using click reaction chemistry for PLA detection of fork associated proteins of interest.

RAD51 is important for the stabilisation of single-stranded nascent DNA at the stalled fork, permitting fork reversal, preventing excessive fork degradation and promoting restart of stalled/collapsed forks. BRCA1 is essential for the exchange of RPA to RAD51 and MRE11 is required for the DNA resection necessary for homologous recombination and fork restart. To assess their recruitment to active replication forks, HeLa cells were labelled with EdU and fixed untreated or labelled prior to 4mM HU treatment for 3h.

For the EdU-RAD51 PLA, no significant difference in the mean number of foci was observed between HeLa WT cells and *DTX3L*$^{-/-}$ cells. Untreated cells produced a mean number of foci in the range of 1.4 to 2.0 foci per positive nucleus. In cells treated with 4mM HU for 3h, the difference in mean number of foci for *DTX3L*$^{-/-}$ cells was statistically insignificant with foci increasing from 2.6 to 3.5 for clone 20 and 3.3 for clone 24 (**Figure *42***).

In **Figure *43*** where BRCA1 recruitment to nascent DNA was investigated, no difference was observed in untreated cells between WT and *DTX3L*$^{-/-}$. For HU treated cells, a slight increase was observed above WT in clone 24, but not for clone 20, with mean foci of 8.0, 9.9 and 8.2 respectively.

Finally, recruitment of MRE11 to replicating DNA is shown (**Figure *44***). In untreated cells, the number of foci observed for HeLa WT was 9.5 compared to KO clones 20 and 24 with 10.1 and 6.7 respectively, resulting in non-statistically significant differences with WT. In HU treated cells, HDKO clone 24 resulted in a slightly statistically significant decrease in mean foci from 13.6 to 9.2, and 13.1 for clone 20.

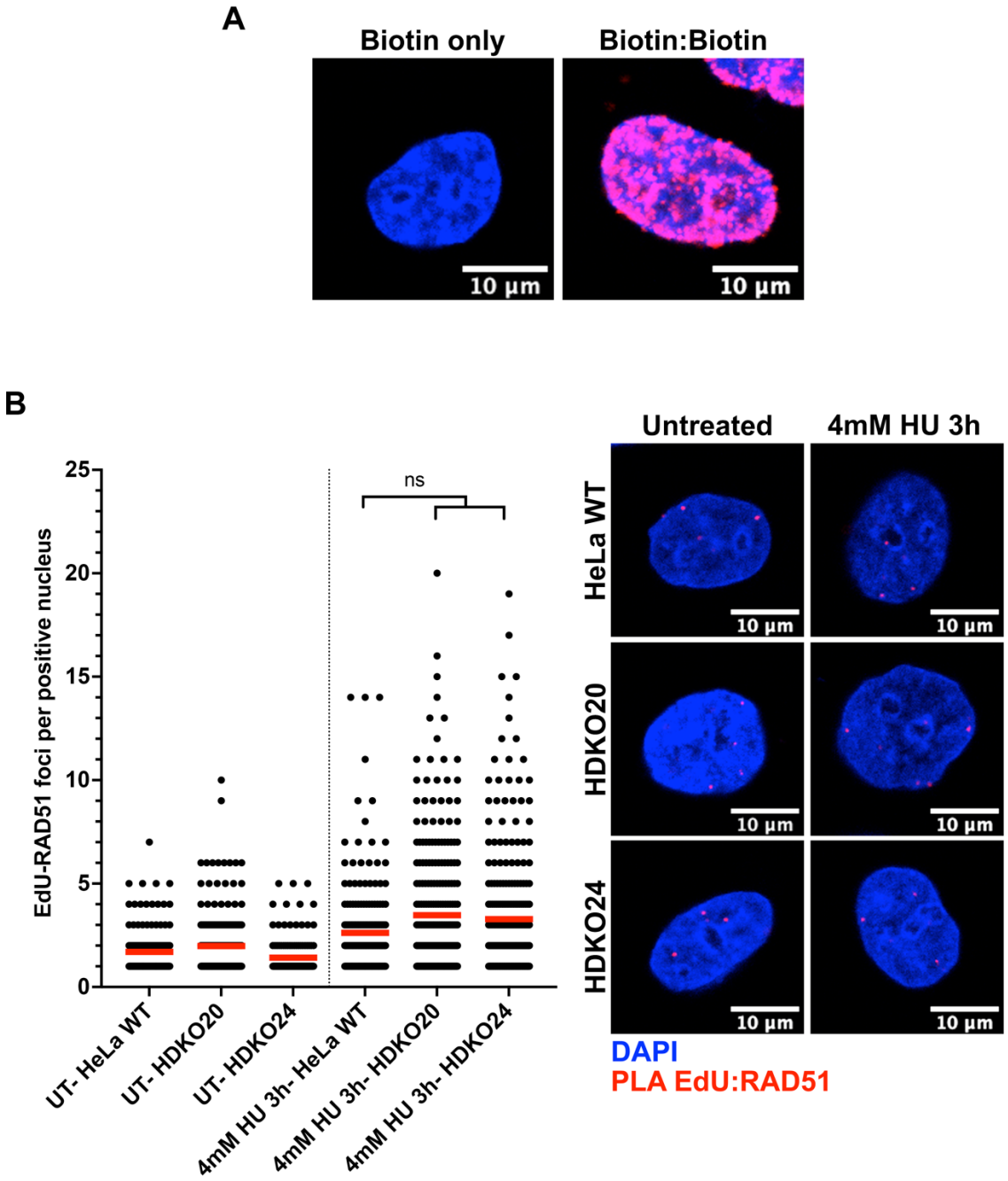

Figure 42. Recruitment of RAD51 to the replication fork is not affected by DTX3L deficiency.

A) *Single species biotin antibody immunostaining acts as negative control for PLA assay, and mouse & rabbit biotin antibodies immunostaining acts as positive control for PLA assay.* ***B)*** *PLA foci formation resulting from RAD51 recruitment to EdU labelled forks. n ≥ 144 foci-positive nuclei from three independent repeats. Red lines show mean (ns = non-significant, analysed by Mann-Whitney). Representative images of nuclei shown; white scale bars are 10µm.*

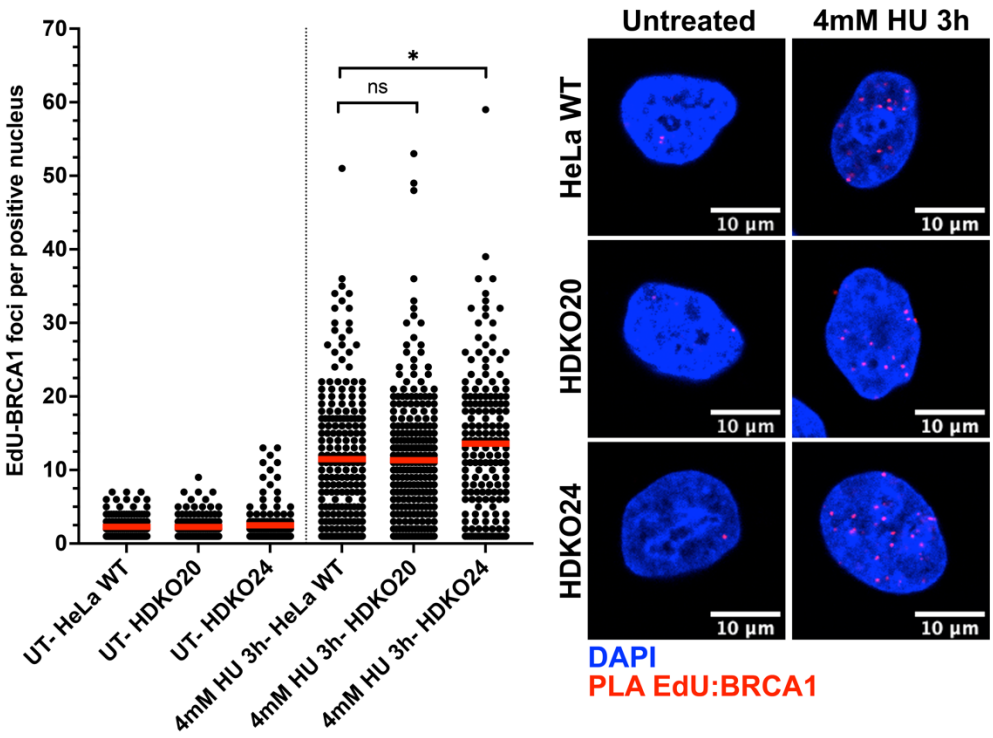

Figure 43. Recruitment of BRCA1 to the replication fork is not affected by DTX3L deficiency.

*PLA foci from BRCA1 recruitment. n ≥ 114 foci-positive nuclei from three independent repeats. Red lines show mean (ns = non-significant, * = P > 0.02, analysed by Mann-Whitney). Representative images of nuclei shown; white scale bar is 10µm.*

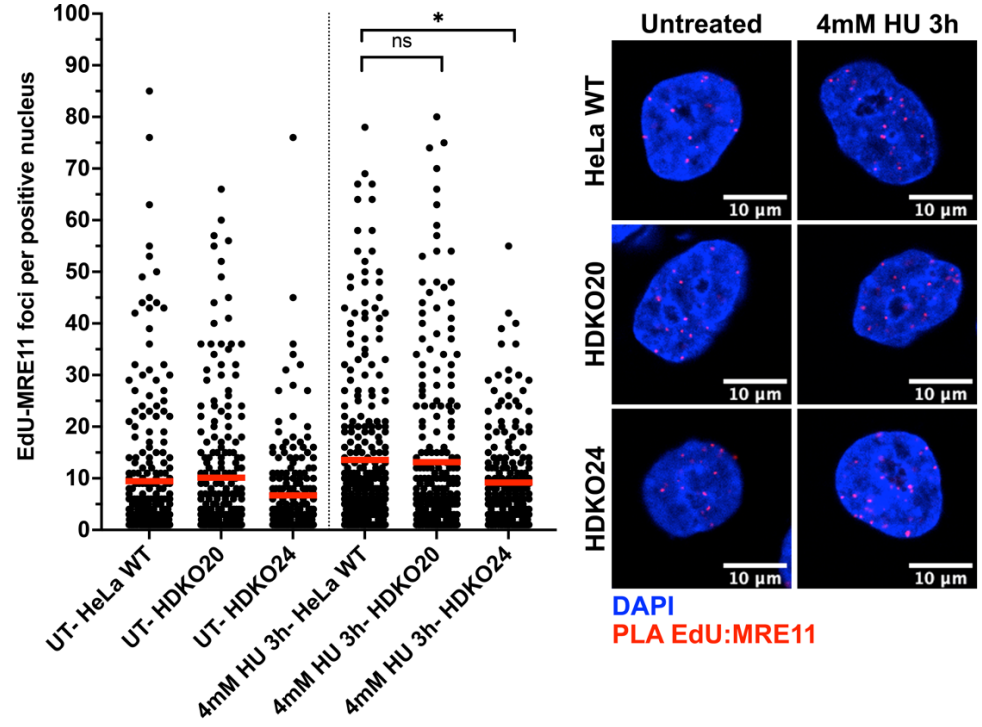

Figure 44. Recruitment of MRE11 to the replication fork is not affected by DTX3L deficiency.

*PLA foci from MRE11 recruitment. n ≥ 193 foci-positive nuclei from three independent repeats. Red lines show mean. (ns = non-significant, * = P > 0.02, analysed by Mann-Whitney).*

6.3. Complementation of HeLa *DTX3L*$^{-/-}$ Cells by Ectopic Expression of GFP-DTX3L

6.3.1. Generation and Characterisation of HeLa *DTX3L*$^{-/-}$ Cells Recomplemented With GFP-DTX3L

A gateway destination vector based on the Clontech pEGFP-C1 backbone (a generous gift from Prof. C. Green) was used to clone the DTX3L cDNA from a DNASU repository entry vector via LR clonase reaction (see **Chapter 2.2.3**). This pDEST-GFP-DTX3L construct was transfected into the HeLa *DTX3L*$^{-/-}$ clones (clone 20 and clone 24) under G418 selection to generate stable GFP-DTX3L expressing clones.

Transfected cells were single cell sorted and expanded from 96 well plates. Upon further expansion under selection, cells were harvested and analysed by western blot to determine transgene expression. Unexpectedly, despite these clones being resistant to selection, the presence of GFP from the transfected construct was not detectable by western blot despite detection of GFP in the positive control (data not shown).

I then decided to blot with DTX3L antibody to see if ectopic DTX3L expression could be detected this way. Surprisingly, compared to the parental controls, DTX3L was present in the transfected samples suggesting that exogenous DTX3L expression was occurring (**Figure *45, A***). To further characterise the expression of this transgene, I then examined the subcellular localisation of GFP-DTX3L by immunofluorescent imaging. Compared to the parental control, GFP was seen above background in the nuclei of transfected cells, suggesting that GFP-DTX3L expression is predominantly nuclear as anticipated by the presence of NLS domains in DTX3L (**Figure *45, B***).

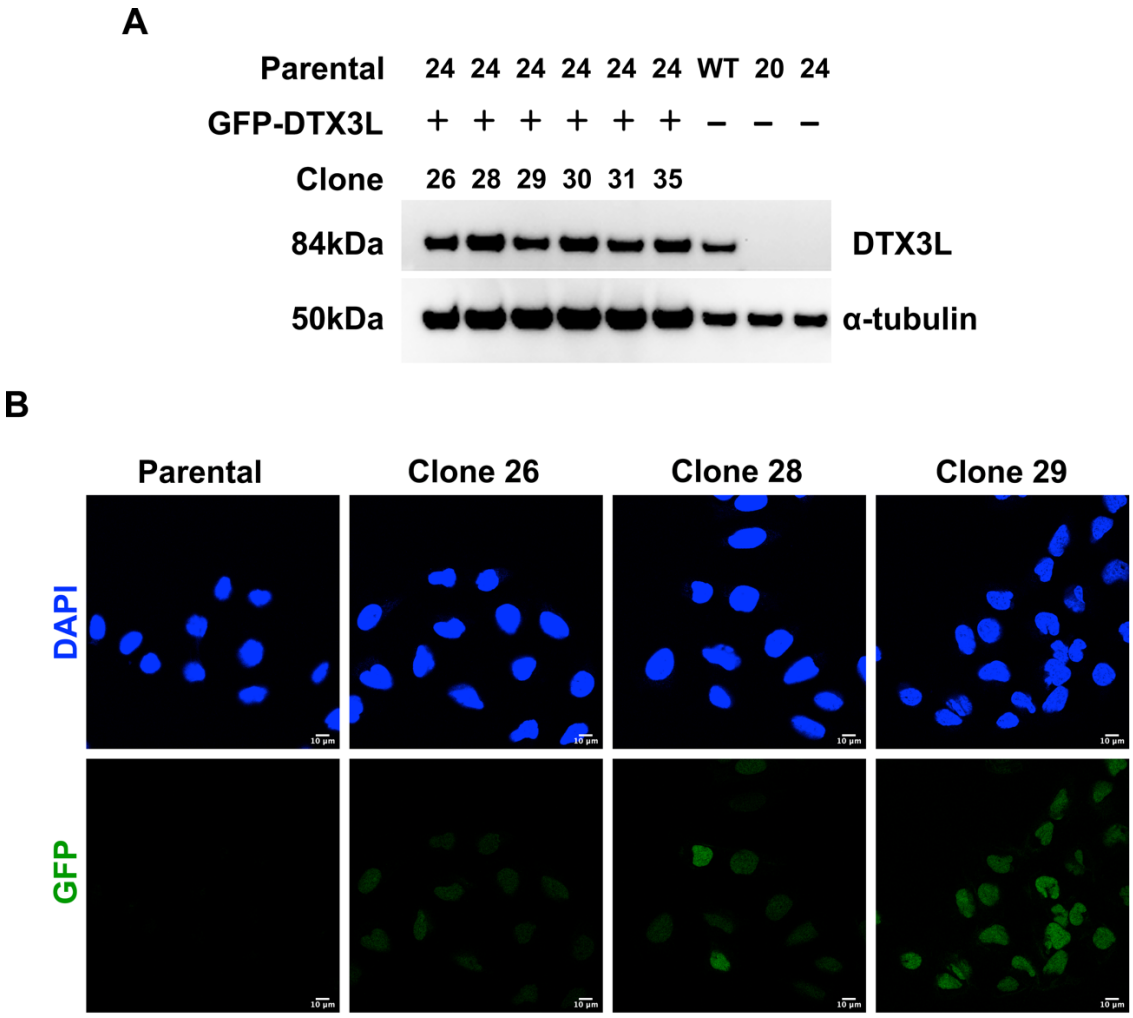

Figure 45. DTX3L is transgenically expressed in HeLa *DTX3L*$^{-/-}$ cells via the pDEST-GFP-DTX3L construct and localises to the nucleus.

A) *Western blot analysis of HeLa DTX3L$^{-/-}$ cells transfected with pDEST-GFP-DTX3L. Samples were immunoblotted with antibody against DTX3L. α-tubulin serves as loading control.* ***B)*** *Fluorescent imaging of HeLa DTX3L$^{-/-}$ GFP-DTX3L stable clones for direct GFP fluorescence. Cells were seeded onto coverslips, fixed and mounted. Parental cells were included as a control for background fluorescence detectable in the 488nm channel. White scale bars are 10μm in length.*

6.3.2. Exploring the DTX3L Interactome Through GFP-Nanotrap Co-Immunoprecipitation Coupled to LC-MS/MS

To shed further light on the molecular mechanism of DTX3L in the replication stress response, the pDEST-GFP-DTX3L construct was used to transiently express GFP-DTX3L in HEK293FT cells in order to perform GFP nanotrap pulldown of the transgene and DTX3L associated proteins. Transient transfection of GFP-DTX3L in HEK293FT cells was performed 48h prior to IP. An untransfected control was included to account for unspecific pulldown through low affinity binding to the GFP nanotrap beads. For transfected cells, cells were either untreated or treated prior to harvesting with 1mM HU for 1h, or 4mM HU 3h to see whether enhanced replication stress resulted in altered protein-protein interactions. I immunoblotted for DTX3L to ensure successful pulldown of GFP-DTX3L by the GFP nanotrap beads (**Figure *46, A***).

To ascertain whether any proteins were being coimmunoprecipitated with the GFP-DTX3L protein, and given that DTX3L has few known interactors, the IP was submitted for analysis by LC-MS/MS. Mass spectrometry profiling of the co-immunoprecipitated samples revealed the identification of 221 unique proteins. DTX3L and GFP were identified as most abundant, as expected in the transfected samples (**Figure *46, B***). Other relevant hits identified included positive interactors histone 4 and PARP9. Histone 4 was also detected in the control, however PARP9 was identified in at least one GFP-DTX3L transfected sample specifically. Interestingly, DNA damage response related proteins PARP1 and TOPBP1 were also identified. PARP1 was found in the untreated IP sample but was also detected in the untransfected control sample. TOPBP1 was present in samples treated with 1mM HU for 1h and in greater abundance in samples treated with 4mM HU 3h. Other peptides identified were not relevant to the current

investigation and the majority consisted of cell matrix proteins or ribosomal proteins.

A

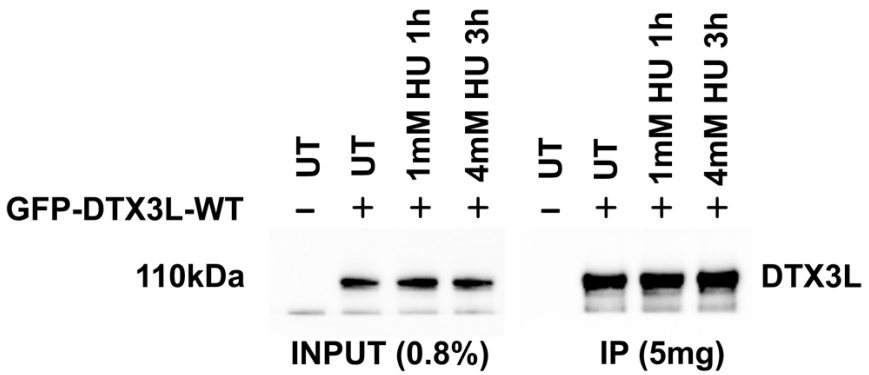

B

Abundance Count	NT	UT GFP-DTX3L	1HU GFP-DTX3L	4HU GFP-DTX3L
DTX3L	6	29	29	32
GFP	1	7	4	5
H4	8	6	5	6
PARP9		1		
TOPBP1			1	2
PARP1	1	1		

Figure 46. TOPBP1 interaction in vivo with DTX3L is suggested by GFP co-IP-MS.

A) *Western blot for detection of target proteins in input (pre-immunoprecipitation) and immunoprecipitated samples. Whole cell lysate from HEK293FT cells transiently transfected with GFP-DTX3L plasmid construct was obtained and 40μg used as input (0.8% of total protein used in IP).* ***B)*** *GFP-DTX3L Nanotrap IP coupled to LC-MS/MS results. Table shows peptide abundance count relative to IP sample. NT: non-transfected. UT: untreated. 1HU: 1mM HU, 1h. 4HU: 4mM HU 3h.*

6.4. TOPBP1 Associates With DTX3L

6.4.1. FLAG-DTX3L-WT Co-IP Corroborates DTX3L and TOPBP1 Interact *In Vivo*

To continue work initiated using the GFP-DTX3L construct exploring the interactome of DTX3L, I wanted to validate the finding that immunoprecipitation of DTX3L leads to co-immunoprecipitation of TOPBP1. To see whether TOPBP1 was present in the immunoprecipitated lysate, lysate was analysed by western blot. TOPBP1 was identified in all FLAG-DTX3L IP samples, reaffirming the ability for TOPBP1 to co-immunoprecipitate with DTX3L independently of the beads used, or the tag that permits DTX3L binding to the beads (**Figure *47***). TOPBP1 pulldown was found to be most abundant in cells treated for 1mM HU for 1h, despite equal pulldown of DTX3L in all FLAG-DTX3L transfected samples, suggesting the *in vivo* interaction of TOPBP1 and DTX3L is enhanced in conditions of increased replication stress.

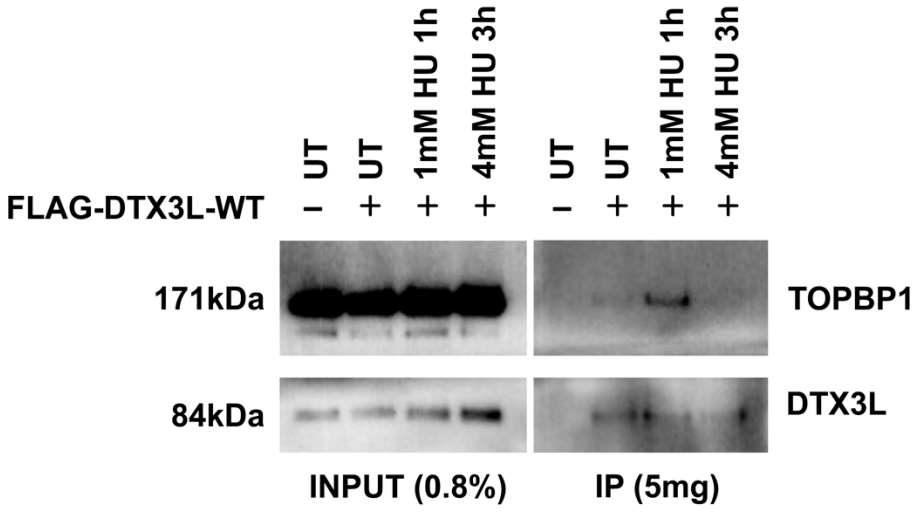

Figure 47. TOPBP1 *in vivo* interaction with DTX3L is validated by FLAG co-IP.

Western blot for detection of TOPBP1 in input (pre-immunoprecipitation) and immunoprecipitation samples generated from HEK293FT cells transiently transfected with FLAG-DTX3L plasmid construct (input samples represent 0.8% of total protein used in IP).

6.4.2. DTX3L and TOPBP1 Associate More Frequently Under Conditions of Replication Stress

Utilising the proximity ligation assay, an alternative approach was employed to validate the interaction between DTX3L and TOPBP1.

U2OS cells stably expressing GFP-tagged TOPBP1 (U2OS GFP-TOPBP1, generated by Dr. Peter Martin (ICR)) were used, with cells either untreated, treated with 1mM HU for 1h or 4mM HU 3h. U2OS GFP expressing cell lines were used as control. All three GFP samples had mean foci counts of 0.3-0.5 foci per nucleus, suggesting that this is the background level of foci to be expected for this assay for these antibodies, of which unspecific binding and chance proximity may account for this (**Figure *48***).

In support of the interaction observed between TOPBP1 and DTX3L from the co-immunoprecipitations presented in the previous section, a significant increase in PLA foci was observed for GFP-TOPBP1 untreated cells compared to the GFP only control, from a mean of 0.5 foci per nucleus to a mean of 1.8 foci per nucleus. Interestingly, the mean foci for cells treated with 1mM HU for 1h and 4mM HU for 3h were 2.3 and 2.8 respectively, suggesting the incidence of TOPBP1 and DTX3L association is increased in conditions of enhanced replication stress. In combination with co-IP data, this suggests that DTX3L and TOPBP1 are interacting proteins, and interaction is more frequently observed when there are challenges to DNA replication.

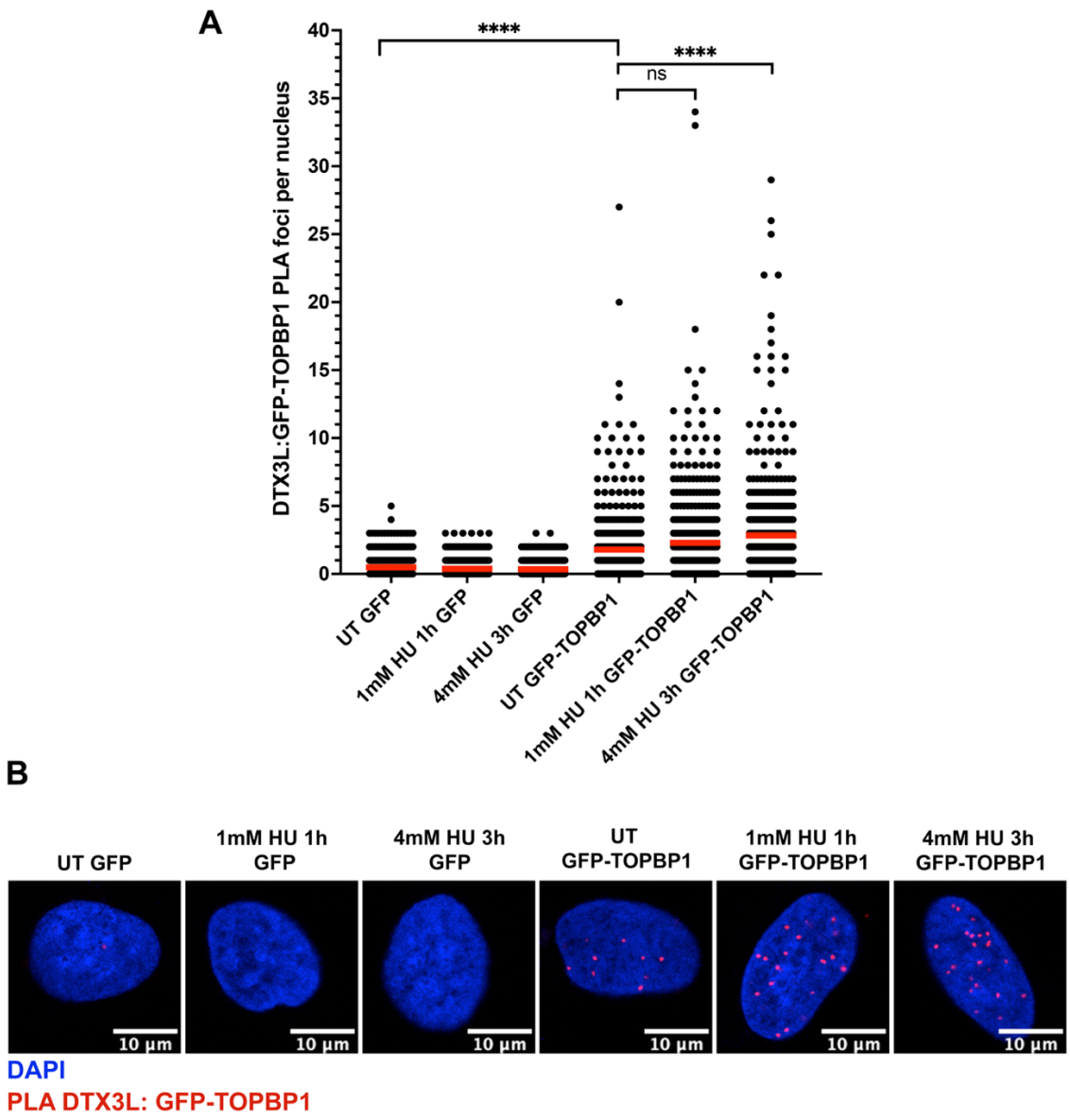

Figure 48. Frequency of TOPBP1 and DTX3L association *in vivo* is greater in conditions of enhanced replication stress.

A) *PLA assay using antibodies against GFP and DTX3L. Red line shows mean; each point represents a nucleus. Cells expressing GFP only were used as a negative control. (**** = P < 0.0001, Mann-Whitney test, n ≥ 256 nuclei from three independent experiments).* ***B)*** *Representative images of nuclei stained with DAPI and DTX3L:GFP PLA foci in red.*

6.5. Ubiquitome Enrichment Profiling of *DTX3L*$^{-/-}$ Cells

Due to the challenge of delineating the numerous substrate targets of E3 ubiquitin ligases, loss of function ubiquitome enrichment analysis was performed to identify a cohort of DTX3L substrates that may contribute to its role in the RSR (Bakos et al., 2018; Fulzele & Bennett, 2018; Thompson et al., 2014).

Here, ubiquitin peptide (diGly remnant) immunoprecipitation resulted in retrieval of >20,000 ubiquitinated peptides. Samples were scaled, filtered and statistically analysed as described in **Chapter 2.2.14.4,** accounting for a cell culture batch effect determined by Pearson sample correlation (**Figure *49***).

Two sample t-test comparisons were performed for investigation of ubiquitin enrichment upon enhanced replication stress (Untreated (UT) vs 3mM HU 4h (HU) treatment, in HeLa WT/*DTX3L*$^{-/-}$ (KO)), or through DTX3L deficiency (HeLa WT vs *DTX3L*$^{-/-}$, in UT/HU). >480 peptides were found to be differentially ubiquitinated in at least one comparison, of which 147 were differentially regulated in HU-treated *DTX3L*$^{-/-}$ vs WT and 168 in untreated *DTX3L*$^{-/-}$ vs WT. Of these, 5 were regulated in both.

In a group wide comparison by ANOVA, >300 peptides were determined to be significantly ($P < 0.05$) differentially ubiquitinated (enrichment factor >1.3) in at least one group (e.g. HU *DTX3L*$^{-/-}$). Both statistical methods were used to compare the data in multiple ways for informing the identification of potentially interesting, differentially regulated peptides that may be functionally validated hereafter.

The following work is the result of a collaborative effort between myself, Lu Yu (Choudhary Lab, ICR) and Theo Roumeliotis (Choudhary Lab, ICR). Cell culture and sample pellet preparation were carried out by myself. Cell pellet lysis, protein digest, ubiquitin remnant enrichment IP, elution and desalting were carried out by myself with the guidance of Lu Yu. TMT labelling, hpH fractionation, concatenation and LC-MS/MS were performed by Lu Yu. Statistical analysis for ubiquitin peptide enrichment and GOBP pathway enrichment were performed by Theo Roumeliotis using Perseus software (version 1.6.2.2).

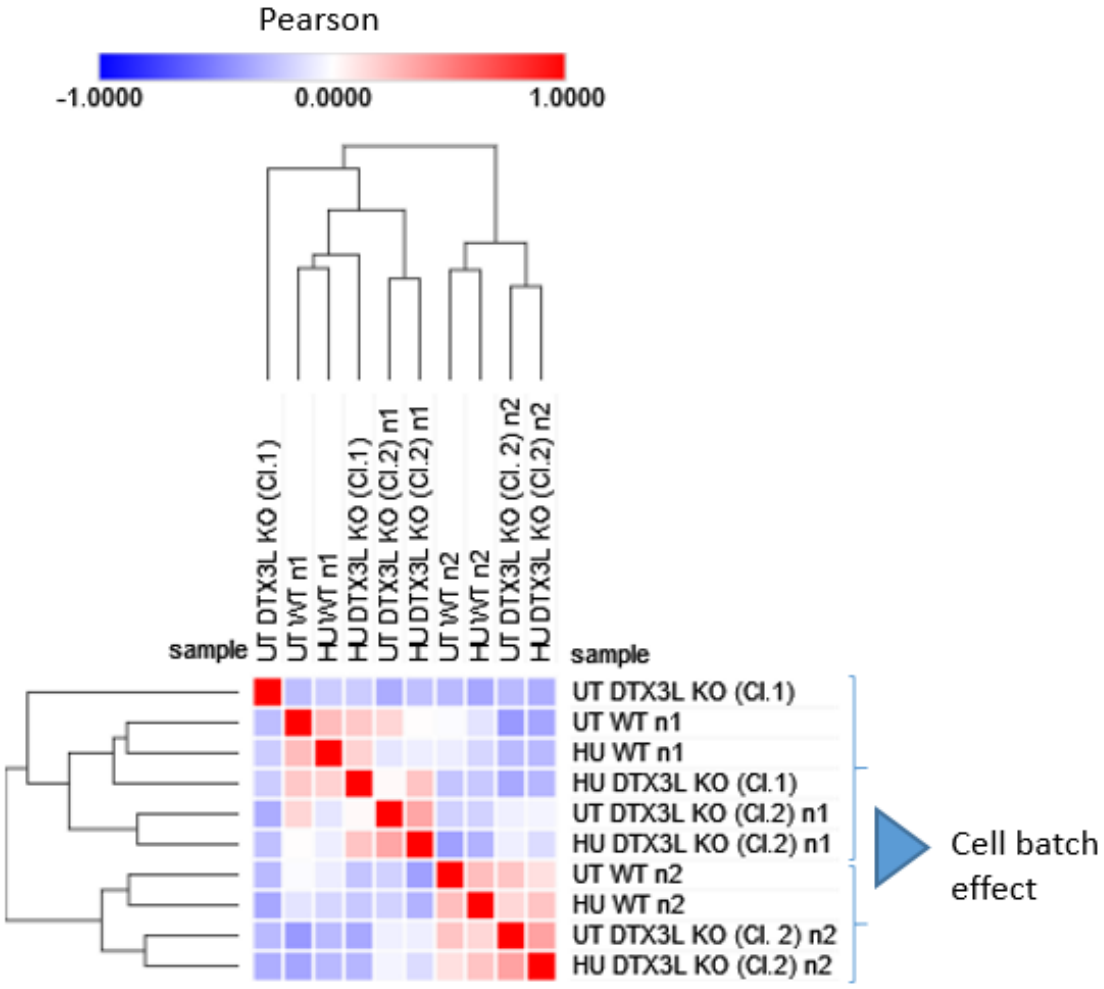

Figure 49. Pearson sample correlation analysed using scaled abundances.

Correlation within biological repeats suggests a cell batch effect. Samples were re-scaled within each batch. (Theo Roumeliotis)

6.5.1. Pathway Enrichment Analysis of Ubiquitinated Peptides

Pathway enrichment analysis was performed using the GOBP (Gene Ontology Biological Processes) database to identify biological processes where retrieved ubiquitinated peptides were significantly ($P < 0.05$, Fisher exact test) over/under-represented (enrichment factor >1.3) in their respective comparisons (**Table *8***). 103 GOBP annotated pathways were identified across all 4 comparisons.

The most relevant comparisons for this study include pathway enrichment for *DTX3L*$^{-/-}$ vs HeLa WT in untreated conditions and in 3mM HU 4h treated conditions. In the untreated comparison, 38 pathways were enriched (**Table *8, A***). These include immunologically related biological processes such as Notch signalling, cytokine-mediated signalling, leukocyte migration and neutrophil degranulation. Additionally, pathways such as cell proliferation and regulation of RNA Pol II transcription were also identified.

Concerning the RSR more specifically, by comparing *DTX3L*$^{-/-}$ vs WT in treated conditions 31 pathways were identified (**Table *8, B***). These include detection of DNA damage and the DNA damage response, regulation of cell growth & cell division, DSBR (via NHEJ), regulation of apoptosis, and the G1/S transition of mitosis. Modifications in pathways pertaining to gene expression, through transcription and translation were also featured. Immunologically related biological processes were also identified such as NFκB (nuclear factor kappa B) activity, neutrophil degranulation and cytokine-mediated signalling.

A

GOBP Name	Enrichment factor	P value
protein K48-linked ubiquitination	8.3647	5.54E-05
response to nutrient	7.8071	8.31E-05
response to drug	4.5041	0.00012
vasculogenesis	9.2942	0.00014
positive regulation of protein phosphorylation	4.8794	0.00043
transmembrane transport	5.323	0.0007
blood vessel development	8.6745	0.00089
positive regulation of smooth muscle cell proliferation	8.218	0.0011
apoptotic process	2.405	0.00182
regulation of gene expression	5.1362	0.00225
regulation of cholesterol biosynthetic process	6.7888	0.00226
protein stabilization	3.2194	0.00244
response to organic cyclic compound	6.2457	0.00307
positive regulation of cold-induced thermogenesis	6.0055	0.00354
positive regulation of ERK1 and ERK2 cascade	4.539	0.00381
wound healing	5.5765	0.00461
protein localization	5.3842	0.00521
regulation of cell migration	5.2047	0.00587
ubiquitin-dependent protein catabolic process	2.5458	0.00591
Notch signaling pathway	4.8794	0.00732
cellular response to heat	4.8794	0.00732
positive regulation of cell migration	3.253	0.00763
cell adhesion	2.7882	0.00898
response to hypoxia	3.4242	0.01164
aging	3.3651	0.01242
cellular protein modification process	3.7177	0.01767
protein deubiquitination	2.1992	0.01841
cytokine-mediated signaling pathway	3.0027	0.01876
extracellular matrix organization	3.5487	0.02037
leukocyte migration	3.3222	0.0248
in utero embryonic development	2.749	0.0254
positive regulation of cell proliferation	2.0018	0.02797
proteasome-mediated ubiquitin-dependent protein catabolic process	2.2739	0.03193
neutrophil degranulation	1.7121	0.03532
spermatogenesis	2.1487	0.03885
negative regulation of apoptotic process	1.7479	0.03914
regulation of transcription by RNA polymerase II	1.9108	0.04363
heart development	2.6921	0.04458

B

GOBP Name	Enrichment factor	P value
protein ubiquitination	3.368	4.58E-05
positive regulation of translation	8.609	4.73E-05
protein K11-linked ubiquitination	11.16	5.55E-05
response to ethanol	6.8872	0.0001718
positive regulation of protein serine/threonine kinase activity	11.479	0.0002881
regulation of mRNA stability	5.1507	0.0022352
cellular protein modification process	4.7828	0.0030689
DNA damage response, detection of DNA damage	6.1808	0.0032045
translational initiation	3.061	0.0032804
negative regulation of cell growth	4.4639	0.0040957
osteoblast differentiation	4.274	0.0048965
cellular response to DNA damage stimulus	2.5644	0.0056619
protein deubiquitination	2.5463	0.0059007
telomere maintenance	4.8697	0.007384
nuclear-transcribed mRNA catabolic process, nonsense-mediated decay	2.8697	0.0078248
double-strand break repair via nonhomologous end joining	4.4639	0.0098728
negative regulation of translation	4.229	0.011777
cellular response to lipopolysaccharide	4.229	0.011777
positive regulation of NF-kappaB transcription factor activity	3.293	0.013473
ubiquitin-dependent protein catabolic process	2.329	0.014019
neutrophil degranulation	1.9383	0.015133
negative regulation of apoptotic process	1.9988	0.016465
cytokine-mediated signaling pathway	3.0904	0.016956
cellular response to leukemia inhibitory factor	3.7372	0.017408
cell division	1.9503	0.018752
positive regulation of gene expression	2.5644	0.020459
viral process	1.7544	0.031599
SRP-dependent cotranslational protein targeting to membrane	2.4202	0.038274
translation	2.0603	0.044668
DNA repair	1.8748	0.046631
G1/S transition of mitotic cell cycle	2.5919	0.049216

Table 8. DNA damage repair and immune system related pathways are significantly represented in ubiquitome enrichment analysis comparing *DTX3L*$^{-/-}$ against WT cells.

*GOBP pathway enrichment analysis of retrieved ubiquitinated peptides in comparisons of **A)** untreated DTX3L$^{-/-}$ vs WT samples **B)** 3mM HU 4h treated DTX3L$^{-/-}$ vs WT samples, where pathway enrichment is >1.3 and statistically significant ($P < 0.05$, Fisher exact test).*

6.5.2. Ubiquitin Peptide Enrichment between HeLa WT and *DTX3L*$^{-/-}$ cells

Investigating specific peptide enrichment, and pertaining to the work presented here proposing TOPBP1 as a potential substrate of DTX3L, no significant difference was identified in the single retrieved ubiquitinated peptide for TOPBP1 between HeLa WT and *DTX3L*$^{-/-}$ in untreated or HU treated samples.

Other potentially relevant ubiquitinated-peptide fold changes were identified through result filtering. Retrieved peptides in HU treated samples with significant fold changes ($\geq$ +/- $\log_2$ 0.5, two sample t-test $P < 0.05$) were filtered for GOBP name matches including the term 'DNA damage' and a subselection of peptides were returned. These include cyclin D1 (CCND1), involved in cell cycle regulation during the G1/S phase transition. In both untreated and HU treated samples, retrieved ubiquitinated cyclin D1-K95 was significantly reduced ($\log_2$ -1.6744 FC and $\log_2$ -1.4910 FC, respectively) in *DTX3L*$^{-/-}$ samples compared to WT. Similarly, peptides such as USP1-K683 (deubiquitinates FANCD2) and HERC2-K2008 (E3 ubiquitin ligase, associated with DSBR via NHEJ) were found to be significantly reduced ($\log_2$ FC -0.5305 and -0.6467). Conversely, other filtered ubiquitinated peptides include POLD2-K90 ($\log_2$ FC +0.5905, DNA polymerase delta subunit), XRCC6-K443 ($\log_2$ FC +1.0153, regulatory subunit of DNA-PK) and MSH6-K1233 ($\log_2$ FC +0.6861, mismatch repair protein), found to be significantly enriched in *DTX3L*$^{-/-}$ compared to WT. In both UT and HU treated samples, UBE2A (ubiquitin conjugating enzyme) was enriched ($\log_2$ FC +0.6861 and +0.7180) in *DTX3L*$^{-/-}$ vs WT.

Additional peptides were identified with a $\log_2$ FC determined to be statistically significant upon group-wise comparison through ANOVA ($P < 0.05$). This included two RAD21 ubiquitinated peptides (ubiquitinated at K406 and K335).

RAD21 is a member of the cohesion complex involved in proper chromosome segregation. RAD21-K406 and RAD21-K335 were found to be reduced in HU treated *DTX3L*$^{-/-}$ samples (log_2 FC -0.4234 and -0.4467 respectively) and in UT *DTX3L*$^{-/-}$ samples (log_2 FC -0.6402 and -0.5292 respectively). POLD1-K648 (-0.1906), POLD1-K676 (-0.1110), POLD1-K1087 (-0.1238), POLE-K168 (-0.3444), DNA2-K968 (-0.2912, DNA nuclease) were also downregulated. SETX-K544 (+0.4719, DNA:RNA helicase), RAP80-K305 (+0.4908, BRCA1-A complex subunit), PCNA-K248 (+0.6437), NEDD8-K33 (+0.5544) were upregulated.

Many more peptides were retrieved (**Figure *50***) and may be interesting for further investigation. Additionally, many ubiquitinated peptides were identified as being significantly regulated (by two sample t-test, data not shown due to dataset size) in HU treated *DTX3L*$^{-/-}$ cells compared to WT, however these did not meet the threshold for log_2 FC or were not included after filtering for 'DNA damage' GOBP annotation. Despite this, these may also be interesting proteins to investigate for elucidating the role of DTX3L in the replication stress response, DNA damage response or cell physiology more widely.

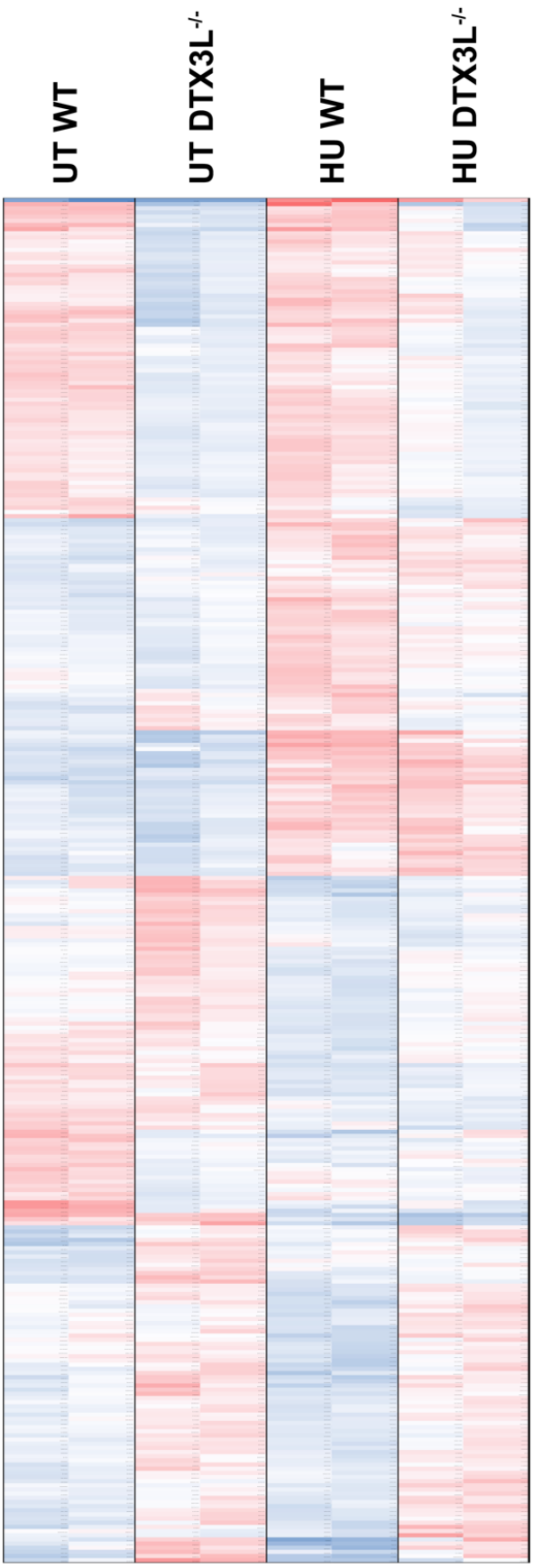

Figure 50. Differentially ubiquitinated peptides.

Ubiquitinated peptides were retrieved through ubiquitin remnant peptide IP and LC-MS/MS. Red indicates enrichment, blue indicates reduction. Over 300 retrieved ubiquitinated peptides are shown, determined to be significantly differentially ubiquitinated in at least one group as determined by ANOVA ($P < 0.05$).

6.6. Conclusion

With a previously explored role in the DNA damage response, and now a newly identified role being revealed in DNA replication and the tolerance of replication stress, it is important to understand how DTX3L mechanistically contributes to these processes.

Here, complementation studies have established the importance of ubiquitination activity to the role of DTX3L. Abrogation of the E3 ubiquitin ligase RING domain through previously described ‘M2’ point mutations resulted in a failure to rescue the replication fork defects observed with DTX3L depletion. Additionally, clinical mutations Y403X and A502V in DTX3L were investigated and Y403X was found to result in a similar defective resection phenotype, suggesting an underlying molecular cause for the condition. Additionally, heterodimerisation partner PARP9 was found to produce an additive fork degradation defect to DTX3L.

Excessive fork degradation exhibited by DTX3L deficiency was rescued through the inhibition of SMARCAL1, indicating a translocase responsible and supporting unscheduled fork regression arising through absence of DTX3L. Inhibition of MRE11 also rescued fork degradation, indicating a responsible nuclease. Investigating upstream factors that may be defective for this aberrant fork regression and degradation, or through fork repair by HR, DTX3L deficiency did not have an effect on the recruitment of RAD51 or BRCA1, suggesting an unaffected capacity to stabilise forks and initiate HR mediated recovery of stalled forks.

An exploratory approach was taken to identify targets of DTX3L responsible for the replication fork defects. Through IP-MS, TOPBP1 was identified as a potential interacting partner of DTX3L. Association of TOPBP1 and DTX3L was further validated by PLA and their increased association was observed in conditions of HU induced replication stress. Furthermore, ubiquitome enrichment analysis has identified a vast array of differentially ubiquitinated peptides upon DTX3L deficiency and in untreated and HU treated conditions, many of which may prove interesting for follow-up investigation. Pathway enrichment has indicated DTX3L regulates peptides involved in DNA damage and cell proliferation, as well as other pathways with previously described roles such as notch signalling and inflammation. This stands in support of the data shown in this study and of that generated by others (L. Wang et al., 2021; Yan et al., 2009, 2013; Y. Zhang et al., 2015).

This study provides a strong foundation establishing DTX3L as a factor involved in the replication stress response and in maintenance of genome stability. Building from this work, it will be important to explore potential targets of DTX3L ubiquitination pertaining to the maintenance of replication, of which targets such as TOPBP1 and CCND1 may be relevant.

Chapter 7: Discussion

This study aims to further our understanding of how cells maintain genome stability in the face of replication stress. Numerous factors have already been identified that contribute to maintenance of the replication programme, such as EXD2 and BOD1L, through the use of technologies that interrogate the replication fork at a molecular level (Higgs et al., 2015; Nieminuszczy et al., 2019). These factors have been evidenced to play crucial roles in maintaining fork stability and preventing severe genome instability as a result of replication stress. However, full understanding of the replication stress response and the factors involved in this process is still a work in progress. Here, DTX3L has been identified as a factor of the RSR and work has been instigated to identify mechanistically how this E3 ubiquitin ligase contributes to the RSR.

7.1. Summary

From the work carried out here, loss of DTX3L has been shown to lead to defective replication fork dynamics, both in unchallenged conditions and conditions of enhanced replication stress. A reduced ability to maintain fork progression, fork recovery from stalling and appropriate fork regression was observed with DTX3L deficiency. Cellular proliferation was also reduced in DTX3L deficient cells, however the cell cycle distribution of these cells was largely unaffected. Furthermore, depletion of DTX3L enhanced sensitivity to clinically relevant drugs that impede DNA replication.

An increase in DNA damage was observed upon DTX3L loss, likely arising through enhanced replication stress burden and a reduced stress tolerance. Interestingly, and in accordance with this, silencing of DTX3L resulted in a reduction in CHK1 phosphorylation. This suggests defective ATR activation and downstream RSR signalling, thus hinting at a putative role for DTX3L in promoting S-phase checkpoint activation.

Complementation studies revealed that DTX3L ubiquitination activity (through abrogation of the RING domain) is important for the prevention of excessive fork regression and unscheduled fork degradation. This was further supported through the investigation of clinically relevant mutations in DTX3L, where truncation mutation Y403X, omitting the RING domain of DTX3L, was also found to produce excessive fork reversal and degradation.

The defective fork regression exhibited by DTX3L deficiency was found to occur independently of the role of heterodimerisation partner PARP9, standing in contrast to an apparent requirement of PARP9 for DTX3L recruitment to DSBs (Yan et al., 2013). Additionally, fork regression was rescued through inhibition of fork repair factors SMARCAL1 and MRE11, indicating unscheduled fork reversal

and degradation by these factors as responsible for the defective RSR in DTX3L deficient cells. Recruitment of fork protection and repair factors RAD51, BRCA1 and MRE11 were largely unaffected by DTX3L depletion.

Furthermore, an *in vivo* association of DTX3L and TOPBP1 was identified, which is of interest given the role of TOPBP1 in ATR activation. Importantly, this association was found to be upregulated in conditions of HU-induced replication stress; further studies will be required to functionally characterise this interaction.

Finally, through ubiquitome enrichment analysis, a vast dataset of differentially ubiquitinated proteins were identified in the presence and absence of DTX3L, in unchallenged and replication stress induced conditions. Pathway enrichment analysis revealed an enrichment of these differentially ubiquitinated peptides in pathways that include DNA damage repair and cell proliferation, as well as other pathways where DTX3L is known to function such as notch signalling and immuno-modulation.

7.2. DTX3L Acts at the Stalled Replication Fork to Overcome Challenges to Replication

Previously to this study, work carried out by others has suggested a role for DTX3L in the DNA damage response (Yan et al., 2009, 2013). These studies proposed that abrogation of DTX3L, through associated mono-ubiquitination at H4K91, leads to defective H4K20 methylation and a delay in 53BP1 recruitment kinetics to sites of DNA damage. Given this association of DTX3L with DNA damage recruitment and repair, and the identification of DTX3L at the challenged replication fork through iPOND-MS, we sought to investigate if DTX3L had a role in maintaining replication through the RSR.

The DNA fibre analysis technique is a powerful method to interrogate the role of genetic factors in DNA replication and the tolerance of challenges to this process, at single molecule resolution. Different versions of the assay exist, varying on how DNA fibres are distributed and how actively replicating DNA is labelled. Variants of the technique have been employed by numerous labs, with fluorography-based techniques being utilised and developed for over twenty years (D. A. Jackson & Pombo, 1998).

In this study, DNA fibre analysis was employed to investigate alterations in active fork dynamics as a result of the abolishment of select E3 ubiquitin ligases found to be present at the replication fork. This served as a starting point for the identification of novel factors that contribute to the tolerance of replication stress in eukaryotic cells. E3 ligases such as RFWD3 were identified at the fork through iPOND-MS and, through DNA fibre, exhibited to produce fork defects upon their depletion. RFWD3 has recently been identified to polyubiquitinate RPA, promoting damage bypass and fork restart, demonstrating a known role for

RFWD3 in the RSR and validating these approaches in the identification of RSR factors (Elia, Wang, et al., 2015; Gong & Chen, 2011; Lin et al., 2018).

To our knowledge, this is the first study to demonstrate the contribution of DTX3L to maintaining active replication fork dynamics. Here, DTX3L was identified from iPOND-MS in unchallenged conditions, and through fibre analysis DTX3L abrogation was found to impair global replication fork dynamics in unchallenged conditions, suggesting a role for DTX3L even in unchallenged DNA replication and/or overcoming endogenous replication stress (as well as in response to enhanced replication stress). This proposes the question as to whether DTX3L is constitutively present at the replication fork or recruited rapidly in the face of potential lesions. Through laser microirradiation studies in HeLa cells, DTX3L was found to be recruited to sites of DNA damage in less than 1 minute, with maximal recruitment for approximately 10 minutes and subsequent release thereafter (Yan et al., 2013). This suggests that DTX3L is capable of being rapidly recruited and localised in the nucleus, but it remains to be seen whether this is the case when responding to lesions challenging active DNA replication.

Employing CRISPR gene editing, the altered fork dynamics in RNAi treated cells were validated in stable cellular models of DTX3L deficiency, demonstrating that DTX3L contributes to maintenance of the actively progressing replication fork in both a model of cancer (HeLa cells) as well as non-cancer cells (RPE-1 cells).

7.3. DTX3L and the Maintenance of Genome Stability

Concerning the role of DTX3L in the DDR, work here also stands in support of this. Previously published work demonstrated an increase in DNA damage as a result of DTX3L silencing through comet assay in response to low-dose ionising radiation (200cGy), with up to 24h recovery (Yan et al., 2013). Here, DTX3L depletion also resulted in an increase in DSB DNA damage (indicated by γH2AX foci, in response to 10Gy ionising radiation with 6h recovery). While interesting, high dose IR also has the potential to introduce complex DNA damage. Many resultant DSBs are less able to be repaired, resulting in apoptosis, necrosis or senescence (Adjemian et al. 2020). Additional experiments utilising lower dose radiation may be even more informative on the specific DNA repair dynamics of cells depleted for DTX3L compared to WT, revealing a greater difference between the number of resultant DSBs, and additionally doses such as 2-3Gy will be more clinically relevant (Mavragani et al. 2019).

One aspect where findings differ concern 53BP1 foci analysis. In this study, 53BP1 foci were increased upon HU treatment and upon silencing of DTX3L, suggesting increased DNA damage as a result of enhanced replication stress. Interestingly, this stands in contrast with previously published work showing a delay in 53BP1 kinetics of accumulation at damage sites at 1, 2 and 4 hours compared to control (Yan et al., 2009). Differences in procedure could account for this; in the latter case, cells were treated with doxorubicin and the percentage of cells with foci were counted, as opposed to number of foci per cell. Lesions formed through HU treatment may necessitate different kinetics of repair compared to doxorubicin treatment (requiring nucleolytic excision of the adduct or proteolytic degradation of TOPII leads to DSBs necessitating DSBR by NHEJ)

(Nitiss, 2009). Conversely, collapsed forks forming DSBs induced by HU may be repaired by HRR.

Also pertaining to the quantification of genomic instability, micronuclei scoring is widely used to assess the consequences of genetic abrogation or genotoxin exposure. In the present study, an increase in micronuclei was observed in hydroxyurea treated cells depleted for DTX3L, suggesting DTX3L contributes to genome stability. The origin of these micronuclei may be be determined by analysing the presence of centromeres (indicating their origin from acentric fragments or lagging whole chromosomes excluded from daughter cells post-mitosis). Additionally, staining with γH2AX antibody can indicate their formation originating from DSBs, as opposed to microtubule dissociation defects. A supplementary approach that permits detection of a subtle increase in genome instability is through flow-cytometry based micronuclei scoring and may be useful for further quantization.

Additionally in this study, it was observed that both HeLa and U2OS cells depleted for DTX3L and treated with hydroxyurea produced an increase in RPA foci intensity, suggesting ssDNA formation from replication fork stalling. Interestingly, of note in U2OS cells specifically, an increase in ssDNA was observed upon DTX3L depletion even in untreated cells. One possible reason for this could be due to genetic differences in these cell lines; indeed, U2OS cells possess a break-induced repair mechanism for the alternative lengthening of telomeres (ALT pathway); it is possible that factors in this pathway contribute to the maintenance of DNA replication at other loci, or that U2OS possess subtle differences in other DDR pathways enabling more extensive ssDNA formation.

7.4. Mechanistic Action of DTX3L in the RSR

In the previous two chapters, evidence has been provided suggesting a role for DTX3L more specifically in the replication stress response. Here, foundations have been established to elucidate the mechanism by which DTX3L contributes to DNA replication and replication stress tolerance, with many avenues generated for further investigation.

7.4.1. DTX3L Requires Ubiquitination Function to Mediate Replication Stress Tolerance

DTX3L is an E3 ubiquitin ligase in possession of a C-terminal region RING domain, capable of ubiquitinating other proteins as well as self-ubiquitination (Takeyama, 2003). It has been shown that deletion of this domain (Takeyama, 2003, Yan 2009) leads to abrogation of ubiquitination activity and, more specifically, loss of mono-ubiquitination on histone 4 (H4). Additionally, it has also been shown that co-expression of DTX3L with a mutated RING domain, compared to WT DTX3L, failed to rescue the DNA damage phenotype associated with defective H4K91 ubiquitination (Tessadori 2017). The data presented here provides evidence to suggest that the DTX3L RING mutant (M2) was inadequate for the rescue of the fork resection defect, suggesting that the E3 ubiquitin ligase activity of DTX3L specifically is integral for regulation of fork stability, likely *via* its role in modulating fork regression and resection.

In light of this, it will be important to identify the ubiquitination target(s) of DTX3L that mechanistically contribute to the replication stress response. Given the role of H4K91 ubiquitination in the DNA damage response, it is yet to be investigated if this residue modification is relevant to the replication stress response, and may

be an interesting future avenue of study, especially given its association with genomic instability and developmental disorders (Tessadori et al., 2017; Yan et al., 2009).

Histone modifications are known to play a crucial role in the reorganisation of chromatin for DNA damage repair processes as well as DNA replication and transcription. Additionally, maintenance of epigenetic information is dependent on chromatin restoration on nascent DNA (Alabert & Groth, 2012; Groth et al., 2007; Jasencakova & Groth, 2010). It remains to be seen whether H4K91 mono-ubiquitination is involved in regulation of chromatin architecture, or whether this histone PTM leads to associated modification of other histone PTMs important for fork repair factor recruitment. Indeed, newly synthesized histones have been found to be acetylated at H4K91 prior to their incorporation into chromatin, however mutations at this residue, associating the abolishment of this modification (through mutation of the modified residue) with sensitivity to replication impeding agents, do not distinguish between the loss of acetylation or ubiquitination at this residue (Ye et al., 2005).

In relation to developmental disorders, the DNA fibre analysis performed here has permitted modelling of clinically relevant mutations of DTX3L in a system that elucidates detail on the molecular level. Given that the Y403X mutation was predicted to result in a truncation protein with exclusion of the functional E3 ubiquitin ligase RING domain, it is unsurprising that transfection of this construct alone does not result in rescue of the fork resection defect and confirms the observation that a functional RING domain is required for maintenance of appropriate fork regression and resection. This is further validated through the observation that rescue is achieved through introduction of the WT construct, and

also through introduction of the A502V mutant construct. While presence of the A502V mutation was found to have little consequence on the function of DTX3L pertaining to maintenance of fork stability, it is possible that this residue may modulate other potential aspects of DTX3L function in other cellular pathways unrelated to that discussed here.

In the case of co-transfection with both Y403X and A502V constructs, only a partial rescue in the fork regression defect is observed which, on the surface, may suggest that a certain level of DTX3L expression and regulation is required for scheduled fork regression and avoidance of excessive resection. Due to HeLa cells being genetically abnormal compared to non-cancer cells and having high endogenous expression of DTX3L protein (Juszczynski et al., 2006; Yan et al., 2009), it is difficult to translate what the requirement for DTX3L would be in a patient background and thus necessitates further study on patient derived cells. It may be speculated that in the case of our patient, at least two functional copies of the WT DTX3L gene are required and the presence of Y403X in one inherited allele produces haploinsufficiency, instead of the initial suggestion of compound heterozygosity with the A502V allele. Acquiring relevant clinical information, if any, from the patient's parent contributing the Y403X allele may validate this. Unfortunately, we were unable to gain further information on the clinical phenotypes of the patient due to limited correspondence from the patient's clinician.

7.4.2. Contribution of PARP9 to Observed Fork Defects

As mentioned, DTX3L forms heterodimers with binding partner PARP9. Here, depletion of PARP9 was found to partially produce a mild fork degradation defect

compared to control, but this was not as severe as that observed upon DTX3L depletion. Upon co-depletion, fork defects were found to be compounding suggesting an absence of epistasis.

The observation that PARP9 depletion leads to a mild fork resection defect appears counterintuitive, given PARP9 restrains ubiquitination activity of DTX3L (Yang et al., 2017). However, PARP9 is required for DTX3L recruitment to laser microirradiation induced DNA breaks and therefore may also be required for DTX3L recruitment to fork lesions (Yan et al., 2013). Investigating the recruitment of DTX3L to the replication fork upon PARP9 depletion will be an interesting aspect of future work. PARP9 depletion, similarly to DTX3L depletion, has also been found to reduce cell proliferation (Yan et al., 2013), providing impetus for the future investigation of the contribution of PARP9 to the RSR.

7.4.3. Fork Resection Arising Through DTX3L Deficiency is Mediated by SMARCAL1 and MRE11

Given that the evidence here suggests an absence of DTX3L leads to greater fork resection, likely through loss of DTX3L-mediated ubiquitination, it was important to understand if this was due to extensive fork reversal, and identify the factors involved to further understand how DTX3L contributes to fork stability.

A number of fork protection factors exist to shield DNA ends from degradation upon fork regression, driven by remodellers such as SMARCAL1, ZRANB3, HLTF and F-box DNA helicase 1 (FBH1) (W. Liu et al., 2020). Here, we observe that the fork degradation observed in cells deficient for DTX3L is dependent on fork remodeller mediated regression, as knockdown of SMARCAL1 leads to a complete rescue of the fork resection defect. This is similar to the rescue observed upon SMARCAL1 knockdown in BRCA1/2 deficient cells (Taglialatela

et al., 2017). Given that ZRANB3 and HLTF have been suggested to act in a concerted manner with SMARCAL1 (Taglialatela et al., 2017), and their knockdown prevents fork degradation in BRCA2-deficient cells (W. Liu et al., 2020; Mijic et al., 2017), as well as other mutant backgrounds (W. Liu et al., 2021), it is likely that knockdown of these factors may also suppress fork degradation upon DTX3L loss.

Following on from this, it was also important to characterise the factors contributing to excessive fork resection. Here we observe that MRE11 is likely to be the nuclease responsible for degradation of reversed forks in *DTX3L*$^{-/-}$ cells, as inhibition by mirin also resulted in a complete rescue. Other nucleases such as DNA2 may also contribute to resection, but due to time constraints were not investigated.

7.4.4. Recruitment of Fork Repair Factors is Not Significantly Affected by DTX3L Depletion

Fork repair factor recruitment of factors such as RAD51, BRCA1 and MRE11 are important for the HR mediated repair of stalled forks (or BIR of forks in S-phase) and for protection of stalled forks (Ait Saada et al., 2018; Schlacher et al., 2012). There appeared to be no defect in RAD51 recruitment to nascent DNA upon loss of DTX3L, suggesting the MRE11-mediated fork resection defect may not be a result of unprotected ssDNA arising through defective RAD51 recruitment or retention. Conversely, the low number of EdU-RAD51 PLA foci detected should also be taken into consideration; given that mirin treatment was found to rescue the over-resection phenotype in DTX3L deficient cells, one would expect enhanced RAD51 recruitment or nucleofilament formation to produce a

corresponding increase in EdU-RAD51 foci detection resulting from extensive resection. Analysis of EdU-RPA PLA foci may corroborate this. Based on the increase in RPA foci detected by IF, it may be possible that DTX3L-mediated nascent DNA protection is interrupted downstream of RPA accumulation, possibly due to an impairment of RAD51 loading. This RAD51 loading at stalled forks could in turn could be related to perturbed histone modifications (Xu et al., 2021), such as that of H4K20me associated DTX3L depletion (Yan et al., 2009). It would be interesting to explore whether RAD51 overexpression in DTX3L deficient cells can rescue the over resection phenotype. Additionally, previous work has shown that RAD51 foci are induced during late replication blocks, therefore it may be interesting to investigate RAD51 foci formation with hydroxyurea treatment across a prolonged time course, beyond 3 hours (Petermann et al., 2010).

Here, BRCA1 recruitment at EdU labelled forks was also found to be unaffected, implying an intact capacity for HR repair of stalled forks, antagonization of 53BP1 binding and adequate RAD51 loading onto ssDNA. The inclusion of BRCA2 recruitment will further validate this. Perhaps surprisingly, MRE11 recruitment was observed to be reduced in one clone (clone 24); this stands in contrast to the fibre analysis data where inhibition of MRE11 by mirin was found to rescue the regression defect in *DTX3L*$^{-/-}$ cells. However, given that the defect was relatively small and only observed in one clone, it is unlikely to be biologically relevant in this context.

Given the defective ATR activation observed in *DTX3L*$^{-/-}$ cells and the role of ATR in restraining SMARCAL1 activity (Couch et al., 2013), it is likely that the observed fork degradation defect in *DTX3L*$^{-/-}$ cells is at least partially due to

misregulation of fork remodelling. For future work, it will be important to investigate the effect of ATR inhibition on the fork resection defect in *DTX3L*$^{-/-}$ cells.

Overall, these experiments suggest that the unscheduled fork regression and excessive resection observed in the absence of DTX3L is a consequence of some other mechanism, but unscheduled resection by MRE11 is not a result of defect in RAD51 or BRCA1 recruitment to regressed replication forks, or defective HR repair of stalled forks.

7.4.5. DTX3L Associates With TOPBP1 Under Conditions of Enhanced Replication Stress

Due to the numerous factors involved in replication fork maintenance, protection and repair, it was important to take an exploratory approach to identify targets of DTX3L that may facilitate its role in the RSR. PARP9 and H4K91 have been evidenced in the literature to be a binding partner and target respectively of DTX3L, however no extensive analysis has been performed on the interactome of DTX3L and it is likely many other proteins are yet to be identified. Here, GFP-DTX3L was used to interrogate the interactome through co-IP. Characterisation of the GFP-DTX3L construct in stable GFP-DTX3L expressing clones demonstrated nuclear localisation of the protein, as expected given the presence of an NLS in the N-terminal region of DTX3L and corroborates what has been seen previously (Yan et al., 2013), suggesting the transgene was being expressed as expected.

Utilising this construct for co-immunoprecipitation coupled to mass spectrometry in HEK293 cells revealed the presence of TOPBP1, suggesting that DTX3L and

TOPBP1 may interact in vivo. This interaction was validated in HeLa cells by co-IP, using a FLAG-DTX3L construct and an antibody against endogenous TOPBP1 to ensure a tag-independent interaction. From these experiments, it seems likely that a DTX3L and do interact, and that this interaction is enhanced in conditions of replication stress. These observations have not, to my knowledge, been documented previously in the literature. Further characterisation of the DTX3L-TOPBP1 interaction is essential to establish a possible role of this protein in promoting ATR activation.

With regards to how DTX3L and TOPBP1 may interact on a domain level, computational annotated motif prediction suggests that DTX3L may possess BRCT-phosphopeptide ligand sites (ELM Resource, (ELM - DTX3L_HUMAN, 2021). Indeed, many BRCT domain containing proteins function in the DDR (Day et al., 2021; Gerloff et al., 2012), of which potential DTX3L BRCT phosphopeptides may act as a ligand. TOPBP1 has been structurally well-characterised and is composed of multiple BRCT modular domains that can bind to these phosphorylated serine motifs (Wardlaw et al., 2014). Indeed, phospholigands on repair proteins such as BLM and FANCJ have been evidenced to bind to BRCT domains of TOPBP1; it is unclear however whether these associations have a role on ligand protein function, or just their recruitment (Day et al., 2021). Mutations of these regions in future work may elucidate a potential role of these putative DTX3L BRCT phosphopeptide ligands and establish their relevance to DTX3L function.

TOPBP1 is a crucial protein for DNA replication and is a factor important for the activation of ATR/CHK1 in the replication stress response (Kim et al., 2021;

Velichko et al., 2021). Interestingly, it has recently been reported that while TOPBP1 is important for activation of the replication stress response, overexpression of TOPBP1 has also been shown to hinder activation of the ATR/CHK1 response (K. Liu et al., 2021). One angle of speculation incites a theory that deregulation of TOPBP1 may arise through an absence of interaction with DTX3L, leading to the observed defective replication stress response. Given the canonical role of ubiquitination in the ubiquitin proteosomal system (UPS), it is possible that stability of TOPBP1 is at least in part regulated by DTX3L ubiquitination. Indeed, TOPBP1 turnover is regulated via ubiquitination by hHYD in unstressed conditions (Honda et al., 2002). Irradiation leads to diminished TOPBP1 ubiquitination, resulting in its stable colocalization with γH2AX damage induced foci (Honda et al., 2002). Unfortunately, due to time limitations this avenue of investigation was not pursued, however future work investigating the role of enhanced replication stress and the effect of DTX3L deficiency on TOPBP1 ubiquitination and cellular stability of TOPBP1 is required. Perhaps counterintuitively, here we see that association between TOPBP1 and DTX3L is upregulated in conditions of enhanced replication stress, presumably leading to increased TOPBP1 ubiquitination. It is important to consider that this increased interaction (***Figure 48***) may be an artefact of increased TOPBP1 expression in response to increased DNA damage, therefore increasing the proportion of DTX3L-TOPBP1 binding observed. It is also possible there is a greater availability of substrate (stalled/regressed forks) for DTX3L and TOPBP1 recruitment, resulting their increased association. It will therefore be important to directly investigate the effect of DTX3L deficiency on TOPBP1 ubiquitination and stability under these conditions. Additionally, USP13 is a de-ubiquitinating enzyme (DUB) that stabilises TOPBP1, of which depletion of USP13 has been found to impede

ATR activation and hypersensitize cells to replication-stress inducing agents (Kim et al., 2021). It is likely that the fine-tuning of TOPBP1 stability, modulated by ubiquitination, is crucial for the cell in maintaining an appropriate ATR response to DNA damage, and future work will elucidate if DTX3L contributes to this.

As discussed in Chapter 1.7, ubiquitination is a dynamic process that also performs an array of non-proteolytic functions which include localisation, mediation of PPIs, and modulation of protein activity (Z. J. Chen & Sun, 2009). It may also be possible that direct TOPBP1 ubiquitination by DTX3L may instead regulate TOPBP1 activity or localisation to sites of replication fork challenge, or indirectly through modification of other factors at the fork, of which future work may elucidate this. Indeed, ubiquitination of BLM at stalled replication forks by E3 ubiquitin ligase TRIM25 enhances BLM recruitment, demonstrating a non-proteolytic role of this PTM in the RSR (Zhao et al., 2017).

Future work exploring the recruitment of TOPBP1, as well as the recruitment and activation of ATR at stalled replication forks in *DTX3L*$^{-/-}$ cells will be important.

7.4.6. *DTX3L*$^{-/-}$ Ubiquitome Enrichment Analysis

Ubiquitome enrichment analysis in loss of function experiments have been used to elucidate substrates of numerous E3 ubiquitin ligases such as HUWE1, but this study is the first to do so with DTX3L (Thompson et al., 2014). While being a powerful exploratory technique for overcoming the challenge of identifying substrates of E3 ubiquitin ligases, ubiquitome enrichment analysis is also limited by its ability to distinguish between ubiquitination events that are degradational or non-degradational. This may be overcome through the inclusion of non MG-

132 (proteosome inhibitor) treated samples, however this was not feasible due to expense limitations.

Despite this, a multitude of differentially ubiquitinated peptides were differentially enriched in cells deficient for DTX3L compared to wild-type under HU treated conditions. Cell cycle regulator cyclin D1, USP1, a deubiquitinating factor of FANCD2 and HERC2, an E3 ubiquitin ligase associated with DSBR by NHEJ were relevant hits found to be significantly reduced, suggesting that DTX3L may directly ubiquitinate these proteins as part of the RSR. Additionally, some ubiquitinated peptides were found to be upregulated in HU treated *DTX3L*$^{-/-}$ cells such as POLD2, DNA-PK regulatory subunit XRCC6 and mismatch repair protein MSH6. In the absence of DTX3L, this ubiquitination must be mediated by other E3 ligases and will be more complex to elucidate the mechanism of DTX3L here; it is possible that loss of ubiquitination by DTX3L leads to stabilisation of other E3 ubiquitin ligases, or these ubiquitination events may be compensatory in the absence of DTX3L.

Identification of cyclin D1 as a potential substrate of DTX3L ubiquitination is interesting given the importance of cyclin D1 regulation by the proteosome degradation system for the prevention of cancer. Indeed, inhibition of cyclin D1 degradation inhibits G1 arrest and increases cell sensitivity to DNA damage and carcinogenesis, of which lysine modifications including that of K95-ubiquitination has been found to contribute to cyclin D1 degradation (Q. Feng et al., 2007). In the absence of DTX3L, it may be possible that the increased stability of this oncogene product leads to an increased burden of replication stress. Indeed, overexpression of cyclin D1 has been found to perturb replication fork

progression, and lead to an increase in DSBs (Shimura et al., 2013). Furthermore, high expression of DTX3L was found to result in cell cycle arrest in multiple myeloma cells (Shen et al., 2017). Follow-up functional studies will help elucidate the role of DTX3L on cyclin D1 regulation.

Given the role of FANCD2 in regressed fork protection and restart (Kais et al., 2016; W. Liu et al., 2021), and the role of USP1 in regulating DNA repair mechanisms including the FA pathway (Nijman et al., 2005), it is also interesting to observe that USP1 is also a potential substrate of DTX3L ubiquitination.

Interestingly, HERC2 is required for HRR but has also been shown to be a component of the DNA replication fork complex, interacting with claspin and playing a critical role in DNA elongation and origin firing (Izawa et al., 2011). HERC2 has also been suggested to regulate stability of deubiquitinating enzyme USP20, which regulates claspin stability and CHK1 phosphorylation (Zhu et al., 2014). Unpicking these complex and dynamic ubiquitin signalling networks will require further functional characterisation to elucidate the significance of DTX3L deficiency on their regulation.

Furthermore, in the case of TOPBP1, only a single ubiquitinated peptide was retrieved. Although fold change enrichment in peptides can provide a useful indication for targets to follow up in functional studies, absence of enrichment does not indicate an absence of regulation and may be consequence of technical limitation.

While the results obtained here are a valuable starting point for further investigation into the targets of DTX3L ubiquitination concerning the RSR, they are limited by the presence of a cell batch effect introduced through sample acquisition; this may be attributed to differences in confluency upon harvesting

(despite attempts to ensure consistency), batch differences in drug treatments or technical variation in cell culture practice or sample handling. Additionally, some ubiquitination events are short-lived and may therefore require DUB inhibitors to detect, while other ubiquitination events may be sparsely observed, requiring even greater amounts of starting material. Furthermore, a degree of clonal variation was observed between *DTX3L*$^{-/-}$ clones; this may be the consequence of single-cell expansion and passaging (from CRISPR selection), resulting in deviating genetic backgrounds between clone 20 and clone 24. As a consequence, despite the retrieval of >20,000 ubiquitinated peptides, many ubiquitinated peptides may not meet the $\log_2$ FC and statistical significance thresholds despite potentially being biologically relevant.

Due to time constraints, the ubiquitinated peptides retrieved could not be followed up through functional experiments for validation but do provide ample opportunity for the project to be taken forward. Pathway enrichment adds weight to the involvement of DTX3L in regulation of the DNA damage and replication stress response pathways and is also supported by presence of immunological pathways where DTX3L has also been evidenced to play a role (see **Chapter 1.7.1**) (Juszczynski et al., 2006; Y. Zhang et al., 2015).

Pathway enrichment analysis also showed ubiquitome enrichment in pathways relating to viral processing. Antiviral DNA processing is mediated by the cGAS-STING pathway, resulting in interferon stimulated gene expression (Wu et al., 2019). Interestingly, DTX3L, and PARP9, are expressed via an interferon stimulated gene promoter and have been suggested to have a role in protection against viral infection (Wu et al., 2019; Y. Zhang et al., 2015). This could also

suggest that DTX3L has a role in responding to cytoplasmic DNA as a consequence of nuclear repair processes instigated by the RSR, leading to further response induction (Ho et al., 2016; Ragu et al., 2020). Indeed, the accumulation of cytoplasmic DNA is a common feature of tumours and cancer cell lines, of which cytoplasmic ssDNA fragments are released during stalled fork processing (Coquel et al., 2019, 2020; Gasser et al., 2017). Furthermore, a recent study exploring the cGAS interactome provides evidence showing enriched association of cGAS with DTX3L (Lum et al., 2018).

To summarise, the evidence presented here provides a compelling case for the involvement of DTX3L in the response to DNA damage and replication stress. In terms of clinical relevance, DTX3L has been found to be overexpressed in numerous cancers and in light of the work carried out here, this overexpression could reflect a dependency on the replication stress response to tolerate higher levels of replication stress and increased DNA damage intrinsic to cancer cells. Accordingly, DTX3L overexpression has been found to provide a chemoprotective effect to HU and doxorubicin treated HEK293 cells (Yan et al., 2009). Additionally, work carried out here demonstrates enhanced sensitivity to clastogens upon depletion of DTX3L. This may indicate DTX3L as a potential therapeutic target in cancers to abrogate an already established chemoresistance, or in cancers with a background (such as BRCA1/BRCA2 deficiency) that are already vulnerable to replication defects. Further experiments investigating sensitivity in a double deficient background may prove interesting.

The mechanism by which DTX3L elicits its function remains unclear, however it is likely that this function requires its E3 ligase activity and may be driven by a role in promoting ATR activation and/or fork remodelling. Ultimately, DTX3L may be a novel target for the selective treatment of cancer, or for abrogation of chemoresistance.

References

Abdel-Fatah, T. M. A., Middleton, F. K., Arora, A., Agarwal, D., Chen, T., Moseley, P. M., Perry, C., Doherty, R., Chan, S., Green, A. R., Rakha, E., Ball, G., Ellis, I. O., Curtin, N. J., & Madhusudan, S. (2015). Untangling the ATR-CHEK1 network for prognostication, prediction and therapeutic target validation in breast cancer. *Molecular Oncology*, *9*(3), 569. https://doi.org/10.1016/J.MOLONC.2014.10.013

Adjemian, S., Oltean, T., Martens, S. *et al.* (2020). Ionizing radiation results in a mixture of cellular outcomes including mitotic catastrophe, senescence, methuosis, and iron-dependent cell death. *Cell Death Dis 11,* 100. https://doi.org/10.1038/s41419-020-03209-y

Aguiar, R. C. T., Takeyama, K., He, C., Kreinbrink, K., & Shipp, M. A. (2005). B-aggressive lymphoma family proteins have unique domains that modulate transcription and exhibit poly(ADP-ribose) polymerase activity. *Journal of Biological Chemistry*, *280*(40), 33756–33765. https://doi.org/10.1074/jbc.M505408200

Ait Saada, A., Lambert, S. A. E., & Carr, A. M. (2018). Preserving replication fork integrity and competence via the homologous recombination pathway. *DNA Repair*, *71*, 135–147. https://doi.org/10.1016/J.DNAREP.2018.08.017

Alabert, C., & Groth, A. (2012). Chromatin replication and epigenome maintenance. In *Nature Reviews Molecular Cell Biology* (Vol. 13, Issue 3, pp. 153–167). Nature Publishing Group. https://doi.org/10.1038/nrm3288

Alderton, G. K., Joenje, H., Varon, R., Børglum, A. D., Jeggo, P. A., & O'Driscoll, M. (2004). Seckel syndrome exhibits cellular features demonstrating defects in the ATR-signalling pathway. *Human Molecular Genetics*, *13*(24), 3127–3138. https://doi.org/10.1093/HMG/DDH335

Al-Hakim, A., Escribano-Diaz, C., Landry, M.-C., O'Donnell, L., Panier, S., Szilard, R. K., & Durocher, D. (2010). The ubiquitous role of ubiquitin in the DNA damage response. *DNA Repair*, *9*(12), 1229–1240. https://doi.org/10.1016/J.DNAREP.2010.09.011

Andreassen, P. R., D'Andrea, A. D., & Taniguchi, T. (2004). ATR couples FANCD2 monoubiquitination to the DNA-damage response. *Genes & Development*, *18*(16), 1958. https://doi.org/10.1101/GAD.1196104

Artavanis-Tsakonas, S., Rand, M. D., & Lake, R. J. (1999). Notch signaling: Cell fate control and signal integration in development. In *Science* (Vol. 284, Issue 5415, pp. 770–776). American Association for the Advancement of Science. https://doi.org/10.1126/science.284.5415.770

Audeh, M. W., Carmichael, J., Penson, R. T., Friedlander, M., Powell, B., Bell-McGuinn, K. M., Scott, C., Weitzel, J. N., Oaknin, A., Loman, N., Lu, K., Schmutzler, R. K., Matulonis, U., Wickens, M., & Tutt, A. (2010). Oral poly(ADP-ribose) polymerase inhibitor olaparib in patients with BRCA1 or BRCA2 mutations and recurrent ovarian cancer: a proof-of-concept trial. *Lancet (London, England)*, *376*(9737), 245–251. https://doi.org/10.1016/S0140-6736(10)60893-8

Audoynaud, C., Vagner, S., & Lambert, S. (2021). Non-homologous end-joining at challenged replication forks: an RNA connection? *Trends in Genetics*, *37*(11), 973–985. https://doi.org/10.1016/J.TIG.2021.06.010

Bakos, G., Yu, L., Gak, I. A., Roumeliotis, T. I., Liakopoulos, D., Choudhary, J. S., & Mansfeld, J. (2018). An E2-ubiquitin thioester-driven approach to identify substrates modified with ubiquitin and ubiquitin-like molecules. *Nature Communications*, *9*(1). https://doi.org/10.1038/s41467-018-07251-5

Bansbach, C. E., Bétous, R., Lovejoy, C. A., Glick, G. G., & Cortez, D. (2009). The annealing helicase SMARCAL1 maintains genome integrity at stalled replication forks. *Genes & Development*, *23*(20), 2405. https://doi.org/10.1101/GAD.1839909

Bartkova, J., Hořejší, Z., Koed, K., Krämer, A., Tort, F., Zleger, K., Guldberg, P., Sehested, M., Nesland, J. M., Lukas, C., Orntoft, T., Lukas, J., & Bartek, J. (2005). DNA damage response as a candidate anti-cancer barrier in early human tumorigenesis. *Nature*, *434*(7035), 864–870. https://doi.org/10.1038/nature03482

Bekker-Jensen, S., & Mailand, N. (2011). The ubiquitin- and SUMO-dependent signaling response to DNA double-strand breaks. In *FEBS Letters* (Vol. 585, Issue 18, pp. 2914–2919). https://doi.org/10.1016/j.febslet.2011.05.056

Bermejo, R., Lai, M. S., & Foiani, M. (2012). Preventing Replication Stress to Maintain Genome Stability: Resolving Conflicts between Replication and Transcription. *Molecular Cell*, *45*(6), 710–718. https://doi.org/10.1016/J.MOLCEL.2012.03.001

Berti, M., Chaudhuri, A. R., Thangavel, S., Gomathinayagam, S., Kenig, S., Vujanovic, M., Odreman, F., Glatter, T., Graziano, S., Mendoza-Maldonado, R., Marino, F., Lucic, B., Biasin, V., Gstaiger, M., Aebersold, R., Sidorova, J. M., Monnat, R. J., Lopes, M., & Vindigni, A. (2013). Human RECQ1 promotes restart of replication forks reversed by DNA topoisomerase I inhibition. *Nature Structural & Molecular Biology*, *20*(3), 347. https://doi.org/10.1038/NSMB.2501

Berti, M., & Vindigni, A. (2016). Replication stress: Getting back on track. In *Nature Structural and Molecular Biology* (Vol. 23, Issue 2, pp. 103–109). Nature Publishing Group. https://doi.org/10.1038/nsmb.3163

Bétous, R., Couch, F. B., Mason, A. C., Eichman, B. F., Manosas, M., & Cortez, D. (2013). Substrate-selective repair and restart of replication forks by DNA translocases. *Cell Reports*, *3*(6), 1958–1969. https://doi.org/10.1016/J.CELREP.2013.05.002

Bétous, R., Goullet de Rugy, T., Pelegrini, A. L., Queille, S., de Villartay, J. P., & Hoffmann, J. S. (2018). DNA replication stress triggers rapid DNA replication fork breakage by Artemis and XPF. *PLOS Genetics*, *14*(7), e1007541. https://doi.org/10.1371/JOURNAL.PGEN.1007541

Boerkoel, C. F., Takashima, H., John, J., Yan, J., Stankiewicz, P., Rosenbarker, L., André, J. L., Bogdanovic, R., Burguet, A., Cockfield, S., Cordeiro, I., Fründ, S., Illies, F., Joseph, M., Kaitila, I., Lama, G., Loirat, C., McLeod, D. R., Milford, D. v., … Stockton, D. W. (2002). Mutant chromatin remodeling protein SMARCAL1 causes Schimke immuno-osseous dysplasia. *Nature Genetics 2002 30:2*, *30*(2), 215–220. https://doi.org/10.1038/ng821

Bouwman, P., Aly, A., Escandell, J. M., Pieterse, M., Bartkova, J., van der Gulden, H., Hiddingh, S., Thanasoula, M., Kulkarni, A., Yang, Q., Haffty, B. G., Tommiska, J., Blomqvist, C., Drapkin, R., Adams, D. J., Nevanlinna, H., Bartek, J., Tarsounas, M., Ganesan, S., & Jonkers, J. (2010). 53BP1 loss rescues BRCA1 deficiency and is associated with triple-negative and BRCA-mutated breast cancers. *Nature Structural & Molecular Biology*, *17*(6), 688–695. https://doi.org/10.1038/NSMB.1831

Broderick, R., Nieminuszczy, J., Baddock, H. T., Deshpande, R. A., Gileadi, O., Paull, T. T., McHugh, P. J., & Niedzwiedz, W. (2016). EXD2 promotes homologous recombination by facilitating DNA end resection. *Nature Cell Biology*, *18*(3), 271–280. https://doi.org/10.1038/ncb3303

Brown, E. J., & Baltimore, D. (2000). ATR disruption leads to chromosomal fragmentation and early embryonic lethality. *Genes and Development*, *14*(4), 397–402. https://doi.org/10.1101/gad.14.4.397

Bunting, S. F., Callén, E., Wong, N., Chen, H. T., Polato, F., Gunn, A., Bothmer, A., Feldhahn, N., Fernandez-Capetillo, O., Cao, L., Xu, X., Deng, C. X., Finkel, T.,

Nussenzweig, M., Stark, J. M., & Nussenzweig, A. (2010). 53BP1 inhibits homologous recombination in Brca1-deficient cells by blocking resection of DNA breaks. *Cell*, *141*(2), 243–254. https://doi.org/10.1016/J.CELL.2010.03.012

Byun, T. S., Pacek, M., Yee, M. C., Walter, J. C., & Cimprich, K. A. (2005). Functional uncoupling of MCM helicase and DNA polymerase activities activates the ATR-dependent checkpoint. *Genes and Development*, *19*(9), 1040–1052. https://doi.org/10.1101/gad.1301205

Ceccaldi, R., Liu, J. C., Amunugama, R., Hajdu, I., Primack, B., Petalcorin, M. I. R., O'Connor, K. W., Konstantinopoulos, P. A., Elledge, S. J., Boulton, S. J., Yusufzai, T., & D'Andrea, A. D. (2015). Homologous-recombination-deficient tumours are dependent on Polθ-mediated repair. *Nature*, *518*(7538), 258–262. https://doi.org/10.1038/NATURE14184

Chang, H. H. Y., Pannunzio, N. R., Adachi, N., & Lieber, M. R. (2017). *Non-homologous DNA end joining and alternative pathways to double-strand break repair*. https://doi.org/10.1038/nrm.2017.48

Chapman, J. R., Barral, P., Vannier, J. B., Borel, V., Steger, M., Tomas-Loba, A., Sartori, A. A., Adams, I. R., Batista, F. D., & Boulton, S. J. (2013). RIF1 Is Essential for 53BP1-Dependent Nonhomologous End Joining and Suppression of DNA Double-Strand Break Resection. *Molecular Cell*, *49*(5), 858–871. https://doi.org/10.1016/J.MOLCEL.2013.01.002/ATTACHMENT/466B9ED5-FBE8-489B-92AB-E7E4C789EAAF/MMC1.PDF

Chaudhuri, A. R., Callen, E., Ding, X., Gogola, E., Duarte, A. A., Lee, J. E., Wong, N., Lafarga, V., Calvo, J. A., Panzarino, N. J., John, S., Day, A., Crespo, A. V., Shen, B., Starnes, L. M., de Ruiter, J. R., Daniel, J. A., Konstantinopoulos, P. A., Cortez, D., … Nussenzweig, A. (2016). Replication fork stability confers chemoresistance in BRCA-deficient cells. *Nature*, *535*(7612), 382–387. https://doi.org/10.1038/nature18325

Chen, C.-C., Feng, W., Lim, P. X., Kass, E. M., & Jasin, M. (2018). Homology-Directed Repair and the Role of BRCA1, BRCA2, and Related Proteins in Genome Integrity and Cancer. *Annual Review of Cancer Biology*, *2*, 313–336. https://doi.org/10.1146/annurev-cancerbio-030617-050502

Chen, J., Feng, W., Jiang, J., Deng, Y., & Huen, M. S. Y. (2012). Ring finger protein RNF169 antagonizes the ubiquitin-dependent signaling cascade at sites of DNA damage. *Journal of Biological Chemistry*, *287*(33), 27715–27722. https://doi.org/10.1074/jbc.M112.373530

Chen, Y. H., Jones, M. J. K., Yin, Y., Crist, S. B., Colnaghi, L., Sims, R. J., Rothenberg, E., Jallepalli, P. v., & Huang, T. T. (2015). ATR-mediated phosphorylation of FANCI regulates dormant origin firing in response to replication stress. *Molecular Cell*, *58*(2), 323–338. https://doi.org/10.1016/J.MOLCEL.2015.02.031

Chen, Z. J., & Sun, L. J. (2009). Nonproteolytic functions of ubiquitin in cell signaling. *Molecular Cell*, *33*(3), 275–286. https://doi.org/10.1016/J.MOLCEL.2009.01.014

Ciccia, A., Bredemeyer, A. L., Sowa, M. E., Terret, M. E., Jallepalli, P. v., Harper, J. W., & Elledge, S. J. (2009). The SIOD disorder protein SMARCAL1 is an RPA-interacting protein involved in replication fork restart. *Genes & Development*, *23*(20), 2415. https://doi.org/10.1101/GAD.1832309

Ciccia, A., & Elledge, S. J. (2010). The DNA Damage Response: Making It Safe to Play with Knives. In *Molecular Cell* (Vol. 40, Issue 2, pp. 179–204). https://doi.org/10.1016/j.molcel.2010.09.019

Cimprich, K. A., & Cortez, D. (2008). ATR: An essential regulator of genome integrity. In *Nature Reviews Molecular Cell Biology* (Vol. 9, Issue 8, pp. 616–627). https://doi.org/10.1038/nrm2450

Connor, F., Bertwistle, D., Joseph Mee, P., Ross, G. M., Swift, S., Grigorieva, E., Tybulewicz, V. L. J., & Ashworth, A. (1997). Tumorigenesis and a DNA repair defect in mice with a truncating Brca2 mutation. *Nature Genetics 1997 17:4*, *17*(4), 423–430. https://doi.org/10.1038/ng1297-423

Couch, F. B., Bansbach, C. E., Driscoll, R., Luzwick, J. W., Glick, G. G., Bétous, R., Carroll, C. M., Jung, S. Y., Qin, J., Cimprich, K. A., & Cortez, D. (2013). ATR phosphorylates SMARCAL1 to prevent replication fork collapse. *Genes and Development*, *27*(14), 1610–1623. https://doi.org/10.1101/gad.214080.113

Curti, L., & Campaner, S. (2021). MYC-Induced Replicative Stress: A Double-Edged Sword for Cancer Development and Treatment. *International Journal of Molecular Sciences*, *22*(12). https://doi.org/10.3390/IJMS22126168

Davis, A. J., & Chen, D. J. (2013). DNA double strand break repair via non-homologous end-joining. *Translational Cancer Research*, *2*(3), 130–143. https://doi.org/10.3978/J.ISSN.2218-676X.2013.04.02

Day, M., Oliver, A. W., & Pearl, L. H. (2021). Phosphorylation-dependent assembly of DNA damage response systems and the central roles of TOPBP1. *DNA Repair*, *108*, 103232. https://doi.org/10.1016/J.DNAREP.2021.103232

de Klein, A., Muijtjens, M., van Os, R., Verhoeven, Y., Smit, B., Carr, A. M., Lehmann, A. R., & Hoeijmakers, J. H. J. (2000). Targeted disruption of the cell-cycle checkpoint gene ATR leads to early embryonic lethality in mice. *Current Biology : CB*, *10*(8), 479–482. https://doi.org/10.1016/S0960-9822(00)00447-4

Dehé, P. M., & Gaillard, P. H. L. (2017). Control of structure-specific endonucleases to maintain genome stability. *Nature Reviews Molecular Cell Biology 2017 18:5*, *18*(5), 315–330. https://doi.org/10.1038/nrm.2016.177

Doil, C., Mailand, N., Bekker-Jensen, S., Menard, P., Larsen, D. H., Pepperkok, R., Ellenberg, J., Panier, S., Durocher, D., Bartek, J., Lukas, J., & Lukas, C. (2009). RNF168 binds and amplifies ubiquitin conjugates on damaged chromosomes to allow accumulation of repair proteins. *Cell*, *136*(3), 435–446. https://doi.org/10.1016/J.CELL.2008.12.041

Dungrawala, H., Rose, K. L., Bhat, K. P., Mohni, K. N., Glick, G. G., Couch, F. B., & Cortez, D. (2015). The Replication Checkpoint Prevents Two Types of Fork Collapse without Regulating Replisome Stability. *Molecular Cell*. https://doi.org/10.1016/j.molcel.2015.07.030

Dupré, A., Boyer-Chatenet, L., Sattler, R. M., Modi, A. P., Lee, J. H., Nicolette, M. L., Kopelovich, L., Jasin, M., Baer, R., Paull, T. T., & Gautier, J. (2008). A forward chemical genetic screen reveals an inhibitor of the Mre11-Rad50-Nbs1 complex. *Nature Chemical Biology*, *4*(2), 119–125. https://doi.org/10.1038/NCHEMBIO.63

Duxin, J. P., & Walter, J. C. (2015). What is the DNA repair defect underlying Fanconi anemia? In *Current Opinion in Cell Biology*. https://doi.org/10.1016/j.ceb.2015.09.002

Elia, A. E. H., Boardman, A. P., Wang, D. C., Huttlin, E. L., Everley, R. A., Dephoure, N., Zhou, C., Koren, I., Gygi, S. P., & Elledge, S. J. (2015). Quantitative Proteomic Atlas of Ubiquitination and Acetylation in the DNA Damage Response. *Molecular Cell*, *59*(5), 867–881. https://doi.org/10.1016/j.molcel.2015.05.006

Elia, A. E. H., Wang, D. C., Willis, N. A., Boardman, A. P., Hajdu, I., Adeyemi, R. O., Lowry, E., Gygi, S. P., Scully, R., & Elledge, S. J. (2015). RFWD3-Dependent Ubiquitination of RPA Regulates Repair at Stalled Replication Forks. *Molecular Cell*, *60*(2), 280–293. https://doi.org/10.1016/j.molcel.2015.09.011

ELM - DTX3L_HUMAN. (2021). http://elm.eu.org/cgimodel.py?fun=smartResult&userId=QiKQoW85uS&EXPECT_CUTOFF=100&r=1&bg=on

Fanning, E., Klimovich, V., & Nager, A. R. (2006). A dynamic model for replication protein A (RPA) function in DNA processing pathways. *Nucleic Acids Research*, *34*(15), 4126–4137. https://doi.org/10.1093/NAR/GKL550

Feeney, L., Muñoz, I. M., Lachaud, C., Toth, R., Appleton, P. L., Schindler, D., & Rouse, J. (2017). RPA-Mediated Recruitment of the E3 Ligase RFWD3 Is Vital for Interstrand Crosslink Repair and Human Health. *Molecular Cell*, *66*(5), 610-621.e4. https://doi.org/10.1016/j.molcel.2017.04.021

Feng, Q., Sekula, D., Muïler, R., Freemantle, S. J., & Dmitrovsky, E. (2007). Uncovering residues that regulate cyclin D1 proteasomal degradation. *Oncogene*, *26*, 5098–5106. https://doi.org/10.1038/sj.onc.1210309

Feng, W., Simpson, D. A., Carvajal-Garcia, J., Price, B. A., Kumar, R. J., Mose, L. E., Wood, R. D., Rashid, N., Purvis, J. E., Parker, J. S., Ramsden, D. A., & Gupta, G. P. (2019). Genetic determinants of cellular addiction to DNA polymerase theta. *Nature Communications 2019 10:1*, *10*(1), 1–13. https://doi.org/10.1038/s41467-019-12234-1

Ferlay, J., Ervik, M., Lam, F., Colombet, M., Mery, L., & Piñeros, M. (2020). *Global Cancer Observatory: Cancer Today*. International Agency for Research on Cancer. https://www.who.int/news-room/fact-sheets/detail/cancer

Foiani, M., Lucchini, G., & Plevani, P. (1997). The DNA polymerase α-primase complex couples DNA replication, cell-cycle progression and DNA-damage response. *Trends in Biochemical Sciences*, *22*(11), 424–427. https://doi.org/10.1016/S0968-0004(97)01109-2

Fong, P. C., Boss, D. S., Yap, T. A., Tutt, A., Wu, P., Mergui-Roelvink, M., Mortimer, P., Swaisland, H., Lau, A., O'Connor, M. J., Ashworth, A., Carmichael, J., Kaye, S. B., Schellens, J. H. M., & de Bono, J. S. (2009). Inhibition of poly(ADP-ribose) polymerase in tumors from BRCA mutation carriers. *The New England Journal of Medicine*, *361*(2), 123–134. https://doi.org/10.1056/NEJMOA0900212

Forment, J. v., & O'Connor, M. J. (2018). Targeting the replication stress response in cancer. In *Pharmacology and Therapeutics* (Vol. 188, pp. 155–167). https://doi.org/10.1016/j.pharmthera.2018.03.005

Fouché, N., Özgür, S., Roy, D., & Griffith, J. D. (2006). Replication fork regression in repetitive DNAs. *Nucleic Acids Research*, *34*(20), 6044. https://doi.org/10.1093/NAR/GKL757

Fulzele, A., & Bennett, E. J. (2018). Ubiquitin diGLY proteomics as an approach to identify and quantify the ubiquitin-modified proteome. In *Methods in Molecular Biology* (Vol. 1844, pp. 363–384). Humana Press Inc. https://doi.org/10.1007/978-1-4939-8706-1_23

Furnari, B., Rhind, N., & Russell, P. (1997). Cdc25 mitotic inducer targeted by chk1 DNA damage checkpoint kinase. *Science (New York, N.Y.)*, *277*(5331), 1495–1497. https://doi.org/10.1126/SCIENCE.277.5331.1495

Gaillard, H., García-Muse, T., & Aguilera, A. (2015). Replication stress and cancer. *Nature Reviews Cancer*. https://doi.org/10.1038/nrc3916

Gambus, A., Khoudoli, G. A., Jones, R. C., & Blow, J. J. (2011). MCM2-7 form double hexamers at licensed origins in Xenopus egg extract. *The Journal of Biological Chemistry*, *286*(13), 11855–11864. https://doi.org/10.1074/JBC.M110.199521

Gao, Y., Mutter-Rottmayer, E., Zlatanou, A., Vaziri, C., & Yang, Y. (2017). Mechanisms of Post-Replication DNA Repair. *Genes*, *8*(2). https://doi.org/10.3390/GENES8020064

Garaycoechea, J. I., Crossan, G. P., Langevin, F., Mulderrig, L., Louzada, S., Yang, F., Guilbaud, G., Park, N., Roerink, S., Nik-Zainal, S., Stratton, M. R., & Patel, K. J. (2018). Alcohol and endogenous aldehydes damage chromosomes and mutate stem

cells. *Nature 2018 553:7687*, *553*(7687), 171–177. https://doi.org/10.1038/nature25154

Garzón, J., Ursich, S., Lopes, M., Hiraga, S. ichiro, & Donaldson, A. D. (2019). Human RIF1-Protein Phosphatase 1 Prevents Degradation and Breakage of Nascent DNA on Replication Stalling. *Cell Reports*, *27*(9), 2558-2566.e4. https://doi.org/10.1016/j.celrep.2019.05.002

Gasser, S., Zhang, W. Y. L., Tan, N. Y. J., Tripathi, S., Suter, M. A., Chew, Z. H., Khatoo, M., Ngeow, J., & Cheung, F. S. G. (2017). Sensing of dangerous DNA. *Mechanisms of Ageing and Development*, *165*, 33–46. https://doi.org/10.1016/J.MAD.2016.09.001

Ge, X. Q., & Blow, J. J. (2010). Chk1 inhibits replication factory activation but allows dormant origin firing in existing factories. *The Journal of Cell Biology*, *191*(7), 1285–1297. https://doi.org/10.1083/JCB.201007074

George, A. J., Hoffiz, Y. C., Charles, A. J., Zhu, Y., & Mabb, A. M. (2018). A comprehensive atlas of E3 ubiquitin ligase mutations in neurological disorders. *Frontiers in Genetics*, *9*(FEB), 29. https://doi.org/10.3389/FGENE.2018.00029/BIBTEX

Gerloff, D. L., Woods, N. T., Farago, A. A., & Monteiro, A. N. A. (2012). BRCT Domains: a little more than kin, and less than kind. *FEBS Letters*, *586*(17), 2711. https://doi.org/10.1016/J.FEBSLET.2012.05.005

Gong, Z., & Chen, J. (2011). E3 ligase RFWD3 participates in replication checkpoint control. *Journal of Biological Chemistry*, *286*(25), 22308–22313. https://doi.org/10.1074/jbc.M111.222869

Goodarzi, A. A., & Jeggo, P. A. (2013). The Repair and Signaling Responses to DNA Double-Strand Breaks. *Advances in Genetics*, *82*, 1–45. https://doi.org/10.1016/B978-0-12-407676-1.00001-9

Gorgoulis, V. G., Vassiliou, L. V. F., Karakaidos, P., Zacharatos, P., Kotsinas, A., Liloglou, T., Venere, M., DiTullio, R. A., Kastrinakis, N. G., Levy, B., Kletsas, D., Yoneta, A., Herlyn, M., Kittas, C., & Halazonetis, T. D. (2005). Activation of the DNA damage checkpoint and genomic instability in human precancerous lesions. *Nature 2005 434:7035*, *434*(7035), 907–913. https://doi.org/10.1038/nature03485

Groth, A., Rocha, W., Verreault, A., & Almouzni, G. (2007). Chromatin Challenges during DNA Replication and Repair. In *Cell* (Vol. 128, Issue 4, pp. 721–733). Cell Press. https://doi.org/10.1016/j.cell.2007.01.030

Grunewald, T. G. P., Diebold, I., Esposito, I., Plehm, S., Hauer, K., Thiel, U., da Silva-Buttkus, P., Neff, F., Unland, R., Müller-Tidow, C., Zobywalski, C., Lohrig, K., Lewandrowski, U., Sickmann, A., da Costa, O. P., Görlach, A., Cossarizza, A., Butt, E., Richter, G. H. S., & Burdach, S. (2012). STEAP1 Is Associated with the Invasive and Oxidative Stress Phenotype of Ewing Tumors. *Molecular Cancer Research*, *10*(1), 52–65. https://doi.org/10.1158/1541-7786.MCR-11-0524

Halazonetis, T. D., Gorgoulis, V. G., & Bartek, J. (2008). An Oncogene-Induced DNA Damage Model for Cancer Development. *Science*. https://doi.org/10.1126/science.1140735

Hanahan, D., & Weinberg, R. A. (2000). The hallmarks of cancer. *Cell*, *100*(1), 57–70. https://doi.org/10.1016/S0092-8674(00)81683-9

Hanahan, D., & Weinberg, R. A. (2011). Hallmarks of cancer: The next generation. In *Cell*. https://doi.org/10.1016/j.cell.2011.02.013

Harrigan, J. A., Belotserkovskaya, R., Coates, J., Dimitrova, D. S., Polo, S. E., Bradshaw, C. R., Fraser, P., & Jackson, S. P. (2011). Replication stress induces 53BP1-containing OPT domains in G1 cells. *Journal of Cell Biology*, *193*(1), 97–108. https://doi.org/10.1083/jcb.201011083

Helleday, T. (2011). The underlying mechanism for the PARP and BRCA synthetic lethality: Clearing up the misunderstandings. *Molecular Oncology*, *5*(4), 387. https://doi.org/10.1016/J.MOLONC.2011.07.001

Hershko, A., & Ciechanover, A. (1998). The ubiquitin system. *Annual Review of Biochemistry*, *67*, 425–479. https://doi.org/10.1146/ANNUREV.BIOCHEM.67.1.425

Heyer, W. D., Ehmsen, K. T., & Liu, J. (2010). Regulation of homologous recombination in eukaryotes. *Annual Review of Genetics*, *44*, 113–139. https://doi.org/10.1146/ANNUREV-GENET-051710-150955

Hickson, I. D., & Bhowmick, R. (2017). The "enemies within": regions of the genome that are inherently difficult to replicate. *F1000Research*, *6*. https://doi.org/10.12688/F1000RESEARCH.11024.1

Higgs, M. R., Reynolds, J. J., Winczura, A., Blackford, A. N., Borel, V., Miller, E. S., Zlatanou, A., Nieminuszczy, J., Ryan, E. L., Davies, N. J., Stankovic, T., Boulton, S. J., Niedzwiedz, W., & Stewart, G. S. (2015). BOD1L Is Required to Suppress Deleterious Resection of Stressed Replication Forks. *Molecular Cell*, *59*(3), 462–477. https://doi.org/10.1016/J.MOLCEL.2015.06.007

Ho, S. S. W., Zhang, W. Y. L., Tan, N. Y. J., Khatoo, M., Suter, M. A., Tripathi, S., Cheung, F. S. G., Lim, W. K., Tan, P. H., Ngeow, J., & Gasser, S. (2016). The DNA Structure-Specific Endonuclease MUS81 Mediates DNA Sensor STING-Dependent Host Rejection of Prostate Cancer Cells. *Immunity*, *44*(5), 1177–1189. https://doi.org/10.1016/J.IMMUNI.2016.04.010

Honda, Y., Tojo, M., Matsuzaki, K., Anan, T., Matsumoto, M., Ando, M., Saya, H., & Nakao, M. (2002). Cooperation of HECT-domain ubiquitin ligase hHYD and DNA topoisomerase II-binding protein for DNA damage response. *The Journal of Biological Chemistry*, *277*(5), 3599–3605. https://doi.org/10.1074/JBC.M104347200

Hsiao, K. Y., & Mizzen, C. A. (2013). Histone H4 deacetylation facilitates 53BP1 DNA damage signaling and double-strand break repair. *Journal of Molecular Cell Biology*, *5*(3), 157–165. https://doi.org/10.1093/JMCB/MJS066

Hyland, E. M., Cosgrove, M. S., Molina, H., Wang, D., Pandey, A., Cottee, R. J., & Boeke, J. D. (2005). Insights into the role of histone H3 and histone H4 core modifiable residues in Saccharomyces cerevisiae. *Molecular and Cellular Biology*, *25*(22), 10060–10070. https://doi.org/10.1128/MCB.25.22.10060-10070.2005

Ilves, I., Petojevic, T., Pesavento, J. J., & Botchan, M. R. (2010). Activation of the MCM2-7 helicase by association with Cdc45 and GINS proteins. *Molecular Cell*, *37*(2), 247–258. https://doi.org/10.1016/J.MOLCEL.2009.12.030

Inano, S., Sato, K., Katsuki, Y., Kobayashi, W., Tanaka, H., Nakajima, K., Nakada, S., Miyoshi, H., Knies, K., Takaori-Kondo, A., Schindler, D., Ishiai, M., Kurumizaka, H., & Takata, M. (2017). RFWD3-Mediated Ubiquitination Promotes Timely Removal of Both RPA and RAD51 from DNA Damage Sites to Facilitate Homologous Recombination. *Molecular Cell*, *66*(5), 622-634.e8. https://doi.org/10.1016/J.MOLCEL.2017.04.022

Izawa, N., Wu, W., Sato, K., Nishikawa, H., Kato, A., Boku, N., Itoh, F., & Ohta, T. (2011). HERC2 Interacts with Claspin and regulates DNA origin firing and replication fork progression. *Cancer Research*, *71*(17), 5621–5625. https://doi.org/10.1158/0008-5472.CAN-11-0385

Jackson, D. A., & Pombo, A. (1998). Replicon Clusters Are Stable Units of Chromosome Structure: Evidence That Nuclear Organization Contributes to the Efficient Activation and Propagation of S Phase in Human Cells. *Journal of Cell Biology*, *140*(6), 1285–1295. https://doi.org/10.1083/JCB.140.6.1285

Jackson, S. P., & Durocher, D. (2013). Regulation of DNA Damage Responses by Ubiquitin and SUMO. *Molecular Cell*, *49*(5), 795–807. https://doi.org/10.1016/J.MOLCEL.2013.01.017

Jasencakova, Z., & Groth, A. (2010). Replication stress, a source of epigenetic aberrations in cancer? In *BioEssays* (Vol. 32, Issue 10, pp. 847–855). https://doi.org/10.1002/bies.201000055

Jing Huang, A., Zhang, J., Bellani, M. A., Li, L., Wang, W., & Seidman, M. M. (2019). Remodeling of Interstrand Crosslink Proximal Replisomes Is Dependent on ATR, FANCM, and FANCD2 Correspondence. *CellReports*, *27*, 1794-1808.e5. https://doi.org/10.1016/j.celrep.2019.04.032

Jiricny, J. (2006). The multifaceted mismatch-repair system. *Nature Reviews Molecular Cell Biology 2006 7:5*, *7*(5), 335–346. https://doi.org/10.1038/nrm1907

Jones, R. M., Mortusewicz, O., Afzal, I., Lorvellec, M., García, P., Helleday, T., & Petermann, E. (2012). Increased replication initiation and conflicts with transcription underlie Cyclin E-induced replication stress. *Oncogene 2013 32:32*, *32*(32), 3744–3753. https://doi.org/10.1038/onc.2012.387

Juszczynski, P., Kutok, J. L., Li, C., Mitra, J., Aguiar, R. C. T., & Shipp, M. A. (2006). BAL1 and BBAP Are Regulated by a Gamma Interferon-Responsive Bidirectional Promoter and Are Overexpressed in Diffuse Large B-Cell Lymphomas with a Prominent Inflammatory Infiltrate. *Molecular and Cellular Biology*, *26*(14), 5348–5359. https://doi.org/10.1128/mcb.02351-05

Kabeche, L., Nguyen, H. D., Buisson, R., & Zou, L. (2018). A mitosis-specific and R loop-driven ATR pathway promotes faithful chromosome segregation. *Science (New York, N.Y.)*, *359*(6371), 108–114. https://doi.org/10.1126/SCIENCE.AAN6490

Kais, Z., Rondinelli, B., Holmes, A., O'Leary, C., Kozono, D., D'Andrea, A. D., & Ceccaldi, R. (2016). FANCD2 maintains fork stability in BRCA1/2-deficient tumors and promotes alternative end-joining DNA repair. *Cell Reports*, *15*(11), 2488. https://doi.org/10.1016/J.CELREP.2016.05.031

Kandoth, C., McLellan, M. D., Vandin, F., Ye, K., Niu, B., Lu, C., Xie, M., Zhang, Q., McMichael, J. F., Wyczalkowski, M. A., Leiserson, M. D. M., Miller, C. A., Welch, J. S., Walter, M. J., Wendl, M. C., Ley, T. J., Wilson, R. K., Raphael, B. J., & Ding, L. (2013). Mutational landscape and significance across 12 major cancer types. *Nature*, *502*(7471), 333–339. https://doi.org/10.1038/nature12634

Kannouche, P. L., Wing, J., & Lehmann, A. R. (2004). Interaction of human DNA polymerase eta with monoubiquitinated PCNA: a possible mechanism for the polymerase switch in response to DNA damage. *Molecular Cell*, *14*(4), 491–500. https://doi.org/10.1016/S1097-2765(04)00259-X

Kim, W., Zhao, F., Gao, H., Qin, S., Hou, J., Deng, M., Kloeber, J. A., Huang, J., Zhou, Q., Guo, G., Gao, M., Zeng, X., Zhu, S., Tu, X., Wu, Z., Zhang, Y., Yin, P., Kaufmann, S. H., Luo, K., & Lou, Z. (2021). USP13 regulates the replication stress response by deubiquitinating TopBP1. *DNA Repair*, *100*. https://doi.org/10.1016/J.DNAREP.2021.103063

Knijnenburg, T. A., Wang, L., Zimmermann, M. T., Chambwe, N., Gao, G. F., Cherniack, A. D., Fan, H., Shen, H., Way, G. P., Greene, C. S., Liu, Y., Akbani, R., Feng, B., Donehower, L. A., Miller, C., Shen, Y., Karimi, M., Chen, H., Kim, P., … Wang, C. (2018). Genomic and Molecular Landscape of DNA Damage Repair Deficiency across The Cancer Genome Atlas. *Cell Reports*, *23*(1), 239-254.e6. https://doi.org/10.1016/J.CELREP.2018.03.076

Knipscheer, P., Räschle, M., Smogorzewska, A., Enoiu, M., Ho, T. V., Schärer, O. D., Elledge, S. J., & Walter, J. C. (2009). The Fanconi anemia pathway promotes

replication-dependent DNA interstrand crosslink repair. *Science (New York, N.Y.)*, *326*(5960), 1698. https://doi.org/10.1126/SCIENCE.1182372

Kolas, N. K., Chapman, J. R., Nakada, S., Ylanko, J., Chahwan, R., Sweeney, F. D., Panier, S., Mendez, M., Wildenhain, J., Thomson, T. M., Pelletier, L., Jackson, S. P., & Durocher, D. (2007). Orchestration of the DNA-damage response by the RNF8 ubiquitin ligase. *Science*, *318*(5856), 1637–1640. https://doi.org/10.1126/science.1150034

Komander, D., & Rape, M. (2012). The Ubiquitin Code. *Annual Review of Biochemistry*, *81*(1), 203–229. https://doi.org/10.1146/annurev-biochem-060310-170328

Kramara, J., Osia, B., & Malkova, A. (2018). Break Induced Replication: the where, the why, and the how. *Trends in Genetics : TIG*, *34*(7), 518. https://doi.org/10.1016/J.TIG.2018.04.002

Krokan, H. E., & Bjørås, M. (2013). Base Excision Repair. *Cold Spring Harbor Perspectives in Biology*, *5*(4), 1–22. https://doi.org/10.1101/CSHPERSPECT.A012583

Kumagai, A., Lee, J., Yoo, H. Y., & Dunphy, W. G. (2006). TopBP1 activates the ATR-ATRIP complex. *Cell*, *124*(5), 943–955. https://doi.org/10.1016/J.CELL.2005.12.041

Lange, S. S., Takata, K. I., & Wood, R. D. (2011). DNA polymerases and cancer. *Nature Reviews. Cancer*, *11*(2), 96–110. https://doi.org/10.1038/NRC2998

Langerak, P., & Russell, P. (2011). Regulatory networks integrating cell cycle control with DNA damage checkpoints and double-strand break repair. *Philosophical Transactions of the Royal Society B: Biological Sciences*, *366*(1584), 3562. https://doi.org/10.1098/RSTB.2011.0070

Lecona, E., & Fernández-Capetillo, O. (2014). Replication stress and cancer: It takes two to tango. In *Experimental Cell Research* (Vol. 329, Issue 1, pp. 26–34). Academic Press Inc. https://doi.org/10.1016/j.yexcr.2014.09.019

Lee, J., Kim, S. T., Smith, S., Mortimer, P. G., Loembé, B., Hong, J., Kozarewa, I., Pierce, A., & Dean, E. (2020). Results from a phase I, open-label study of ceralasertib (AZD6738), a novel DNA damage repair agent, in combination with weekly paclitaxel in refractory cancer (NCT02630199). *Https://Doi.Org/10.1200/JCO.2020.38.15_suppl.3503*, *38*(15_suppl), 3503–3503. https://doi.org/10.1200/JCO.2020.38.15_SUPPL.3503

Lemaçon, D., Jackson, J., Quinet, A., Brickner, J. R., Li, S., Yazinski, S., You, Z., Ira, G., Zou, L., Mosammaparast, N., & Vindigni, A. (2017). MRE11 and EXO1 nucleases degrade reversed forks and elicit MUS81-dependent fork rescue in BRCA2-deficient cells. *Nature Communications 2017 8:1*, *8*(1), 1–12. https://doi.org/10.1038/s41467-017-01180-5

Leonard, A. C., & Grimwade, J. E. (2017). Regulation of Replication Origin Firing. *Reference Module in Life Sciences*. https://doi.org/10.1016/B978-0-12-809633-8.12304-0

Liang, Y., Lin, S. Y., Brunicardi, F. C., Goss, J., & Li, K. (2008). DNA Damage Response Pathways in Tumor Suppression and Cancer Treatment. *World Journal of Surgery 2008 33:4*, *33*(4), 661–666. https://doi.org/10.1007/S00268-008-9840-1

Lin, Y. C., Wang, Y., Hsu, R., Giri, S., Wopat, S., Arif, M. K., Chakraborty, A., Prasanth, K. v., & Prasanth, S. G. (2018). PCNA-mediated stabilization of E3 ligase RFWD3 at the replication fork is essential for DNA replication. *Proceedings of the National Academy of Sciences of the United States of America*, *115*(52), 13282–13287. https://doi.org/10.1073/pnas.1814521115

Liu, K., Graves, J. D., Lin, F. T., & Lin, W. C. (2021). Overexpression of TopBP1, a canonical ATR/Chk1 activator, paradoxically hinders ATR/Chk1 activation in

cancer. *The Journal of Biological Chemistry*, *296*. https://doi.org/10.1016/J.JBC.2021.100382

Liu, W., Krishnamoorthy, A., Zhao, R., & Cortez, D. (2020). Two replication fork remodeling pathways generate nuclease substrates for distinct fork protection factors. *Science Advances*, *6*(46). https://doi.org/10.1126/sciadv.abc3598

Liu, W., Roubal, I., Polaczek, P., Meng, Y., Choe, W.-C., Caron, M.-C., Sedgeman, C. A., Xi, Y., Liu, C., Wu, Q., Zheng, L., Masson, J.-Y., Shen, B., & Campbell, J. L. (2021). FANCD2 directly inhibits DNA2 nuclease at stalled replication forks and acts as a RAD51 mediator in strand exchange. *BioRxiv Preprint*. https://doi.org/10.1101/2021.07.08.450798

Liu, X. L., Wang, T., Huang, X. J., Zhou, H. Y., Luan, X. H., Shen, J. Y., Chen, S. di, & Cao, L. (2016). Novel ATM mutations with ataxia-telangiectasia. *Neuroscience Letters*, *611*, 112–115. https://doi.org/10.1016/J.NEULET.2015.11.036

Lopes, M., Cotta-Ramusino, C., Pellicioli, A., Liberi, G., Plevani, P., Muzi-Falconi, M., Newlon, C. S., & Foiani, M. (2001). The DNA replication checkpoint response stabilizes stalled replication forks. *Nature*, *412*(6846), 557–561. https://doi.org/10.1038/35087613

López-Contreras, A. J., & Fernandez-Capetillo, O. (2010). The ATR barrier to replication-born DNA damage. In *DNA Repair* (Vol. 9, Issue 12, pp. 1249–1255). Elsevier. https://doi.org/10.1016/j.dnarep.2010.09.012

López-Contreras, A. J., Gutierrez-Martinez, P., Specks, J., Rodrigo-Perez, S., & Fernandez-Capetillo, O. (2012). An extra allele of Chk1 limits oncogene-induced replicative stress and promotes transformation. *The Journal of Experimental Medicine*. https://doi.org/10.1084/jem.20112147

Ludwig, T., Fisher, P., Ganesan, S., & Efstratiadis, A. (2001). Tumorigenesis in mice carrying a truncating Brca1 mutation. *Genes & Development*, *15*(10), 1188. https://doi.org/10.1101/GAD.879201

Lukas, C., Savic, V., Bekker-Jensen, S., Doil, C., Neumann, B., Sølvhøj Pedersen, R., Grøfte, M., Chan, K. L., Hickson, I. D., Bartek, J., & Lukas, J. (2011). 53BP1 nuclear bodies form around DNA lesions generated by mitotic transmission of chromosomes under replication stress. *Nature Cell Biology*, *13*(3), 243–253. https://doi.org/10.1038/ncb2201

Lum, K. K., Song, B., Federspiel, J. D., Diner, B. A., Howard, T., & Cristea, I. M. (2018). Interactome and Proteome Dynamics Uncover Immune Modulatory Associations of the Pathogen Sensing Factor cGAS. *Cell Systems*, *7*(6), 627-642.e6. https://doi.org/10.1016/J.CELS.2018.10.010

Luzhna, L., Kathiria, P., & Kovalchuk, O. (2013). Micronuclei in genotoxicity assessment: From genetics to epigenetics and beyond. *Frontiers in Genetics*, *4*(JUL), 131. https://doi.org/10.3389/FGENE.2013.00131/BIBTEX

Ma, C. X., Ellis, M. J. C., Petroni, G. R., Guo, Z., Cai, S. R., Ryan, C. E., Craig Lockhart, A., Naughton, M. J., Pluard, T. J., Brenin, C. M., Picus, J., Creekmore, A. N., Mwandoro, T., Yarde, E. R., Reed, J., Ebbert, M., Bernard, P. S., Watson, M., Doyle, L. A., … Fracasso, P. M. (2013). A phase II study of UCN-01 in combination with irinotecan in patients with metastatic triple negative breast cancer. *Breast Cancer Research and Treatment*, *137*(2), 483. https://doi.org/10.1007/S10549-012-2378-9

Macheret, M., & Halazonetis, T. D. (2015). DNA replication stress as a hallmark of cancer. *Annual Review of Pathology: Mechanisms of Disease*, *10*, 425–448. https://doi.org/10.1146/ANNUREV-PATHOL-012414-040424

Madhani, H. D. (2006). Functional analysis of protein kinase networks in living cells: beyond “knock-outs” and “knock-downs.” *Methods (San Diego, Calif.)*, *40*(3), 251–254. https://doi.org/10.1016/J.YMETH.2006.06.006

Mailand, N., Bekker-Jensen, S., Faustrup, H., Melander, F., Bartek, J., Lukas, C., & Lukas, J. (2007). RNF8 Ubiquitylates Histones at DNA Double-Strand Breaks and Promotes Assembly of Repair Proteins. *Cell*, *131*(5), 887–900. https://doi.org/10.1016/j.cell.2007.09.040

Malacaria, E., Franchitto, A., & Pichierri, P. (2017). SLX4 Prevents GEN1-Dependent DSBs During DNA Replication Arrest Under Pathological Conditions in Human Cells. *Scientific Reports 2017 7:1*, *7*(1), 1–14. https://doi.org/10.1038/srep44464

Marteijn, J. A., Lans, H., Vermeulen, W., & Hoeijmakers, J. H. J. (2014). Understanding nucleotide excision repair and its roles in cancer and ageing. *Nature Reviews Molecular Cell Biology 2014 15:7*, *15*(7), 465–481. https://doi.org/10.1038/nrm3822

Masai, H., Matsumoto, S., You, Z., Yoshizawa-Sugata, N., & Oda, M. (2010). Eukaryotic Chromosome DNA Replication: Where, When, and How? *Http://Dx.Doi.Org/10.1146/Annurev.Biochem.052308.103205*, *79*, 89–130. https://doi.org/10.1146/ANNUREV.BIOCHEM.052308.103205

Mateos-Gomez, P. A., Gong, F., Nair, N., Miller, K. M., Lazzerini-Denchi, E., & Sfeir, A. (2015). Mammalian polymerase θ promotes alternative NHEJ and suppresses recombination. *Nature*, *518*(7538), 254–257. https://doi.org/10.1038/NATURE14157

Mattiroli, F., Vissers, J. H. A., van Dijk, W. J., Ikpa, P., Citterio, E., Vermeulen, W., Marteijn, J. A., & Sixma, T. K. (2012). RNF168 ubiquitinates K13-15 on H2A/H2AX to drive DNA damage signaling. *Cell*, *150*(6), 1182–1195. https://doi.org/10.1016/j.cell.2012.08.005

Mavragani, Ifigeneia V., Zacharenia Nikitaki, Spyridon A. Kalospyros, and Alexandros G. Georgakilas. (2019). Ionizing Radiation and Complex DNA Damage: From Prediction to Detection Challenges and Biological Significance. *Cancers* 11, no. 11: 1789. https://doi.org/10.3390/cancers11111789

Mccabe, N., Turner, N. C., Lord, C. J., Kluzek, K., Białkowska, A., Swift, S., Giavara, S., O'connor, M. J., Tutt, A. N., Zdzienicka, M. Z., Smith, G. C. M., & Ashworth, A. (2006). Deficiency in the Repair of DNA Damage by Homologous Recombination and Sensitivity to Poly(ADP-Ribose) Polymerase Inhibition. *Cancer Res*, *66*(16), 8109–8124. https://doi.org/10.1158/0008-5472.CAN-06-0140

McKinnon, P. J. (2009). DNA Repair Deficiency and Neurological Disease. *Nature Reviews. Neuroscience*, *10*(2), 100. https://doi.org/10.1038/NRN2559

McKinnon, P. J. (2012). ATM and the molecular pathogenesis of ataxia telangiectasia. *Annual Review of Pathology*, *7*, 303–321. https://doi.org/10.1146/ANNUREV-PATHOL-011811-132509

Menoyo, A., Alazzouzi, H., Espín, E., Armengol, M., Yamamoto, H., & Schwartz, S. (2001). Somatic Mutations in the DNA Damage-Response Genes ATR and CHK1 in Sporadic Stomach Tumors with Microsatellite Instability. *Cancer Research*, *61*(21).

Messick, T. E., & Greenberg, R. A. (2009). The ubiquitin landscape at DNA double-strand breaks. *Journal of Cell Biology*, *187*(3), 319–326. https://doi.org/10.1083/JCB.200908074

Metzger, M. B., Hristova, V. A., & Weissman, A. M. (2012). HECT and RING finger families of E3 ubiquitin ligases at a glance. *Journal of Cell Science*, *125*(3), 531–537. https://doi.org/10.1242/JCS.091777/-/DC1

Mijic, S., Zellweger, R., Chappidi, N., Berti, M., Jacobs, K., Mutreja, K., Ursich, S., Ray Chaudhuri, A., Nussenzweig, A., Janscak, P., & Lopes, M. (2017). Replication fork reversal triggers fork degradation in BRCA2-defective cells. *Nature Communications 2017 8:1*, *8*(1), 1–11. https://doi.org/10.1038/s41467-017-01164-5

Miyabe, I., Kunkel, T. A., & Carr, A. M. (2011). The Major Roles of DNA Polymerases Epsilon and Delta at the Eukaryotic Replication Fork Are Evolutionarily Conserved. *PLoS Genetics*, *7*(12), 1002407. https://doi.org/10.1371/JOURNAL.PGEN.1002407

Monti, S., Savage, K. J., Kutok, J. L., Feuerhake, F., Kurtin, P., Mihm, M., Wu, B., Pasqualucci, L., Neuberg, D., Aguiar, R. C. T., Cin, P. D., Ladd, C., Pinkus, G. S., Salles, G., Harris, N. L., Dalla-Favera, R., Habermann, T. M., Aster, J. C., Golub, T. R., & Shipp, M. A. (2005). Molecular profiling of diffuse large B-cell lymphoma identifies robust subtypes including one characterized by host inflammatory response. *Blood*, *105*(5), 1851–1861. https://doi.org/10.1182/BLOOD-2004-07-2947

Mordes, D. A., & Cortez, D. (2008). Activation of ATR and related PIKKs. In *Cell Cycle* (Vol. 7, Issue 18, pp. 2809–2812). Taylor and Francis Inc. https://doi.org/10.4161/cc.7.18.6689

Mouli Kolinjivadi, A., Sannino, V., de Antoni, A., echer, H. T., Baldi, G., & Costanzo, V. (2017). *Moonlighting at replication forks-a new life for homologous recombination proteins BRCA1, BRCA2 and RAD51*. https://doi.org/10.1002/1873-3468.12556

Mukherjee, C., Tripathi, V., Manolika, E. M., Heijink, A. M., Ricci, G., Merzouk, S., de Boer, H. R., Demmers, J., van Vugt, M. A. T. M., & Ray Chaudhuri, A. (2019). RIF1 promotes replication fork protection and efficient restart to maintain genome stability. *Nature Communications*, *10*(1). https://doi.org/10.1038/S41467-019-11246-1

Nam, E. A., & Cortez, D. (2011). ATR signalling: More than meeting at the fork. In *Biochemical Journal* (Vol. 436, Issue 3, pp. 527–536). NIH Public Access. https://doi.org/10.1042/BJ20102162

Nedelcheva-Veleva, M. N., Krastev, D. B., & Stoynov, S. S. (2006). Coordination of DNA synthesis and replicative unwinding by the S-phase checkpoint pathways. *Nucleic Acids Research*, *34*(15), 4138. https://doi.org/10.1093/NAR/GKL528

Neelsen, K. J., & Lopes, M. (2015). Replication fork reversal in eukaryotes: from dead end to dynamic response. *Nature Reviews Molecular Cell Biology*, *16*(4), 207–220. https://doi.org/10.1038/nrm3935

Nieminuszczy, J., Broderick, R., Bellani, M. A., Smethurst, E., Schwab, R. A., Cherdyntseva, V., Evmorfopoulou, T., Lin, Y. L., Minczuk, M., Pasero, P., Gagos, S., Seidman, M. M., & Niedzwiedz, W. (2019). EXD2 Protects Stressed Replication Forks and Is Required for Cell Viability in the Absence of BRCA1/2. *Molecular Cell*, *75*(3), 605-619.e6. https://doi.org/10.1016/j.molcel.2019.05.026

Nijman, S. M. B., Huang, T. T., Dirac, A. M. G., Brummelkamp, T. R., Kerkhoven, R. M., D'Andrea, A. D., & Bernards, R. (2005). The deubiquitinating enzyme USP1 regulates the Fanconi anemia pathway. *Molecular Cell*, *17*(3), 331–339. https://doi.org/10.1016/J.MOLCEL.2005.01.008

Nitiss, J. L. (2009). Targeting DNA topoisomerase II in cancer chemotherapy. *Nature Reviews Cancer 2009 9:5*, *9*(5), 338–350. https://doi.org/10.1038/nrc2607

Ochs, F., Somyajit, K., Altmeyer, M., Rask, M. B., Lukas, J., & Lukas, C. (2016). 53BP1 fosters fidelity of homology-directed DNA repair. *Nature Structural & Molecular Biology 2016 23:8*, *23*(8), 714–721. https://doi.org/10.1038/nsmb.3251

O'Connell, M. J., Raleigh, J. M., Verkade, H. M., & Nurse, P. (1997). Chk1 is a wee1 kinase in the G2 DNA damage checkpoint inhibiting cdc2 by Y15 phosphorylation. *EMBO Journal*, *16*(3), 545–554. https://doi.org/10.1093/emboj/16.3.545

O'Connor, M. J. (2015). Targeting the DNA Damage Response in Cancer. In *Molecular Cell* (Vol. 60, Issue 4, pp. 547–560). https://doi.org/10.1016/j.molcel.2015.10.040

O'Driscoll, M., & Jeggo, P. (2002). Immunological disorders and DNA repair. *Mutation Research/Fundamental and Molecular Mechanisms of Mutagenesis*, *509*(1–2), 109–126. https://doi.org/10.1016/S0027-5107(02)00221-X

O'Driscoll, M., & Jeggo, P. A. (2003). Clinical impact of ATR checkpoint signalling failure in humans. *Cell Cycle (Georgetown, Tex.)*, *2*(3), 193–194. https://doi.org/10.4161/CC.2.3.404

O'Neil, N. J., Bailey, M. L., & Hieter, P. (2017). Synthetic lethality and cancer. *Nature Reviews Genetics 2017 18:10*, *18*(10), 613–623. https://doi.org/10.1038/nrg.2017.47

Osborn, A. J., Elledge, S. J., & Zou, L. (2002). Checking on the fork: The DNA-replication stress-response pathway. In *Trends in Cell Biology* (Vol. 12, Issue 11, pp. 509–516). Elsevier Current Trends. https://doi.org/10.1016/S0962-8924(02)02380-2

Pan, Q., Fang, Y., Xu, Y., Zhang, K., & Hu, X. (2005). Down-regulation of DNA polymerases kappa, eta, iota, and zeta in human lung, stomach, and colorectal cancers. *Cancer Letters*, *217*(2), 139–147. https://doi.org/10.1016/J.CANLET.2004.07.021

Peller, S., & Rotter, V. (2003). TP53 in Hematological Cancer: Low Incidence of Mutations With Significant Clinical Relevance. *HUMAN MUTATION*, *21*, 277–284. https://doi.org/10.1002/humu.10190

Peng, J., Schwartz, D., Elias, J. E., Thoreen, C. C., Cheng, D., Marsischky, G., Roelofs, J., Finley, D., & Gygi, S. P. (2003). A proteomics approach to understanding protein ubiquitination. *Nature Biotechnology*, *21*(8), 921–926. https://doi.org/10.1038/nbt849

Petermann, E., Orta, M. L., Issaeva, N., Schultz, N., & Helleday, T. (2010). Hydroxyurea-Stalled Replication Forks Become Progressively Inactivated and Require Two Different RAD51-Mediated Pathways for Restart and Repair. *Molecular Cell*, *37*(4), 492–502. https://doi.org/10.1016/j.molcel.2010.01.021

Petersen, B. O., Lukas, J., Sørensen, C. S., Bartek, J., & Helin, K. (1999). Phosphorylation of mammalian CDC6 by cyclin A/CDK2 regulates its subcellular localization. *The EMBO Journal*, *18*(2), 396–410. https://doi.org/10.1093/EMBOJ/18.2.396

Petitjean, A., Achatz, M. I. W., Borresen-Dale, A. L., Hainaut, P., & Olivier, M. (2007). TP53 mutations in human cancers: functional selection and impact on cancer prognosis and outcomes. *Oncogene*, *26*(15), 2157–2165. https://doi.org/10.1038/SJ.ONC.1210302

Petitjean, A., Mathe, E., Kato, S., Ishioka, C., Tavtigian, S. v., Hainaut, P., & Olivier, M. (2007). Impact of mutant p53 functional properties on TP53 mutation patterns and tumor phenotype: lessons from recent developments in the IARC TP53 database. *Human Mutation*, *28*(6), 622–629. https://doi.org/10.1002/HUMU.20495

Pfeifer, G. P., Denissenko, M. F., Olivier, M., Tretyakova, N., Hecht, S. S., & Hainaut, P. (2002). Tobacco smoke carcinogens, DNA damage and p53 mutations in smoking-associated cancers. *Oncogene 2002 21:48*, *21*(48), 7435–7451. https://doi.org/10.1038/sj.onc.1205803

Poole, L. A., & Cortez, D. (2017). Functions of SMARCAL1, ZRANB3, and HLTF in maintaining genome stability. *Critical Reviews in Biochemistry and Molecular Biology*, *52*(6), 696–714. https://doi.org/10.1080/10409238.2017.1380597

Qin, W., Wu, H. J., Cao, L. Q., Li, H. J., He, C. X., Zhao, D., Xing, L., Li, P. Q., Jin, X., & Cao, H. L. (2019). Research Progress on PARP14 as a Drug Target. *Frontiers in Pharmacology*, *10*, 172. https://doi.org/10.3389/FPHAR.2019.00172

Ragland, R. L., Patel, S., Rivard, R. S., Smith, K., Peters, A. A., Bielinsky, A. K., & Brown, E. J. (2013). RNF4 and PLK1 are required for replication fork collapse in

ATR-deficient cells. *Genes & Development*, *27*(20), 2259–2273. https://doi.org/10.1101/GAD.223180.113

Ragu, S., Matos-Rodrigues, G., & Lopez, B. S. (2020). Replication Stress, DNA Damage, Inflammatory Cytokines and Innate Immune Response. *Genes*, *11*(4). https://doi.org/10.3390/GENES11040409

Riccio, A. A., Schellenberg, M. J., & Williams, R. S. (2020). Molecular mechanisms of topoisomerase 2 DNA-protein crosslink resolution. *Cellular and Molecular Life Sciences : CMLS*, *77*(1), 81–91. https://doi.org/10.1007/S00018-019-03367-Z

Rose Li, Y., Halliwill, K. D., Adams, C. J., Iyer, V., Riva, L., Mamunur, R., Jen, K. Y., del Rosario, R., Fredlund, E., Hirst, G., Alexandrov, L. B., Adams, D., & Balmain, A. (2020). Mutational signatures in tumours induced by high and low energy radiation in Trp53 deficient mice. *Nature Communications 2020 11:1*, *11*(1), 1–15. https://doi.org/10.1038/s41467-019-14261-4

Saldivar, J. C., Cortez, D., & Cimprich, K. A. (2017). The essential kinase ATR: Ensuring faithful duplication of a challenging genome. In *Nature Reviews Molecular Cell Biology* (Vol. 18, Issue 10, pp. 622–636). https://doi.org/10.1038/nrm.2017.67

Saurin, A. J., Borden, K. L. B., Boddy, M. N., & Freemont, P. S. (1996). Does this have a familiar RING? In *Trends in Biochemical Sciences* (Vol. 21, Issue 6, pp. 208–214). Elsevier Ltd. https://doi.org/10.1016/S0968-0004(96)80017-X

Schlacher, K., Christ, N., Siaud, N., Egashira, A., Wu, H., & Jasin, M. (2011). Double-strand break repair-independent role for BRCA2 in blocking stalled replication fork degradation by MRE11. *Cell*, *145*(4), 529–542. https://doi.org/10.1016/J.CELL.2011.03.041

Schlacher, K., Wu, H., & Jasin, M. (2012). A Distinct Replication Fork Protection Pathway Connects Fanconi Anemia Tumor Suppressors to RAD51-BRCA1/2. *Cancer Cell*, *22*, 106–116. https://doi.org/10.1016/j.ccr.2012.05.015

Schmid, J. A., Berti, M., Walser, F., Raso, M. C., Schmid, F., Krietsch, J., Stoy, H., Zwicky, K., Ursich, S., Freire, R., Lopes, M., & Penengo, L. (2018). Histone Ubiquitination by the DNA Damage Response Is Required for Efficient DNA Replication in Unperturbed S Phase. *Molecular Cell*, *71*(6), 897-910.e8. https://doi.org/10.1016/j.molcel.2018.07.011

Schwab, R. A., Blackford, A. N., & Niedzwiedz, W. (2010). ATR activation and replication fork restart are defective in FANCM-deficient cells. *EMBO Journal*, *29*(4), 806–818. https://doi.org/10.1038/emboj.2009.385

Schwab, R. A., Nieminuszczy, J., Shah, F., Langton, J., Lopez Martinez, D., Liang, C. C., Cohn, M. A., Gibbons, R. J., Deans, A. J., & Niedzwiedz, W. (2015). The Fanconi Anemia Pathway Maintains Genome Stability by Coordinating Replication and Transcription. *Molecular Cell*, *60*(3), 351–361. https://doi.org/10.1016/j.molcel.2015.09.012

Sclafani, R. A., & Holzen, T. M. (2007). Cell cycle regulation of DNA replication. *Annual Review of Genetics*, *41*, 237–280. https://doi.org/10.1146/ANNUREV.GENET.41.110306.130308

Setiaputra, D., & Durocher, D. (2019). Shieldin-the protector of DNA ends. *EMBO Reports*, *447560*. https://doi.org/10.15252/embr.201847560

Shapiro, G. I., Wesolowski, R., Devoe, C., Lord, S., Pollard, J., Hendriks, B. S., Falk, M., Diaz-Padilla, I., Plummer, R., & Yap, T. A. (2021). Phase 1 study of the ATR inhibitor berzosertib in combination with cisplatin in patients with advanced solid tumours. *British Journal of Cancer 2021 125:4*, *125*(4), 520–527. https://doi.org/10.1038/s41416-021-01406-w

Sharma, A., Singh, K., & Almasan, A. (2012). Histone H2AX Phosphorylation: A Marker for DNA Damage. *Methods in Molecular Biology*, *920*, 613–626. https://doi.org/10.1007/978-1-61779-998-3_40

Shen, Y., Sun, Y., Zhang, L., & Liu, H. (2017). Effects of DTX3L on the cell proliferation, adhesion, and drug resistance of multiple myeloma cells. *Tumor Biology*, *39*(6), 1010428317703941. https://doi.org/10.1177/1010428317703941

Shimura, T., Ochiai, Y., Noma, N., Oikawa, T., Sano, Y., & Fukumoto, M. (2013). Cyclin D1 overexpression perturbs DNA replication and induces replication-associated DNA double-strand breaks in acquired radioresistant cells. *Cell Cycle*, *12*(5), 773. https://doi.org/10.4161/CC.23719

Sirbu, B. M., Couch, F. B., & Cortez, D. (2012). Monitoring the spatiotemporal dynamics of proteins at replication forks and in assembled chromatin using isolation of proteins on nascent DNA. *Nature Protocols*, *7*. https://doi.org/10.1038/nprot.2012.010

Sirbu, B. M., Couch, F. B., Feigerle, J. T., Bhaskara, S., Hiebert, S. W., & Cortez, D. (2011). Analysis of protein dynamics at active, stalled, and collapsed replication forks. *Genes and Development*, *25*(12), 1320–1327. https://doi.org/10.1101/gad.2053211

Soehnge, H., Ouhtit, A., & Ananthaswamy, H. N. (1997). MECHANISMS OF INDUCTION OF SKIN CANCER BY UV RADIATION. *Frontiers in Bioscience*, *2*, 538.

Stec, A. A., Dickens, K. E., Salden, M., Hewitt, F. E., Watts, D. P., Houldsworth, P. E., & Martin, F. L. (2018). Occupational Exposure to Polycyclic Aromatic Hydrocarbons and Elevated Cancer Incidence in Firefighters. *Scientific Reports 2018 8:1*, *8*(1), 1–8. https://doi.org/10.1038/s41598-018-20616-6

Stewart, G. S. (2009). Solving the RIDDLE of 53BP1 recruitment to sites of damage. *Http://Dx.Doi.Org/10.4161/Cc.8.10.8351*, *8*(10), 1532–1538. https://doi.org/10.4161/CC.8.10.8351

Stewart, G. S., Panier, S., Townsend, K., Al-Hakim, A. K., Kolas, N. K., Miller, E. S., Nakada, S., Ylanko, J., Olivarius, S., Mendez, M., Oldreive, C., Wildenhain, J., Tagliaferro, A., Pelletier, L., Taubenheim, N., Durandy, A., Byrd, P. J., Stankovic, T., Taylor, A. M. R., & Durocher, D. (2009). The RIDDLE syndrome protein mediates a ubiquitin-dependent signaling cascade at sites of DNA damage. *Cell*, *136*(3), 420–434. https://doi.org/10.1016/J.CELL.2008.12.042

Stewart, G. S., Wang, B., Bigneli, C. R., Taylor, A. M. R., & Elledge, S. J. (2003). MDC1 is a mediator of the mammalian DNA damage checkpoint. *Nature 2003 421:6926*, *421*(6926), 961–966. https://doi.org/10.1038/nature01446

Stingele, J., Bellelli, R., & Boulton, S. J. (2017). Mechanisms of DNA–protein crosslink repair. *Nature Publishing Group*, *18*. https://doi.org/10.1038/nrm.2017.56

Sung, H., Ferlay, J., Siegel, R. L., Laversanne, M., Soerjomataram, I., Jemal, A., & Bray, F. (2021). Global Cancer Statistics 2020: GLOBOCAN Estimates of Incidence and Mortality Worldwide for 36 Cancers in 185 Countries. *CA: A Cancer Journal for Clinicians*, *71*(3), 209–249. https://doi.org/10.3322/CAAC.21660

Symington, L. S. (2014). End resection at double-strand breaks: Mechanism and regulation. *Cold Spring Harbor Perspectives in Biology*. https://doi.org/10.1101/cshperspect.a016436

Symington, L. S., & Gautier, J. (2011). Double-Strand Break End Resection and Repair Pathway Choice. *Annual Review of Genetics*. https://doi.org/10.1146/annurev-genet-110410-132435

Taglialatela, A., Alvarez, S., Leuzzi, G., Sannino, V., Ranjha, L., Huang, J. W., Madubata, C., Anand, R., Levy, B., Rabadan, R., Cejka, P., Costanzo, V., &

Ciccia, A. (2017a). Restoration of Replication Fork Stability in BRCA1- and BRCA2-Deficient Cells by Inactivation of SNF2-Family Fork Remodelers. *Molecular Cell*, *68*(2), 414-430.e8. https://doi.org/10.1016/j.molcel.2017.09.036

Taglialatela, A., Alvarez, S., Leuzzi, G., Sannino, V., Ranjha, L., Huang, J. W., Madubata, C., Anand, R., Levy, B., Rabadan, R., Cejka, P., Costanzo, V., & Ciccia, A. (2017b). Restoration of Replication Fork Stability in BRCA1- and BRCA2-Deficient Cells by Inactivation of SNF2-Family Fork Remodelers. *Molecular Cell*, *68*(2), 414-430.e8. https://doi.org/10.1016/J.MOLCEL.2017.09.036

Takahashi, T. S., Wollscheid, H.-P., Lowther, J., & Ulrich, H. D. (2020). Effects of chain length and geometry on the activation of DNA damage bypass by polyubiquitylated PCNA. *Nucleic Acids Research*, *48*(6), 3042–3052. https://doi.org/10.1093/nar/gkaa053

Takeyama, K., Aguiar, R. C. T., Gu, L., He, C., Freeman, G. J., Kutok, J. L., Aster, J. C., & Shipp, M. A. (2003). The BAL-binding protein BBAP and related deltex family members exhibit ubiquitin-protein isopeptide ligase activity. *Journal of Biological Chemistry*, *278*(24), 21930–21937. https://doi.org/10.1074/jbc.M301157200

Técher, H., Koundrioukoff, S., Nicolas, A., & Debatisse, M. (2017). The impact of replication stress on replication dynamics and DNA damage in vertebrate cells. *Nature Reviews. Genetics*, *18*(9), 535–550. https://doi.org/10.1038/NRG.2017.46

Tessadori, F., Giltay, J. C., Hurst, J. A., Massink, M. P., Duran, K., Vos, H. R., van Es, R. M., Scott, R. H., van Gassen, K. L. I., Bakkers, J., & van Haaften, G. (2017). Germline mutations affecting the histone H4 core cause a developmental syndrome by altering DNA damage response and cell cycle control. *Nature Genetics*, *49*(11), 1642–1646. https://doi.org/10.1038/ng.3956

Thada, V., & Cortez, D. (2021). ATR activation is regulated by dimerization of ATR activating proteins. *The Journal of Biological Chemistry*, *296*. https://doi.org/10.1016/J.JBC.2021.100455

Thakar, T., Leung, W., Nicolae, C. M., Clements, K. E., Shen, B., Bielinsky, A. K., & Moldovan, G. L. (2020). Ubiquitinated-PCNA protects replication forks from DNA2-mediated degradation by regulating Okazaki fragment maturation and chromatin assembly. *Nature Communications 2020 11:1*, *11*(1), 1–14. https://doi.org/10.1038/s41467-020-16096-w

Thang, N. D., Yajima, I., Kumasaka, M. Y., Iida, M., Suzuki, T., & Kato, M. (2015). Deltex-3-like (DTX3L) stimulates metastasis of melanoma through FAK/PI3K/AKT but not MEK/ERK pathway. *Oncotarget*, *6*(16), 14290–14299. https://doi.org/10.18632/ONCOTARGET.3742

Thompson, J. W., Nagel, J., Hoving, S., Gerrits, B., Bauer, A., Thomas, J. R., Kirschner, M. W., Schirle, M., & Luchansky, S. J. (2014). Quantitative Lys-ϵ-Gly-Gly (diGly) Proteomics Coupled with Inducible RNAi Reveals Ubiquitin-mediated Proteolysis of DNA Damage-inducible Transcript 4 (DDIT4) by the E3 Ligase HUWE1. *The Journal of Biological Chemistry*, *289*(42), 28942. https://doi.org/10.1074/JBC.M114.573352

Toledo, L. I., Altmeyer, M., Rask, M. B., Lukas, C., Larsen, D. H., Povlsen, L. K., Bekker-Jensen, S., Mailand, N., Bartek, J., & Lukas, J. (2013). ATR prohibits replication catastrophe by preventing global exhaustion of RPA. *Cell*, *155*(5), 1088. https://doi.org/10.1016/j.cell.2013.10.043

Tutt, A., Robson, M., Garber, J. E., Domchek, S. M., Audeh, M. W., Weitzel, J. N., Friedlander, M., Arun, B., Loman, N., Schmutzler, R. K., Wardley, A., Mitchell, G., Earl, H., Wickens, M., & Carmichael, J. (2010). Oral poly(ADP-ribose) polymerase inhibitor olaparib in patients with BRCA1 or BRCA2 mutations and

advanced breast cancer: a proof-of-concept trial. *Lancet (London, England)*, *376*(9737), 235–244. https://doi.org/10.1016/S0140-6736(10)60892-6

Uchida, C., & Kitagawa, M. (2016). RING-, HECT-, and RBR-type E3 Ubiquitin Ligases: Involvement in Human Cancer. *Current Cancer Drug Targets*, *16*(2), 157–174. https://doi.org/10.2174/1568009616666151112122801

Vaisman, A., & Woodgate, R. (2017). Translesion DNA polymerases in eukaryotes: what makes them tick? *Critical Reviews in Biochemistry and Molecular Biology*, *52*(3), 274–303. https://doi.org/10.1080/10409238.2017.1291576

Vannier, J. B., Pavicic-Kaltenbrunner, V., Petalcorin, M. I. R., Ding, H., & Boulton, S. J. (2012). RTEL1 Dismantles T Loops and Counteracts Telomeric G4-DNA to Maintain Telomere Integrity. *Cell*, *149*(4), 795–806. https://doi.org/10.1016/J.CELL.2012.03.030

Vassileva, V., Millar, A., Briollais, L., Chapman, W., & Bapat, B. (2002). Genes Involved in DNA Repair Are Mutational Targets in Endometrial Cancers with Microsatellite Instability. *Cancer Research*, *62*(14).

Velichko, A. K., Ovsyannikova, N., Petrova, N. v., Luzhin, A. v., Vorobjeva, M., Gavrikov, A. S., Mishin, A. S., Kireev, I. I., Razin, S. v., & Kantidze, O. L. (2021). Treacle and topbp1 control replication stress response in the nucleolus. *Journal of Cell Biology*, *220*(8). https://doi.org/10.1083/JCB.202008085/212262

Venitt, S., & Phillips, D. H. (2012). Philip D. Lawley (1927–2011). *Nature 2012 482:7383*, *482*(7383), 36–36. https://doi.org/10.1038/482036a

Vujanovic, M., Krietsch, J., Raso, M. C., Terraneo, N., Zellweger, R., Schmid, J. A., Taglialatela, A., Huang, J. W., Holland, C. L., Zwicky, K., Herrador, R., Jacobs, H., Cortez, D., Ciccia, A., Penengo, L., & Lopes, M. (2017). Replication Fork Slowing and Reversal upon DNA Damage Require PCNA Polyubiquitination and ZRANB3 DNA Translocase Activity. *Molecular Cell*, *67*(5), 882-890.e5. https://doi.org/10.1016/J.MOLCEL.2017.08.010

Wagner, J. M., & Karnitz, L. M. (2009). Cisplatin-induced DNA damage activates replication checkpoint signaling components that differentially affect tumor cell survival. *Molecular Pharmacology*, *76*(1), 208–214. https://doi.org/10.1124/MOL.109.055178

Wang, L. C., & Gautier, J. (2010). The Fanconi anemia pathway and ICL repair: implications for cancer therapy. *Critical Reviews in Biochemistry and Molecular Biology*, *45*(5), 424. https://doi.org/10.3109/10409238.2010.502166

Wang, L., Sun, X., He, J., & Liu, Z. (2021). Functions and Molecular Mechanisms of Deltex Family Ubiquitin E3 Ligases in Development and Disease. *Frontiers in Cell and Developmental Biology*, *9*, 2355. https://doi.org/10.3389/FCELL.2021.706997/BIBTEX

Wardlaw, C. P., Carr, A. M., & Oliver, A. W. (2014). TopBP1: A BRCT-scaffold protein functioning in multiple cellular pathways. In *DNA Repair* (Vol. 22, pp. 165–174). Elsevier. https://doi.org/10.1016/j.dnarep.2014.06.004

Watanabe, K., Tateishi, S., Kawasuji, M., Tsurimoto, T., Inoue, H., & Yamaizumi, M. (2004). Rad18 guides polη to replication stalling sites through physical interaction and PCNA monoubiquitination. *The EMBO Journal*, *23*(19), 3886. https://doi.org/10.1038/SJ.EMBOJ.7600383

Werner, B., Case, J., Williams, M. J., Chkhaidze, K., Temko, D., Fernández-Mateos, J., Cresswell, G. D., Nichol, D., Cross, W., Spiteri, I., Huang, W., Tomlinson, I. P. M., Barnes, C. P., Graham, T. A., & Sottoriva, A. (2020). Measuring single cell divisions in human tissues from multi-region sequencing data. *Nature Communications*, *11*(1). https://doi.org/10.1038/S41467-020-14844-6

Weterings, E., & Chen, D. J. (2008). The endless tale of non-homologous end-joining. *Cell Research 2008 18:1*, *18*(1), 114–124. https://doi.org/10.1038/cr.2008.3

Weterings, E., & van Gent, D. C. (2004). The mechanism of non-homologous end-joining: a synopsis of synapsis. *DNA Repair*, *3*(11), 1425–1435. https://doi.org/10.1016/J.DNAREP.2004.06.003

Wilkinson, K. D. (2000). Ubiquitination and deubiquitination: targeting of proteins for degradation by the proteasome. *Seminars in Cell & Developmental Biology*, *11*(3), 141–148. https://doi.org/10.1006/SCDB.2000.0164

Wilting, S. M., de Wilde, J., Meijer, C. J. L. M., Berkhof, J., Yi, Y., van Wieringen, W. N., Braakhuis, B. J. M., Meijer, G. A., Ylstra, B., Snijders, P. J. F., & Steenbergen, R. D. M. (2008). Integrated genomic and transcriptional profiling identifies chromosomal loci with altered gene expression in cervical cancer. *Genes, Chromosomes & Cancer*, *47*(10), 890–905. https://doi.org/10.1002/GCC.20590

Wright, W. D., Shah, S. S., & Heyer, W. D. (2018). Homologous recombination and the repair of DNA double-strand breaks. *The Journal of Biological Chemistry*, *293*(27), 10524–10535. https://doi.org/10.1074/JBC.TM118.000372

Wu, Z., Oeck, S., West, A. P., Mangalhara, K. C., Sainz, A. G., Newman, L. E., Zhang, X. O., Wu, L., Yan, Q., Bosenberg, M., Liu, Y., Sulkowski, P. L., Tripple, V., Kaech, S. M., Glazer, P. M., & Shadel, G. S. (2019). Mitochondrial DNA stress signalling protects the nuclear genome. *Nature Metabolism 2019 1:12*, *1*(12), 1209–1218. https://doi.org/10.1038/s42255-019-0150-8

Wyatt, H. D. M., Sarbajna, S., Matos, J., & West, S. C. (2013). Coordinated actions of SLX1-SLX4 and MUS81-EME1 for Holliday junction resolution in human cells. *Molecular Cell*, *52*(2), 234–247. https://doi.org/10.1016/J.MOLCEL.2013.08.035

Xie, M., Yen, Y., Owonikoko, T. K., Ramalingam, S. S., Khuri, F. R., Curran, W. J., Doetsch, P. W., & Deng, X. (2014). Bcl2 induces DNA replication stress by inhibiting ribonucleotide reductase. *Cancer Research*, *74*(1), 212–223. https://doi.org/10.1158/0008-5472.CAN-13-1536-T

Xu, G., & Jaffrey, S. R. (2013). Proteomic identification of protein ubiquitination events. *Biotechnology and Genetic Engineering Reviews*, *29*(1), 73–109. https://doi.org/10.1080/02648725.2013.801232

Xu, P., & Peng, J. (2006). Dissecting the ubiquitin pathway by mass spectrometry. In *Biochimica et Biophysica Acta - Proteins and Proteomics* (Vol. 1764, Issue 12, pp. 1940–1947). https://doi.org/10.1016/j.bbapap.2006.09.004

Xu, P., Tao, X., Zhao, C., Huang, Q., Chang, H., Ban, N., Bei, Y., Xia, X., Shen, C., Wang, K., Xu, L., Wu, P., Ren, J., & Wang, D. (2017). DTX3L is upregulated in glioma and is associated with glioma progression. *International Journal of Molecular Medicine*, *40*(2), 491–498. https://doi.org/10.3892/IJMM.2017.3023/HTML

Yan, Q., Dutt, S., Xu, R., Graves, K., Juszczynski, P., Manis, J. P., & Shipp, M. A. (2009). BBAP Monoubiquitylates Histone H4 at Lysine 91 and Selectively Modulates the DNA Damage Response. *Molecular Cell*, *36*(1), 110–120. https://doi.org/10.1016/j.molcel.2009.08.019

Yan, Q., Xu, R., Zhu, L., Cheng, X., Wang, Z., Manis, J., & Shipp, M. A. (2013). BAL1 and Its Partner E3 Ligase, BBAP, Link Poly(ADP-Ribose) Activation, Ubiquitylation, and Double-Strand DNA Repair Independent of ATM, MDC1, and RNF8. *Molecular and Cellular Biology*, *33*(4), 845–857. https://doi.org/10.1128/mcb.00990-12

Yang, C. S., Jividen, K., Spencer, A., Dworak, N., Ni, L., Oostdyk, L. T., Chatterjee, M., Kuśmider, B., Reon, B., Parlak, M., Gorbunova, V., Abbas, T., Jeffery, E., Sherman, N. E., & Paschal, B. M. (2017). Ubiquitin Modification by the E3 Ligase/ADP-Ribosyltransferase Dtx3L/Parp9. *Molecular Cell*, *66*(4), 503-516.e5. https://doi.org/10.1016/j.molcel.2017.04.028

Yazinski, S. A., Comaills, V., Buisson, R., Genois, M. M., Nguyen, H. D., Ho, C. K., Kwan, T. T., Morris, R., Lauffer, S., Nussenzweig, A., Ramaswamy, S., Benes, C. H., Haber, D. A., Maheswaran, S., Birrer, M. J., & Zou, L. (2017). ATR inhibition disrupts rewired homologous recombination and fork protection pathways in PARP inhibitor-resistant BRCA-deficient cancer cells. *Genes & Development*, *31*(3), 318–332. https://doi.org/10.1101/GAD.290957.116

Ye, J., Ai, X., Eugeni, E. E., Zhang, L., Carpenter, L. R., Jelinek, M. A., Freitas, M. A., & Parthun, M. R. (2005). Histone H4 Lysine 91 Acetylation: A Core Domain ModificationAssociated with Chromatin Assembly. *Molecular Cell*, *18*(1), 123–130. https://doi.org/10.1016/j.molcel.2005.02.031

Zhang, J., Dewar, J. M., Budzowska, M., Motnenko, A., Cohn, M. A., & Walter, J. C. (2015). DNA interstrand cross-link repair requires replication fork convergence. *Nature Structural & Molecular Biology*, *22*(3), 242. https://doi.org/10.1038/NSMB.2956

Zhang, P., Elabd, S., Hammer, S., Solozobova, V., Yan, H., Bartel, F., Inoue, S., Henrich, T., Wittbrodt, J., Loosli, F., Davidson, G., & Blattner, C. (2015). TRIM25 has a dual function in the p53/Mdm2 circuit. *Oncogene*, *34*(46), 5729–5738. https://doi.org/10.1038/ONC.2015.21

Zhang, Y., Mao, D., Roswit, W. T., Jin, X., Patel, A. C., Patel, D. A., Agapov, E., Wang, Z., Tidwell, R. M., Atkinson, J. J., Huang, G., McCarthy, R., Yu, J., Yun, N. E., Paessler, S., Lawson, T. G., Omattage, N. S., Brett, T. J., & Holtzman, M. J. (2015). PARP9-DTX3L ubiquitin ligase targets host histone H2BJ and viral 3C protease to enhance interferon signaling and control viral infection. *Nature Immunology*, *16*(12), 1215–1227. https://doi.org/10.1038/ni.3279

Zhao, B., Zhang, W., Cun, Y., Li, J., Liu, Y., Gao, J., Zhu, H., Zhou, H., Zhang, R., & Zheng, P. (2017). Mouse embryonic stem cells have increased capacity for replication fork restart driven by the specific Filia-Floped protein complex. *Cell Research 2018 28:1*, *28*(1), 69–89. https://doi.org/10.1038/cr.2017.139

Zhu, M., Zhao, H., Liao, J., & Xu, X. (2014). HERC2/USP20 coordinates CHK1 activation by modulating CLASPIN stability. *Nucleic Acids Research*, *42*(21), 13074–13081. https://doi.org/10.1093/nar/gku978